Peptide-Driven Tri-Modal Gene Delivery Systems (PDTMG): Novel Versatile Peptide-Based Lipopolyplexes Incorporating Peptide-Functionalized Gemini Surfactants for Targeted Gene Therapy- Implementation of RGD Motifs as a Means for Endosomal Escape

by

Amirreza Rafiee

A thesis
presented to the University of Waterloo
in fulfilment of the
thesis requirement for the degree of
Doctor of Philosophy
in
Pharmacy
Waterloo, Ontario, Canada, 2018

Examining Committee Membership

The following served on the Examining Committee for this thesis. The decision of the Examining Committee is by majority vote.

External Examiner	Dr. Elizabeth Gillies Professor, Department of Chemistry, The University of Western Ontario
Supervisor	Dr. David Edwards Professor, School of Pharmacy
Internal Members	Dr. Praveen P. Nekkar Rao Associate Professor, School of Pharmacy
	Dr. Shawn Wettig Associate Professor, School of Pharmacy
Internal-External Member	Dr. John Honek Professor, Department of Chemistry

AUTHOR'S DECLARATION

I hereby declare that I am the sole author of this thesis. This is a true copy of the thesis, including any required final revisions, as accepted by my examiners. I understand that my thesis may be made electronically available to the public.

Abstract

The development of non-viral gene delivery vectors is highly challenging and aims to provide a safe while cost-effective manufacturing alternative to viral vectors. Eleven novel gemini surfactants (G**4**-G**14**) were designed and synthesized by covalent linking of 10 different functional moieties (R = R_1-R_{10}) to the spacer regions of gemini surfactants (chemical formula m-s-m; m = saturated 12, 18 carbon alkyl chains, s = R-linked-imino-substituted-7 methylene spacer group (7NR)). These R-functionalities include imidazole and thiol containing functional groups (R_1 = imidazolepropionyl, R_2 = thiopropionyl; for synthesis of G**4** (18-7NR_1-18) and G**5** (18-7NR_2-18)), linear RGD derivatives (R_3 = RGDG, R_4 = GRGDSPG; for synthesis of G**6** (12-7NR_3-12), G**7** (18-7NR_3-18), G**8** (18-7NR_4-18)), polyhistidine derivatives (R_5 = $E(H)_5$; for synthesis of G**9** (18-7NR_5-18)), bifunctional RGD-polyhistidine peptides (R_6 = $EGRGDSPG(H)_5$; for synthesis of G**10** (18-7NR_6-18)), and arginine-rich peptide motifs (R_7 = Suc-$(E)_2G(R)_2$, R_8 = Suc-$(E)_2G(R)_3$, R_9 = Suc-$(E)_2(G)_3(R)_3$, R_{10} = Suc-$DE(G)_3(R)_3$); for synthesis of G**11** (18-7NR_7-18), G**12** (18-7NR_8-18), G**13** (18-7NR_9-18), G**14** (18-7NR_{10}-18)]. The RGD-functionalized gemini surfactants were evaluated for targeted gene delivery.

Further, the impact of non-covalent addition of designed peptide enhancers (7 types; P_A-P_G) [zwitterionic RGD peptide enhancer (P_A), cationic peptide enhancers rich in histidine and/or arginine (P_B, P_D, P_F), or bifunctional cationic, RGD peptide enhancers (P_C = P_A+ P_B, P_E = P_A+ P_D, P_G = P_A+ P_F)] were examined for development of peptide-based lipopolyplexes, named peptide-driven tri-modal gene delivery systems (PDTMG). The PDTMG were formulated using peptide enhancers/gemini surfactants/1,2-dioleyl-*sn*-glycero-3-phosphoethanolamine (DOPE) helper lipid, for *in vitro* delivery of green fluorescent protein (GFP)-expressing plasmid DNA.

Using quantitative flow cytometry, transfection activity was investigated by both the percentage of the transfected cells and the intensity of GFP expression level determined by mean fluorescence intensities (MFI). The correlation of the transfection activity and viability to the physicochemical properties of delivery systems, size and zeta potential, were identified to advance formulation strategies for development of a potent delivery system with negligible cytotoxicity. These include optimization of cationic quaternary ammonium of gemini surfactants/anionic phosphate of DNA (N/P) mole ratios ($\rho_{\pm}$ values), DOPE/gemini molar ratios (r values), and the molarity of the compositional elements in the formulation mixtures (M_P, M_G and M_L for molar concentrations of peptide enhancers (P), gemini surfactants (G) and DOPE helper lipids (L), respectively).

In vitro transfection studies demonstrated that among PDTMG delivery systems formulated using fourteen different gemini surfactants [G**1**-G**14**] differing in their headgroups and alkyl tails lengths (i.e., s = 3, 7NH, $7NR_{1\text{-}10}$; m = 12, 18), remarkably gemini surfactants with short RGD functional headgroups and C18 alkyl tails (G**7** and G**8**) provided elevated cell-penetrating activity and endosomal rupturing functionality. The G**7**-based PDTMG formulation (prepared at $\rho_{\pm}$ = 1.1 and r = 6.8; M_P = 267 μM, M_G = 17 μM, M_L = 113 μM) revealed up to 120-fold increase in MFI as compared to bi-modal gemini/DOPE formulation (prepared at $\rho_{\pm}$ = 10 and r = 3.3). Compared to the PDTMG systems formulated using G**1**-G**6** and G**9**-G**14** gemini surfactants (prepared at $\rho_{\pm}$ = 1.1 and r = 6.8), G**7** counterparts resulted up to 38-fold higher in MFI. Further, the G**7**- and G**8**-based PDTMG nanoparticles demonstrated comparable transfection activity with the gold-standard Lipofectamine 3000 transfection reagent.

It is believed that the short RGD functional peptides (R_3, R_4) covalently linked to 18-series gemini surfactants provided reduced steric hindrance on the surface of the PDTMG nanoparticles when compared to other functional peptides (R_5-R_{10}), and exhibited endosomal destabilizing effects in

response to cellular environment. The non-covalent addition of cationic peptide enhancers in formulation of the PDTMG delivery systems demonstrated a synergistic effect for DNA condensation, particle stability, cellular uptake, amplified endosomal release, protecting and facilitating the intracellular delivery of the pDNA.

This project has demonstrated that G**7**- and G**8**-based PDTMG nanoparticles have the capability to undergo conformational changes in response to the cellular environment, disrupt the endosome, and release genetic materials into the cell cytoplasm. The development of these novel peptide-based lipopolyplexes provided a solid foundation for design of the versatile derivatives for *in vivo* targeted delivery of nucleotide-based therapeutics.

ACKNOWLEDGMENTS

The completion of this PhD work would not have been possible without the support of many people who influenced my life and work.

First, I would like to thank my supervisor Dr. Dave Edwards, Hallman Director of the School of Pharmacy, for his time, and all his help and support during my PhD program, and my former supervisors Dr. Marianna Foldvari for supplying all the materials and instruments throughout this project, and Dr. Roderick Slavcev for his guidance, enormous support, and encouragement throughout the writing of my thesis. I would like to express my sincere gratitude to Dr. Praveen Nekkar for his patient guidance, encouragement, and constant support as well as providing access to his lab and instruments. I would like to extend my thanks to Dr. Shawn Wettig for his valuable feedback, advice and assistance over the course of my thesis, and for allowing me to use his benchtop freeze dry system. I would also like to thank the members of my committee, Dr. Elizabeth Gillies and Dr. John Honek, for taking their time and providing valuable insight on this project.

I would also like to express my gratitude to the School of Pharmacy and other departments of University of Waterloo for their continuous help, financial and technical support throughout the course of my PhD program. I also thank Dr. Richard Smith, manager at the University of Waterloo Mass Spectrometry Facility (UWMSF) for his technical assistance and coordination with mass spectrometry throughout this work.

I thank both current and former members of Dr. Foldvari's lab and Dr. Slavcev's lab, especially Dr. Marjan Gharagozloo for her time, and countless helpful discussions. I would also like to thank all my colleagues from different labs for their help, assistance and friendship, especially Ding Wen (Roger) Chen, Arash Shakeri, Dr. Nafiseh Nafissi, and Dr. Aula Al Muslim.

I am incredibly grateful to my friend, Kaveh Fazli, for his time and technical assistance on creating 3D images.

Finally, I would like to express my deepest gratitude and appreciation to my fiancé, Maygol, for her love, encouragement and her patience, and to her loving family for their continuous support. To my dear parents and my sisters, Bahareh and Azadeh, for their endless love and encouragement. My parents have always encouraged me in all my pursuits and supported me to follow my dreams. Thank you.

DEDICATION

To my beloved fiancé, Maygol, and my dear parents, Mehdi and Masoumeh.

Table of Contents

List of Figures

List of Tables

List of Abbreviations

AAV2	adeno-associated virus serotype 2
ADA-SCID	adenosine deaminase severe combined immunodeficiency
ALL	acute lymphoblastic leukemia
AON	antisense oligonucleotide
BM [G/L]	Bi-Modal [gemini surfactant/DOPE lipid] gene delivery systems
BM [P/G]	Bi-Modal [peptide enhancer/gemini surfactant] gene delivery systems
BM [P/L]	Bi-Modal [peptide enhancer/DOPE lipid] gene delivery systems
CAR T	chimeric antigen receptor T-cell therapy
Cas9	CRISPR associated protein 9
CCV	clathrin-coated vesicle
CDs	cyclodextrins
CIE	clathrin- and caveolae-independent endocytosis
CMC	critical micelle concentration
CME	clathrin-mediated endocytosis
CPPs	cell-penetrating peptides
CRISPR	Clustered Regularly Interspaced Short Palindromic Repeats
CSF-1	colony-stimulating factor-1
CSPGs	chondroitin sulfate proteoglycans
CvME	caveolae-mediated endocytosis
DC-Chol	3β-[*N-(N″,N″*-dimethylaminoethane)-carbomoyl]cholestrol
DIPEA	*N,N*-diisopropylethylamine
DLBCL	diffuse large B-cell lymphoma
DLS	dynamic light scattering
DMEM	Dulbecco's modified Eagle's medium
DMF	*N,N*-dimethylformamide
DOGS	dioctadecylamidoglycylspermine
DOPC	1,2-dioleoyl-sn-glycero-3-phosphatidylcholine
DOPE	1,2-dioleoyl-sn-glycero-3-phosphatidylethanolamine
DOSPA	2,3-dioleyloxy-*N*-[2(sperminecarboxamido)-ethyl]-*N,N*-dimethyl-l-propanaminium trifluoroacetate
DOTAP	1,2-dioleoyloxy-3-trimethylammonium-propane
DOTMA	*N*-[1-(2,3-dioleyloxy)propyl-*N,N,N*-trimethylammonium chloride
DPPE	1,2-dipalmitoyl-sn-glycero-3-phosphatidylehanolamine
DSBs	double-strand breaks
DTS	DNA nuclear targeting sequences

EDT	1,2-ethanedithiol
EGF	epidermal growth factor
EMA	European Medicines Agency
EPR	enhanced permeability and retention
ESI-MS	Electrospray ionization mass spectrometry
FBS	fetal bovine serum
FDA	Food and Drug Administration
FG	fibrinogen
FN	fibronectin
GAGs	glycosaminoglycans
GFP	green fluorescent protein
HATU	1-[bis(dimethylamino)methylene]-1-*H*-1,2,3-triazolo[4,5-*b*]pyridimium 3-oxid hexafluorophosphate
HDR	homology-directed repair
HPLC	high performance liquid chromatography
HSC	hematopoietic stem cell
HSPGs	heparan sulfate proteoglycan
MeCN	acetonitrile
MFI	mean fluorescence intensity
miRNA	microRNA
MPS	mononuclear phagocytic system
NHEJ	non-homologous end joining
NLS	nuclear localization signals
NPC	nuclear pore complex
OTC	ornithine transcarbamylase
P	packing parameter
PAMAM	polyamidoamine
PDGF	platelet-derived growth factor
pDNA	plasmid DNA
PDTMG	Peptide-Driven Tri-Modal [peptide enhancer/gemini surfactant/DOPE lipid] gene delivery systems
PEG	poly(ethylene glycol)
PEI	polyethyleneimine
PLL	poly(L-Lysine)
PPI	poly(propylenimine)
RES	reticuloendothelial system
RPE	retinal pigment epithelial
SANS	small angle neutron scattering

SAXS	small angle X-ray scattering
sgRNA	single guide RNA
shRNA	small hairpin RNA
siRNA	small interfering RNA
TALENs	Transcription Activator-Like Effector Nucleases
TEM	transmission electron microscopy
TFA	trifluoroacetic acid
TIL	tumor-infiltrating lymphocytes
TIS	triisopropylsilane
UM [G]	Uni-Modal [gemini surfactant] gene delivery systems
UM [P]	Uni-Modal [peptide enhancer] gene delivery systems
UPLC	ultra-performance liquid chromatography
VEGF R2	vascular endothelial growth factor receptor-2
VN	vitronectin
VWF	von Willebrand Factor
X-SCID	X-linked severe combined immunodeficiency disorder
ZFNs	Zinc Finger Nucleases

Chapter 1

Introduction

1.1 Introduction to gene delivery

Gene therapy is a cutting-edge technology that uses therapeutic nucleic acids to cure or prevent wide range of inherited conditions (such as hemophilia [1], thalassemia [2], cystic fibrosis [3], Wiskott-Aldrich syndrome [4]) and acquired diseases (including cancer [5, 6], infectious diseases [7], neurodegenerative disorders [8] and cardiovascular conditions [9]) at the genetic level. This can be achieved by either replacing a malfunctioning gene, or introducing a therapeutic gene for transient expression of a defective gene, or inactivating an overexpressing gene through gene silencing techniques [10-14]. Gene therapy can be classified into two major categories: germ line gene therapy and somatic gene therapy that target germ line cells (egg or sperm) and somatic cells (non-reproductive cells or body cells), respectively [15, 16]. Germ line gene therapy offers a permanent therapeutic effect that can potentially eliminate an inherited genetic disorder from a family and possibly from the population [17]. However, the idea surrounding germline gene therapy is controversial due to unresolved ethical challenges and unpredictable side effects which are yet to be known and may affect future generations [18-23]. Somatic gene therapy is considered a safe approach where modifications and effects are limited to the individual and are not passed on to the next generations [24].

In addition to the common classes of therapeutic nuclei acids (e.g., plasmid DNA (pDNA), antisense oligonucleotide (AON), small interfering RNA (siRNA), small hairpin RNA (shRNA), microRNA (miRNA)) used in gene therapy, the emergence of programmable nuclease-based

genome editing technologies over the past decade dramatically impacted scientific research [25, 26]. The genome editing technologies utilize chimeric nucleases that are engineered by fusing sequence-specific DNA-binding domains to a nonspecific DNA cleavage domain. These engineered nucleases generate targeted DNA double-strand breaks (DSBs) into the genome, resulting in efficient and precise genome modification through cellular DNA repair mechanisms, including error-prone non-homologous end joining (NHEJ) and homology-directed repair (HDR) using exogenous DNA [14]. Zinc Finger Nucleases (ZFNs), Transcription Activator-Like Effector Nucleases (TALENs) and more recently, the innate bacterial based immune system Clustered Regularly Interspaced Short Palindromic Repeats (CRISPR)/ associated protein 9 (CRISPR/Cas9) technology are the major tools used in the field of genome editing [10, 11, 27]. In contrast to ZFNs and TALENs that use proteins to recognise the target DNA sequence, CRISPR/Cas9 employs single guide RNA (sgRNA) for site recognition; hence, it provides a simple, easy-to-use and highly efficient gene editing tool for therapeutic applications in human [14]. For a comprehensive review of genome editing techniques, their mechanism of action and delivery strategies for therapeutic applications refer to [12, 26, 28].

Despite the substantial progress in the field of gene therapy, there are fundamental challenges for safe and effective delivery of therapeutic nucleic acids to target cells in human body. This has consequently resulted in limited success of gene therapy in clinical trials.

1.2 Current position of gene therapy: progress and limitations

In 1989, the first clinical protocol was approved to test the safety and feasibility of the gene therapy process using retroviral-mediated “marked” tumor-infiltrating lymphocytes (TIL) concomitant with interleukin-2 in treatment of advanced melanoma [29] and the first human gene therapy

clinical trial was approved by FDA on September 14th 1990 to treat two unrelated girls, ages 4 and 9, suffering from adenosine deaminase deficiency, a very rare autosomal monogenic disorder that causes severe combined immunodeficiency (ADA-SCID) [30]. Since then, there have been almost 2,600 gene therapy clinical trials undertaken that have utilized both viral vectors and non-viral vectors as a method of gene transfer [31]. Viral vectors are the amongst the most used vectors in clinical trials. Approximately 70% of gene therapy clinical trials carried out so far have utilized recombinant viruses such as adenoviruses (20.5%), retroviruses (17.9%), adeno-associated viruses (7.6%) and lentivirus (7.3%)- based on online available database on The Journal of Gene Medicine Gene Therapy Clinical Trials Worldwide (updated November 2017). To date, cancer has been the most targeted disease in clinical gene therapy trials (approximately 65%), followed by monogenic diseases (11.1%), infectious diseases (7%) and cardiovascular diseases (6.9%) [31]. Gendicine™, developed by SiBiono GenTech, was the first human gene therapy product that was approved by the State Food and Drug Administration of China (SFDA) in 2003 [32]. Gendicine™ is a recombinant adenoviral expressing human p53 (Ad-p53 gene therapy) for treatment of head and neck squamous cell carcinoma [32]. This breakthrough, later, resulted in accelerating in development of several other gene therapy products such as Glybera® (alipogene tiparvovec), Strimvelis™, Kymriah® (tisagenlecleucel), Yescarta™ (axicabtagene ciloleucel) and Luxturna™ (voretigene neparvovec-rzyl) [33-36]. Glybera® (alipogene tiparvovec) is an adeno-associated virus serotype 1 (AAV1)-based gene therapy that delivers human lipoprotein lipase (LPL) gene to muscle cells for the treatment of severe lipoprotein lipase deficiency (LPLD), a rare autosomal monogenic disorder of triglyceride metabolism. Glybera®, marketed by uniQure, was the first gene therapy product to gain approval by the European Medicines Agency (EMA) in the Western world back in 2012 [33]. However, 5 years later, due to the high market price, at an average of $1 million

per treatment, uniQure's Glybera® was withdrawn from the European market [37, 38]. GlaxoSmithKline (GSK)'s Strimvelis®, the second approved gene therapy by EMA in May 2016, is an ex-vivo genetically modified hematopoietic stem cell (HSC) gene therapy for the treatment of patients with ADA-SCID. Strimvelis® is prepared by inserting a functional ADA gene into the cells from the patient's own bone marrow using gammaretrovirus [34]. At the expensive cost of the treatment, $665,000 for a single dose of Strimvelis®, and the low number of treated patients (only two patients as of July 2017), in July 2017, GSK has announced that the company is considering eliminating its rare disease unit [39]. On Aug 30, 2017, the U.S. Food and Drug Administration (FDA) has approved the cell-based gene therapy Kymriah®, which became the first gene therapy available in the United States [40]. Kymriah®, marketed by Novartis Pharmaceutical Corporation, is a chimeric antigen receptor (CAR)-T-cell therapy for the treatment of patients up to 25 years of age with B-cell precursor acute lymphoblastic leukemia (ALL) [35, 41]. The second FDA approved CAR-T-based gene therapy is granted to Yescarta™ (Gilead Science Inc.'s Kite Pharma) on October 18, 2017 to treat patients with diffuse large B-cell lymphoma (DLBCL) [42]. Both Kymriah® and Yescarta™ are customized treatments that use patient's own T cells to target and kill cancer cells, which have a specific antigen (CD19) on their surface [40, 42]. More recently, on December 19, 2017, FDA granted gene therapy approval to Luxturna™, developed by Spark Pharmaceutics Inc., to treat patients with biallelic RPE65 mutation-associated retinal dystrophy, a rare form of inherited retinal disease [43]. Luxturna™ is a recombinant adeno-associated virus serotype 2 (AAV2)-based gene therapy that is administered via subretinal injection where it delivers a functional copy of human retinal pigment epithelium-specific protein 65kDa (RPE65) gene to retinal pigment epithelial (RPE) cells [44].

Despite these recent advancements of viral of gene therapy, there are fundamental limitations associated with viral vectors, including immunogenicity, carcinogenesis, cytotoxicity, broad tropism, limited DNA packaging capacity [45-47].

In 1999, a patient suffered from deficiency of ornithine transcarbamylase (OTC; a liver enzyme responsible for removal of ammonia from the blood) died in an adenovirus-mediated gene therapy clinical trial due to an unexpected severe immune response triggered by the virus capsid protein [48]. In addition, in a French clinical trial begun in 1999 for the treatment of X-linked severe combined immunodeficiency disorder (X-SCID) by *Ex vivo* retrovirus-mediated gene transfer into hematopoietic stem cells, two patients developed leukemia-like syndrome in late 2002. The disease was shown to be due to the oncogenic insertional mutagenesis resulting from random retroviral integration to the LMO2 proto-oncogene promoter of host cells [45, 49, 50]. Recently, complications with CAR-T products (Kymriah® and Yescarta™) including life-threatening side effects, such as cytokine release syndrome and neurological toxicities, are increasingly getting attention [51]. As a result, many of viral gene products are used in combination with various immune modulatory regimens [52]. These events highlight some of the major safety concerns with the use of viral gene therapy products.

In addition, the high price tags of viral gene therapy products (e.g., Kymriah®: $475,000, Yescarta™: 373,000 and Luxturna™: $425,000 for single dose per eye or $850,000 for both eyes) raise the question of affordability and present considerable financial challenges for health-care providers and insurance companies [37, 41, 53]. Moreover, difficulty in production and manufacturing process, possibility of large-scale contamination of bioreactor batches [54], encourage the research for the potential alternatives that can circumvent many of these limitations.

Non-viral gene therapy can fall into two categories: physical methods and non-viral vectors. Physical technology including electroporation [55], gene gun [56], ultrasound [57], and hydrodynamic injection [58] utilize physical forces to deliver naked nucleic acids into the targeted cells by creating transient membrane holes or defects in the cell membrane [16, 59]. However, these strategies are generally invasive that may cause cell trauma, cell death and/or physical damage to the samples [60]. In addition, their applications are limited to the local tissues (such as skin and muscles) and are not feasible for systemic gene delivery [61]. Non-viral vectors are highly sought after because of their low toxicity and immunogenicity, potential for repeated administration, low cost and ease of large scale production, potential platform for surface engineering with receptor-specific ligands for targeted gene delivery, and capacity to deliver unlimited size of nucleic acid payloads. Various non-viral vectors have been developed, including lipid-based vectors and polymer-based nanoparticles, dendrimer-based vectors and cell penetrating peptides [62]. Unlike viruses that have evolved mechanisms to deliver their genomes efficiently to host cells, non-viral vectors are not capable to effectively transport their cargos across various extra- and intra-cellular barriers. As a result, they have comparatively lower transfection efficiency and none of the non-viral based gene therapeutics has so far been approved by the US FDA despite the progress in their clinical developments [25, 63]. Therefore, development of non-viral gene delivery systems that can mimic the virus effective gene transfer is highly desirable [64-66].

1.3 Barriers to non-viral gene delivery

1.3.1 Extra-cellular barriers

Systematic delivery of non-viral vectors is hindered by enzymatic degradation, serum inactivation, and clearance by host defence mechanism. After *in vivo* administration of the

therapeutic nucleic acids, free nucleic acids can be rapidly degraded by various nucleases existing in circulation and extracellular environment. In a study, it was shown that the half-life of naked plasmid DNA in mouse whole blood was about 10 minutes at a concentration of 100 μg/ml [67]. Therefore, it is necessary to use vector systems that can efficiently condense and protect the large nucleic acid macromolecules against enzymatic degradation. Condensation and protection are generally proceeded by electrostatic interaction between negatively charged phosphate backbone of nucleic acids and cationic agents (such as lipids and polymers) to form thermodynamically stable particles (e.g., lipoplex and polyplex). The size, stability and the degree of complexation are largely dependent on the type and the amount of materials being used [68]. For example, these parameters can be controlled by adjusting cationic lipids/polymers to nucleic acids charge ratios (N/P).

The administration of neutral and cationic gene delivery vectors, however, can lead to aggregation owing to colloidal instability of cationic complexes at high physiological salt concentration or interaction with negatively charged erythrocyte membrane. Therefore, these aggregates may result in vascular blockage and lung embolization [69]. Preventing aggregation by increasing electrostatic repulsion using excessive cationic charge can further increase the opsonisation of the positively charged particles with plasma proteins (opsonins) in which the opsonized particles induce rapid clearance by circulating macrophages (through activation of the complement system) and phagocytic cells of the mononuclear phagocytic system (MPS) located in the liver, spleen, bone marrow and lungs (also known as reticuloendothelial system (RES)) [70, 71]. Increased colloidal stability is typically achieved by modification of non-viral vectors with hydrophilic polymers (e.g., poly(ethylene glycol) (PEG)), which creates a hydrophilic layer around the particle surface and confers steric hindrance between the opsonins and the delivery systems, thus avoiding

recognition by the RES system and prolonging circulation time in bloodstream [72, 73]. Therefore, the PEGylated nanoparticles (also referred as “stealth” nanoparticles) with reduced cytotoxicity can accumulate at pathological regions such as solid tumors (the so-called passive targeting) due to the cut-off size of their leaky vasculature, a phenomenon termed as “enhanced permeability and retention (EPR) effect” [66, 74]. Targeting ligand moieties such as peptides, antibodies and sugars have been grafted on the surface of gene delivery vectors to target organs/tissues of interest. However, the improved stability of PEG-shielded nanoparticles without efficient cleavable PEG systems have shown to inhibit cellular uptake and interfere with endosomal escape of the gene delivery systems, resulting in reduced gene expression [75, 76].

In addition to physiological barriers after systemic administration, the gene delivery vectors must cross anatomical barriers such as epithelial tissue of the blood vessels and the extracellular matrix to gain access to the targeted cells.

Gene delivery vectors using non-systemic administration are subjected to the sets of barriers associated with each organ involved (skin, eye, lung and other mucosal barriers) [25]. Following the extracellular barriers, the intracellular hurdles include cellular uptake, intracellular delivery, endosomal escape, nuclear translocation (in case of pDNA delivery) as described below.

1.3.2 Intra-cellular barriers

1.3.2.1 Cell binding and uptake mechanism

The uptake of naked nucleic acids across the lipophilic cell membrane is hindered due to the large, hydrophilic and high negative charge density of nucleic acids. Cationic complexes such as lipoplex, polyplex or other nanocarriers are typically used to facilitate internalization of nucleic acids through a process called endocytosis, by which the portion of the cell membrane

progressively encloses the vector, invaginates into a vesicle and then pinches off from the cell membrane to form an intracellular vesicle [77]. It is generally accepted that cell membrane interactions with cationic complexes are non-specific and mainly driven by the electrostatic interactions between the cationic complexes and the negatively charged proteoglycans carrying various glycosaminoglycans (GAGs) (e.g., chondroitin sulfate proteoglycans (CSPGs) and heparan sulfate proteoglycan (HSPGs)) on the cell surface [78-80]. Several viruses have also been shown to utilize these highly negatively charged GAGs as binding receptors to bring them closer to cells where they can interact with other receptors triggering internalization process [81-84]. The internalization of cationic complexes can be mediated either by electrostatic interaction with generic binding sites on the cell membrane in a non-specific manner (adsorptive-mediated endocytosis) and/or by specific ligands that bind to specific cell surface receptors (receptor-mediated endocytosis). Receptor-mediated endocytosis is believed to be a more efficient method for targeted gene delivery with reduced cytotoxicity. Cell surface binding and internalization, however, was found to be specific only within a narrow window of charge ratios close to neutrality [85, 86].

Targeted gene delivery can be achieved by surface modification of nanoparticles with specific ligands that can efficiently target certain receptors or antigens that are overexpressed in a disease or condition. Arg-Gly-Asp (RGD) [87], folate [88], transferrin [89], mannose [90] and cell-specific antibodies [91], are a few examples of nanoparticles surface modifications that have been investigated for targeted gene delivery.

As a particular example, RGD peptide motif ligands, found in many extra-cellular matrix (ECM) proteins such as collagen, laminin, fibronectin (FN), vitronectin (VN), von Willebrand Factor (VWF) and fibrinogen (FG), bind to integrins, a large family of transmembrane heterodimeric

glycoprotein receptors made of α and β subunits, and have been exploited for integrin-mediated targeted gene delivery. Many integrins, including $\alpha_5\beta_1$ and α_v integrins (such as $\alpha_v\beta_3$, and $\alpha_v\beta_5$), recognize the RGD peptide motif. Integrin-mediated uptake are also exploited by certain viruses, including adenovirus, echovirus and foot-and mouth disease virus [92-94]. The grafting of synthetic RGD peptides or peptidomimetics to the surface of gene complexes have been investigated for cancer gene therapy through targeting of $\alpha_v\beta_3$ integrin, which is involved in tumor angiogenesis and progression [95-98]. The integrin $\alpha_v\beta_3$ is highly expressed on cancer cells and tumor vasculatures, but it is absent in resting endothelial cells and most normal cells, making it an attractive target for cancer gene therapy [99]. In a study, polyethyleneimine (PEI) nanoparticles, which were PEGylated with a cyclic RGD ligand at the distal end of the PEG, were used for tumor-targeting delivery of siRNAs inhibiting vascular endothelial growth factor receptor-2 (VEGF R2) expression and tumor angiogenesis [100]. It was shown that the intravenous administration of the gene complex in tumor-bearing mice decreased protein expression with the tumor, resulting in inhibition of tumor growth and reduction in angiogenesis.

Endocytosis mechanism can also be classified in two broad categories: phagocytosis and pinocytosis. Phagocytosis is only limited to the specialized cells such as macrophages, monocytes and dendritic cells. Pinocytosis, however, occurs in all cell types and based on the composition of the coated vesicle, the size of the detached vesicle and the subsequent intracellular trafficking of the internalized particles are typically subdivided into four distinct pathways: 1- clathrin-mediated endocytosis (CME), 2- caveolae-mediated endocytosis (CvME), 3- macropinocytosis and 4- clathrin- and caveolae-independent endocytosis (CIE) [101]. The details of non-viral vectors cellular uptake mechanism have been extensively reviewed in the literature [102-104].

Briefly, CME includes the internalization of nutrients, antigens, growth factors and pathogens by binding to a cell surface receptor, followed by clustering of the ligand-receptor complexes into coated pits, which are then taken up into a clathrin-coated vesicle (CCV) with the size range of up to 200 nm [104]. The clathrin then depolymerized to form uncoated vesicles, which are then fused with each other and/or other vesicles, resulting in formation of early endosome, followed by acidification by proton pumps and maturation into late endosome and eventually lysosome to form an endolysosome where the particles are degraded at pH around 4.5.

CvME are small (60-80 nm), flask-shaped invagination of plasma membrane that are enriched in cholesterol and glycosphingololipids. CvME are involved in transcytosis (specially in endothelial cells) and endocytosis and are characterized by the presence of caveolin-1 located at the inner leaflet of the membrane bilayer [105, 106]. The density of caveola varies between cell types, tissues and can vary by the physiological conditions or disease states [106]. CvME is generally reported to be a non-acidic and non-digestive route of internalization where the internalized cargos are directly transferred to the Golgi and/or endoplasmic reticulum thus bypassing endolysosomal degradation [107]. However, the recent evidence suggests that some of the internalized caveosomes can join the classical endocytic degradative pathway [103, 105].

Macropinocytosis refers to the formation of large heterogeneous vesicles that are not induced by the cargos but rather stimulated in response to growth factors such as colony-stimulating factor-1 (CSF-1), epidermal growth factor (EGF) and platelet-derived growth factor (PDGF). Macropinocytosis is an actin-based process by which the internalization of fluids and particles occurs through cell surface ruffling that collapses onto and fuse with the plasma membrane [77, 108]. The endocytic vesicles, called macropinosomes, can be as large as 5 μM in diameter (usually bigger than 1 μM) and reported to have no coat. The intracellular fate of the macropinosomes are

largely dependent on the cell type, but generally they become acidified and shrink. The macropinosomes either recycle their content back to the cell exterior or mature and fuse with other late endosomes or with lysosomes [104, 109].

Phagocytosis is an actin-based membrane protrusions zippering up around the ligand-coated large particles (0.5> μM), followed by internalization into uncoated vesicles called phagosomes, which then readily fuse to early endosomes and late endosomes and eventually mature into phagolysosome where the internalized cargos are degraded [110]. Particle internalization is mediated by opsonic receptors, including complement receptors and Fc receptors.

In addition to the professional phagocytes (neutrophils, monocytes and macrophages, dendritic cells), other cell types such epithelial cells, endothelial cells and fibroblasts may uptake large cationic gene complexes (lipoplex and polyplex) through phagocytosis-like mechanism [77, 110].

Other endocytosis pathways independent of clathrin and caveolin (CIE) have been described to take place in lipid rafts and can include flotillin-dependent endocytosis, GTPase regulator associated with focal adhesion kinase-1 (CRAF1)-dependent endocytosis, adenosine diphosphate-ribosylation factor 6 (Arf6)-dependent endocytosis, and RhoA-dependent endocytosis [104].

Among all these endocytic pathways, clathrin-mediated endocytosis has been reported to be the major internalization pathway for non-targeting cationic gene delivery systems (i.e. adsorptive-mediated endocytosis). In addition, most of the current ligands used in targeted gene delivery (receptor-mediated endocytosis), including asialoglycoprotein, epidermal growth factor (EGF), folate, integrin-binding motifs, lactose, mannose and transferrin, are internalized via clathrin-mediated endocytosis [77].

The use of cell-penetrating peptides (CPPs) also referred to as protein transduction domains (e.g., TAT (48-60), penetratin, transportan) has also been investigated for internalization of nucleic acid

cargos [111]. It was initially suggested that these peptides can directly penetrate through the cell membrane by the localized positive charge of the peptides or formation of inverted micelles in an energy-independent mechanism (non-endocytic pathways). However, more evidence found that the major uptake mechanism of these peptides and their cargos are mediated through endocytosis pathways- primary macropinocytosis, in a non-specific manner driven by enhanced electrostatic interaction with the cell [112].

1.3.2.2 Endosomal escape

Regardless of the route of the endocytosis, the endocytosed gene complexes are trapped in endosomes, which then they are either degraded by lysosomal proteases or recycled back to the extracellular milieu through multiple pathways [113, 114]. In addition, it was reported that nanoparticles that are directly delivered into the cell cytoplasm (e.g., by microinjection) can be captured by an autophagy response (also known as 'self-eating') and are delivered to the lysosomal compartment for degradation [115]. These observations indicated that the escaped nanoparticles from single endosomal escape event can also be recaptured in endocytic vesicles, leading to entrapment in the endosomal compartment and hence limited therapeutic efficiency.

Therefore, design of gene delivery systems that can efficiently escape from endosomes and release the nucleic acid cargos into cytoplasm is crucial for high transfection efficiency. Zabner and colleagues., showed that direct injection of cationic lipoplex into the nucleus do not induce high gene expression, indicating that dissociation of DNA from cationic complex must occur before transcription [116]. Following this, a model, explaining the underlying mechanism for the release of naked DNA from the complex, was proposed by Xu and Szoka, suggesting that flip-flop of anionic phospholipids from the cytoplasmic side of the endosomal membrane to the endosomal

lumen form charge-neutralized ion-pairs with cationic lipids of lipoplex, resulting in destabilizing the endosomal membrane and displacement of pDNA from the complex into the cytoplasm [117]. The incorporation of neutral phospholipid, 1,2-dioleoyl-sn-glycero-3-phosphatidylethanolamine (DOPE), as a helper lipid in formulating cationic complexes promotes membrane fusion and endosomal destabilization by adopting inverted hexagonal (H_{II}) phase at acidic pH [118, 119]. It was shown that the addition of lysosomotropic agent chloroquine, known to elevate the pH by buffering the endosomes, resulted in inhibition of the transfection efficiency of DOPE-containing cationic complex, denoting the necessity of the acidic pH of the endosomes for the DOPE helper lipid activity [120]. Similarly, adenoviruses exploit the low pH of endosome to destabilize the endosome where the Ad penton base protein containing five RGD motifs undergoes a conformational change at pH 6, exposing its hydrophobic regions and penetrates to the endosomal membrane and escape from endo-lysosomal degradation [121-124].

Replacement of the un-saturated DOPE helper lipid with a phospholipid of the same acyl chain groups, 1,2-dioleoyl-sn-glycero-3-phosphatidylcholine (DOPC) or with a phospholipid made up of the same head group, 1,2-dipalmitoyl-sn-glycero-3-phosphatidylehanolamine (DPPE), was shown to result in low transfection efficiency [120, 125]. In addition, the inclusion of cationic lipids with long saturated tails (≥ C16:0) or with large charged head groups or bilayer-stabilizing lipids (e.g., PEGylated lipids) was reported to have inhibitory effects on intracellular delivery and thereby reducing lipoplex transfection efficiency [80, 126]. This has been observed to be the strong correlation between the transfection efficiency and the capability of the lipoplexes in inducing lamellar to nonlamellar phase transition [80]. The geometrical shape of the lipids has been used to predict the occurrence of such phases. Lipids with a cone-like geometry (i.e., headgroup surface area is larger than hydrocarbon area) self-assemble into micelles, exhibiting positive membrane

curvature, and lipids with a cylindrical geometry (i.e., headgroup and hydrocarbon surface areas are about equal) favourably adopt the bilayer phase, whereas inverted cone shaped lipids (i.e., having a headgroup area smaller than hydrocarbon domain) obtain the hexagonal H_{II} phase or inverted micelles (cubic phase), exhibiting negative membrane curvature [118, 127, 128]. The complementary mixtures of positively curved cone and negatively curved inverted cone-shaped lipids can adopt lamellar system that maybe capable of undergoing non-lamellar phases and destabilizing endosomal membrane. For example, the mixture of cone shaped DOPE, which adopts the inverted hexagonal phase in isolation at above 10°C, with cationic lipids are used to complex DNA in a bilayer structure [128, 129]. Safinya's group studied the supramolecular structures of cationic lipoplex in correlation with their transfection efficiency using synchrotron small angle X-ray scattering (SAXS) and optical microscopy [129, 130]. The SAXS scans of the self-assembled cationic lipoplex revealed either the formation of lamellar H_{α}^{C} phase where the DNA monolayers intercalated (sandwiched) between cationic bilayers, or columnar inverted hexagonal phase H_{II}^{C} structure consisting of DNA surrounded with cationic lipid monolayers arranged on a 2D hexagonal lattice [129, 130]. Optical microscopy showed that H_{II}^{C} complexes rapidly fused and released DNA upon interaction with anionic endosomal vesicles.

Cationic polyplexes such as polyethylenimine (PEI), polyamidoamine (PAMAM) dendrimers and imidazole-containing polymers, however, are suggested to exert a distinct approach known as "proton-sponge" mechanism [86, 131, 132]. This hypothesis is correlated with the buffering capacity of polymers below physiological pH. During endosomal acidification and maturation, the unprotonated amine groups (secondary or tertiary amines with pK_a values between 5.5-6) act as a sponge by absorbing protons, resulting in more influx of H^+ ions, leading to an increased influx of Cl^- counterions which causes increased osmotic pressure inside the endosomes. Consequently, the

influx of water into the endosomes causes osmotic swelling and the eventual rupture of the endosomal membrane, thus resulting in subsequent release of polyplexes in the cytoplasm [133]. For other cationic polymers such as polylysine, which contains only primary amine groups, the addition of chloroquine at the time of transfection can considerably improve their transfection efficiency by inhibiting lysosomal DNA degradation. The practicality of this approach, however, is only limited for *in vitro* gene delivery [134, 135].

The details of the escape mechanism of lipoplexes and polyplexes are still debatable as no direct evidence has supported these mechanisms [80, 135-138].

Other strategies to overcome endosomal barriers include the utilization of fusogenic viral peptides derived from viral proteins (e.g., fusogenic peptide derived from the N-terminal sequence of the influenza virus hamagglutinin subunit HA-2) or synthetic fusogenic peptides (e.g., amphipathic peptides GALA and cationic amphipathic peptide KALA) that can be either covalently or non-covalently attached to the gene delivery systems [139-142]. These peptides can undergo a conformational change at endosomal pH and adopt an α-helical structure that can interact with the endosomal membrane and result in destabilization and pore formation [143]. For example, influenza HA-2 subunit (23 mer: GLFGAIAGFIENGWEGMIDGWYG) at neutral pH forms a hydrophilic non-helical structure due to the charge repulsion arising from the negatively charged glutamic acid (E) residues (located at position 11 and 15) and aspartic acid (D) residue (at position 19) and speculated that the protonation of the acidic residues at low endosomal pH promotes transition to a hydrophobic helical conformation, hence inducing the peptide's membrane fusion and leakage activity [139, 144]. It was shown that the DNA complexes made up of polylysine as the nucleic acid packaging module, polylysine-modified transferrin as the receptor-mediated transport module and polylysine bound to HA-2 peptide, forming a simple model of an "artificial

membrane-free virus" (for example similar to adenoviruses), can enhance endosomal escape and gene expression [139, 145].

1.3.2.3 Nuclear translocation

Delivery of DNA across the double-bilayer nuclear membrane is essential to access the transcriptional machinery for subsequent transcription of their encoding transgenes in the nucleus. In quiescent or slow dividing cells with intact nuclear envelope, the nuclear uptake is considered as the rate-limiting barrier. However, this barrier is not as important in rapidly dividing cells as DNA can reach the nucleus during cell division where the breakdown of the nuclear envelope takes place [146]. To promote nuclear uptake, nuclear localization signals (NLS), which are short cationic peptide sequences, have been utilized to actively deliver DNA through the nuclear pore complex (NPC). The NPC are 125 MDa assembly of 30 different nucleoproteins that allow passive diffusion of small molecules but require active transport for macromolecules larger than ~40 kDa [146, 147]. Many proteins bearing NLS are recognized by specific proteins called karyopherins (for example importins), which mediate nuclear transport through the nuclear pore [86, 146]. Therefore, many studies have been devising various methods to promote nuclear localization. These include attachment of karyopherins to the delivery system, coupling of linear or plasmid DNA with NLS-peptides, and covalent linkage of DNA nuclear targeting sequences (DTS) to vectors [148-151]. For example. the SV40 enhancer is a DTS that is believed to contain a binding site for transcription factors bearing NLSs that allow the plasmid vector containing the SV40 DTS with NLSs to shuttle into the nucleus [151]. Cationic polyplexes may also serve as NLS to some extent, due to their positive surface charge [152, 153].

1.4 Non-viral gene delivery systems

Due to the limitations associated with the viral vectors, since the mid 1970's many types of synthetic vectors have been developed to overcome the extra- and intra-cellular barriers [68]. Some of the most common synthetic polymer-, dendrimer- and lipid-based vectors (Fig. 1.1 and Fig. 1.2) are described here.

1.4.1 Poly(L-Lysine) (PLL)

Poly(L-Lysine) (PLL) was the first cationic polymer introduced in 1987 by Wu and Wu [154, 155]. The PLL is the most widely studied cationic polymer and has been used as linear or branched in a variety of polymerizations including PLL-containing peptides [156]. In the absence of lysosomal disruption agent such as chloroquine, PLL has poor transfection activity. This is because all the primary amine groups of PLL are protonated at physiological pH, and therefore have low buffering capacity for endosomal escape [62, 68]. In addition, as the molecular weight of the cationic polymer increases, this results in increasing the net positive charge leading to tighter complexation of DNA, hence, forming more stable particles. However, increasing the length of the cationic PLL is often associated with increasing the cytotoxicity profile of the delivery complexes. PEG-grafted PLL have shown to reduce toxicity and increase circulation half-life by preventing plasma protein binding [156, 157]. The conjugation of PLL with asialoorosomucoid glycoprotein, folate, RGD peptides, and antibodies have also been investigated for targeted gene delivery [154, 158-160].

1.4.2 Polyethylenimine (PEI)

Polyethylenimine (PEI) was introduced by Behr *et al.* in 1995 [131] and similar to PLL has been widely used in linear or branched forms as gene delivery vehicles. Examples of commercially

available transfection reagents based on linear PEI include ExGen500, and jetPEI [161, 162]. The strong buffering capacity of PEI owing to the great number of primary, secondary, and tertiary amines, make PEI and its variants as potent delivery systems. Conjugation of various targeting ligands such as RGD motifs, galactose, transferrin, and specific antibodies to PEI have been explored to improve their uptake for targeted delivery [163-165]. For example, synthetic virus-like particles were developed by conjugation of RGD integrin-binding motif (i.e., CYGGRGDTP) to thiol-derivatized PEI via disulphide bridges to follow adenovirus properties such as size, centrally protected DNA core, integrin-mediated cellular uptake, and acid-triggered endosome escape [163]. One of the drawbacks of the PEI is its non-biodegradable nature, causing substantial toxicity *in vivo*. Several approaches to decrease the cytotoxicity of PEI include PEGylation, functionalization of the PEG-PEI block copolymer with targeting moieties (e.g., RGD and galactose), and conjugation with biodegradable linkers (e.g., disulphide- and ester-crosslinked PEIs) [166-169].

1.4.3 Carbohydrate-based vectors

Carbohydrate-based vectors have been investigated as gene delivery vectors for their excellent biodegradability, biocompatibility and low toxicity properties [68, 170]. Chitosan and cyclodextrins are amongst the most frequently studied carbohydrate-based gene delivery systems. Chitosan is obtained by the alkaline deacetylation of chitin, a naturally occurring polymer, and composed of β(1→4)-linked D-glucosamine (GlcN) and *N*-acetyl-D-glucosamine (GlcNAc) repeating units (Fig. 1.1) [170-172]. The transfection activity of chitosan polyplexes have been shown to be affected by several factors such as degree of deacetylation, molecular weight, the number of chitosan nitrogen atoms per DNA phosphorus atoms charge ratio, pH, and their physicochemical properties (size and zeta potential) [173, 174]. The bioadhesive and permeation-

enhancing properties of chitosan-based polyplexes, make them suitable vectors in oral and nasal gene delivery. This is due to the electrostatic interactions between the cationic chitosan with negatively charged sialic acid residues (pK_a = 2.6) on mucins, which are highly hydrated glycoprotein constituents of mucus and primarily responsible for viscoelastic properties of mucus [175-179]. However, their applications for *in vivo* gene delivery are limited due to several drawbacks that include low solubility at physiological pH and low transfection activity [180]. To enhance their solubility and improve colloidal stability of the chitosan polyplexes for prolonged circulation time, chemical modification of chitosan has been investigated by quaternization of the D-glucosamine or grafting certain polymers such as PEG and dextran to chitosan [172, 181]. Targeted gene delivery of chitosan-based polyplexes has also been achieved by grafting cellular targeting ligands on chitosan (e.g., galactose for targeted delivery to liver cells, folate for pulmonary tumor targeting) [182, 183]. Moreover, functional groups such as histidine, imidazole, urocanic acid or PEI were coupled to chitosan to confer proton sponge capacity, thus facilitating their endosomal escape and increasing their transfection activity [184-189].

Cyclodextrins (CDs) are naturally occurring cyclic $\alpha(1\rightarrow4)$-linked oligosaccharides of D-glucopyranose units [190]. CDs possess a basket-shaped topology with a hydrophilic cavity exterior and an inner hydrophobic cavity, which allows inclusion and solubilisation of hydrophobic "guest" molecules [170, 190]. The most common CDs are α-, β- and γ-CDs, which are comprised of 6, 7, and 8 D-glucopyranose units, respectively [190]. CDs with abundant hydroxyl groups are soluble in water and can also be easily functionalized with multiple targeting ligands. While the transfection efficiency of native CDs is much lower compared with conventional polymeric vectors, such as chitosan, PEI and PLL (that is perhaps due to their poor capability to form stable complexes with pDNA), CDs have been exploited as a central dendritic core for coupling of

various functional groups, as linking agents for development of larger gene delivery constructs, or as structural modifier to modulate the performance of existing gene delivery vectors [170, 190]. Other carbohydrate-based vectors used as gene delivery vectors include dextran, arabinogalactan, hyaluronan, alginate, pullulan, pectin, and schizophyllan [191-197].

1.4.4 Dendrimer-based vectors

Dendrimers are hyperbranched macromolecules with three-dimensional well-defined architectures constructed using both divergent and convergent methods [198-200]. A few examples of dendrimers used in gene delivery include polyamidoamine (PAMAM) dendrimer, poly(propylenimine) (PPI) dendrimer, triazine dendrimer, carbosilane dendrimer, phosphorus dendrimer, and PLL dendrimer [201-208]. Superfect and PolyFect are the two commercially available transfection reagents prepared using activated PAMAM dendrimer technology [209]. Dendrimers can efficiently condense nucleic acids by electrostatic interactions, protect them from enzymatic degradation, and promote their cellular uptake and endosomal escape. The primary amine groups at the periphery of dendrimers bind to and compact nucleic acids, while the high density of tertiary amines within the interior of dendrimers function as an endosomal pH buffer, hence enhancing intracellular delivery of nucleic acids [198, 210]. The transfection activity of dendrimers is dependent on the dendrimer generation (i.e., number of repeated branching cycles during dendrimer synthesis) [169]. However, the increased transfection efficiency of high generation dendrimers is often accompanied with serious cytotoxicity. Therefore, to improve transfection activity and lower cytotoxicity, surface modification of dendrimers with various functional ligands such as lipids, sugars, peptides and proteins have been explored [211-217].

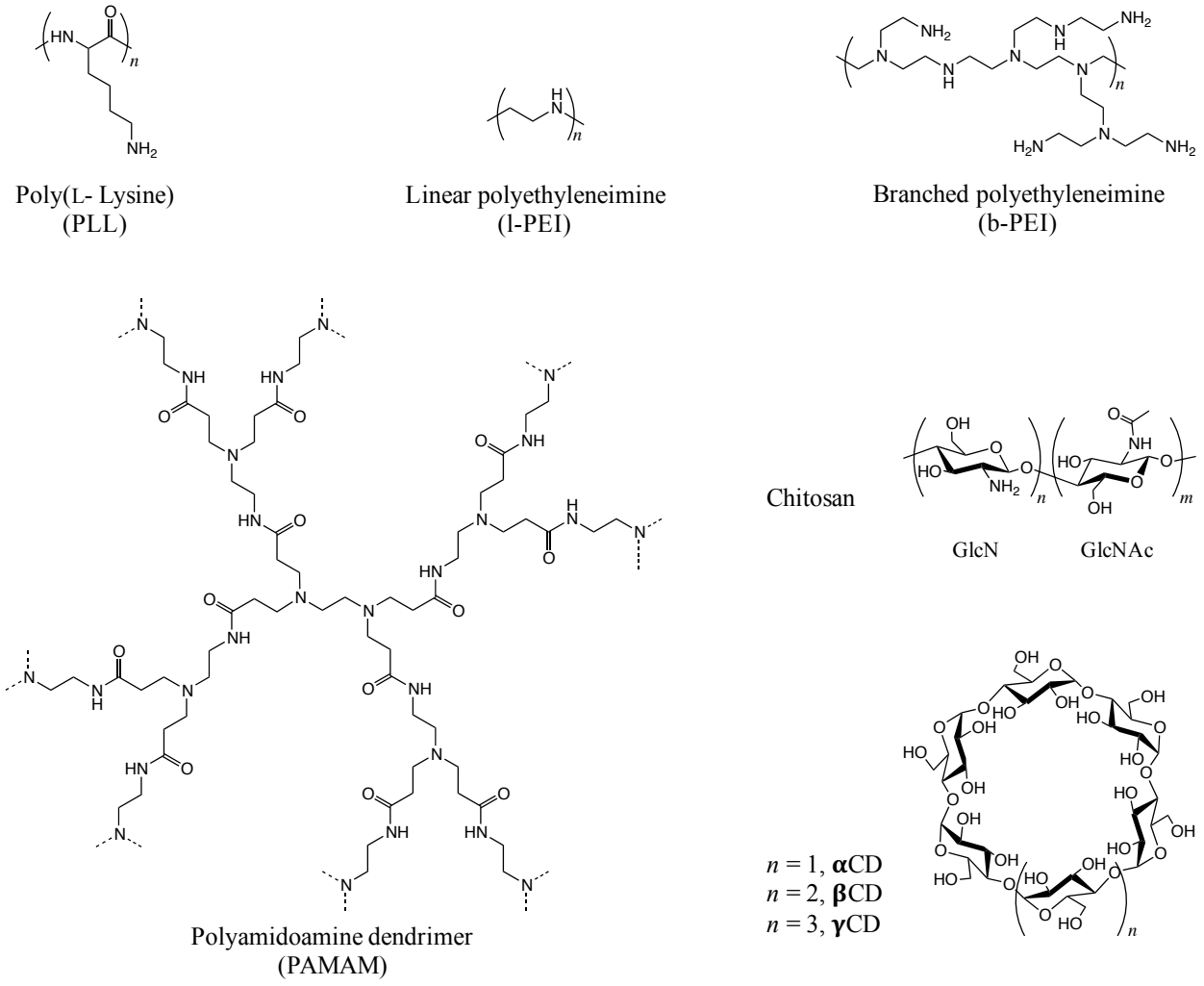

Fig. 1.1. Chemical structures of selected cationic polymers used for non-viral gene delivery.

1.4.5 Polypeptides

Polypeptides hold great promise in the field of gene therapy owing to their inherent biocompatibility, biodegradability, and bioactivity. The diversity of polypeptides confers peptide-based gene delivery systems with various functions such as DNA condensation and protection, cell targeting, cell penetrating, endosomal escape capacity, cellular trafficking of DNA and nuclear localization [142, 143, 218].

Neurotensin, LHRH, Tf, RGD, trastuzumab are a few examples of targeted peptides used for targeted gene delivery [139, 219-223]. Table 1.1 also lists the most important functional peptides that have been used in gene delivery systems. These peptides can be readily synthesized using solid phase peptide synthesis methods and can be used as a single peptide sequence or in combination by covalent conjugation of different functional peptides to a single multifunctional molecule [142, 224].

Table 1.1. Cell penetrating peptides (CPP_s), endosomolytic peptides, and nuclear localization signal (NLS) peptides used for gene delivery.

Function	Name	Sequence	Reference
CPPs	TAT (48-60)	GRKKRRQRRRPPQ	[225]
	Penetratin	RQIKIWFQNRRMKWKK	[226]
	Transportan	GWTLNSAGYLLGKINLKALAALAKKIL	[227]
	VP22	NAKTRRHERRRKLAIER	[228, 229]
	MAP	KLALKLALKALKAALKLA	[230]
	Pep-1	KETWWETWWTEWSQPKKKRKV	[231]
	Polyarginine	$(R)_9$	[232]
Endosomolytic	GALA	WEAALAEALAEALAEHLAEALAEALEALAA	[140]
	KALA	WEAKLAKALAKALAKHLAKALAKALKACEA	[233]
	JST-1	GLFEALLELLESLWELLLEA	[234]
	ppTG1	GLFKALLKLLKSLWKLLLKA	[235]
	ppTG20	GLFRALLRLLRSLWRLLLRA	[235]
	His-rich peptides	HHHHHWYG	[236]
	His-rich peptides	CHKKKKKKHC	[237]
NLS	SV40 T antigen	PKKKRKV	[238]
	Nucleoplasmin	KRPAATKKAGQAKKKK	[239]
	PARP	KRKGDEVDGVDECAKKSKK	[240]
	M9	YTAIAWVKAFIRKLRK	[241]

1.4.6 Cationic lipids

Over the past three decades, various cationic lipid-based gene delivery systems have been developed. These complexes mimic natural viruses where the synthetic carriers transfer gene across cell membranes and resulted in expression of exogenous DNA [130]. Cationic lipids are constructed from hydrophilic head group connected to hydrophobic hydrocarbon tails (often two alkyl tails with 12-18 carbons in length) via a linker group. In aqueous environment, most cationic lipids in combination with neutral helper lipids such as DOPE or cholesterol are self-assembled into closed lipid bilayer membrane shells (liposomes) in an entropically favorable manner [242, 243].

It was first demonstrated in 1980 that liposomes composed of natural anionic phosphatidylserine were capable of encapsulating and delivering Simian virus 40 (SV40) DNA into cells [244]. In 1987, the first synthetic cationic lipid, *N*-[1-(2,3-dioleyloxy)propyl-*N,N,N*-trimethylammonium chloride (DOTMA), was produced by Felgner *et al.* [245]. It was shown that cationic small unilamellar liposomes containing DOTMA could interact spontaneously with DNA and more efficiently encapsulate DNA (100% entrapment) than conventional liposomes (less than 10% entrapment). In addition, cationic DOTMA in combination with DOPE, in a 1:1 (wt/wt) ratio, could form small cationic liposome that could efficiently transfect various mammalian cell lines [245]. Since then, many commercially available cationic lipid reagents were developed, including dioctadecylamidoglycylspermine (DOGS; TRANSFECTAM^{TM}) [246]; 1,2-dioleoyloxy-3-trimethylammonium-propane (DOTAP) [247, 248], 3β-[*N-(N″,N″*-dimethylaminoethane)-carbomoyl]cholestrol (DC-Chol) [249], 2,3-dioleyloxy-*N*-[2(sperminecarboxamido)-ethyl]-*N,N*-dimethyl-l-propanaminium trifluoroacetate (DOSPA; Lipofectamine) [250] (Fig. 1.2).

DOTMA (Lipofectin)

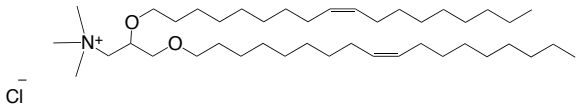

DOTAP

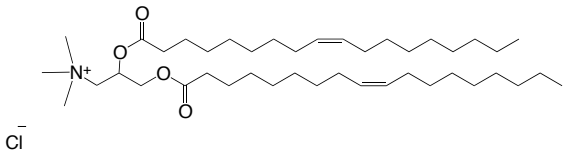

DOGS (Transfectam)

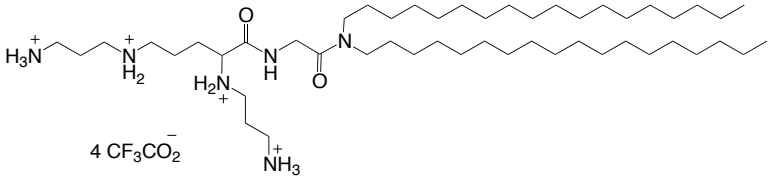

DOSPA (Lipofecamine)

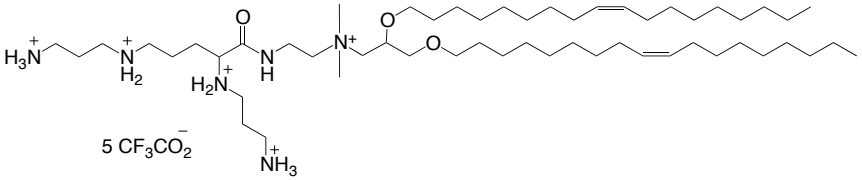

DC-Chol

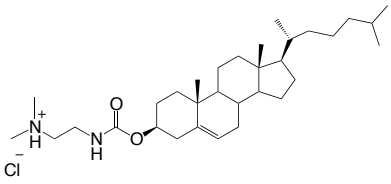

DOPE

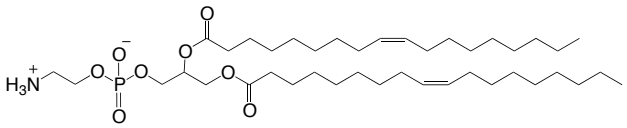

DPPC

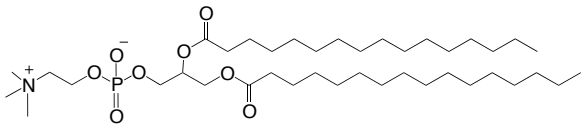

Fig. 1.2. Chemical structures of cationic lipids (DOTMA, DOTAP, DOGS, DOSPA and DC-Chol) and neutral helper lipids (DOPE, DPPC).

The addition of polycations such as poly(L-Lysine), histone, and protamine into cationic liposomes (Lipofectamine, DC-Chol, Lipofectin) containing nucleic acids have been shown to considerably reduce the particle size of the complexes, improve DNA stability against nuclease activity, and significantly enhance the level of gene expression [251, 252]. These ternary complexes which are formed by non-covalent interactions (electrostatic interactions and hydrophobic effects) are denoted as lipopolyplexes.

In attempt to construct integrin-mediated gene delivery, lipofectin (DOTMA/DOPE) (L) was incorporated into integrin-targeting peptide/DNA (ID) complex to form LID vector [253, 254]. It was demonstrated that the peptide-based lipopolyplex increased luciferase expression by more than 100-fold and was capable to efficiently transfect several cell types *in vitro* [253, 254]. Colin *et al.* examined transfection efficiency of lipofectamine/$[K]_{16}$RGD/DNA in tracheal cell line. The ternary complex increased the transfection about three orders of magnitude as compared with the $[K]_{16}$RGD/DNA and about 6-fold higher than that of lipofectamine/$[K]_{16}$/DNA [255]. Jenkins *et al.* reported that intratracheal delivery of LID vector formulated by complexation of Lipofectin, integrin targeting peptide (K16-GACRRETAWACG) specific to $\alpha_5\beta_1$ integrin and pCI-Luc plasmid DNA in water resulted in 10-fold increase in luciferase activity in comparison to that prepared in phosphate-buffered saline (PBS) [256]. Kudsiova *et al.* investigated the transfection efficiencies of lipid/DNA (LD) lipoplexes and lipid/peptide/DNA (LPD) lipopolyplexes in relation to alteration of the alkyl chain geometry of cationic lipids using novel C14-DOTMA analogues (containing *cis*- or *trans*-double bonds at positions Δ9 or Δ11 or an alkyne at position C9; Fig. 1.3) in MDA-MB-231 breast cancer cell line [257, 258]. It was shown that lipoplexes incorporating *trans*-lipids (co-formulated with DOPE and using gWiz-luc plasmid) at lipid: pDNA weight ratio of 4:1 had higher transfection efficiency than those with *cis*-lipids or alkyne lipids, and among

trans isomers, lipoplexes formulated with *E*-Δ11 was more efficient than *E*-Δ9. In addition, lipoplexes formulated with alkyne lipids at lipid: pDNA weight ratio of 4:1 or 16:1 were more efficient than that of with *cis*-lipids, and at 16:1 lipid: pDNA weight ratio was comparable to the luciferase expression in cells transfected with *E*-Δ9 lipids-formulated lipoplexes prepared at the 4:1 lipid: pDNA weight ratio [257]. While there was no clear explanation to justify the direct correlation between the geometry of the cationic lipids and their correlated transfection efficiency, it was hypothesized that *E*-lipids presumably occupy a smaller area per molecule than the *Z*-lipids or alkyne lipids, resulting in more efficient complexation and thus higher transfection efficiency. The transfection study of the LPD lipopolyplexes, however, suggested superiority of the *cis*-lipids in LPD formulations. The *Z*-lipids (*cis*-lipids) pack less tightly due to the significantly larger area per molecule than the *E*-lipids with *trans* double bonds in their alkyl chains. As a consequence, bilayers formed by *Z*-lipids are more fluid and permeable than those containing *E*-lipids. This therefore, was hypothesized, to allow more of the integrin targeting sequence to protrude through the lipid bilayer from the central core of the tightly bound cationic peptide-DNA complex, and leading to better targeting and transfection activity [258]. This proposed structure was in alignment with the previous work performed by Mustapa *et al.* who studied the structure of the ternary LID complex (prepared from Lipofectin (1:1 DOTMA:DOPE), a bi-functional cationic, targeting peptide component, and pDNA) using fluorescence quenching experiments and freeze-fracture electron microscopy [259]. These experiments concluded that the cationic portion of the peptide (polylysine domain- K16) interacts with pDNA and forms a condensed DNA-peptide inner core surrounded by an irregular lipid layer, from which the targeting moiety of the peptide partially protrudes (Fig. 1.4). Freeze-fracture electron microscopy of LID and LK16D lipopolyplexes displayed a soft outer-shell/hard inner core morphology (Fig. 1.5). Similar structures were also

observed by Tagawa *et al.* in formulating LMD virus-like nanoparticles self-assembled from cationic liposomes (DC-Chol/DOPE), adenovirus core peptide μ (mu) and pDNA [260]. The cryo-electron microscopy of LMD particles (prepared at 12:0.6:1 lipid:mu:DNA w/w/w ratio), however, revealed encapsulation of the MD core within a DC-Chol/DOPE cationic bilammellar liposome, described as a double-walled virus-like nanoparticle (VNP) with the particle size of 120 ± 30 nm [260].

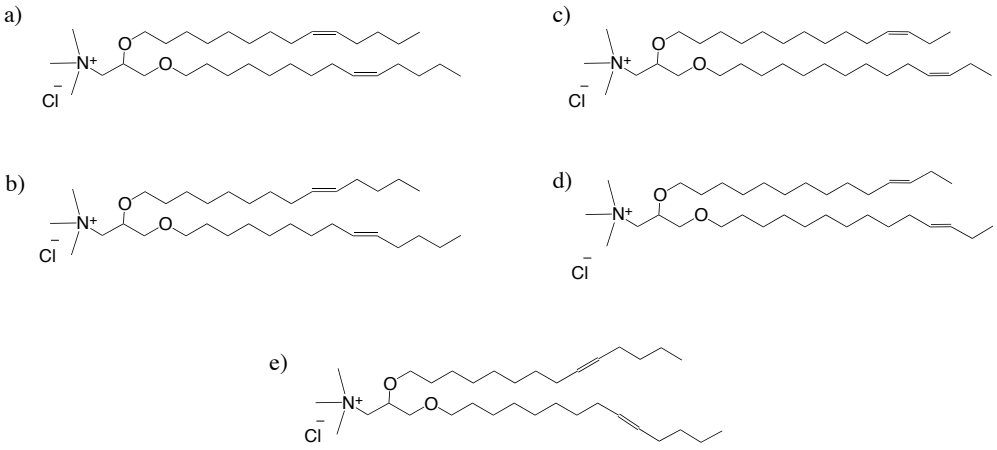

Fig. 1.3. The structures of C14 analogue of DOTMA containing cis- or trans-double bonds at positions C9 or C11 (*Z*-Δ9 (a), *E*-Δ9 (b), *Z*-Δ11 (c), *E*-Δ11 (d)) or triple bonds at position C9 (e) in their alkyl chains, depicted from reference [258].

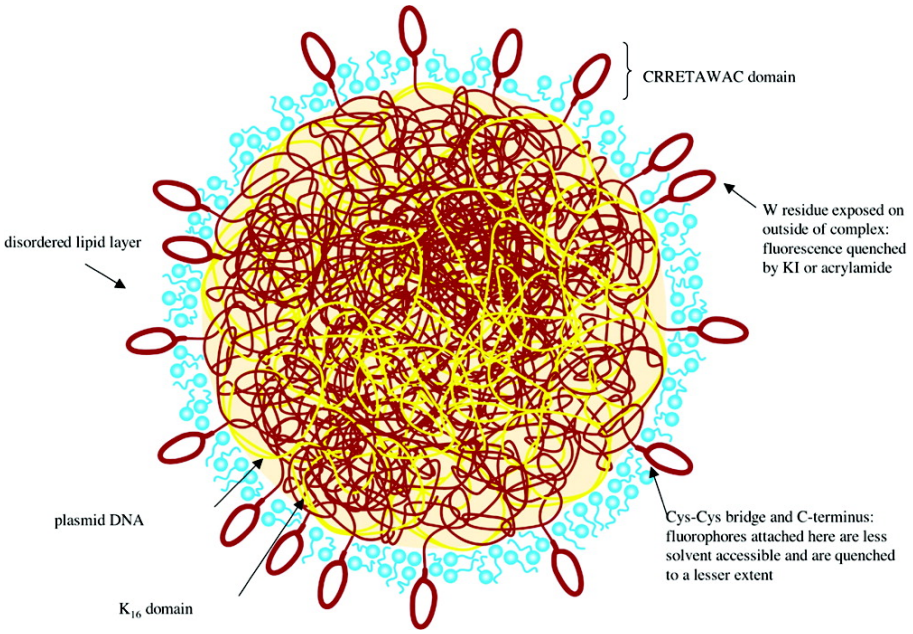

Fig. 1.4. A model for the molecular organization of the LID lipopolyplex. Adapted with permission from [259]. Copyright (2007) American Chemical Society.

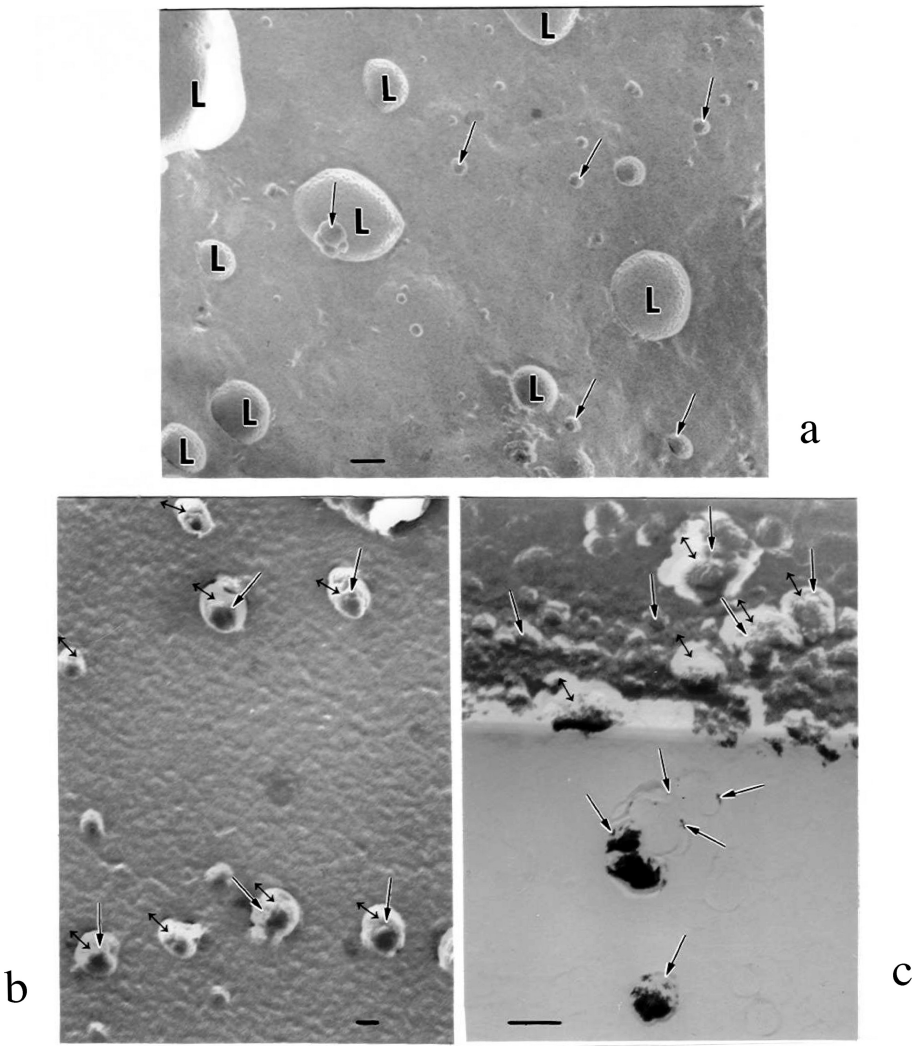

Fig. 1.5. Freeze-fracture electron micrographs of LID lipopolyplexes (a) and LK16D (b, c) displaying particles having a “hard” inner core with an irregular “soft” outer shell. Adapted with permission from [259]. Copyright (2007) American Chemical Society.

1.4.7 Gemini surfactants

In addition to the cationic congeners of classical glycerophospholipids and cholesterol derivatives presented above, a novel class of cationic dimeric surfactants, known as gemini surfactants, have been investigated for gene delivery application [261-263]. In 1991, the name "gemini surfactants" was assigned by Menger to a family of synthetic amphiphilic molecules consisting of two head groups and two aliphatic chains that are linked at the level or close to the head group by a rigid spacer group (e.g., a benzene or stilbene unit) [264]. Since then, the term has been broadened to include all dimeric surfactants with rigid or flexible (e.g., a hydrocarbon chain) spacer region, those contain multiple heads and multiple tails whether they are symmetrical or asymmetrical, and even those surfactants studied preceding Mengers's work [265-270]. Gemini surfactants provide high levels of interfacial activity and promote self-assembly at concentrations about hundredfold lower as compared to the monomeric surfactants [271-273]. The synergistic behaviour observed for gemini surfactants impart with the structural flexibility in their design make them of special interest for development of non-viral vectors for gene therapy [274].

Gemini surfactants can be categorized based on their functionalities such as ammonium-, pyridinium-, carbohydrate-, cholesterol-based and disulfide-containing gemini surfactants [263, 275].

The propensity of the surfactant to self-assemble in water can be quantitatively measured by determining the critical micelle concentration (CMC), which is defined as the concentration above which monomeric surfactants self-assemble into supramolecular aggregates. Therefore, the lower the CMC the higher the tendency of surfactants is to self-assemble in water. The solution properties of *N,N*-bis(dimethylalkyl)-α,ω-alkanediammonium, also called m-s-m gemini surfactant (where m and s refer to number of carbon atoms of the alkyl tail and spacer groups, respectively) has been

well studied [263]. The CMC value of simple surfactants is associated with their structural parameters such as the length of the alkyl tail, the size and charge of the polar head and of the counterions. In gemini surfactants, the linker connecting the monomeric surfactant structural units limits their individual mobility and thus the increased hydrophobic forces lower the CMC of gemini surfactants as compared with corresponding monomeric surfactants of equivalent chain length, polar head and counterion [265]. For example, the CMC of 12-3-12 gemini surfactant, $[C_{12}H_{25}N^{+}(CH_3)_2\text{-}(CH_2)_3\text{-}N^{+}(CH_3)_2C_{12}H_{25}]\ 2Br^{-}$, was found to be approximately 1 mM, which is 16 times lower than the CMC value of dodecyltrimethylammonium bromide (DTAB; CMC: 16 mM), $[C_{12}H_{25}N^{+}(CH_3)_3]\ Br^{-}$ [271, 273, 276]. While increasing the alkyl tail length of gemini surfactants linearly decreases the CMC value, the effect of variation in length and polarity of short spacer groups (2-8 atoms) on CMC values are not prominent. A longer hydrocarbon spacer (s >10), however, was found to reduce the CMC value due to the folding of the spacer and thus bringing the quaternary ammonium head groups in closer proximity, thus increasing the overall hydrophobicity of the gemini surfactant and resulting in an enhanced tendency to self-assemble ([263, 265, 277].

The morphology of the supramolecular assemblies formed by gemini surfactants can be determined by various techniques such as light scattering, cryo-transmission electron microscopy (cryo-TEM) and small angle neutron scattering (SANS) methods. Gemini surfactants in aqueous solution can form a variety of shape ranging from spherical to thread-like micelles, rod-like, disk-like micelles and lamellar shapes [278, 279]. For example, 12-s-12 gemini surfactants with short spacer (s = 2,3) tend to form threadlike micelles and as the length of the spacer increases they form spherical micelles (for medium length, s = 5-12) and vesicles (for very like spacer region, s = 16) [278].

Many factors such as concentration, temperature and ionic strength of the solution can impact the morphology of the aggregates [279]. For example, at low concentration, 12-2-12 gemini surfactants form spherical micelles and by increasing concentration, their morphologies change to elongated micelles and grow both in length and number [280].

The morphology of the aggregates can be predicted by surfactant structure using the surfactant packing parameter "*P*", a method introduced by Israelachvili *et al.* (Fig. 1.6).

$$P = \frac{v}{a_\circ l_c}$$

where v is the surfactant alkyl tail volume, l_c is the alkyl tail length and $a_\circ$ is the surface area occupied by the head-group at the aggregate interface. For example, surfactants with large head group areas have $P < 1/3$, forming into spherical micelles, whereas $P = 1$ indicates planar bilayer formation, and small polar heads $P > 1$ form inverted micellar phases (inverted hexagonal (H_{II}) structures).

As discussed earlier, lipoplexes that are capable to induce transition from lamellar (L_α^C) to inverted hexagonal (H_{II}^C) structures are more transfection-efficient than those remaining their lamellar structures. Since, most cationic lipids including gemini surfactants have $P < 1$, they are mixed with non-aggregate forming helper lipids ($P > 1$) such as DOPE and cholesterol in certain proportions in order to induce an average P around 1 or over 1. The addition of helper lipids also reduces the electrostatic repulsions between cationic head groups and strengthens the hydrophobic forces, allowing lipids to pack together and forming a stable lipoplex [281, 282].

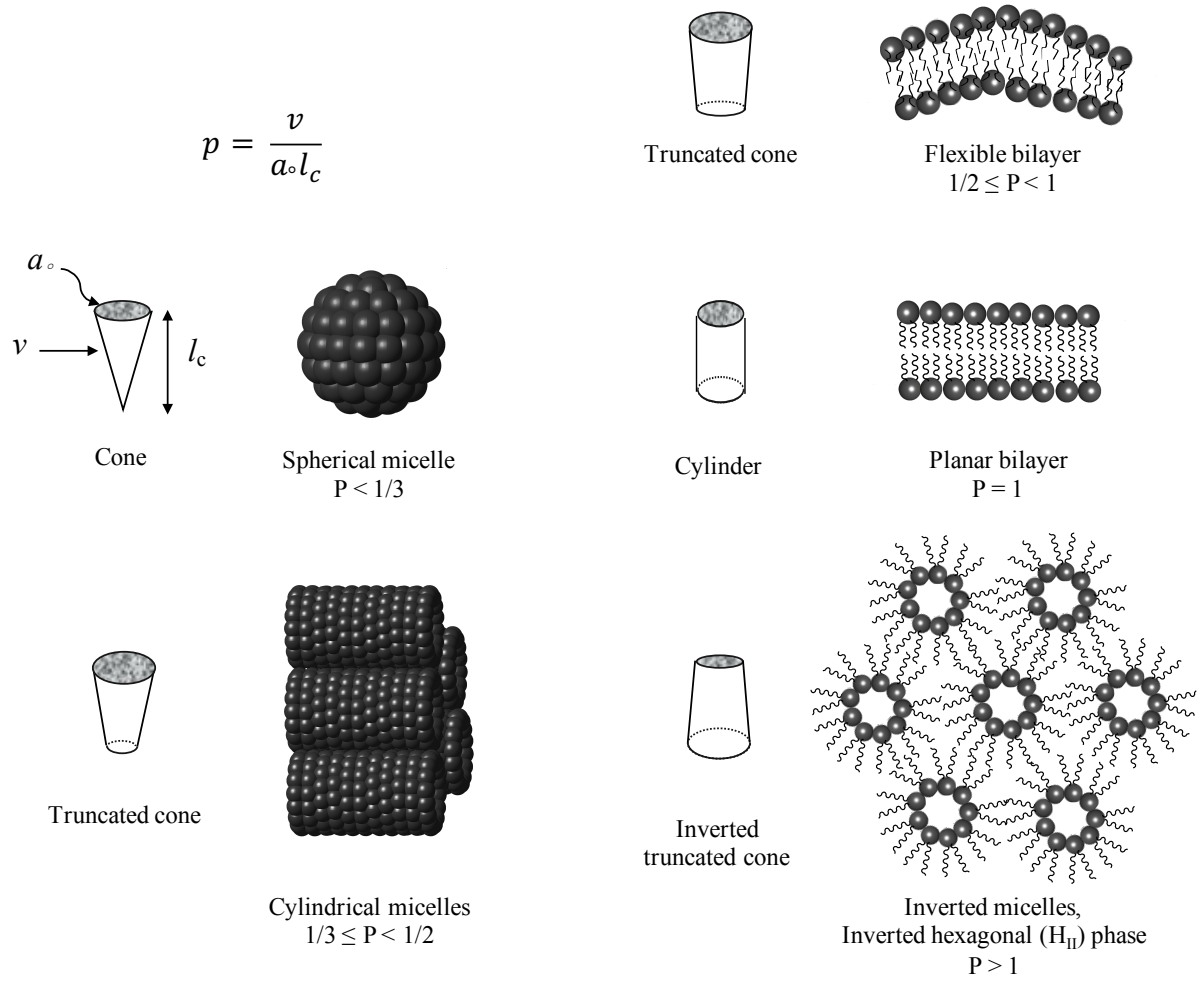

Fig. 1.6. The packing parameter "*P*" of surfactants with various molecular geometries and the predicted morphologies of the supramolecular assemblies formed by surfactant structure [243, 281, 282].

1.4.7.1 Transfection using gemini surfactants

Rosenzweig *et al.* demonstrated the use of ammonium-based gemini surfactants made up of saturated C16 or unsaturated alkyl tails C18:1 with various length spacer groups (2, 3 and 6 methylene units) to transfect BHK cells with pCMV-*β*-gal plasmid [283]. It was shown that unsaturated surfactant with 6 methylene spacer group exhibited highest transfection activity. In

addition, the incorporation of DOPE as a helper lipid resulted in reduction of the transfection efficiency. Badea *et al*. investigated series of gemini surfactants (alkyl tail = 12 or 16; spacer length = 2-16) formulated with/without DOPE helper lipid for delivery of the pGTmCMV.IFN-GFP plasmid in PAM 212 keratinocyte at various gemini/plasmid charge ratios (5:1; 10:1; 20:1; 40:1) [284]. The maximum expression of IFNγ was observed for the pDNA/16-3-16/DOPE (P/G/L) complex at 10:1 gemini/plasmid charge ratio, whereas cells transfected with 12-n-12 gemini surfactants in the absence of DOPE showed no IFNγ detection [284]. Replacement of one C16 chain of gemini surfactant with a phyntanyl moiety (dissymmetric phytanyl-gemini surfactant; phy-3-16) increased the transfection efficiency as compared to 16-3-16 in OVAR-3 cells using pVGtekRL plasmid encoding green fluorescent protein (GFP) [285]. Following a study examining DNA condensation using polyamine-DNA complexes and the effect of spacing between amine groups for DNA transfection, a series of aza- ($N\text{-}CH_3$) and imino (N-H) substituted gemini surfactants were designed to increase the transfection efficiency of gemini surfactants [286-288]. It was shown that 12-7N-12 and 12-7NH-12 gemini surfactants, both with a three-methylene unit separation between adjacent nitrogen centers, increased transfection as compared with the gemini surfactants with a two-methylene unit separation (12-5N-12 and 12-8N-12) [288]. In addition, the higher transfection efficiency of imino-substituted 12-7NH-12 gemini surfactant than aza-substituted 12-7N-12 was hypothesized to be associated with the pH-sensitive imino-group that facilitate membrane fusion and release of DNA upon cellular uptake [288]. The variations in alkyl tail length of m-7NH-m gemini surfactants (m = 12, 16, 18, 18:1) were investigated for keratinocyte transfection at various gemini/plasmid charge ratios ($\rho_{\pm}$ = 0.5:1; 1:1; 2.5:1; 5:1; 10:1) (Fig. 1.7). It was demonstrated that the transfection efficiencies increased by increasing alkyl tail length (18 > 16 > 12) and were highest in cells transfected using pDNA/gemini/DOPE complexes

with $\rho_{\pm}$ = 10 [289]. The unsaturated 18:1-7NH-18:1 resulted in lower transfection efficiency as compared with 18-7NH-18 and the reason behind this was suggested to be due to oxidation of the double bond during either complex preparation or storage [289]. Upon further investigation, it was shown that the attachment of a glycine moiety on 12-7NH-12 gemini surfactant resulted in higher gene expression in COS-7, PAM212 and SF 1EP cells [290]. Recently, Cardoso *et al.* investigated the transfection efficiency of series of serine-derived gemini surfactants (with varying alkyl chain lengths and linker groups (amine, amide and ester) connecting the spacer region to the head groups) formulated with DOPE and cholesterol for delivery of pEGFP-C1 plasmid DNA encoding GFP at gemini/plasmid charge ratios ranging from 1:1 to 8:1 in HeLa cells (human epithelial cervical carcinoma cell line) [291]. The flow cytometry result analysis showed that the percentage of the transfected cells was highest for gemini surfactants with C12 alkyl tails at the lowest charge ratios (1:1-2:1) and interestingly C14 and C16 alkyl tails had highest percentage of transfection with their highest charge ratios (8:1) (C14 > C16) whereas the transfection efficiency of C18 at 2:1 was higher than that of the highest of C14 and C16 counterparts. Therefore, no clear trend can be concluded in relation to the variation of the chain lengths and the charge ratios associated with their transfection efficiency.

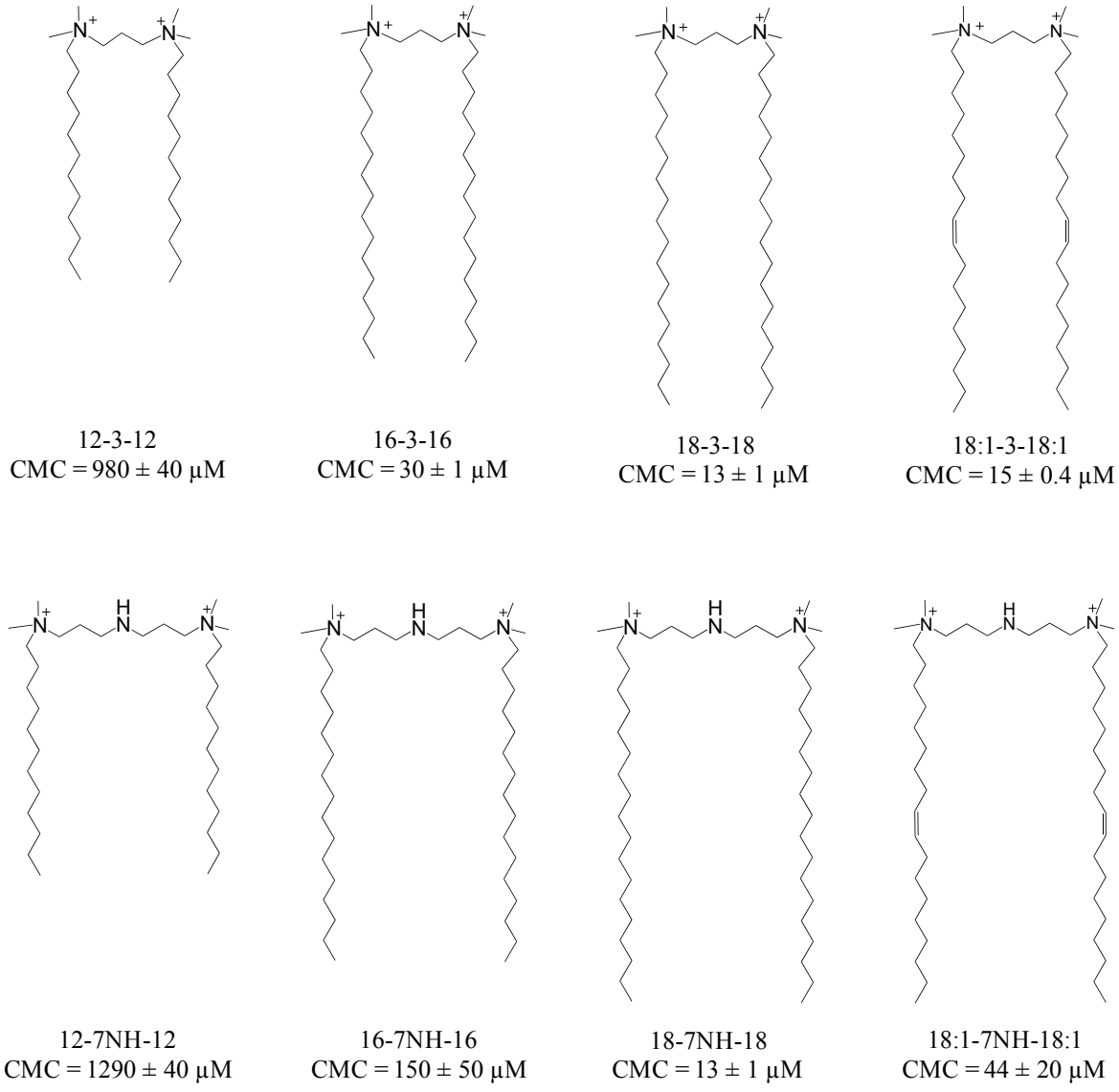

Fig. 1.7. The CMC values of m-3-m and m-7NH-m gemini surfactants obtained from [273, 287, 289, 292].

Sharma et al. studied the effect of pyridinium-based gemini surfactant formulated with DOPE (at 1:2 molar ratio) carrying gWiz-Luc plasmid DNA at a +/– charge ratio 3:1 in correlation with the variation in chain length and the nature of the counterion in NCI-H23 lung cancer cell line [293]. It was demonstrated that the transfection efficiency increased by increasing the chain length, which is in parallel with the decrease in size of lipoplexes. The transfection efficiency showed maximum by chloride counterion (borderline chaotropic/kosmotropic; localized in between the Stern layer and the diffuse layer) as compared with chaotropic (PF_6^- and Br^-, large ions and poorly hydrated; strongly bound to the ionic surface of supramolecular aggregates) and kosmotropic ($H_2PO_4^-$, small ions and well- hydrated; loosely associated with the ionic surface of supramolecular structures) counterions [293, 294]. This was suggested to be due to the chloride counterion contribution to promote aggregation while being loose enough to dissociate upon compaction of DNA. The complexity of this behaviour was revealed where the kosmotropic dihydrogenophosphate resulted in formation of smaller lipoplexes with slightly higher zeta potential than that of chloride counterion.

Bajaj *et al.* synthesized various cholesterol-based gemini surfactants, which differ in the length of the spacer chain (s = 3, 4, 5, 6, 12), and investigated their transfection efficiency in the presence of DOPE helper lipid carrying pEGFP-c3 plasmid DNA by both the number of the transfected cells and the mean fluorescence intensities (MFI) for revealing the level of GFP expression in GFP-positive cells using flow cytometry [295]. All the cholesterol-based gemini surfactants/DOPE showed significantly higher gene transfection activity as compared to their monomeric lipid counterparts. In addition, at 0.5:1 +/– charge ratio, it was found that the cholesterol-based gemini surfactant with pentamethylene spacer region (at 1:4 gemini/DOPE mole

ratio) had the highest transfection efficiency, although the number of transfected cells was found to be less [295].

Zuber *et al.* used disulfide-containing gemini surfactants (formed by dimerization of the tetradecylamide of ornithyl-cysteine; $(C14CO)_2$) co-formulated with DOPE and cyclic RGDfK-grafted lipid (f = D-phenylalanine) for formation of virus-like particles containing pEGFPLuc plasmid to transfect HUVEC and KB cell lines [296]. The result showed the poor transfection efficiency of the virus-like particles compared to PEI/DNA complexes; however, the addition of chloroquine resulted in a further increase of luciferase gene expression [296].

To create virus-like nanoparticles by turning lipoplexes into artificial viruses that mimic virus properties, the system requires a centrally protected DNA core, receptor-mediated uptake, and the ability to undergo structural changes in response to cellular environment in order to trigger endosomal escape. The transfection activity of the system can be quantitatively measured by both the number of cells transfected and the MFI. The transfection percentage and MFI are both imperative factors that indicate the transfection activity of a given gene delivery vector. While the transfection percentage can provide information on the internalization potency of a delivery vector (i.e., indicator of transfection efficiency), the MFI can give insight on the effectiveness of the delivery system for intracellular delivery of the pDNA for successful expression level of the reporter protein (i.e., indicator of transfection efficacy). Therefore, a potent gene delivery system with high transfection activity requires to have both high transfection efficiency and high transfection efficacy.

Chapter 2

Hypothesis and Objectives

2.1 Rationale

Delivery of therapeutic genes to diseased tissues is challenging and highly sought after in the field of therapeutic research. Cellular uptake and effective endosomal escape are the important aspects for *in vivo* application of gene therapy. Non-specific cellular uptake has been attempted by incorporating various alkyl chain lengths into the delivery system, using hydrophobic amino acids, or using cell penetrating peptides to enhance the penetration of nanocarriers across cellular membranes [68]. The quaternizing amine group has frequently been used for increasing the cationic charge density for a given vector and typically reported to improve their transfection efficiency. Promoting endosomal release has been investigated by incorporating various macromolecules bearing unprotonated amine groups with low pK_a values to stage endosomal escape due to so-called "proton sponge" effect [68, 297]. Polyethylenimine (PEI), histidine or imidazole containing polymers, peptides, and lipids are a few examples of such systems [298, 299]. While the increasing charge density of delivery systems may be effective in enhancing cellular uptake and possibly endosomal rupture, cellular toxicity is another challenge when developing a gene delivery system. Histidine or guanidine functional groups have been shown to lower cellular toxicity due to better distribution of positive charges. The guanidine head group of arginine has also been considered to more effectively improve internalization by forming hydrogen bonds with the negatively charged phosphate and sulfates of cell surface membranes as compared to lysine with the same positive charges [112]. Cysteine residues containing thiol groups have been used to improve colloidal stabilization and transfection efficiency through reducible interpeptide

disulfide bonds, therefore forming cross-linked complexes with DNA [300]. Peptide ligands such as transferrin, epidermal growth factor, antibodies and cell adhesion molecules have been grafted to various delivery systems to target cellular uptake in a site-specific manner [301, 302]. The covalently grafting of linear RGD derivatives (GRGDSP) to dioleyl lipid tails via PEG2000 was performed to target genes for integrin-mediated internalization [303]. RGD (arginine-glycine-aspartic acid) peptidomimetics bind to integrin receptors on melanoma, fibroblasts and epithelial cells and have broad application to target drugs and genes to specific cells as well as diagnostic and tissue engineering [122, 301, 304]. Peptide-based lipopolyplexes, which prepared by pre-complexing pDNA with cationic peptides rich in basic amino acid residues (e.g., arginine, lysine or histidine) or with bi-functional receptor-targeting, cationic peptides, and further combining with classical cationic liposomes (i.e., containing DOTMA, or DOTAP or cholesterol derivatives) have been shown to have improved site-specific targeting and enhanced transfection properties [76, 141, 253, 305-307].

Cationic gemini surfactant-based lipoplexes formulated with neutral helper lipids, such as DOPE and DPPC, have been widely used as non-viral gene delivery systems [261, 308]. Through functionalization of the spacer group and the alteration of alkyl chain lengths of gemini surfactants, the development of new compounds can potentially enhance the transfection efficiency and safety profile of gene delivery vectors.

The main focus of this project is to: 1- design and synthesize novel gemini surfactants with various functional headgroups such as imidazole- and thiol-containing functional groups, linear RGD derivatives, polyhistidine derivatives, bi-functional RGD-polyhistidine peptide, zwitterionic and cationic arginine-rich peptide motifs, 2- design several peptide enhancers that include zwitterionic RGD peptide enhancer, DNA-binding cationic peptide enhancers rich in histidine and/or arginine,

and bifunctional cationic, RGD peptide enhancers, 3- systematically optimize lipoplex delivery systems incorporating gemini surfactants of varying alkyl chain lengths, spacer groups and functional headgroups with the aim to provide a clear pattern correlating the physicochemical properties of delivery systems to their transfection efficiency, 4- investigate the impact of the designed peptide enhancers for development of gene delivery formulations containing peptide enhancers and/or gemini surfactants and/or DOPE helper lipids and evaluate the impact of the compositional elements on transfection properties and cell viability, 5- explore the impact of the headgroups of gemini surfactants by systematic variation of the functional moieties in conjunction with alteration of their alkyl chain lengths to elucidate the biophysical mechanism of the formulated lipopolyplex delivery systems.

2.2 Hypothesis

It is hypothesized that development of multifunctional, multicomponent gene delivery systems that contain 1- cationic peptide enhancers that interact and protect DNA at the core of the delivery systems, 2- targeting peptides at the surface of the nanoparticles that bind to cell surface receptors and mediate endocytosis, 3- a lipid shell that can fuse with the endosomal lipid membrane, leading to the cytoplasmic release of DNA- representing synthetic virus-like nanoparticles similar to "envelope-type viruses", will be a potent alternative to viral gene delivery vectors. The success of the *in vitro* gene transfer will provide a potent platform for designing and developing of its kind for targeted *in vivo* non-viral gene therapy.

2.3 Objectives

The objectives of this project are explained as follows:

1. Design, synthesis and characterization of 11 novel R-functionalized gemini surfactants (G**4**-G**14**) with 10 different functional moieties (m-7NR-m; m = 12, 18) (Table 2.1, Fig. 2.1).
2. Optimization and physicochemical characterization of lipoplex formulations by measuring their particle size and zeta potential.
3. Development and optimization of peptide-based lipopolyplexes, and the impact of various designed peptide enhancers (7-types, with various charges and different lengths- Table 2.2) on transfection efficiency and cell viability of the formulated lipopolyplexes.
4. Physicochemical characterization of lipopolyplex formulations.
5. Screening 14 different gemini surfactants (G**1**-G**14**) formulated lipopolyplexes to evaluate the relationships between the structure of gemini surfactants and their transfection efficiency and cytotoxicity.
6. Proposing a unifying model-mechanism based on transfection efficiency results and physicochemical characterization of gene delivery systems for rationalization of surface engineering in development of synthetic virus-like nanoparticles.

The significance outcome of this work has been filed for patent with the United States Patent and Trademark Office (USPTO) (filed: Sep 6, 2017) [309] and the Canadian Intellectual Property Office (CIPO) (filed: June 28, 2018) [310]. The details of this research project are presented in the following chapters.

Table 2.1. Fifteen gemini surfactants (m-s-m formula) studied in this research. m = 12 and 18 carbon alkyl chains, s = 3 (3 methylene unit), 7NH (imino-substituted-7 methylene unit), 7NR (R-linked-imino-substituted-7-methylene unit) spacer groups. R = R1-R10 functional moieties.

Compound		**Compound formula (m-s-m)**	
#	**Names**		
G**0**	12-3-12	m-3-m	12-3-12
G**1**	18-3-18		18-3-18
G**2**	12-7NH-12	m-7NH-m	12-7NH-12
G**3**	18-7NH-18		18-7NH-18
G**4**	Imid-18	m-7NR-m	18-7NR$_1$-18 (R$_1$ = imidazolpropionyl)
G**5**	Thiol-18		18-7NR$_2$-18 (R$_2$ = thiopropionyl)
G**6**	RGDG-12		12-7NR$_3$-12 (R$_3$ = RGDG-)
G**7**	RGDG-18		18-7NR$_3$-18 (R$_3$ = RGDG-)
G**8**	GRGDSPG-18		18-7NR$_4$-18 (R$_4$ = GRGDSPG-)
G**9**	18-E-PepD		18-7NR$_5$-18 (R$_5$ = -E(H)$_5$)
G**10**	18-E-PepE		18-7NR$_6$-18 (R$_6$ = -EGRGDSPG(H)$_5$)
G**11**	18-Suc-E$_2$GR$_2$		18-7NR$_7$-18 (R$_7$ = -Suc-(E)$_2$G(R)$_2$)
G**12**	18-Suc-E$_2$GR$_3$		18-7NR$_8$-18 (R$_8$ = -Suc-(E)$_2$G(R)$_3$)
G**13**	18-Suc-E$_2$G$_3$R$_3$		18-7NR$_9$-18 (R$_9$ = -Suc-(E)$_2$(G)$_3$(R)$_3$)
G**14**	18-Suc-DEG$_3$R$_3$		18-7NR$_{10}$-18 (R$_{10}$ = -Suc-DE(G)$_3$(R)$_3$)

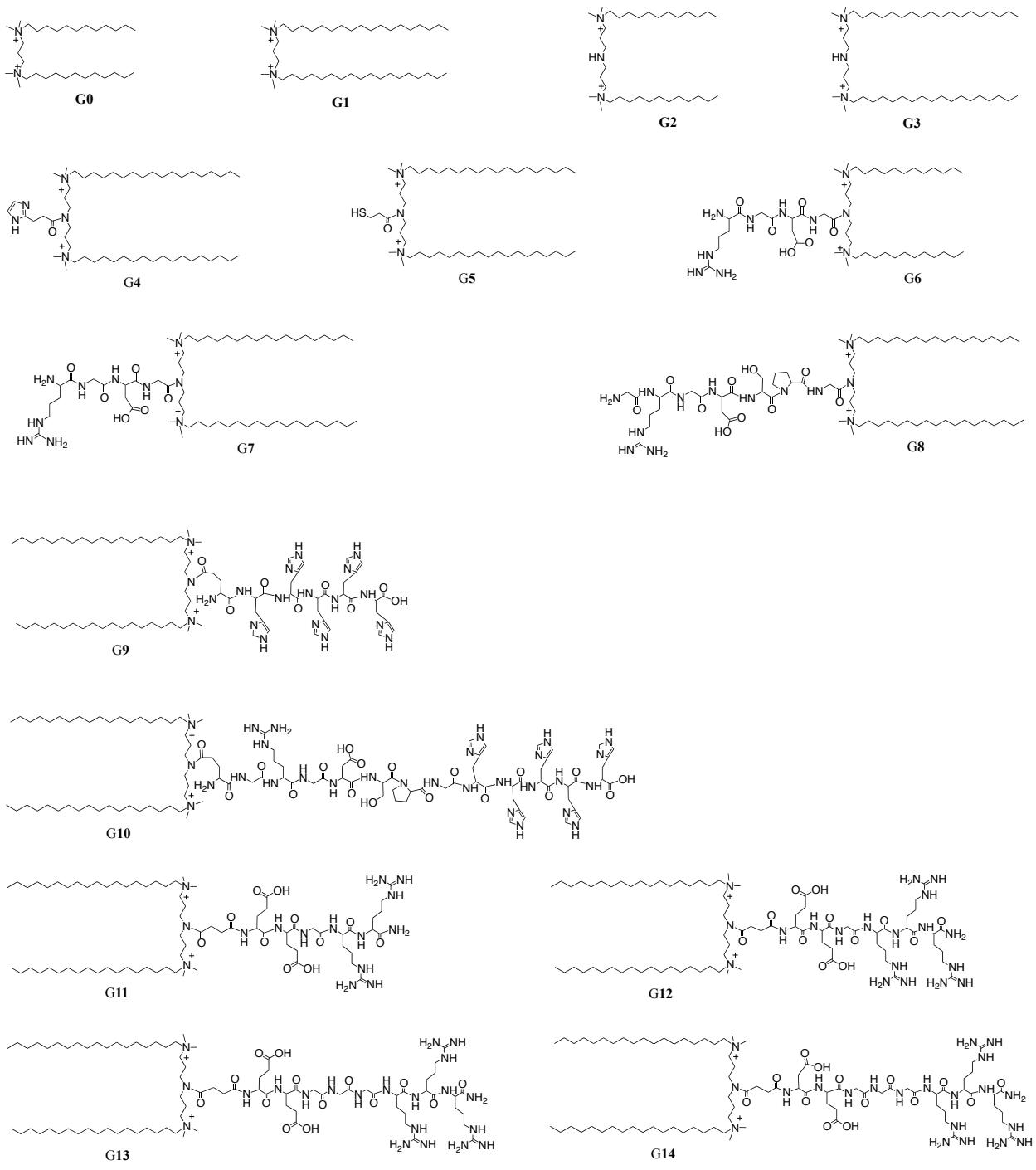

Fig. 2.1. The general structures of 15 different gemini surfactants differing in alkyl chain lengths and/or spacer groups and/or functional headgroups.

Table 2.2. Amino acid sequence, net charge (at pH = 7) and molecular weight of seven peptide enhancers: zwitterionic RGD peptide enhancer (P_A), cationic histidine and/or arginine rich peptide enhancers (P_B, P_D, P_F), or bifunctional cationic, RGD peptide enhancers ($P_C = P_A + P_B$, $P_E = P_A + P_D$, $P_G = P_A + P_F$).

Peptide enhancer	Name	Sequence (N- to C-terminus)	Net charge at pH 7	MW (g/mol)
P_A (7a.a.)	RGD	GRGDSPG	0	664.63
P_B (10a.a.)	$(R)_6$-H_3	$H(R)_3H(R)_3HG$	6.3	1423.6
P_C (17a.a.)	RGD-$(R)_6$-H_3	$GRGDSPGH(R)_3H(R)_3HG$	6.3	2050.22
P_D (5a.a.)	$(H)_5$	$(H)_5$	0.5	703.71
P_E (12a.a.)	RGD-$(H)_5$	$GRGDSPG(H)_5$	0.5	1330.33
P_F (15a.a.)	$(H)_{12}$-$(R)_2$	$(H)_2R(H)_7R(H)_3G$	3.2	2033.11
P_G (22a.a.)	RGD-$(H)_{12}$-$(R)_2$	$GRGDSPG(H)_2R(H)_7R(H)_3G$	3.2	2659.73

Chapter 3

Experimental Procedures

3.1 Materials

Custom designed peptide enhancers (7 types: P_A (GRGDSPG); P_B ($H(R)_3H(R)_3HG$); P_C ($GRGDSPGH(R)_3H(R)_3HG$); P_D ($(H)_5$); P_E ($GRGDSPG(H)_5$); P_F ($(H)_2R(H)_7R(H)_3G$); P_G ($GRGDSPG(H)_2R(H)_7R(H)_3G$)) were purchased from Biomatik Corporation (Cambridge, ON, Canada) (purity > 95%). 1-N-trityl-imidazole-2-ylpropionic acid and 3-(tritylthio)propionic acid (protected R_1 and R_2 functional moieties, respectively) were obtained from Sigma-Aldrich (Oakville, ON, Canada). The protected peptide functionalities (R_3-R_{10}) were purchased from Biomatik Corporation (Cambridge, ON, Canada). The resin-cleaved protected R_3 (Boc-Arg(Pbf)-Gly-Asp(OtBu)-Gly-OH) and R_4 (Boc-(Gly)-Arg(Pbf)-Gly-Asp(OtBu)-Ser(tBu)-Pro-Gly-OH) were obtained with the free C-terminal carboxylic groups (purity > 95%). The rest of protected functionalities (R_5-R_{10}) were acquired on resin with the free carboxylic groups at the N-terminus of the peptide (i.e., the free side chain of glutamic acid or succinic acid). The protected R_5 (Boc-Glu-$(His(Trt))_5$) and R_6 (Boc-Glu-Gly-Arg(Pbf)-Gly-Asp(OtBu)-Ser(tBu)-Pro-Gly-$(His(Trt))_5$) were obtained on H-His(Trt)-2-Chlorotrityl Resin (0.342 mmol/g); while the protected R_7 (succinyl-Glu(OtBu)-Glu(OtBu)-Gly-Arg(Pbf)-Arg(Pbf)), R_8 (succinyl-Glu(OtBu)-Glu(OtBu)-Gly-Arg(Pbf)-Arg(Pbf)-Arg(Pbf)), R_9 (succinyl-Glu(OtBu)-Glu(OtBu)-Gly-Gly-Gly-Arg(Pbf)-Arg(Pbf)-Arg(Pbf), and R_{10} (succinyl-Asp(OtBu)-Glu(OtBu)-Gly-Gly-Gly-Arg(Pbf)-Arg(Pbf)-Arg(Pbf)) were procured on Rink amide MBHA Resin (loading capacity: 0.45 mmol/g used for R_7 and R_8 or 0.332 mmol/g used for R_9 and R_{10}). All chemicals including 1-bromooctadecane, 3,3′-iminobis(*N,N*-dimethylpropylamine), 1-[bis(dimethylamino)methylene]-1-*H*-1,2,3-triazolo[4,5-

b]pyridimium 3-oxid hexafluorophosphate (HATU), *N,N*-diisopropylethylamine (DIPEA), trifluoroacetic acid (TFA), triisopropylsilane (TIS), 1,2-ethanedithiol (EDT), *N,N*-demethylformamide (DMF) and HPLC grade acetonitrile (MeCN) were purchased from Sigma-Aldrich (Oakville, ON, Canada). Analytical ultra-performance liquid chromatography (UPLC) was performed on a Waters ACQUITY UPLC H-Class BioSystem (Milford, MA, USA) with a flow rate of 0.2 mL/min and UV detection at 214 nm. Semi-preparative reverse phase high performance liquid chromatography (RP-HPLC) was performed on a Waters instrument (Waters e2695 separations module) (Milford, MA, USA) at a flow rate of 10 mL/min and UV detector set to a wavelength of 214 nm. The mobile phases for both analytical UPLC and semi-preparative HPLC were solvent A (water/TFA: 99.9/0.1, v/v) and solvent B (MeCN/TFA: 99.9/0.1, v/v). Analytical separation was achieved by a linear gradient of solvent B on ACQUITY UPLC BEH C18 column (130 Å pore size, 1.7 μm particle size, 2.1 mm × 50 mm); while, the semi-preparative separation was on 300SB-C18 semi-preparative column (300 Å pore size, 5 μm particle size, 9.4 mm × 250 mm). Electrospray ionization mass spectrometry (ESI-MS) was performed on a Q-Exactive Orbitrap System (Thermo Fisher Scientific, CA, USA) using a mixture of solvent A (water/formic acid, 99.9/0.1, v/v) and solvent B (MeCN/formic acid, 99.9/0.1, v/v).

3.2 Synthesis of gemini surfactants

3.2.1 Synthesis of m-3-m and m-7NH-m (m = 12, 18 alkyl chain length)

Synthesis of m-3-m (i.e., 12-3-12 (G**0**), 18-3-18 (G**1**)) and m-7NH-m (i.e., 12-7NH-12 (G**3**), 18-7NH-18 (G**4**)) gemini surfactants used in this study was carried out prior to this research according to the published procedures [265, 271, 273, 287, 289]. However, to satisfy the sufficient quantities, the synthesis of the 18-7NH-18 gemini surfactant was repeated, as described below.

The 18-7NH-18 gemini surfactant was synthesized by refluxing 1 equivalent of 3,3′-iminobis(*N,N*-dimethylpropylamine) (15 mmol, MW: 187.33) with 2.2 equivalents of 1-bromooctadecane (33 mmol; MW: 333.39) in 50 mL of MeCN at 90°C under a N_2 atmosphere for 24 h (Fig. 3.1). Then, the reactor flask was cooled down and placed on an ice bath for an hour, allowing the precipitation of the product to take place. The resulting precipitated solid was then filtered using a Buchner funnel and washed with a large excess of cold MeCN under vacuum for at least 3 times to remove the reaction mixture. The crude product was dried overnight in a 37°C oven and the identity of the synthesized 18-7NH-18 surfactant was analyzed by ESI-MS (Fig. B1 and B2; Appendix B).

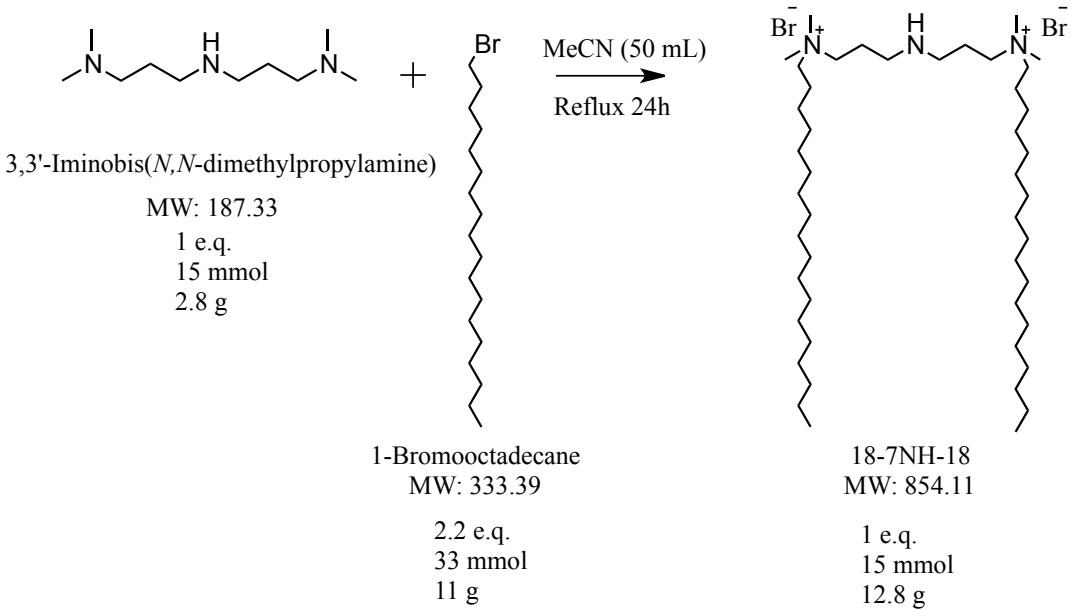

Fig. 3.1. Synthesis scheme of 18-7NH-18 gemini surfactant.

3.2.2 Synthesis and purification of 11 novel functionalized-gemini surfactants (G4-G14; m-7NR-m; R = R_1-R_{10} containing imidazole, thiol or peptide functional groups)

The synthesis of 11 novel functionalized gemini surfactants (G**4**-G**14**, Table 2.1) were performed by covalently linking 10 different functional moieties (R_1-R_{10}; Fig. 3.2 (B)) to the imino spacer of m-7NH-m gemini surfactants (m = 12, 18) as shown in Figure 3.3 either by method A or method B, as described below.

Method A was performed for synthesis of G**4**-G**8** gemini surfactants in solution phase (e.g., at 40 μmol scale in 20 mL of MeCN) and method B was carried out for synthesis of G**9**-G**14** in solid phase on-resin (at 100-200 μmol scale in 10 mL of DMF) (Fig. 3.3 and Fig. 3.4) by amide bond formation between the imino spacer of gemini surfactants (1 eq.) and the pre-activated free carboxylic group of the R-functional moieties (2 eq.) using HATU (1.9 eq.) and DIPEA (2.8 eq.) [311-313]. In method A, in case of peptide-functionalization [R_3-R_4], the m-7NH-m gemini surfactants were coupled to free carboxylic groups at the C-terminus of the resin-cleaved protected peptide moieties (Fig. 3.3 (A)- step 1 and 2). After 3-4 hours' completion of the ligation reactions, the organic solvents were removed by rotary evaporation and then the protected products were separated from the reaction mixture using semi-preparative RP-HPLC (Fig. 3.3 (A)- step 3). In method B, however, following the solid-phase peptide synthesis on resin, the coupling of gemini surfactants took place at the N-terminus of the protected peptide moieties through a carboxyl-containing linker such as glutamic acid with the free side chain carboxyl (used in production of G**9**-G**10**) or succinic acid (used in production of G**11**-G**14**) (Fig. 3.3 (B), step 1). The cleavage/deprotection step was then accomplished using a cocktail of TFA/H_2O/TIS (95:2.5:2.5, v/v/v) (for compounds G**4**, G**6**-G**14**) or TFA/thioanisol/EDT/anisole (90:5:3:2, v/v/v/v) (for compounds G**5**) for over 2-3 hours (Fig. 3.3 (A)- step 4 and (B)-step 2). Crude products were

purified by semi-preparative RP-HPLC (Table 2.2), lyophilized and kept at -20°C. The quantitative and qualitative identification of the synthesized compounds confirmed by analytical RP-UPLC and electrospray ionization-mass spectrometry (ESI-MS) (purity > 95%).

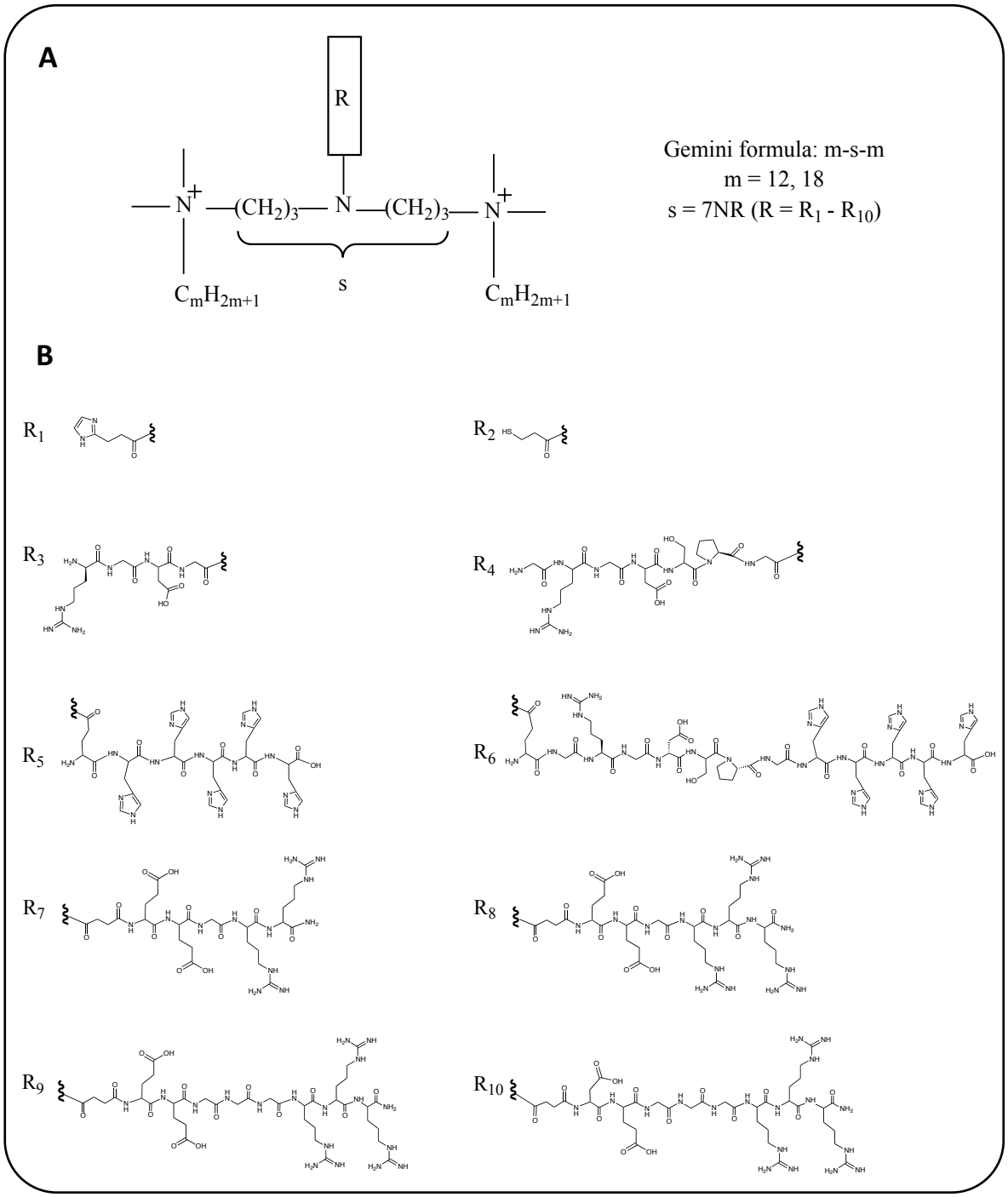

Fig. 3.2. (A) General structure of m-7NR-m gemini surfactants (m= 12, 18; R= R_1-R_{10}). (B) Chemical structure of R functional moieties (R_1-R_{10}).

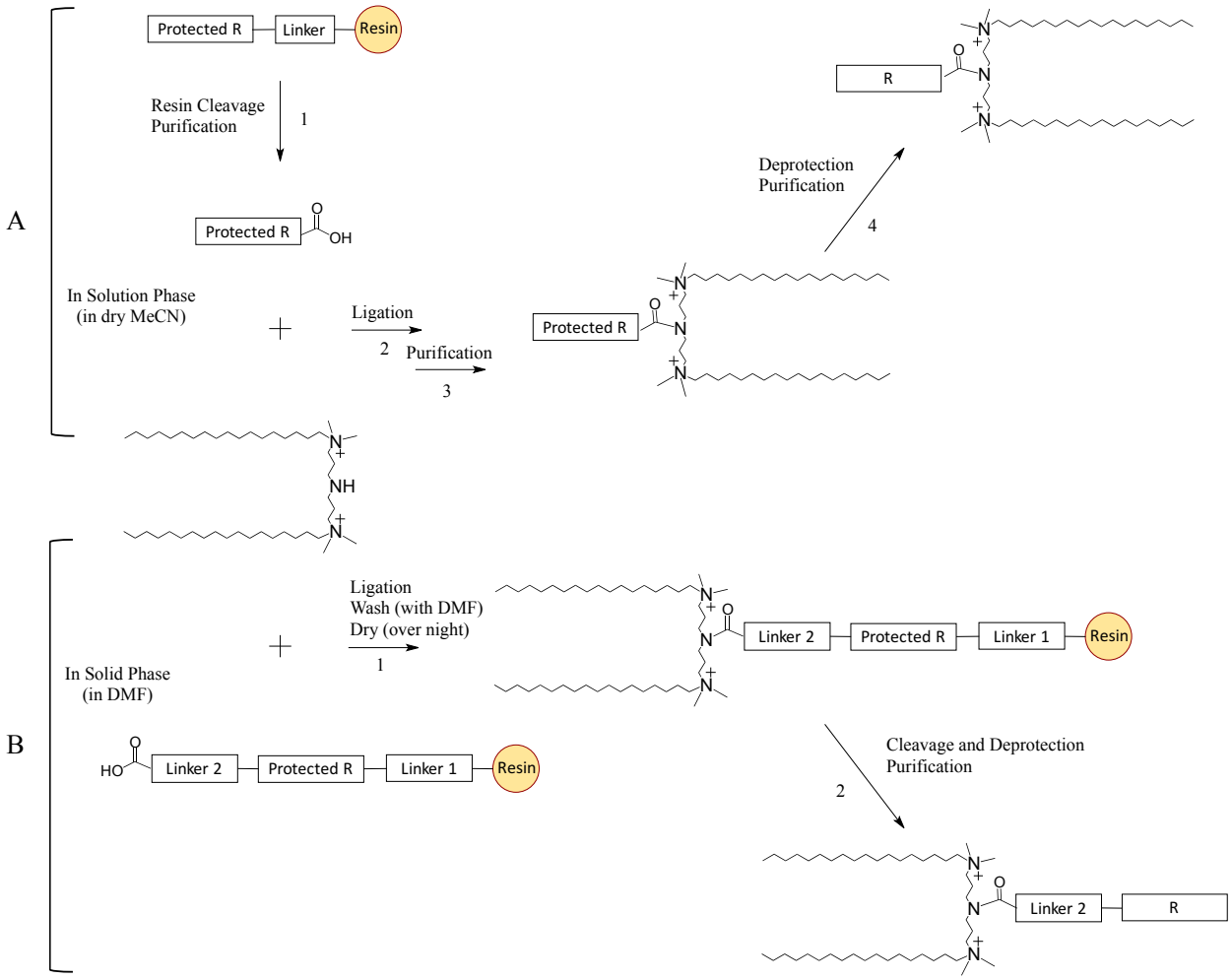

Fig. 3.3. Synthetic scheme for R-functionalization of gemini surfactants by Method (A) in solution (for synthesis of G**4**-G**8** m-7NR-m gemini surfactants (m = 12, 18; R = R_1-R_4)) or by Method (B) in solid phase (for synthesis of G**9**-G**14** m-7NR-m gemini surfactants (m = 18; R = R_5-R_{14})). m-7NR-m gemini surfactants were synthesized by covalent linking of the imino groups of the m-7NH-m gemini surfactants to free carboxylic groups located either at the C-terminus of R functional peptides (using Method (A)) or at the N-terminus of the R functional motifs through a carboxyl-containing linker (using Method (B)). The cleavage and/or deprotection, and purification steps were accomplished to yield G**4**-G**14** m-7NR-m gemini surfactants.

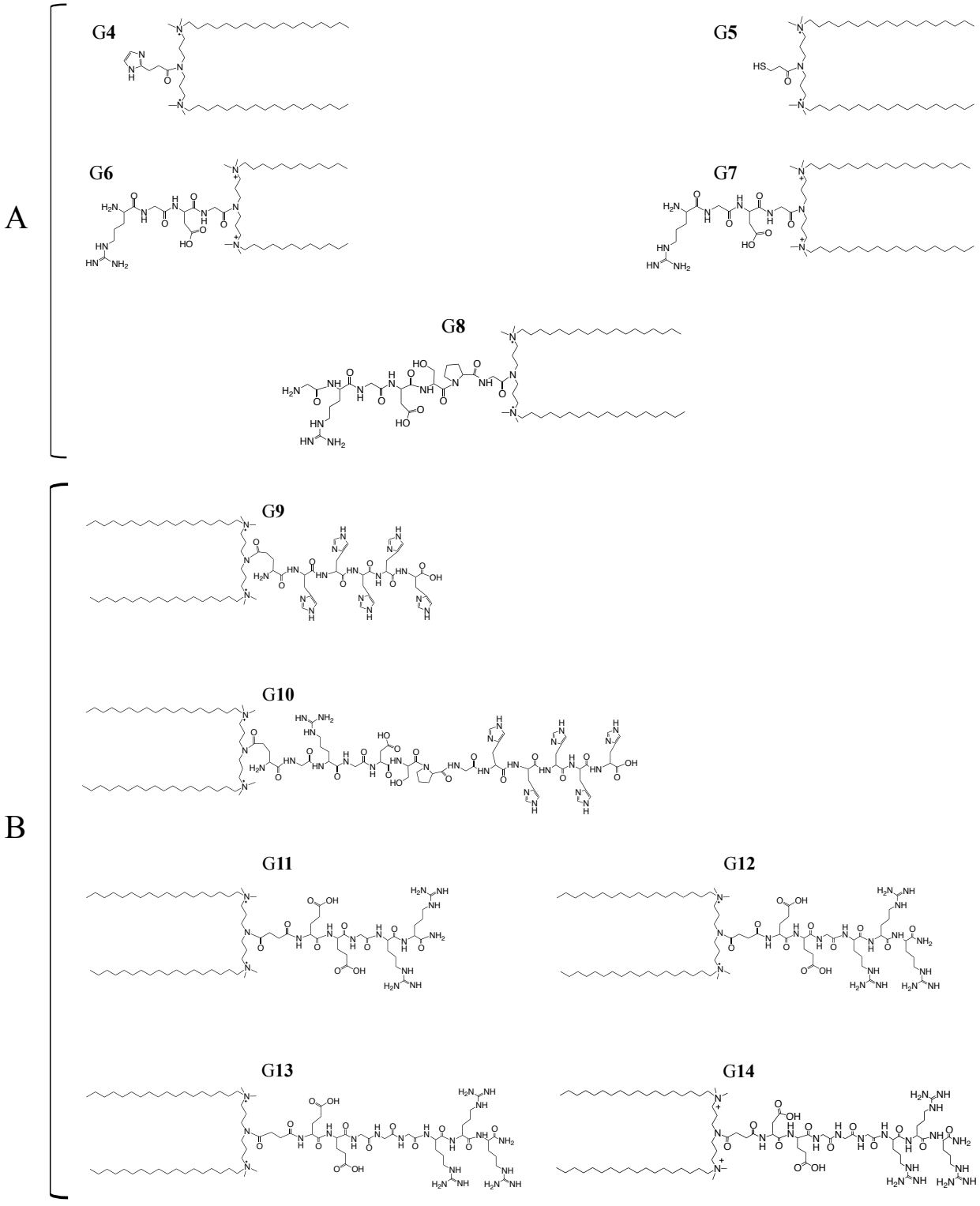

Fig 3.4. (A) The synthesized R-functionalized G**4**-G**8** gemini surfactants by Method (A). (B) The synthesized R-functionalized G**9**-G**14** gemini surfactants by Method (B).

3.3 Preparation of formulations

The freshly made stock solution of DOPE (L) helper lipids (Avanti Polar Lipids, Alabaster, AL, USA) were prepared at 1 mM concentration in sucrose solution (9.25% w/v) by bath sonication (10 min) and high-pressure LV1 Microfluidizer (× 3 at 20,000 psi) as described previously [314, 315]. The aqueous solutions of gemini surfactants (G**1**-**14**) and peptide enhancers (P_A-P_G) were separately prepared in nuclease-free water.

Uni-Modal (UM [P], UM [G]), Bi-Modal (BM [G/L], BM [P/L], BM [P/G]) and Tri-Modal (PDTMG [P/G/L]) gene delivery systems were formulated at various cationic quaternary ammonium of gemini surfactants/anionic phosphate of pDNA (N/P) mole ratios ($\rho_{\pm}$ values), DOPE/gemini molar ratios (r values), and molar concentrations of the compositional elements in the formulation mixtures (M_P, M_G and M_L for molar concentrations of peptide enhancers (P), gemini surfactants (G) and DOPE helper lipids (L), respectively; ; see Table 3.1 for detailed information on the selected formulations). The formulation mixtures were pre-incubated for 30 minutes at room temperature before being used in the transfection assay.

For example, PDTMG [P_C/G**7**/L] formulations were prepared by first pre-complexation of pDNA with P_C cationic peptide enhancer and G**7** gemini surfactant for 15 minutes at room temperature, followed by addition of the DOPE helper lipid to the pDNA/P_C/G**7** mixture and further incubation for another 15 minutes. The pDNA/P_C/G**7**/L mixture were diluted with nuclease-free water to a final volume of 10 μL or 50 μL transfection reagent per well of a 96-well or a 24-well plate, respectively.

The gWiz^{TM} GFP pDNA (5757 bp; Aldevron, Fargo, ND, USA) and tdTomato RFP (red fluorescent protein) pDNA (Clontech Laboratories Inc., Mountain View, CA, USA) were used to monitor the expression level of the reporter genes. A mock pDNA (5688 bp; Blue Heron Biotech,

Bothell, WA, USA) with absent of a fluorescent protein reporter gene was used as negative control. The commercially available Lipofectamine™ 3000 reagents (Invitrogen Life technologies) was used as a reference transfection reagent according to the manufacturer's instructions.

Table 3.1. Selected gene delivery systems formulated using peptide enhancers (P) and/or gemini surfactants (G) and/or DOPE helper lipids (L) at varying molarities of the compositional elements (M_P, M_G, M_L). (A) Detailed information on formulating Uni-Modal (UM [P M_P]), Bi-Modal (BM [G M_G/L M_L], BM [P M_P /L M_L], BM [P M_P/G M_G]) and Tri-Modal (PDTMG [P M_P/G M_G/L M_L]) delivery systems containing 0.5 µg pDNA in 50µL transfection reagent (prepared per well of a 24 well plate). (B) Scaling transfection reagents (10 µL, 50 µL) for formulating 0.1 µg and 0.5 µg of pDNA used per well of 96-well and 24-well.

A) Formulations containing 0.5 µg pDNA per well of a 24-well plate	**Peptide (P)**		**Gemini (G)**		**DOPE (L)**		$\rho_{\pm}$	**r**
	n_P **(nmol)**	M_P **(µM)**	n_G **(nmol)**	M_G **(µM)**	n_L **(nmol)**	M_L **(µM)**		
BM [G 154/L 500]	0.0	0	7.69	154	25.00	500	10	3.3
BM [G 31/L 500]	0.0	0	1.54	31	25.00	500	2	16.1
BM [G 31/L 100]	0.0	0	1.54	31	5.00	100	2	3.3
UM [P 49]	2.4	49	0.00	0	0.00	0	-	-
BM [P 49/L 100]	2.4	49	0.00	0	5.00	100	-	-
BM [P 49/G 31]	2.4	49	1.54	31	0.00	0	2	-
PDTMG [P 49/G 31/L 100]	2.4	49	1.54	31	5.00	100	2	3.3
PDTMG [P 267/G 17/L 100]	13.3	267	0.8	17	5.00	100	1.1	6.0
PDTMG [P 267/G 17/L 113]	13.3	267	0.8	17	5.67	113	1.1	6.8

B) Formulation preparations	**96-well plate**	**24-well plate**
DNA per well	0.1 µg	0.5 µg
Transfection reagent per well	10 µL	50 µL

3.4 Physicochemical characterization of formulations

The gene delivery formulations were prepared as described in Section 3.3. Size measurements were performed at the same concentration used in the transfection assay (60 µL from formulation mixtures were measured in transparent disposable ZEN0118 cuvettes); while, zeta (ζ)-potential measurements were performed by diluting samples to a final volume of 1 mL in nuclease-free water. The size (the Z-average, mean hydrodynamic diameters) and ζ-potential of the particles were measured using 632.8 nm (red) wavelength laser at a 173° scattering angle (detector position), and at 25°C with a 1 min equilibrium time, and automatic measurement cycle using Zetasizer Nano ZS instrument (model number: ZEN3600, Malvern instruments Ltd., Worcestershire, UK). ZEN0040 and DTS1070 cuvettes were used for size and zeta potential measurements, respectively. Data points are the average of three measurements (n = 3) ± standard deviation (SD).

3.5 Cell culture and *in vitro* transfection

Human malignant melanoma A375 cell line (ATCC ® CRL-1619^{TM}) and mouse fibroblasts 3T3-Swiss albino (ATCC ® CCL-92^{TM}) were cultured in Dulbecco's modified Eagle's medium (DMEM) – high Glucose supplemented with 10% fetal bovine serum (FBS) and 1% penicillin/streptomycin and incubated at 37°C under an atmosphere of 5% CO_2. Cells were seeded in 96-well/24-well tissue culture-treated plates (Corning Inc., Corning, NY, USA) at a density of 40,000 cells/cm^2 and 15,000 cells/cm^2 for A-375 and 3T3 cell lines, respectively. After 24 h (when 85-90% confluency was achieved) and 1 h prior to transfection, the complete medium was replaced with the basic DMEM medium without serum and antibiotic. Cells were transfected with formulations containing pDNA (0.1 µg/well of 96-well plate or 0.5 µg/ well of 24-well plate) and

incubated at 37°C for 5 h. The fresh complete growth medium was added to each well without removing transfection formulations and further incubated for 19 h. After 24h of transfection, cells were trypsinized and stained with MitoTracker Deep Red (0.5 μL/mL) for 15 min at 37°C. The percentage of the pDNA-transfected cells, the mean fluorescence intensity (MFI) of the cells expressing GFP, and cell viability were examined by flow cytometry (Attune® Flow Cytometer, Life Technologies, Carlsbad, CA, USA).

3.6 Transfection study and cell viability by flow cytometry

To create a consistent flow cytometry analysis, flow cytometry parameters were adjusted according to fluorescent and non-fluorescent cells prepared by electroporation with PmaxGFP™ reporter pDNA, tdTomato RFP plasmid or mock pDNA using Lonza Nucleofector Kit (Lonza Inc., Basel, Switzerland). Cell viability of the transfected cells was evaluated using MitoTracker® Deep Red FM (a cell permeable far red-fluorescent dye, which stains mitochondria in living cells) by assessing the metabolic activity of the mitochondria and the mitochondrial membrane potential (analysis in all events) [315-317]. The intensity of green or red fluorescence vs. MitoTracker intensity signals were used to evaluate the impact of transfection reagents on the percentage of the transfected cells and protein expression level in viable cell populations. The expressions of the fluorescent proteins were detected in the BL1 channel (emission filter: 530/30 nm for GFP detection) and the BL2 channel (emission filter: 574/26 nm for RFP detection) using 488 nm blue laser as an excitation source. MitoTracker Deep Red mitochondria stain was excited with 638 nm red laser and detected in RL1 channel (emission filter: 650-670 nm). In order to place the events in the appropriate area in the FSC vs. SSC dot plot, FSC (forward scatter) and SSC (side scatter) voltages were set at 1350 (mV) and 2400 (mV), respectively. Meanwhile the BL1, BL2, and RL1

fluorescence channels were adjusted to locate the population in the two-dimensional (2D) density plot of the BL1 or BL2 (on the X axis) vs. RL1 (on the Y axis) by setting the detector voltages for BL1 at 1450 (mV), BL2 at 1450 (mV) and RL1 at 1400 (mV). A total number of 20,000 cell events were recorded for cell cycle analysis. Figure A1 (Appendix A) shows the 2D dot plot (BL1 vs. RL1) of control-untreated cells (Cells only), control-mock pDNA and PmaxGFP^{TM} pDNA transfected cells by electroporation.

Transfection studies were investigated by both the percentage of the transfected cells and the mean fluorescence intensities (MFI) determining the intensity level of expression of the reporter fluorescent proteins (i.e., GFP or RFP). The relative measurement of the percentage of the transfected cells for a given transfection reagent was assessed according to control-untreated cells (with intensity values below 5,000 range on the BL1 logarithmic axis) by setting the outlier at 5,000 (low threshold (LT) analysis) (Figs. A2; Appendix A). To effectively and critically compare the extent of GFP expression levels of gene delivery formulations, the MFI was measured at two different thresholds: low threshold (LT) and high threshold (HT) by setting the outlier at 5,000 and 10,000, respectively, on the BL1 logarithmic axis. Measuring MFI at HT provides a better analysis for understanding and interpretation of flow cytometry data by excluding the events with low fluorescence intensities (i.e., from 5,000-20,000 fluorescence intensity, the background noise from the delivery vehicle were also detected as investigated by various transfection agents carrying mock pDNA), and hence reducing the skewing of MFI. This analysis would be particularly useful in comparing the MFI for transfection agents with high transfection percentages (Figs. A2; Appendix A). Therefore, the difference between the intensity of their GFP expression levels can be measured more appropriately when comparing transfection agents. Both the percentage of the transfected cells and the MFI were normalized by control-untreated cells.

The percentage of cell viability of gene delivery formulations was expressed as 'cell viability index' and investigated according to the percentage of control-untreated-MitoTracker-stained cells (denoted as 'cells only' in untransfected wells), by setting the outlier at 30,000 on the RL1 logarithmic axis, in which the control-untreated cells with intensity values above 30,000 range were considered as 100% viable (with intact mitochondrial membrane potential). The cell viability index was calculated as follows: $\left(V_{treated\ sample}/V_{untreated\ control}\right) \times 100\%$.

3.7 Statistical analysis

All data are presented as means ± SD ($n \geq 2$) and *in vitro* studies of the samples were performed in at least 2 independent experiments to ensure reproducibility. Differences between groups were identified by one-way analysis of variance (ANOVA) followed by Tukey's multiple comparison post-hoc test. GraphPad Prism (version 7.0c, GraphPad Software, Inc.) was used for statistical analyses. Statistical significant differences were considered when $p < 0.05$ ($*p < 0.05$, $**p < 0.01$, $***p < 0.001$, $****p < 0.0001$).

Chapter 4

Results

4.1 Synthesis and characterization of functionalized m-7NR-m gemini surfactants (m = 12, 18) bearing imidazole, thiol, linear RGD motifs, poly-histidine, or arginine-rich peptide functional headgroups

Eleven novel R-functionalized gemini surfactants [G**4**-G**14**] (m-7NR-m formula; m = 12, 18 and R = R_1-R_{10}, Fig. 3.2; Table 2.1) were co-designed and synthesized by covalently linking the amino group of the m-7NH-m gemini surfactants to the free carboxylic groups of functional groups in solution phase (method (A)) or on solid phase support (method (B)).

Using method (A), G**4** (imid-18) and G**5** (thiol-18) were synthesized by functionalization of the gemini surfactants with imidazole- and thiol-containing functional groups (R_1: imidazolepropionyl (R_1), R_2: thiopropionyl), respectively. G**6** (RGDG-12), G**7** (RGDG-18) and G**8** (GRGDSPG-18) were synthesized by conjugating gemini surfactants to the free C-terminus of the RGD peptide motifs (i.e., R_3: RGDG, R_4: GRGDSPG).

Method (B) was used to synthesize G**9** (18-E-PepD) bearing $(H)_5$ functional headgroup (i.e., R_5: $E(H)_5$), G**10** (18-E-PepE) with bifunctional RGD-$(H)_5$ headgroup (i.e., R_6: $EGRGDSPG(H)_5$), and G**11-** G**14** having arginine rich peptide motifs (i.e., R_7: Suc-$(E)_2G(R)_2$, R_8: Suc-$(E)_2G(R)_3$, R_9: Suc-$(E)_2(G)_3(R)_3$ and R_{10} = Suc-$DE(G)_3(R)_3$), by conjugating gemini surfactants to the free carboxylic groups located at the N-terminus of the functional peptides. The modified uncharged C-terminal amide end of the R_7-R_{10} functionalities (generated from the use of Rink amide resin) were designed to increase the biological activity, stability [318] and cell penetrating capability of the G**11-** G**14** gemini surfactant.

The synthesized G**4-** G**14** gemini surfactants were purified to a single peak (purity > 95%) using analytical reverse phase high performance liquid chromatography (RP-HPLC) and the identity of the products were confirmed by ESI-MS (Table 4.1, and Fig. B3-B23 in Appendix B).

Table 4.1. Characterization of m-7NR-m gemini surfactants (m = 12, 18; R = R_1-R_{10}). The identity of the synthesized G**4**-G**14** m-7NR-m gemini surfactants were confirmed by ESI-MS and the purifications were conducted by RP-HPLC with a linear gradient of solvent B on 300SB-C18 semi-preparative column; mobile phases: solvent A (water/TFA: 99.9/0.1, v/v) and solvent B (MeCN/TFA: 99.9/0.1, v/v); flow rate: 10 mL/min; UV detection: 214 nm.

Compounds		**MW (g/mol)**	**ESI-MS (m/z)**	**RP- HPLC**
#	**Names**			
G**4**	Imid-18	816.42	407.92 $[M]^{2+}$, 272.28 $[M]^{3+}$	60-100% B in 15 min
G**5**	Thiol-18	782.43	390.90 $[M]^{2+}$	60%-100% B in 15 min
G**6**	RGDG-12	911.36	303.92 $[M]^{3+}$	40%-60% B in 15 min
G**7**	RGDG-18	1079.67	359.99 $[M]^{3+}$	60%-100% B in 15 min
G**8**	GRGDSPG-18	1320.92	660.03 $[M]^{2+}$, 440.35 $[M]^{3+}$, 330.52 $[M]^{4+}$	60%-100% B in 15 min
G**9**	18-E-PepD	1509.11	754.06 $[M]^{2+}$, 503.04 $[M]^{3+}$, 377.53 $[M]^{4+}$	50%-100% B in 10 min
G**10**	18-E-PepE	2135.73	1067.69 $[M]^{2+}$, 712.13 $[M]^{3+}$, 534.35 $[M]^{4+}$ 427.68 $[M]^{5+}$, 356.57 $[M]^{6+}$	50%-100% B in 20 min
G**11**	18-Suc-E_2GR_2	1421.04	710.06 $[M]^{2+}$, 473.71 $[M]^{3+}$, 355.53 $[M]^{4+}$	50%-100% B in 20 min
G**12**	18-Suc-E_2GR_3	1577.22	525.74 $[M]^{3+}$, 394.56 $[M]^{4+}$	50%-100% B in 20 min
G**13**	18-Suc-$E_2G_3R_3$	1691.32	564.09 $[M]^{3+}$, 423.32 $[M]^{4+}$	50%-100% B in 20 min
G**14**	18-Suc-DEG_3R_3	1677.30	559.42 $[M]^{3+}$, 419.82 $[M]^{4+}$	50%-100% B in 20 min

4.2 Bi-modal gemini/DOPE lipoplexes: Formulation optimization and the impact of RGDG-functionalized gemini surfactants on the transfection activity of gemini-based lipoplexes

Systematic optimization of BM [G/L] lipoplex delivery systems were performed using six different gemini surfactants differing in the spacer groups and hydrocarbon tail lengths (i.e., 12-3-12 (G**0**), 18-3-18 (G**1**), 12-7NH-12 (G**2**), 18-7NH-18 (G**3**), RGDG-12 (G**6**) and RGDG-18 (G**7**)) to correlate molecular architecture of gemini surfactants and physicochemical properties of the lipoplex delivery systems in relation to their transfection activity.

While the physical characterization of the lipoplexes were performed to provide a general pattern and insight to predict an optimized formulation for pDNA delivery, more depth analysis of the effect of the compositional elements of gemini-based lipoplexes was investigated by *in vitro* transfection studies at various gemini to DNA N/P mole ratios (e.g., $\rho_{\pm}$ = 1, 2, 3, 5, 10) and DOPE/gemini molar ratios (e.g., r = 16.2, 9.7, 3.3, 2, 0.7, 0).

In vitro transfection studies of BM [G/L] lipoplexes were investigated for delivery of GFP-encoding gWiz^{TM} pDNA and RFP-encoding tdTomato pDNA to A375 human melanoma cell lines and 3T3-mouse fibroblasts in 96-well plates. However, only the optimization of the selected formulations, investigated using gWiz^{TM} GFP pDNA on 3T3-mouse fibroblasts, are discussed and shown below in order to put the numerous data analysis into perspective. The impact of RGDG-functionalized gemini surfactants (G**6**, G**7**) were compared to the parental gemini surfactants (G**2** and G**3**) on both the number of the transfected cells and the intensity of gene expression level.

4.2.1 Particle size and zeta potential analysis

The physicochemical properties of gene delivery formulations in correlation with their transfection activity portfolio were analyzed to advance formulation strategies for development of a potent delivery system. The hydrodynamic diameters, polydispersity index (PDI) and surface charge (ζ-potential) of various gemini-based lipoplexes formulated at different $\rho_{\pm}$ and r values were characterized by dynamic light scattering (DLS).

As shown in Figures 4.1 and 4.2, the DLS data indicated that lipoplexes formulated using m-3-m, m-7NH-m and m-7N(RGDG)-m at $\rho_{\pm} = 10$ and r = 3.3 (high gemini and DOPE lipid density; M_G = 154 μL, M_L = 500 μM) formed compact particles with the average size diameter of approximately 200-500 nm. However, by decreasing $\rho_{\pm} = 2$ (M_G = 31 μL) with identical DOPE lipid molarity (M_L = 500 μM; r = 16.2), all lipoplexes formed large aggregates (>1.5 μm) with a higher PDI, as observed in Figures 4.1 and 4.2.

Further investigation of the impact of the $\rho_{\pm}$ (2, 10) in conjunction with varying the r values (16.2, 3.3, 0.7, 0) on the physical properties of the lipoplexes was performed for G**6** and G**7** gemini surfactants. As shown in Figure 4.2, at $\rho_{\pm} = 10$ (grey bars), by decreasing the r from 3.3 (BM [G 154/ L500]) to 0.7 (BM [G 154/ L100]) to 0 (UM [G 154]), the size of the G**6**-based lipoplexes increased from 517.5 ± 49.0 nm to 857.9 ± 152.9 nm to large aggregates of 2388.3 ± 147.6 nm, respectively. However, lipoplexes formulated using G**7** gemini surfactants at $\rho_{\pm} = 10$ with varying r values generated small particle sizes; 291.5 ± 20.8 nm, 181.4 ± 2.3 nm and 181.1 ± 4.8 nm for those with r of 3.3, 0.7 and 0, respectively. These observed differences between the G**6** and G**7** in the physical properties of the corresponding lipoplexes are likely due to the various intermolecular repulsive and attractive forces from the hydrophilic cationic heads and the hydrophobic alkyl tails of the gemini surfactants in the formation of the lipoplexes. In the case of the G**7**-based lipoplexes

formulated at $\rho_{\pm}$ = 10 and at varying r values (3.3, 0.7, 0), these opposite forces maybe dominated by the strong hydrophobic forces from the long saturated C18 alkyl tails of G**7** gemini surfactants that yielded much more compact particles as compared to the lipoplex counterparts formulated using G**6** with the short saturated C12 alkyl tails. This is also supported by their zeta potential data indicated that at $\rho_{\pm}$ = 10, G**7**-based lipoplexes exhibited the highest zeta potentials (from ≈ +54 mV to ≈ +64 mV), whereas, G**6** strongly reduced the zeta potentials of the lipoplexes (from ≈ –0.2 mV to ≈ +51 mV) (Fig. 4.2).

It was observed that at $\rho_{\pm}$ = 2 (red bars- Fig 4.2) and r = 0 (without DOPE), the G**6** lipoplexes (i.e., UM [G**6** 31]) formed large aggregates (> 2 μm), while the G**7** lipoplexes (i.e., UM [G**7** 31]) showed an average size diameter of 408.1 ± 6.8 nm. The formation of large aggregates observed for the UM-G**6** lipoplexes (without DOPE) formulated at both $\rho_{\pm}$ of 2 and 10 (as stated above) is perhaps due to the strong repulsion forces between the cationic head groups of gemini surfactants and the weak hydrophobic interactions between the 12C alkyl tails of G**6** gemini surfactants. However, in the case of UM-G**7** lipoplexes (without DOPE), the increased hydrophobic effect from the 18C alkyl tails of G**7** gemini surfactants generated smaller range particles, in that those formulated at $\rho_{\pm}$ = 10 formed more compact particles than that of formulated at $\rho_{\pm}$ = 2. This is believed to be generally due to the lower critical micelle concentration of gemini surfactants with saturated 18C alkyl tails as compared to the gemini surfactants with saturated 12C alkyl tails (see examples shown in Fig 1.7). Further, by incorporation of DOPE, the average size diameters of the G**6**- and G**7**-based lipoplexes formulated at $\rho_{\pm}$ = 2 and r = 3.3 (i.e., BM [G 31/ L 100]) were decreased to 477.1 ± 16.2 nm and 289.4 ± 8.8 nm, respectively. The co-formulations of DOPE lipids with G**6** gemini surfactants at $\rho_{\pm}$ = 2 with r = 3.3 or at $\rho_{\pm}$ = 10 with r = 3.3 are thought to reduce the electrostatic repulsions between the cationic polar heads of gemini surfactants and additionally

increase the hydrophobic effects by balancing the packing of the saturated gemini surfactants with unsaturated DOPE lipids together, thus, resulting in formation of complexes with significantly reduced average size particles. These observations are also in agreement with the results obtained by Sharma *et al.* for DNA compaction with cationic gemini surfactants/DOPE formulations [319]. These effects of DOPE in formulating lipoplexes using G**7** gemini surfactants, however, were found to only be prominent at $\rho_{\pm} = 2$, indicating the extent of compaction is in close relation with the lengths of the alkyl tails and density of the gemini surfactants.

As shown in Figure 4.2, at $\rho_{\pm} = 2$, by increasing the r from 3.3 to 16.2 (BM [G 31/ L 500]), G**6**- and G**7**-based lipoplexes formed large aggregates. As presented in Figure 4.2, the zeta potentials of G**6**- and G**7**-based lipoplexes formulated at $\rho_{\pm} = 2$ and r = 3.3 (ζ-potential: +21.9 ± 1.6 mV and +38.3 ± 0.5 mV for the formulated G**6** and G**7**, respectively) were significantly higher than those formulated at $\rho_{\pm} = 2$ with r of 0 and 16.2; while significantly lower in comparison to their counterparts formulated at $\rho_{\pm} = 10$ with r of 0.7 and 3.3.

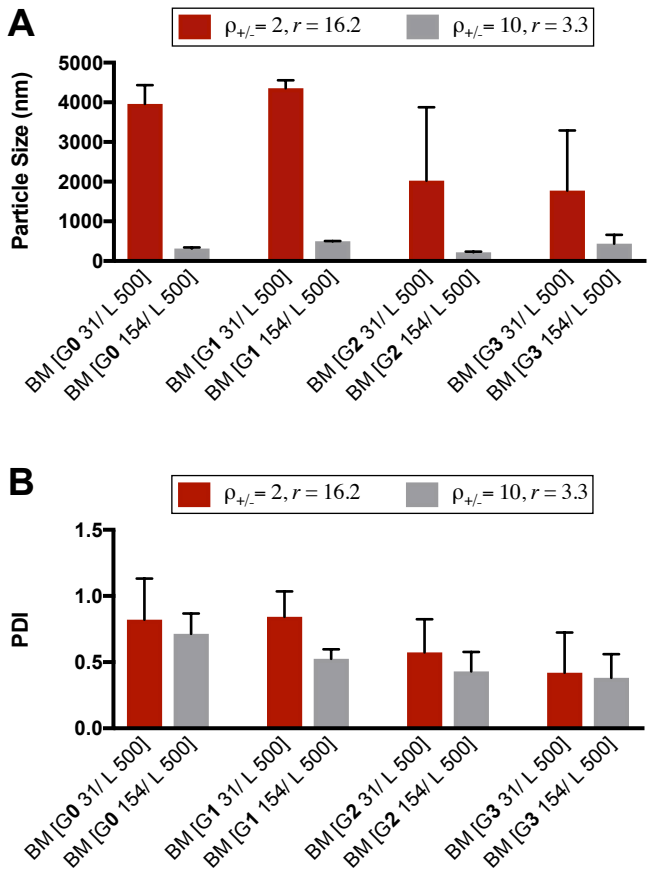

Formulations	Experiment	
	#	n
BM [G**0** 31/L 500]	1	3
BM [G**0** 154/L 500]	1	3
BM [G**1** 31/L 500]	1	3
BM [G**1** 154/L 500]	1	3
BM [G**2** 31/L 500]	2	6
BM [G**2** 154/L 500]	2	6
BM [G**3** 31/L 500]	2	6
BM [G**3** 154/L 500]	3	9

Fig. 4.1. Physical characterization of BM [G/L] lipoplexes formulated using 12-3-12 (G**0**), 18-3-13 (G**1**), 12-7NH-12 (G**2**) and 18-7NH-18 (G**3**) gemini surfactants as a function of $\rho_{\pm}$ = 10, 2 (M_G = 154 µM, 31 µM, respectively) with identical DOPE molarity (M_L = 500 µM). (A) Hydrodynamic diameter and (B) PDI of the lipoplexes were determined by DLS. Results are presented as mean ± SD from one, two or three independent experiments (n = 3 per experiment).

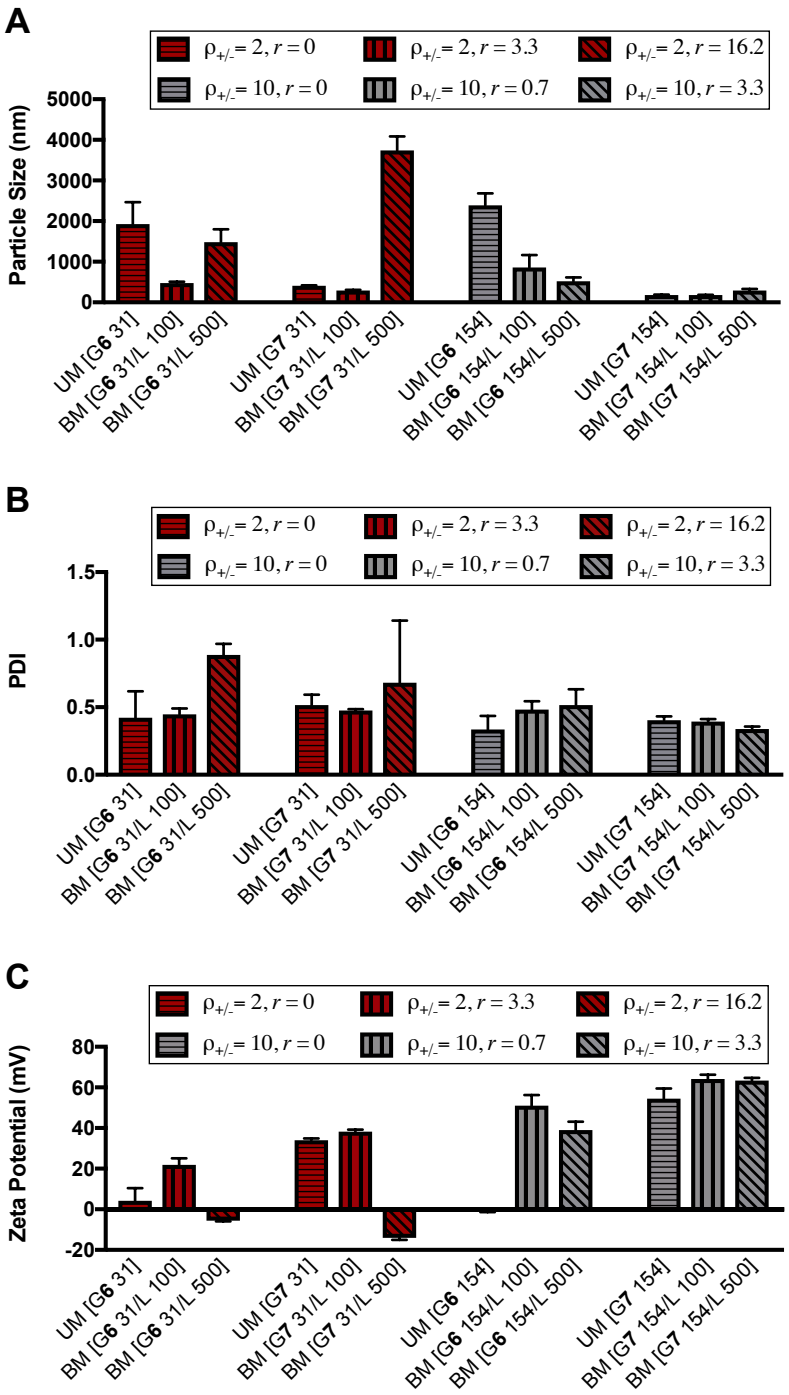

Fig. 4.2. Physical characterization of BM [G/L] lipoplexes formulated using RGDG-12 (G6), RGDG-18 (G7) as a function of $\rho_{\pm}$ (10, 2) and r (0, 0.7, 3.3, 16.2). (A) Hydrodynamic diameter, (B) PDI and (C) zeta potential of the lipoplexes were determined by DLS. Results are presented as mean ± SD from one experiment (n = 3).

4.2.2 *In vitro* transfection studies

The optimization of the BM [G/L] lipoplex delivery systems were also investigated as a function of $\rho_{\pm}$ and r, both for the number of the transfected cells and the intensity of gene expression level determined by MFI, using quantitative flow cytometry.

4.2.2.1 The impact of gemini to DNA N/P mole ratios ($\rho_{\pm}$ values) on transfection properties of BM [G/L] lipoplexes

Transfection activities of BM [G/L] lipoplexes were first investigated by varying $\rho_{\pm}$ values (10, 2) with identical DOPE molarity (M_L = 500) across 6 different gemini surfactants G**0**, G**1**, G**2**, G**3**, G**6**, G**7**, grouped into three categories m-3-m, m-7NH-m and m-7N(RGDG)-m (with m = saturated C12 or C18 alkyl tails). As shown in Figure 4.3, the percentage of the fluorescent positive cells were found to be slightly or significantly higher in all the BM [G/L] lipoplexes formulated at $\rho_{\pm}$ = 10 (with r = 3.3; prepared at M_L = 500) as compared to their counterparts formulated at $\rho_{\pm}$ = 2 (with r = 16.2; prepared at M_L = 500). In addition, the BM [G/L] lipoplexes formulated at $\rho_{\pm}$ = 10 using 18-series gemini surfactants generally resulted in slight or significant higher in the percentage of the fluorescent positive cells as compared to the counterparts with C12 alkyl tails (exception being observed for G**2** vs. G**3** lipoplexes with almost similar transfection percentages). However, in contrast to the high internalization of the BM [G/L] lipoplexes formulated at $\rho_{\pm}$ = 10, no significant increase in intensity of GFP expression levels were observed in the studied gemini surfactants as compared to control-untreated cells (Fig. 4.3 and Fig. D1, Appendix D). Noticeable trends were observed in the GFP expression levels of the BM [G/L] lipoplexes with decrease in $\rho_{\pm}$ values. As shown in Figure 4.3 and Figure D1 (Appendix D), all the BM [G/L] lipoplexes

formulated at $\rho_{\pm} = 2$ (with r = 16.2) resulted in an increase in the intensity of gene expression levels (MFI) as compared to the one formulated at $\rho_{\pm} = 10$ (with r = 3.3) (though statistically insignificant for G**1** and G**7** gemini surfactants).

The transfection activity of the BM [G/L] lipoplexes were also investigated at $\rho_{\pm} = 1$, 3 and 5 using m-7N(RGDG)-m gemini surfactants (G**6**, G**7**) with identical DOPE molarity ($M_L = 500$) (Fig. 4.4). The quantification of the MFI for the transfection agents containing G**6** formulated at $\rho_{\pm} = 5$ (with r = 6.5) or G**7** formulated at $\rho_{\pm} = 5$ (with r = 6.5) or at $\rho_{\pm} = 3$ (with r = 10.8) showed no significant increase in the intensity of GFP expression levels as comparted to that of formulated at $\rho_{\pm} = 10$ (with r = 3.3) or control-untreated cells. However, the G**6** gemini surfactants at $\rho_{\pm} = 3$ (with r = 10.8) resulted in an increase in MFI similar to that of formulated at $\rho_{\pm} = 2$ (with r = 16.2). Further reduction to $\rho_{\pm} = 1$ (with r = 33) resulted in a reduction in MFI for G**6** gemini surfactants whereas an increase in MFI for G**7** gemini surfactants as compared to their counterpart lipoplex formulated at $\rho_{\pm} = 2$ (with r = 16.2). This demonstrates that the protein expression is effective at a narrow range of $\rho_{\pm}$ values (approximately 1-3), and above which further compaction resulted in negligible protein expression. Considering both the percentage of the transfected cells and the MFI, the transfection activity of the BM [G/L] lipoplexes reach to their maximum at $\rho_{\pm} \approx 2$ for G**7**-formulated lipoplex and at $\rho_{\pm} \approx 3$ for G**6**-formulated lipoplex.

The impact of the $\rho_{\pm}$ values together with details on the effect of the alkyl tail lengths of the gemini surfactants on the percentage and MFI of the transfected cells (as explained above) elucidate the correlation between the GFP expression levels and the pDNA compaction of the BM [G/L] lipoplexes. In general, the low MFI levels of the transfected cells with the BM [G/L] lipoplexes formulated at $\rho_{\pm} > 2$ using gemini surfactant with 18C alkyl tails (G**7**) or at $\rho_{\pm} > 3$ using gemini

surfactant with 12C alkyl tails (G**6**) can be explained by the tight compaction of pDNA that hinders the endosomal release of pDNA into the cell cytoplasm. Following these findings, in a recently published work, the impact of lowering the $\rho_{\pm}$ values from 10 to 2.5 was also shown to increase the protein expression level of the lipoplexes formulated using Glycyl-Lysine modified gemini surfactants [320]. While the report discussed that the previous generations of gemini surfactants (i.e., m-3m, m-7NH-m) showed maximum transfection efficiency at $\rho_{\pm}$ = 10, this research, in contrast, provided a foundation that showed the m-3-m, m-7NH-m and functionalized m-7N(RGDG)-m (with m = saturated C12 or C18 alkyl tails) gemini based-lipoplexes all demonstrated GFP expression activity at $\rho_{\pm}$ around 1- 3.

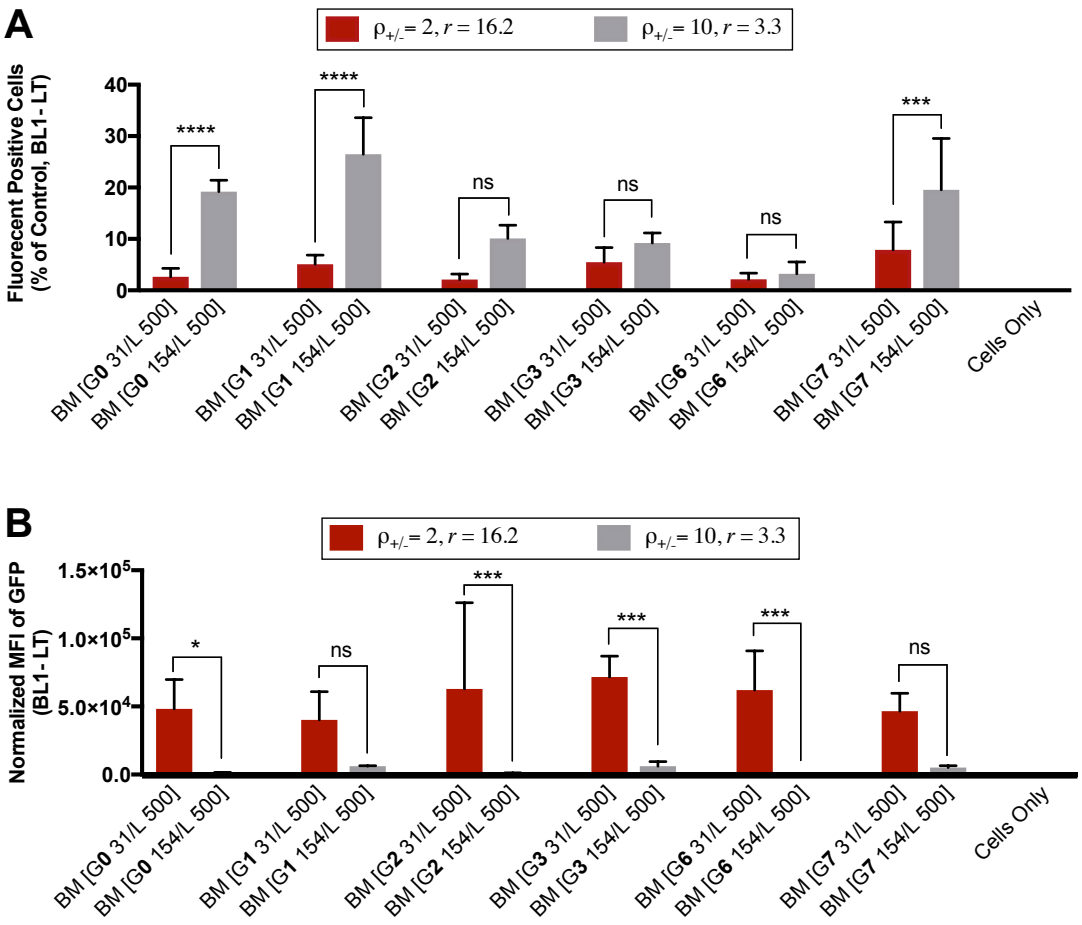

Fig. 4.3. Transfection studies of BM [G/L] lipoplexes formulated using 6 different gemini surfactants as a function of $\rho_{\pm} = 10, 2$ (M_G = 154 µM, 31 µM, respectively) with identical DOPE molarity at M_L = 500 µM, as quantified by flow cytometry. The intensities of GFP expression levels of the BM [G/L] lipoplexes increase at $\rho_{\pm} = 2$ (with r = 16.2) as compared to that of formulated at $\rho_{\pm} = 10$ (with r = 3.3). Results are presented as mean ± SD from two independent experiments (n = 6, 3 repeats per experiment) performed on 3T3 mouse fibroblast in 96-well plates. (A) The percentage of the transfected cells and (B) the intensity of GFP expression level (MFI) were normalized to untreated control (cells only) (* $p < 0.05$, ** $p < 0.01$, *** $p < 0.001$, **** $p < 0.0001$).

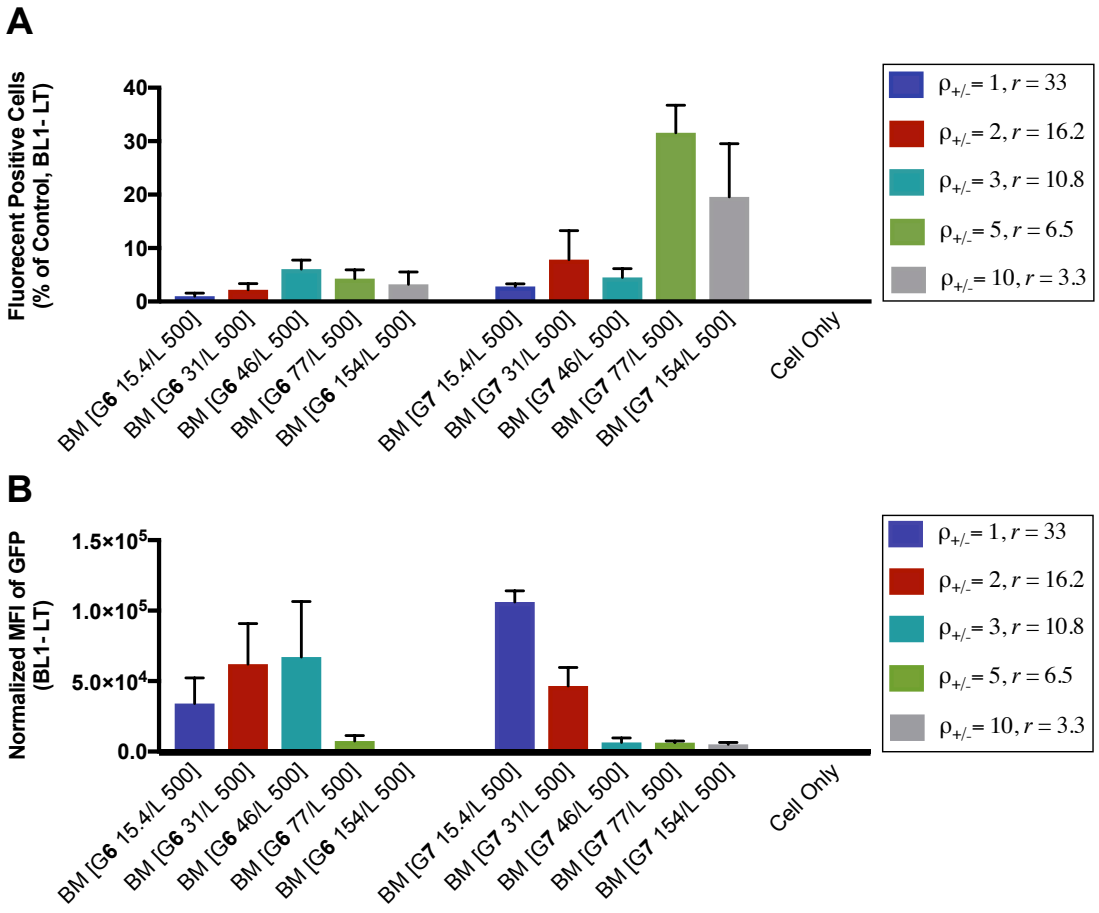

Fig. 4.4. Transfection studies of the BM [G/L] lipoplexes formulated using RGDG-12 (G**6)** and RGDG-18 (G**7)** gemini surfactants for delivery of pDNA to 3T3 mouse fibroblast. Optimization as a function of $\rho_{\pm}$ = 10, 5, 3, 2, 1 (M_G = 154 µM, 77 µM, 46 µM, 31 µM, 15.4 µM, respectively) with identical DOPE molarity at M_L = 500 µM, as quantified by flow cytometry. Results are presented as mean ± SD from one or two independent experiments (3 repeats per experiment) performed in 96-well plates. (A) The percentage of the transfected cells and (B) the intensity of GFP expression level (MFI) were normalized to untreated control (cells only).

4.2.2.2 The impact of DOPE/gemini molar ratios (r values) and RGDG functionalization of gemini surfactants on transfection properties of BM [G/L] lipoplexes

As shown in the previous section, the transfection activities of BM [G/L] lipoplexes using m-3-m, m-7NH-m and m-7NH(RGDG)-m formulated at $\rho_{\pm} = 2$ with r = 16.2 (M_G = 31 μM, M_L = 500 μM) resulted in an elevation in level of protein expression as compared to that formulated at $\rho_{\pm} = 10$ with r = 3.3 (M_G = 154 μM, M_L = 500 μM) (see Section 4.2.1.1.) To investigate the effect of r values on transfection properties of gemini-based lipoplexes, transfection studies were investigated by varying the molar concentration of DOPE (M_L = 500 μM, 300 μM, 100 μM, 0 μM) with identical $\rho_{\pm}$ value (2 or 10) using m-7NH-m (G**2** and G**3**) and m-7NH(RGDG)-m (G**6** and G**7**) gemini surfactants.

As shown in Figure 4.5, a decreasing trend in the percentage of transfection was found for all the gemini surfactants (G**2**, G**3**, G**6** and G**7**) formulated at $\rho_{\pm} = 2$ by decreasing r from 16.2 to 0 (with the only exception for G**6** formulated at r = 16.2 being slightly lower than that of formulated at r = 9.7). In contrast, reducing the lipid density of the lipoplex delivery systems formulated at $\rho_{\pm} = 2$ by decreasing r from 16.2 to 3.3 resulted in an increasing trend in the intensity of protein expression level (Fig. 4.5 and Fig. D2 (Appendix D)). Interestingly, G**3**-based lipoplexes formulated at $\rho_{\pm}$ = 2 and r = 0 (without DOPE helper lipid) resulted in significantly higher MFI as compared to that of formulated using G**2**, G**6** and G**7** (Fig. 4.5 and Fig. D2 (Appendix D)). In general, finding the right concentration of the constituents (M_G, M_L) in correlation with the molecular structures of gemini surfactants (head groups and the alkyl tails) is the determining factor in order to formulate stable particles that can improve internalization of the pDNA while effectively destabilize the endosomal membrane and release pDNA into the cytoplasm. As shown in Figure 4.5, among BM [G/L] lipoplexes formulated at $\rho_{\pm} = 2$ and r = 3.3, only G**7**-formulated lipoplexes showed

statistically significant increase in the percentage of the transfection as compared to control-untreated group (though not significant as compared to high dense particles).

Note that although G**7**-lipoplex formulated at $\rho_{\pm} = 2$ and r = 3.3 (particles with low lipid density) was observed to have the highest transfection activity, as shown in Figure 4.4, the intensity of the GFP expression level, determined at low threshold (LT) analysis, showed no significant improvement as compared to the control-untreated group, and even significantly lower as compared to that of formulated using G**3** or G**6** gemini surfactants (as shown in Figure 4.5). This is partly due to the skewing of the MFI by the background noise as described in Section 3.6. To avoid misinterpretation and better understand the flow cytometry data, it was necessary to compare the MFIs of all transfection reagents at high threshold (HT) analysis, as shown in Section 4.3. Therefore, in Section 4.3.2.1, the MFI of the G**7**-lipoplexes formulated at $\rho_{\pm}$ of 2 or 10 and r = 3.3 will be reassessed and compared with other formulations at HT. While quantification of the percentage of the fluorescent positive cells at LT can provide general information on the transfection percentage/penetration activity of various delivery formulations studied throughout this project, analysing the MFI at HT can allow us to better investigate their transfection activities and measure their GFP expression levels by flow cytometry (refer to Section 4.3).

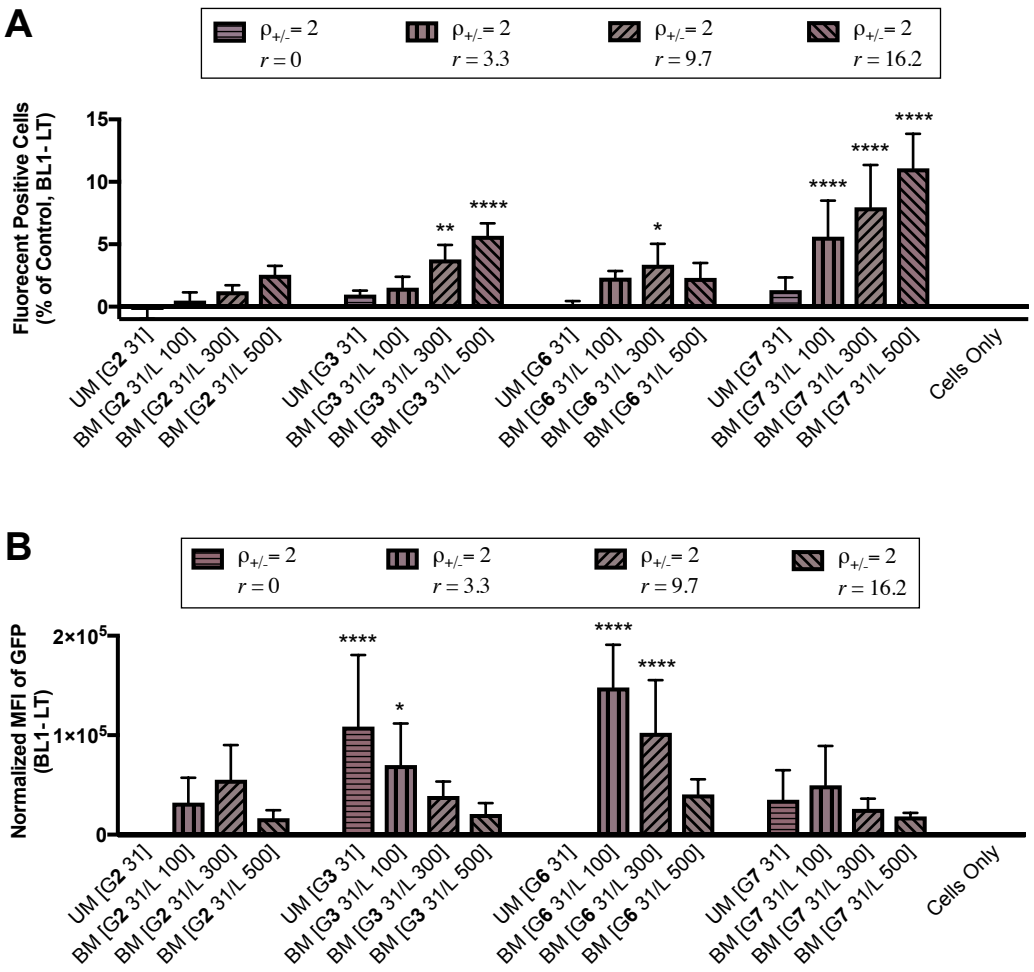

Fig. 4.5. Transfection studies of the gemini-based lipoplexes formulated using 12-7NH-12 (G**2**), 18-7NH-18 (G**3**), RGDG-12 (G**6**) and RGDG-18 (G**7**) gemini surfactants as a function of r = 16.2, 9.7, 3.3, 0 (prepared at M_L = 500 μM, 300 μM, 100 μM, 0 μM, respectively) with identical $\rho_{\pm} = 2$ (prepared at M_G = 31 μM), as quantified by flow cytometry. Results are presented as mean ± SD from two independent experiments (n = 6, 3 repeats per experiment) performed on 3T3 mouse fibroblast in 96-well plates. (A) The percentage of the transfected cells and (B) the intensity of GFP expression level (MFI) were normalized to untreated control (cells only). *Asterisks* indicate statistical significance compared to untreated control (* $p < 0.05$, ** $p < 0.01$, **** $p < 0.0001$).

The impact of r values on transfection activity of the G**7**-based lipoplexes was further investigated at $\rho_{\pm}$ = 10 by varying the DOPE lipid density (e.g., r = 3.3, 2, 0.7, 0) and compared to the G**7** lipoplexes formulated at $\rho_{\pm}$ = 2 and r = 3.3 (Fig. 4.6). It was shown that decreasing the lipid density at $\rho_{\pm}$ = 10 by reducing the r value from 3.3 to 2, to 0.7 and finally 0 (without DOPE), as shown in Figures 4.6 and Figure D3 (Appendix D), revealed no significant improvements in the intensity of GFP expression levels as compared to the control-untreated cells. In addition, further increasing the DOPE lipid density at $\rho_{\pm}$ = 10 by increasing the DOPE molarity above 500 μM (r above 3.3) also showed no effect in intensity of protein expression levels (data not shown). As shown in Figure 4.6, the MFI at LT analysis demonstrated that the intensity of GFP expression level was increased approximately up to 27-fold for G**7**–based lipoplex formulated at $\rho_{\pm}$ = 2 with r = 3.3 as compared to that of formulated at $\rho_{\pm}$ = 10 with varying lipid density (e.g., r = 3.3, 2, 0.7, 0).

Therefore, as per data shown above, at $\rho_{\pm}$ = 10, changing the r values showed no effect on the transfection activities of the G**7**-based lipoplexes. This is thought to be due to the tight compaction capability of the cationic gemini surfactants that regardless of the DOPE lipid density of the lipoplex delivery systems, hinder the release of pDNA. However, at $\rho_{\pm}$ = 2, reducing the r value could form particles with a thin lipid membrane that although resulted in reduced penetration activity, had further improvements on the pDNA release into the cytoplasm. Among the lipoplexes with low lipid density formulated at $\rho_{\pm}$ = 2 and r = 3.3, G**7** (formula: 18-7N(RGDG)-18) gemini surfactant having long alkyl tails with RGDG surface functional headgroup resulted in higher transfection activity (both the percentage of the transfected cells and the intensity of protein expression level) comparing to that of formulated using G**2** (formula: 12-7NH-12) and G**3** (formula: 18-7NH-18) as well as RGDG-functionalized G**6** (formula: 12-7N(RGDG)-12) gemini surfactants (Fig. D2, Appendix D).

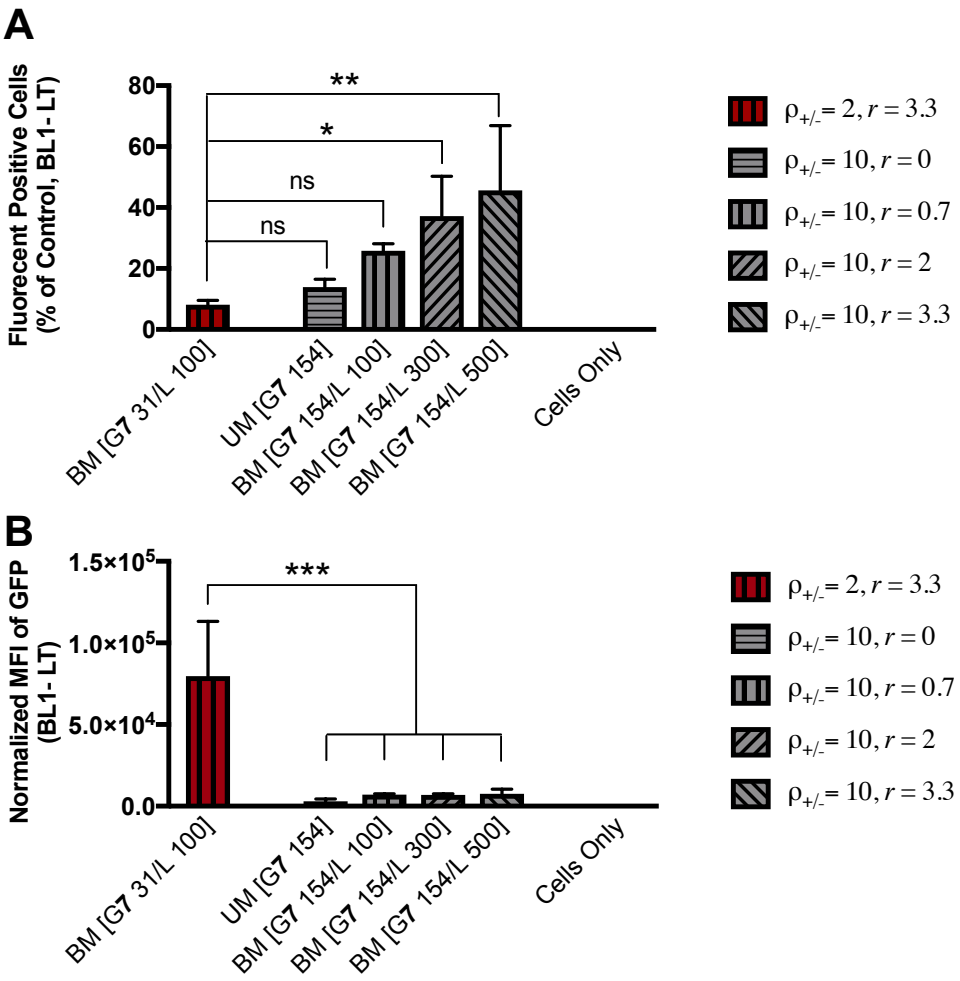

Fig. 4.6. Transfection studies of the RGDG-18 (G**7**)-based lipoplexes as a function of r = 3.3, 2, 0.7, 0 (prepared at M_L = 500 μM, 300 μM, 100 μM, 0 μM, respectively) with identical $\rho_{\pm}$ = 10 (prepared at M_G = 154 μM) as compared to the optimized G**7**-based lipoplexes formulated at $\rho_{\pm}$ = 2, r = 3.3 (i.e., BM [G**7** 31/L 100]). Results are presented as mean ± SD from one experiments (n = 3) performed on 3T3 mouse fibroblast in 96-well plates, as detected by flow cytometry. (A) The percentage of the transfected cells and (B) the intensity of GFP expression level (MFI) were normalized to untreated control (cells only) (* $p < 0.05$, ** $p < 0.01$, *** $p < 0.001$).

4.3 Development of versatile peptide-based lipopolyplexes: peptide-driven tri-modal gene delivery systems (PDTMG)

As shown in the Section 4.2, the BM [G/L] lipoplexes formulated using m-7NH-m (G**2** and G**3**) and m-7N(RGDG)-m (G**6** and G**7**) were found to have the highest transfection activity at $\rho_{\pm} = 2$ and r = 3.3 (prepared at $M_G = 31$ μM, $M_L = 100$ μM). However, the transfection percentages and the stability of the particles were low. That was shown to be due to both reduced lipid densities and the low zeta potentials of the gemini-based lipoplexes. To improve the physicochemical properties and the transfection activity of the delivery systems, the impact of non-covalent addition of several peptide enhancers that differ in their charges (0, 0.5, 3.2, 6.3) and lengths (consisting of histidine and/or arginine residues and/or targeting RGD motif (GRGDSP); as listed in Table 2.2) were investigated using DLS and flow cytometry. These include zwitterionic RGD peptide enhancers (i.e., P_A), cationic $(R)_6$-$(H)_3$ peptide enhancers (i.e., P_B), bi-functional cationic RGD-$(R)_6$-$(H)_3$ peptide enhancers (i.e., P_C), cationic $(H)_5$ peptide enhancers (i.e., P_D), bi-functional cationic RGD-$(H)_5$ peptide enhancers (i.e., P_E), cationic $(H)_{12}$-$(R)_2$ peptide enhancers (i.e., P_F) and bi-functional cationic RGD-$(H)_{12}$-$(R)_2$ peptide enhancers (i.e., P_G). In addition, the impact of structural variations in the spacer groups and functional headgroups of gemini surfactants in conjunction with alteration of their alkyl chain lengths (G**1**-G**14**, as listed in Table 2.1) were investigated. The GRGDSPG-18 (G**8**), 18-E-PepD (G**9**)**,** and 18-E-PepE (G**10**) gemini surfactants were co-designed and synthesized to include functional headgroups with RGD peptide, $(H)_5$ peptide, and bi-functional cationic RGD-$(H)_5$ peptide, respectively. These provided a comparison on the effect of the covalent linking and non-covalent addition of P_A, P_D and P_E in transfection activity of PDTMG delivery systems. The correlation of the compositional elements and the structural modification of gemini surfactants together with the transfection activity and

cytotoxicity of the delivery systems were identified for development of various peptide-based lipopolyplexes (PDTMG) as shown below.

4.3.1 Particle size and zeta potential analysis: uni-modal, bi-modal and tri-modal gene delivery systems

Due to the numerous possibilities in formulating various gene delivery formulations containing peptide enhancers (7 types) or in combination with gemini surfactants (14 types) and/or DOPE lipid at their optimal ratios, the physicochemical properties of selected delivery formulations were characterized to provide a rational in formulating an effective gene delivery formulation.

To investigate the effect of the peptide enhancers on physical properties of gene delivery complexes, the particle size diameters, PDI and zeta potential of various gene delivery systems (i.e., UM [P], BM [P/L], BM [P/G], PDTMG [P/G/L]) were investigated by DLS at varying molar concentrations of the compositional elements.

4.3.1.1 UM [P] gene delivery systems

As shown in Figure 4.7, the UM [P] gene delivery systems formulated using zwitterionic P_A peptide enhancers or cationic P_B or P_C peptide enhancers all showed small Z-average particle sizes. Zeta potential measurements showed that increasing the peptide molarities of P_B and P_C from 10 μM to 98 μM, increased the zeta potentials of the UM [P] complexes to approximately +20 mV, suggesting the binding of the cationic peptide enhancers to pDNA and neutralization of its negative charge. Increasing the peptide molarity of zwitterionic RGD peptide enhancers (i.e., P_A), however, showed no significant changes in the zeta potentials of the UM [P_A] complexes, indicating the pDNA was not efficiently neutralized nor compacted.

4.3.1.2 BM [P/L] gene delivery systems

The complexation of pDNA with zwitterionic P_A peptide enhancers and DOPE lipid formulated at M_P = 62 μM and high DOPE molarity (M_L = 500 μM), showed small size particles (111.2 ± 0.4 nm for the BM [P_A62 /L 500] formulation; Fig 4.7). As shown in Figure 4.7, increasing the P_A molarity (M_P = 62 μM, 154 μM, 308 μM) did not significantly change the sizes and zeta potentials of the formulated BM [P/L] complexes and interestingly all exhibited strongly negative zeta potential values (approximately −50mV to −40mV), suggesting that pDNA was inefficiently neutralized. In contrast, increasing the peptide molarity of the cationic peptide enhancers (i.e., P_B and P_C; M_P = 10 μM, 25 μM, 49 μM, 98 μM) strongly increased the sizes of the BM [P/L] complexes to large aggregates and noticeably increased the zeta potentials from negative values to positive values. This may indicate that while increasing the cationic peptide molarity resulted in increasing the positive charges of peptide/DNA complexes, the repulsive forces between the cationic peptides resulted in formation of larger aggregates. This may also suggest the inability of the zwitterionic DOPE for sufficient compaction of BM [P/L] complexes. It was found that decreasing the DOPE lipid density of the BM [P/L] complexes by decreasing the DOPE lipid molarity (M_L = 100 μM), the size of the complexes formulated using P_B or P_C strongly decreased (261.1 ± 7.1 nm and 341.9 ± 12.5 nm for BM [P_B 98/L 100] and BM [P_C 98/L 100], respectively; Fig 4.7). The BM [P_B 98/L 100] and [P_C 98/L 100] complexes showed the zeta potentials of approximately +20 mV.

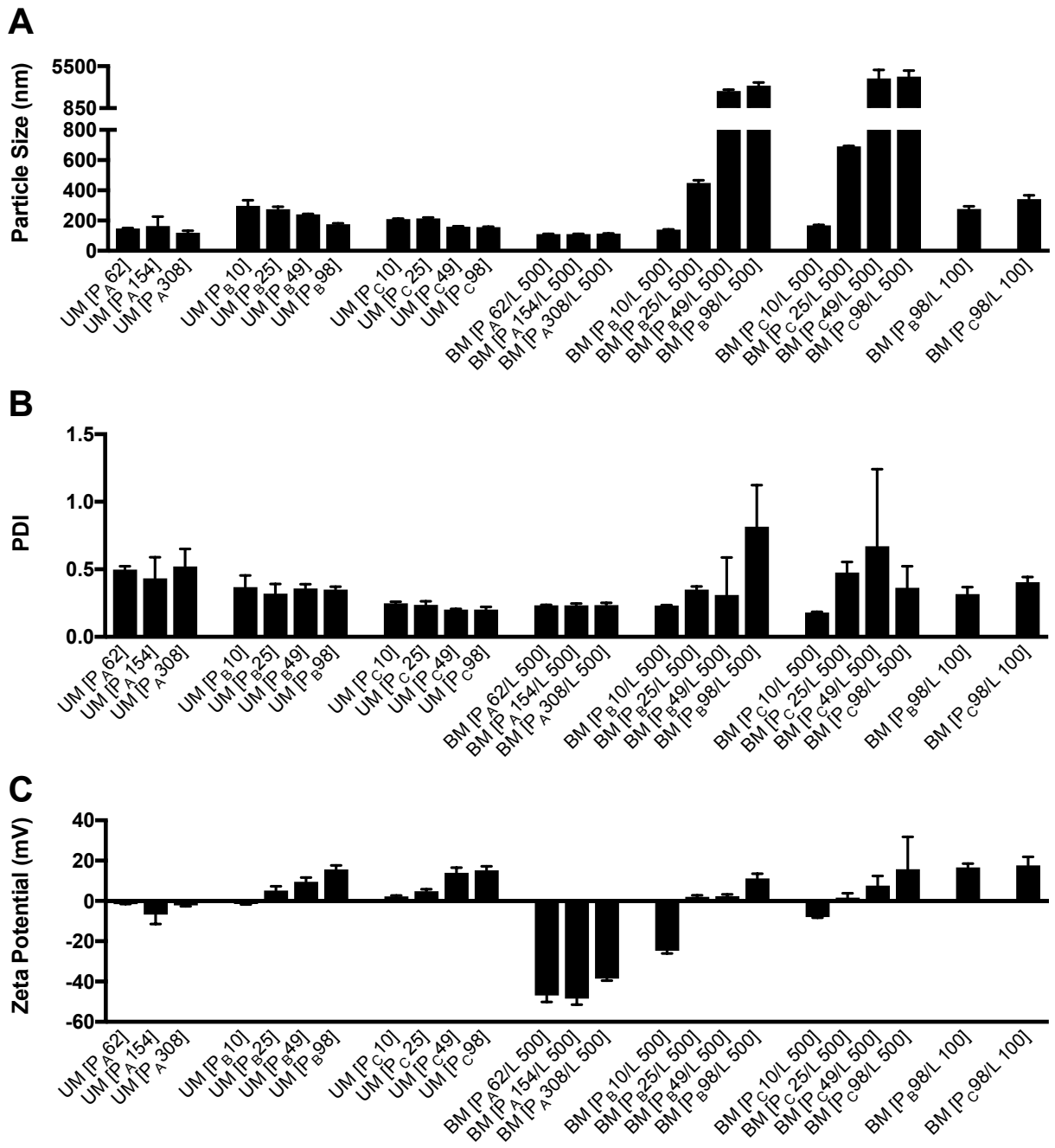

Fig. 4.7. Physical characterization of UM [P] and BM [P/L] gene delivery systems formulated using zwitterionic P_A, cationic P_B or P_C peptide enhancers at varying molar concentration of the compositional elements. (A) Hydrodynamic diameter, (B) PDI and (C) zeta potential of the complexes were determined by DLS. Results are presented as mean ± SD (n = 3).

4.3.1.3 BM [P/G] gene delivery systems

As shown in Figure 4.8, BM [P/G] gene delivery systems formulated using cationic peptide enhancers (i.e., P_B or P_C) at M_P = 49 μM, 98 μM and gemini surfactants (i.e., G**6** or G**7**) at $\rho_{\pm}$ = 2 (prepared at M_G = 31 μM) yielded small size particles (≈136 nm to ≈ 251 nm), indicating the synergistic effects of the cationic peptide enhancers and the gemini surfactants for pDNA condensation as compared to the corresponding UM [G] complexes (G**6** or G**7** formulated at $\rho_{\pm}$ = 2), which formed large aggregates (refer to Section 4.2.1, Fig. 4.2). The zeta potential of all the formulated BM [P/G] gene delivery systems were also found to be substantially higher than BM [P/L] gene delivery complexes, and amongst the BM [P/G] complexes, those formulated with G**7** gemini surfactants generated significantly higher surface charges than that of formulated using G**6** gemini surfactants (e.g., ζ-potential: +40.0 ± 0.8 mV vs. +30.1 ± 1.1 mV vs.+17.6 ± 2.1 mV for BM [P_C 98/G**7** 31], BM [P_C 98/G**6** 31] and BM [P_C 98/L 100], respectively). Comparing with BM [G/L] lipoplexes formulated at $\rho_{\pm}$ = 2 and r = 3.3 (Fig. 4.2), the BM [P/G] complexes formulated at $\rho_{\pm}$ = 2 with cationic peptide enhancers at M_P of 49 μM or 98 μM showed smaller size particles and slightly higher zeta potentials. Further details on the synergistic effects between the cationic peptide enhancers and gemini surfactants in complexation of pDNA will be described in the following section (4.3.1.4).

4.3.1.4 PDTMG gene delivery systems

Systematic characterization of various types of PDTMG formulations were carried out by combining zwitterionic or cationic peptide enhancers (i.e., P_A, P_B, P_C, P_D, P_E, P_F, P_G) with several gemini surfactants (i.e., G**6**, G**7**, G**9**, G**10**) and DOPE lipid at different molarities of the

compositional elements to provide a general view on the physical properties of the numerous PDTMG complexes, studied in this project.

Formulating the pDNA by the zwitterionic P_A peptide enhancers in combination with G**6** gemini surfactants and DOPE at $\rho_{\pm} = 2$ and r = 3.3 (i.e., PDTMG [P_A308, G**6** 31, L 100]) generated large aggregates (≈ 1.9 μm; Fig. 4.8 (A)) with significantly low zeta potentials (+1.1 ± 0.4 mV; Fig. 4.8 (C)), indicating insufficient pDNA charge neutralization and complexation. This may further suggest the role of P_A in preventing the pDNA complexation in the PDTMG [P_A308, G**6** 31, L 100] formulation when compared to the counterpart BM [G**6** 31/L 100] formulation, which were shown to form particles with positive surface charges (refer to data shown in Section 4.2.1, Fig. 4.2). PDTMG complexes formulated using P_A and G**7** gemini surfactants (PDTMG [P_A308, G**7** 31, L 100]), however, resulted in similar average size particles compared with the BM [G**7** 31/L 100] lipoplexes (prepared using G**7** at $\rho_{\pm} = 2$ and r = 3.3) but with significantly reduced zeta potential. This phenomenon is thought to be correlated with the association of gemini surfactants in the presence of peptide enhancers and DNA in which these dynamics affect the effective DNA compaction process. There are several interactions that can be responsible for polymer-surfactant association including hydrophobic interaction and electrostatic interactions [321, 322]. As stated previously (Section 4.2.1), the extent of the pDNA compaction in BM [G/L] lipoplexes is more likely related with the lipid density and the alkyl chain length of gemini surfactants. According to the zeta potential measurements for the UM [P] formulations (Section 4.3.1.1), it was shown that the zwitterionic P_A peptide enhancers generated negatively charged particles, suggesting that pDNA was not sufficiently neutralized nor efficiently compacted, as indicated by the negative zeta potential of the particles (Section 4.3.1.1, Fig. 4.7). Therefore, it is thought that the increased P_A molarity (M_P = 308 μM) resulted in dispersion of pDNA and lowering the association of gemini

surfactants for effective compaction and DNA charge neutralization when compared to the BM [G 31/L 100] lipoplexes formulated using G**6** or G**7** gemini surfactants. This explanation may be further supported, in a complementary manner, by comparing the effect of the cationic peptide enhancers in formation of PDTMG complexes.

As shown in Figure 4.8, the addition of the cationic peptide enhancers (i.e., $P_{B,}$ P_C; M_P = 49 μM-98 μM) in formulating PDTMG, prepared using G**6** or G**7** at $\rho_{\pm}$ = 2 and r = 3.3 (M_G = 31 μM, M_L = 100 μM), all generated smaller size complexes (from ≈ 141 nm to ≈ 246 nm) with significantly increased zeta potentials as compared to the corresponding BM [G 31/L 100] lipoplexes, and amongst the cationic PDTMG complexes, those formulated by G**7** showed higher zeta potentials (from ≈ +45 mV to ≈ +52 mV) than that of formulated by G**6** (from ≈ +35 mV to ≈ +40 mV). As previously shown, the UM [P] complexes formulated using cationic P_B or P_C showed higher zeta potentials than those formulated using zwitterionic P_A, suggesting the higher association/complexation of pDNA for the complexes formulated with the cationic peptide enhancers (i.e., P_B or P_C) compared to that of formulated with the zwitterionic P_A peptide enhancers. Therefore, it is believed that in the PDTMG formulation, the higher association of cationic peptide enhancers with pDNA may lead to the higher association of gemini surfactants to the pDNA-cationic peptide complexes, and hence synergistically resulting in higher degree of complexation and effective DNA charge neutralization in the PDTMG formulations. Therefore, the synergistic contribution of all the components of the PDTMG delivery system (i.e., cationic peptide enhancers, gemini surfactants and DOPE lipids) provided more efficient pDNA compaction as compared to the counterpart lipoplex formulations at the equal lipid molarities and uni-modal peptide-DNA complexes. These collectively may further support the hypothesis of this project, in that, the cationic peptide enhancers intercalating pDNA forms inner core peptide/pDNA

complex, which are surrounded and compacted by the gemini/DOPE lipids. This proposed model is in an alignment with the previous research studying the supramolecular assembly of peptide-based lipopolyplexes [258-260].

Generally, the degree of the pDNA compaction and charge neutralization by cationic peptide enhancers can be correlated with the length and charge of the cationic polymers. As shown in Figure 4.9, the PDTMG [P 67/G 27/ L 100] complexes formulated at $\rho_{\pm} = 1.7$ and r = 3.8, using cationic P_C, P_D, P_E, P_F or P_G peptide enhancers, G**7** gemini surfactants and DOPE, all resulted in formation of particles with high positive zeta potentials (from ≈ +44 mV to ≈ +50 mV). The Z-average particle size for the PDTMG [P 67/G**7** 27/ L 100] complexes formulated using P_C, P_F or P_G peptide enhancers were from ≈ 154 nm to ≈ 165 nm for (Fig. 4.9), and for the ones formulated using P_D and P_E were ≈ 386 nm and ≈ 279 nm, respectively. The higher Z-average particle size for the PDTMG complexes formulated using P_D and P_E might be due to the lower pDNA compaction associated with the low positive charge of the cationic peptide enhancers (i.e., net positive charge at pH 7 = 0.5; Table 2.2) as it was also reported that a minimum of six to eight positive charges in a polypeptide are required for efficient DNA condensation [86, 323-325]. From the data presented above, it was observed and can be predicted that the physical characteristics of various PDTMG delivery systems, formulated in a similar condition using the cationic peptide enhancers, gemini surfactants with the same length saturated alkyl tails, and DOPE, generate particles with similar size and zeta potential, and among the PDTMG complexes, those formulated using gemini surfactants with saturated 18C alkyl tails had higher zeta potentials compared to that of formulated using gemini surfactants with saturated 12C alkyl tails. These observations were in alignment to the physical studies of various lipopolyplex gene delivery systems formulated using various

cationic peptides (whether linear, branched or dendritic) in combination with DOTMA and DOPE, that exhibited also similar size, surface charge and lipid bilayer structure [326, 327].

Further investigation in formulating the compositional elements of the PDTMG delivery systems using cationic P_C peptide enhancers, G**7**, G**9**, G**10** gemini surfactants, and DOPE showed that by increasing the molar concentrations of cationic peptide enhancers (M_P = 67 μM, 133 μM, 267 μM) along with the fine tuning of gemini surfactants and DOPE, as shown in Figures 4.9 and 4.10, could also generate small particles (from ≈ 147 nm to ≈ 174 nm) with highly positive zeta potentials (from ≈ +44 mV to ≈ +60 mV) (Fig. 4.9 and 4.10). For example, PDTMG formulated using P_C at M_P = 267 μM in combination with G**7** gemini and DOPE prepared at $\rho_{\pm}$ = 1.1 and r = 6.8 (i.e., PDTMG [P_C 267/G**7** 17/L 113]) generated particles with Z-average size diameter of 168.6 ± 0.6 nm, PDI of 0.188 ± 0.029 and zeta potential of +51.1 ± 0.3 mV, as presented in Figure 4.9.

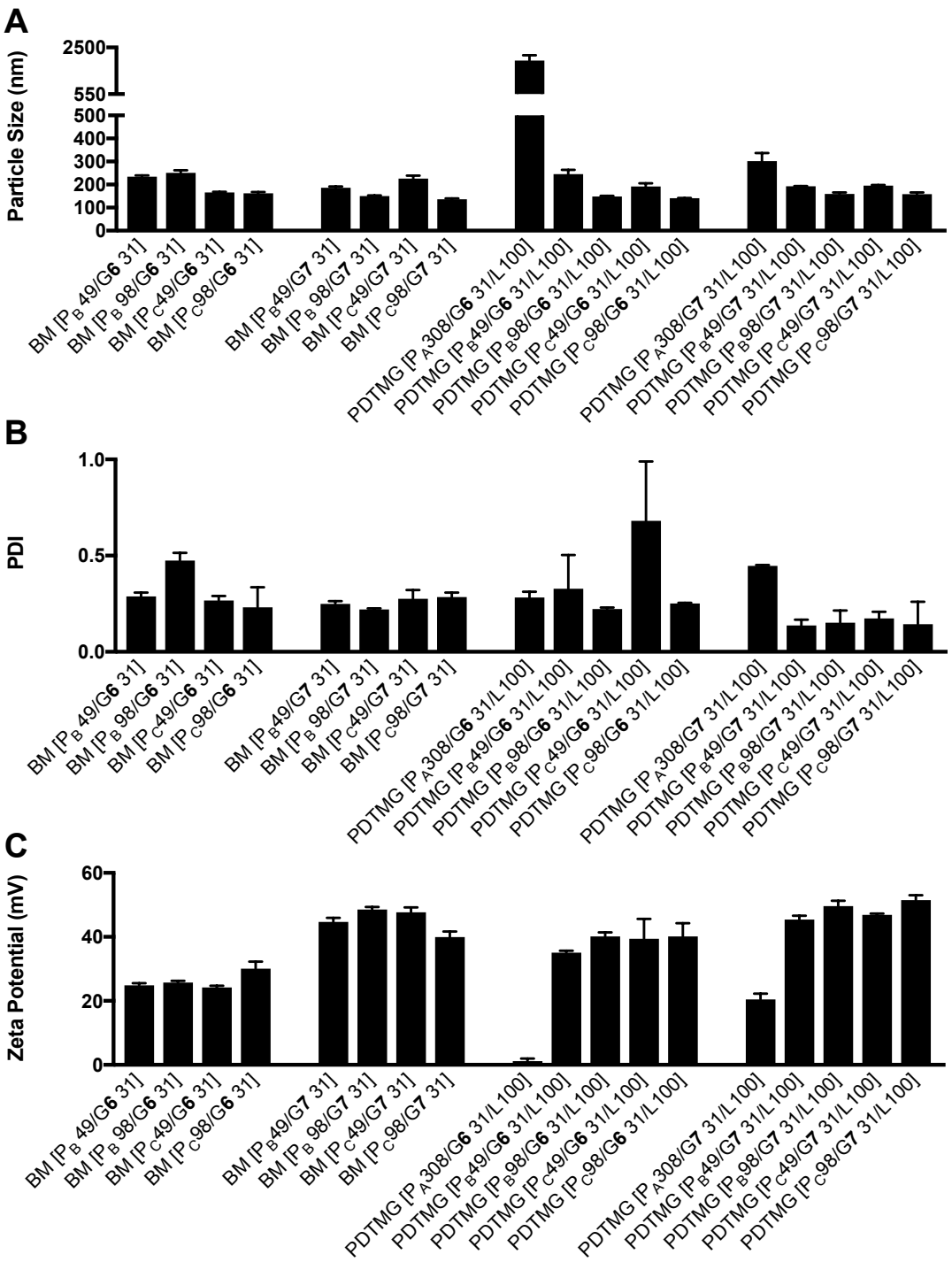

Fig. 4.8. Physical characterization of BM [P/G] and PDTMG [P/G/L] gene delivery systems formulated using P_A, P_B or P_C peptide enhancers in combination with RGDG-12 (G**6**) or RGDG-18 (G**7**) and/or DOPE helper lipid at $\rho_{\pm} = 2$ (prepared at $M_G = 31$ μM). (A) Hydrodynamic diameter, (B) PDI and (C) zeta potential of the complexes were determined by DLS. Results are presented as mean ± SD (n = 3).

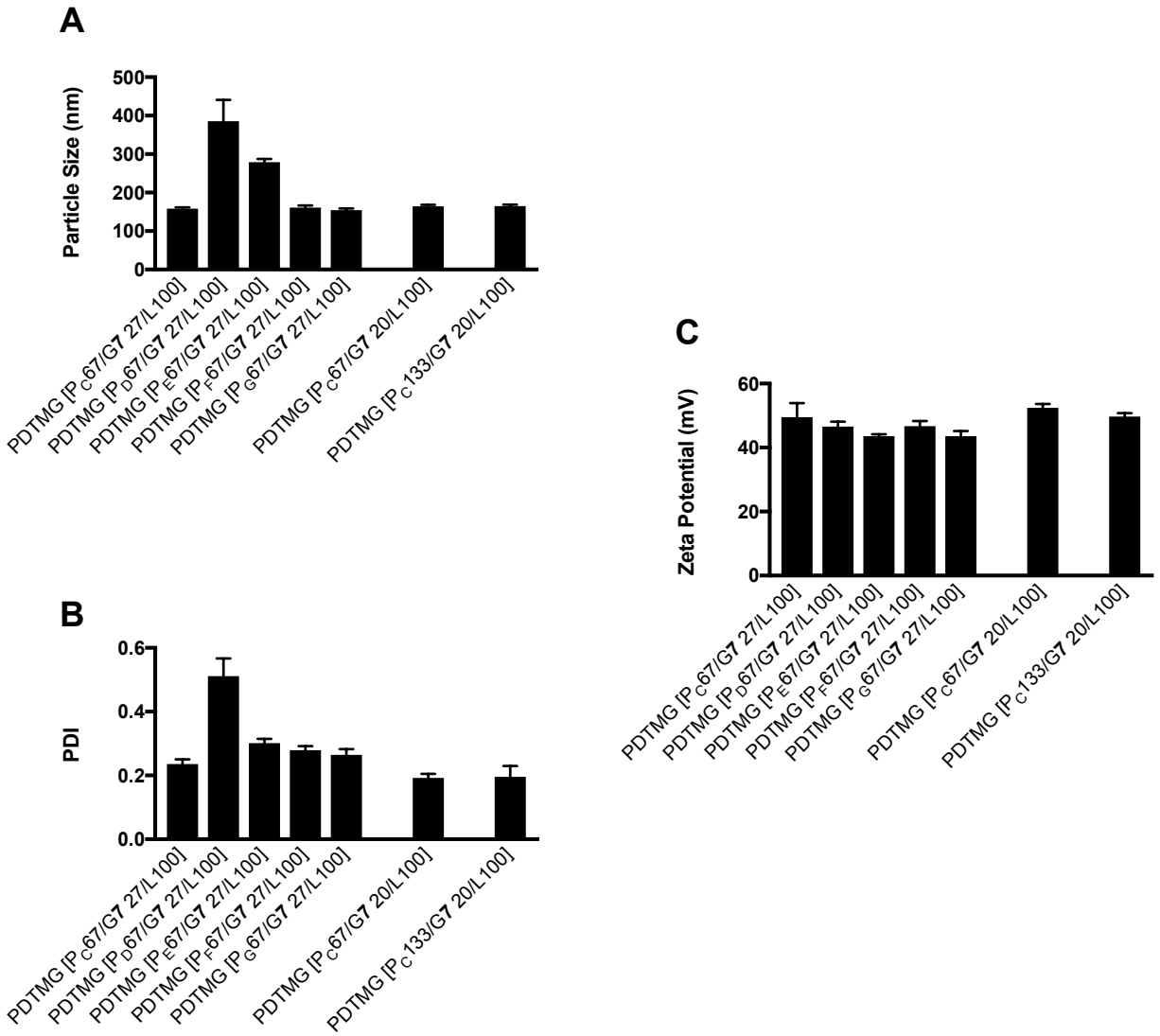

Fig. 4.9. Physical characterization of PDTMG [P/G/L] gene delivery systems formulated using cationic P_C, P_D, P_E, P_F or P_G peptide enhancers in combination with RGDG-18 (G**7**) and DOPE helper lipid at $\rho_{\pm}$ = 1.7 and 1.3 (prepared at M_G = 27 μM and 20 μM, respectively). (A) Hydrodynamic diameter, (B) PDI and (C) zeta potential of the complexes were determined by DLS. Results are presented as mean ± SD (n = 3).

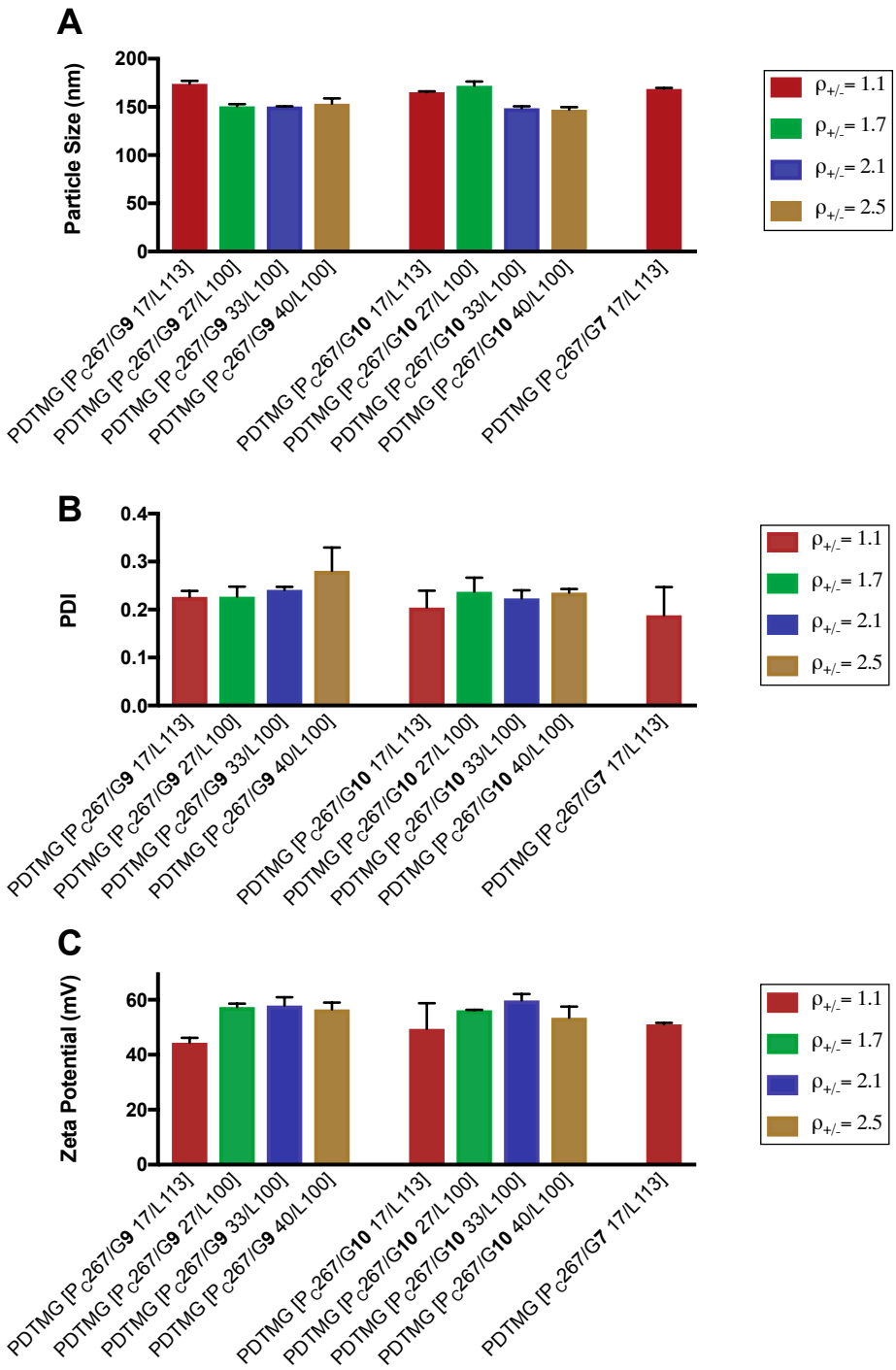

Fig. 4.10. Physical characterization of PDTMG [P/G/L] gene delivery systems formulated using cationic P_C peptide enhancers in combination with RGDG-18 (G**7**), 18-E-PepD (G**9**) or 18-E-PepE (G**10**) gemini surfactants and DOPE lipid at $\rho_{\pm}$ = 2.5, 2.1, 1.7 and 1.1 (prepared at M_G = 40 µM, 33 µM, 27 µM and 17 µM, respectively). (A) Hydrodynamic diameter, (B) PDI and (C) zeta potential of the complexes were determined by DLS. Results are presented as mean ± SD (n = 3).

4.3.2 Formulation strategies for development of potent gene delivery systems

4.3.2.1 *In vitro* transfection activities of uni-modal vs. bi-modal vs. tri-modal (PDTMG) gene delivery systems

In vitro transfection studies of various gene delivery systems, such as BM [G/L], UM [P], BM [P/L], BM [P/G] and PDTMG [P/G/L], were investigated using cationic P_C peptide enhancer, G**6** and G**7** gemini surfactants, and DOPE for delivery of gWiz^{TM} GFP pDNA to 3T3-mouse fibroblasts in 24-well plates. To lower skewing of the MFI and better compare the intensity of protein expression levels, as explained in Section 4.2.2.2, the MFI of various transfection formulations were assessed at HT.

Relative measurements of the intensity of GFP expression level at HT indicated that the MFI was approximately 20-fold higher for the optimized BM [G**7** 31/L 100] lipoplexes (prepared at $\rho_{\pm} = 2$ and r = 3.3) compared to the BM [G**7** 154/L 500] lipoplexes (prepared at $\rho_{\pm} = 10$ and r = 3.3) ($p < 0.001$) (Fig. 4.11 (B)). However, the cell penetration activity of the BM [G**7** 154/L 500] lipoplexes was significantly lower compared to the BM [G**7** 154/L 500] lipoplexes, as shown by the number of the cells transfected.

To further improve transfection activity, the effect of P_C peptide enhancers alone or in combination with G**7** (M_G = 31 μM) and/or DOPE (M_L = 100 μM) was investigated on both transfection percentage and the intensity of GFP expression level. As shown in Figure 4.11 (B), the UM [P_C49] formulation and the BM [P_C 49/L 100] showed no significant increase in the intensity of the GFP expression compared to control-untreated cells ($p > 0.05$). The lipopolyplex delivery system, PDTMG [P_C49/G**7** 31/L 100], showed around 2-fold higher transfection percentage compared to both the BM [G**7** 31/L100] formulation ($p < 0.0001$) and the BM [P_C49/G**7** 31] formulation ($p <$

0.0001). In addition, the MFI with PDTMG [P_C49/G**7** 31/L 100] was 1.8-fold higher than the BM [G**7** 31/L100] formulation ($p < 0.01$) and 3.1-fold higher than the BM [P_C49/G**7** 31] formulation ($p < 0.0001$) (Fig. 4.11 (A) and (B)). These experiments demonstrated the superiority of the transfection activity of the PDTMG [P_C/G**7**/L] complexes compared to the uni-modal (i.e., UM [G], UM [P]) and the bi-modal (i.e., BM [G/L], BM [P/L], BM [P/G]) counterparts. Therefore, it can be inferred that the cationic P_C peptide enhancers in combination with G**7** gemini surfactants and DOPE synergistically contributed to the enhanced GFP expression level of the PDTMG [P_C49/G**7** 31/L 100] complexes, as confirmed by both the increase in the percentage of the transfected cells and the enhanced MFI when compared to the counterpart uni-modal and bi-modal complexes.

Further increasing the amount of the P_C peptide enhancers, the BM [P_C196/G**7** 31] and the PDTMG [P_C244/G**7** 31/L 100] formulations exhibited increased transfection percentages ($p < 0.05$) (Fig. 4.11 (A)) and reduced MFIs (though statistically insignificant) (Fig. 4.11 (B)) compared to their respective counterparts formulated at M_P = 49 μM. In yet another transfection experiment, the PDTMG [P_C49/G**7** 31/L 100] formulation demonstrated an increase in GFP expression level compared to the PDTMG [P_C10/G**7** 31/L 100] formulation, as confirmed by both increase in the transfection percentage ($p < 0.05$) (Fig. 4.12 (A)) and the MFI (though statistically insignificant) (Fig. 4.12 (B)). These experiments collectively indicated that the transfection activity of the PDTMG complexes formulated using P_C, G**7** and DOPE at $\rho_{\pm} = 2$ and r = 3.3 (M_G = 31 μM, M_L = 100 μM) could be effectively improved by small increase in the peptide molarity from M_P = 10 μM to M_P = 49 μM, and above which (i.e., from 49 μM to 244 μM) no apparent differences were observed in the GFP expression levels (for further details, refer to Section 4.3.2.2).

By decreasing the length of the alkyl tails using G**6** gemini surfactants, it was found that there was no significant increase in the transfection percentages for the BM [G**6** 31/L100] lipopolexes and the PDTMG [P_C10/G**6** 31/L 100] complexes compared to control-untreated cells ($p > 0.05$) (Fig. 4.12 (A)). This demonstrated the superiority of the transfection activity of the G**7** gemini surfactants compared to G**6** gemini surfactants in both BM [G/L] and PDTMG [P/G/L] formulations (Fig. 4.12 (A) and (B)). The comparison of the transfection activities of G**6** vs. G**7** gemini surfactants formulated PDTMG delivery systems will be further investigated in Section 4.3.3.

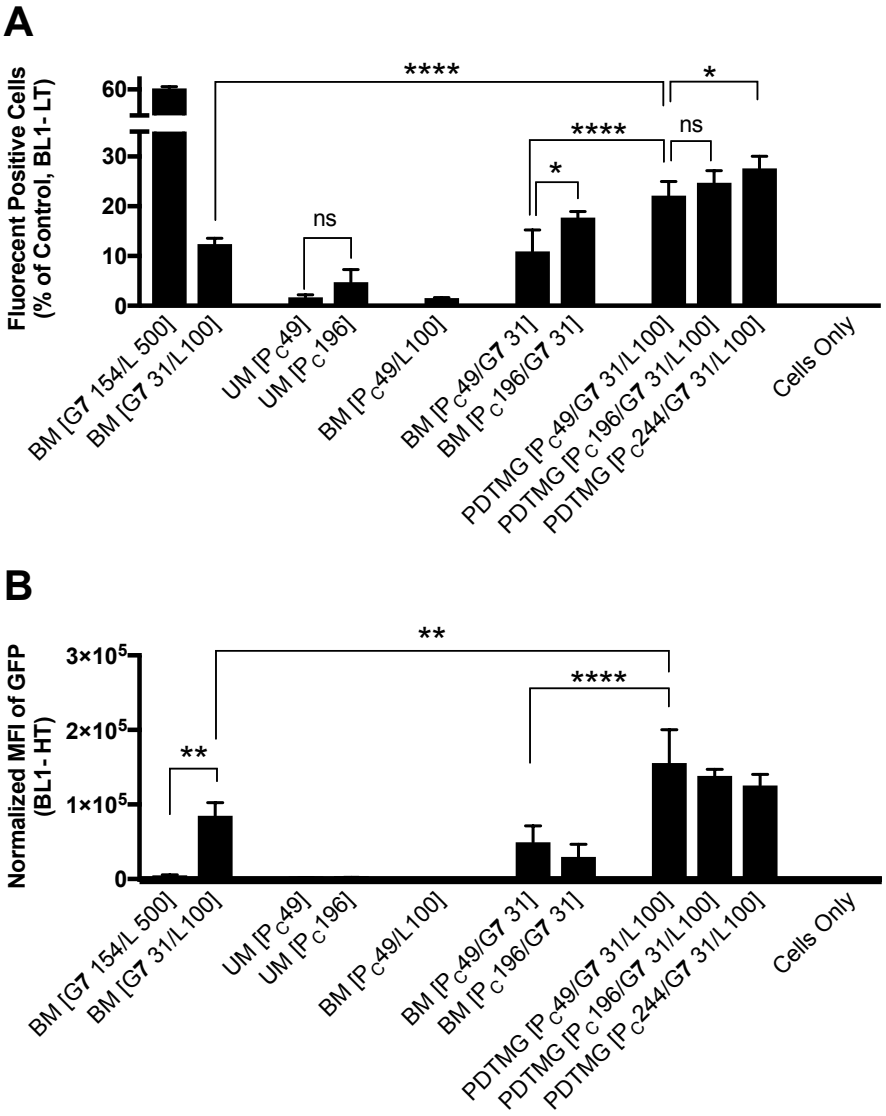

Fig. 4.11. The transfection activities of BM [G/L], UM [P], BM [P/L], BM [P/G] and PDTMG [P/G/L] gene delivery systems formulated from cationic P_C peptide enhancer and/or RGDG-18 (G**7**) gemini surfactant and/or DOPE helper lipid. Results are presented as mean ± SD from one or two independent experiments (n = 3 per experiment) performed in 24-well plate. (A) The percentage of the transfected cells and (B) the intensity of GFP expression levels were normalized to untreated control (cells only) (* $p < 0.05$, ** $p < 0.01$, **** $p < 0.0001$).

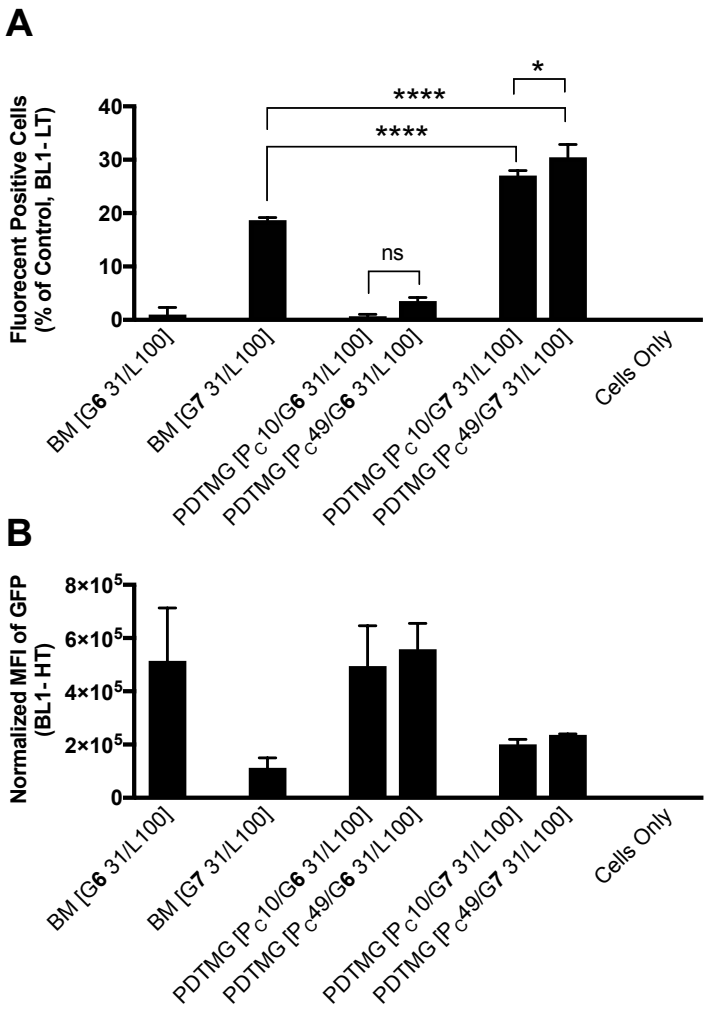

Fig. 4.12. The transfection activities of BM [G/L] lipoplexes and PDTMG [P/G/L] complexes formulated from cationic P_C peptide enhancer, and RGDG-12 (G**6**) or RGDG-18 (G**7**) gemini surfactant and DOPE helper lipid at $\rho_{\pm} = 2$ and r = 3.3. Results are presented as mean ± SD from one experiments (n = 3) performed on 24-well plate. (A) The percentage of the transfected cells and (B) the intensity of GFP expression levels were normalized to untreated control (cells only) (* $p < 0.05$ and **** $p < 0.0001$).

4.3.2.2 Optimization of the PDTMG nanoparticles: synergistic mechanism between peptide enhancer, gemini surfactant and DOPE lipid

Further optimization of the PDTMG [P_C/G**7**/L] nanoparticles by evaluating the transfection percentage and the MFI using flow cytometry led to better understand the synergistic mechanism of the delivery components for improvement in GFP expression level.

As shown previously (Section 4.3.2.1), the addition of cationic P_C peptide enhancers at M_P = 49 μM resulted in a significant increase in GFP expression level for PDTMG formulated at $\rho_{\pm}$ = 2 and r = 3.3 using G**7** gemini surfactants. However, further increase in the peptide molarity showed no improvement in the intensity of GFP expression levels (Fig. 4.11 (B)). As part of an optimization study, it was found that by decreasing the $\rho_{\pm}$ from 2 to 1.1 along with increasing the M_P from 49 μM to 267 μM and fine tuning of DOPE to gemini molar ratio at r = 6.8, PDTMG [P_C267/G**7** 17/L 113] exhibited the highest transfection activity with a 2.3-fold increase in the MFI compared to PDTMG [P_C49/G**7** 31/L 100] (Fig. 4.13). This demonstrated synergistic effects of the components of the PDTMG complexes in formation of nanoparticle for effective cellular and intracellular pDNA delivery. Figure E1 (Appendix E) provide a further detail on the optimization of the compositional elements of the PDTMG nanoparticles in relation to their transfection activities. It is important to note that while decreasing the $\rho_{\pm}$ from 2 to 1.1 by decreasing the gemini molarity from M_G = 31 μM to M_G = 17 μM showed high transfection activity, decreasing the gemini molarity by increasing the volume of the formulation mixture resulted in significant reduction in transfection activity of PDTMG complexes (Fig. 4.14). This demonstrated the dispersion effect in formation of nanoparticles in which at the equal amounts of the peptide, gemini surfactant and DOPE (the same mole amounts) (i.e., PDTMG formulated at $\rho_{\pm}$ = 2 and r = 3.3) reducing the concentration of the compositional elements by increasing the volume of the

formulation mixture did not form effective PDTMG nanoparticles, and led to near total loss of GFP expressions (Fig. 4.14 (B)). This can validate the hypothesis of this project that synergistic effects of the components of the PDTMG resulted in formation of nanoparticles that can effectively complex pDNA for effective cellular uptake and endosomal release. This phenomenon could be further explained by the effect of polymer-surfactant association for effective DNA compaction process. It is thought that the high association of cationic peptide enhancers with pDNA forming a peptide-pDNA core provided a platform for effective association of gemini surfactants along with DOPE at such low lipid molarities (M_G = 17 μM; M_L = 113 μM). Therefore, the PDTMG [P_C267/G**7** 17/L 113] delivery system (prepared at $\rho_{\pm}$ = 1.1 and r = 6.8) could effectively compact pDNA for uptake mechanism and once ingested, could disassemble, rupture endosome and release its peptide-DNA cargo into the cell cytoplasm.

The optimization of the PDTMG formulation provided a better understanding on the formation of PDTMG nanoparticle and further elucidated the effect of the compositional elements and their supramolecular assembly in correlation with their cellular uptake and endosomal release. Further details on the effect of the peptide enhancers and molecular architecture of gemini surfactants on the compaction and release of pDNA will be described in the following sections (refer to Section 4.3.3, 4.3.4 and 4.3.5).

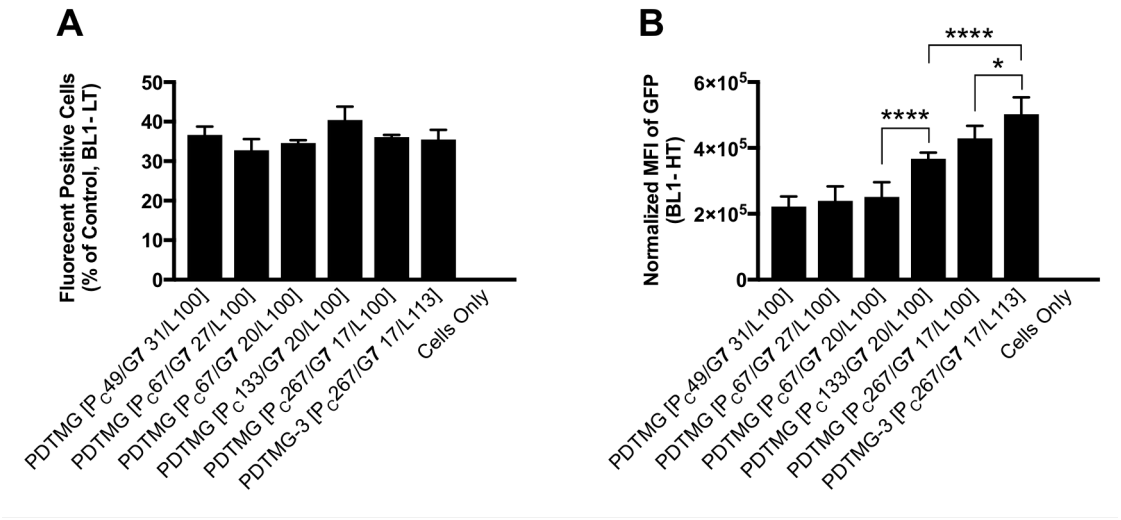

Optimization study: Formulations	**Experiments** #	n	$\rho_{+/-}$	***r***
PDTMG [P_C49/G**7** 31/L100]	1	3	2	3.3
PDTMG [P_C67/G**7** 27/L100]	2	6	1.7	3.8
PDTMG [P_C67/G**7** 20/L100]	1	3	1.3	5.0
PDTMG [P_C133/G**7** 20/L100]	2	5	1.3	5.0
PDTMG [P_C267/G**7** 17/L100]	2	4	1.1	6.0
PDTMG [P_C267/G**7** 17/L113]	3	6	1.1	6.8
Cells Only	6	14	-	-

Fig. 4.13. Optimization of PDTMG complexes formulated from cationic P_C peptide enhancer, RGDG-18 (G**7**) gemini surfactant and DOPE helper lipid at varying $\rho_{\pm}$ from 2 to 1.1, and r from 3.3 to 6.8. Results are presented as mean ± SD from one to six independent experiments as shown in the embedded table (n = 2 or 3 per experiment) performed in 24-well plates. (A) The percentage of the transfected cells and (B) the intensity of GFP expression level were normalized to untreated control (cells only) (* $p < 0.05$ and **** $p < 0.0001$).

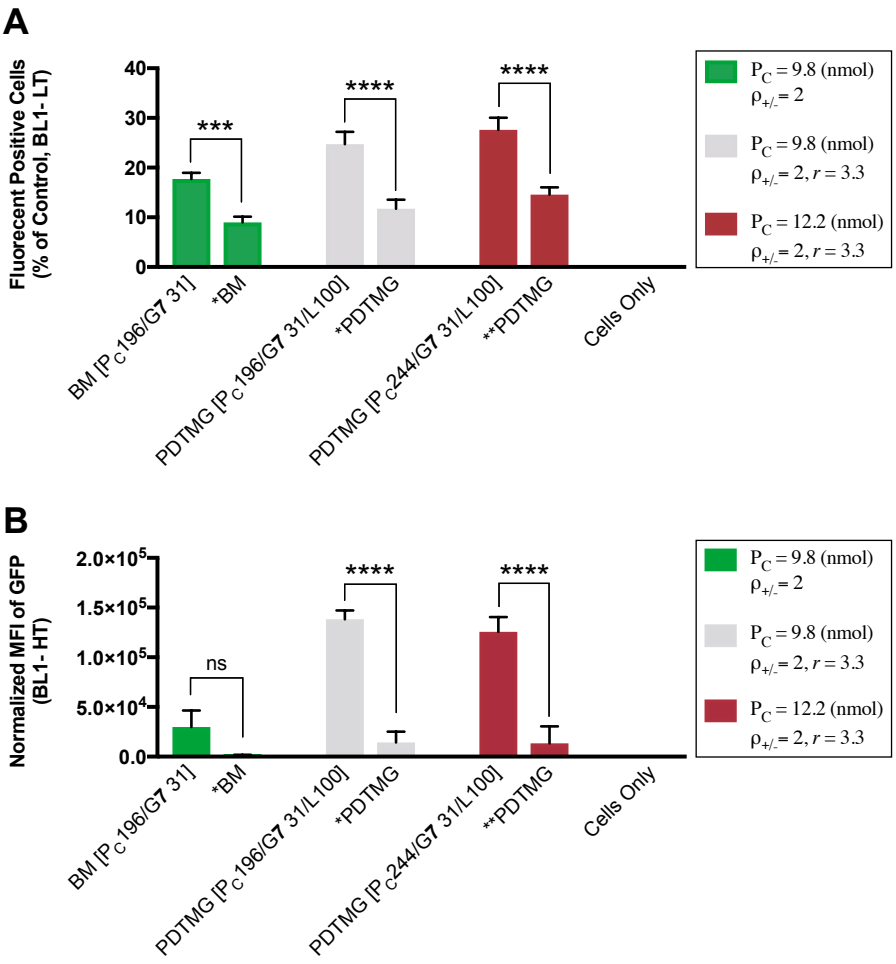

Fig. 4.14. The effect of volume on formulating PDTMG delivery systems in correlation with their transfection activities. BM [P_C196/G**7** 31], PDTMG [P_C196/G**7** 31/L 100] and PDTMG [P_C244/G**7** 31/L 100] were prepared at 0.5 µg pDNA per 50 µL transfection mixture; while *BM and *PDTMG formulations were formulated at 0.5 µg pDNA per 75 µL transfection mixture; and **PDTMG formulations were prepared at 0.5 µg pDNA per 100 µL transfection mixture. Results are presented as mean ± SD from one experiment (n = 3) performed in 24-well plates. (A) The percentage of the transfected cells and (B) the intensity of GFP expression level were normalized to untreated control (cells only) (*** $p < 0.001$ and **** $p < 0.0001$).

4.3.2.3 Cell viability

The condensation of pDNA by various carriers showed some degree of the viability loss (Fig. 4.15). The low complexation of pDNA at low lipid density by the BM [G**7** 31/L 100] lipoplexes formulated at $\rho_{\pm} = 2$ and r = 3.3 showed significant improvement in 3T3 cell viability compared to the BM [G**7** 154/L 500] lipoplexes formulated at $\rho_{\pm} = 10$ and r = 3.3 (Fig. 4.15 (A)). The UM [P_C 49] and BM [P_C 49/L 100] complexes were non-toxic at the expense of losing their transfection activities. The effective complexation of pDNA by the PDTMG [P_C 49/G**7** 31/L 100] complexes showed slight reduction (~ 9%) in cell viability compared to BM [G**7** 31/L 100] lipoplexes (Fig. 4.15 (A)). As shown in Figure 4.15 (B), increasing the peptide molarity while reducing the gemini to DNA ratio at $\rho_{\pm} = 1.1$ in formulating the PDTMG complexes caused minimal reduction (~ 10%) in cell viability compared to untreated control.

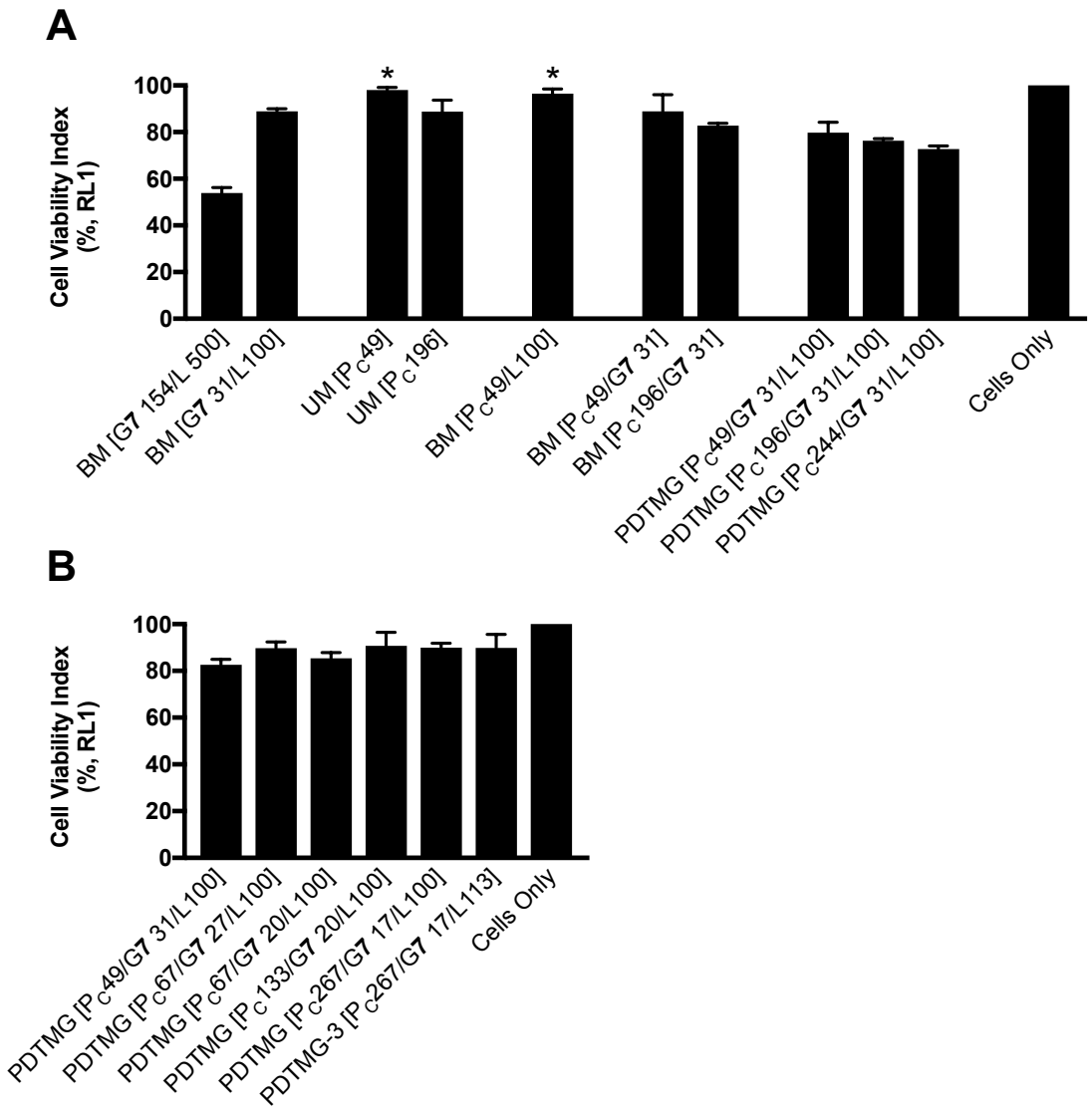

Fig. 4.15. MitoTracker staining for measuring the cytotoxicity of BM [G/L], UM [P], BM [P/L], BM [P/G] and PDTMG [P/G/L] gene delivery systems using flow cytometry. Results are presented as mean ± SD from one or two independent experiments (n = 3) for graph (A) or from one to six independent experiments, as part of an optimization study (n = 2 or 3 repeats per experiment for graph (B) that were performed in 24-well plates. *Asterisks* represent no significant difference from untreated (100%) control ($p > 0.05$).

4.3.3 The impact of peptide enhancers with varying charges and lengths on transfection activity and cell viability of PDTMG nanoparticles

4.3.3.1 *In vitro* transfection activities of PDTMG nanoparticles formulated with various peptide enhancers

As described in the previous section, the PDMTG nanoparticles formulated using cationic P_C peptide enhancers, G**7** and DOPE showed significant transfection activity compared to the counterpart uni-modal [P] complexes and bi-modal [G/L] or [P/G] complexes (refer to Section 4.3.2).

To investigate the impact of peptide enhancers, the transfection activities of various PDTMG delivery systems were assessed using several peptide enhancers, such as zwitterionic peptide enhancer or cationic peptide enhancers with varying charges (net positive charge at pH 7: from 0.5 to 6.3) and peptide lengths (from 5 to 22 amino acid residues), in combination with G**7** gemini surfactant and DOPE lipid.

As shown in Figure 4.16 (A), it was observed that increasing the peptide molarity of the zwitterionic P_A peptide enhancers made no changes in the transfection percentage of the formulated PDTMG complexes (i.e., PDTMG [P_A62/G**7** 31/L 100] and PDTMG [P_A308/G**7** 31/L 100]); however, MFI measurements indicated that by increasing the peptide molarity of the P_A, the transfection activity of the PDTMG [P_A308/G**7** 31/L 100] formulation was reduced ((though not statistically significant) compared to the PDTMG [P_A62/G**7** 31/L 100] formulation (Figure 4.16 (B)). This is more likely due to the low association of the zwitterionic P_A peptide enhancers to pDNA, leading to dispersion effect in formation of nanoparticles.

In comparison with the cationic peptide enhancers, it was found that the transfection activities of the PDTMG complexes formulated using P_B or P_C peptide enhancers (i.e., PDTMG [P_B49/G**7** 31/L

100] and PDTMG [P_C49/G**7** 31/L 100]) were significantly higher compared to the PDTMG complexes formulated using P_A peptide enhancers (Fig. 4.16 (A) and (B)).

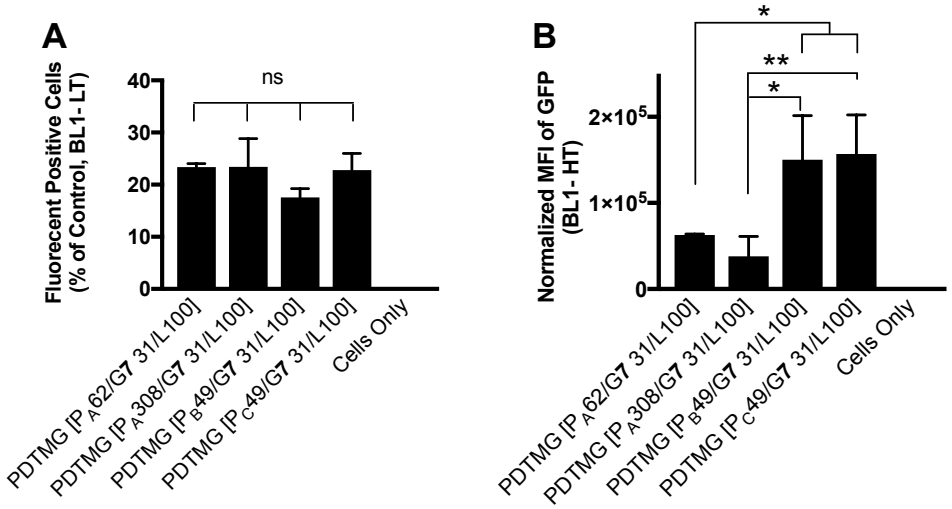

Fig. 4.16. The transfection activities of PDTMG complexes formulated using zwitterionic P_A or cationic P_B or P_C peptide enhancers in combination with RGDG-18 (G**7**) and DOPE lipid at $\rho_{\pm}$ = 2 and r = 3.3. Results are presented as mean ± SD from one experiment (n = 3) performed in 24-well plates. (A) The percentage of the transfected cells and (B) the intensity of GFP expression level were normalized to untreated control (cells only) (* $p < 0.05$ and ** $p < 0.01$).

To analytically compare the impact of the cationic peptide enhancers on transfection activities of the PDTMG complexes, their transfection percentage and MFI were evaluated at two different formulations: PDTMG [P67/G**7** 27/L100] and PDTMG [P267/G**7** 17/L100] (Fig. 4.17). As presented in Figure 4.17, all the PDTMG complexes formulated from cationic P_C, P_D, P_E, P_F, P_G peptide enhancers exhibited similar transfection activities (only exception being PDTMG [P_D 67/G**7** 27/L100] with lower transfection percentage). This data suggests that the "proton-sponge" effect of the cationic peptide enhancers is not significant in the PDTMG complexes as the cationic peptides (i.e., P_B, P_C, P_D, P_E, P_F, P_G) with different numbers of His residues (ranging from 3-12

His residues, Table 2.2) resulted in similar transfection activities. Comparing the transfection activities of the PDTMG complexes formulated from the cationic peptide enhancers with or without targeting sequence (i.e., P_C, P_E, P_G containing RGD sequence and P_B, P_D, P_F not containing RGD sequence; Table 2.2), it is inferred that the targeting RGD peptide sequence of the cationic peptide enhancers had a negligible effect in the PDTMG formulations. Therefore, the above experiments demonstrated that rather than the targeting RGD sequence and/or polyhistidine and/or polyarginine or their combination thereof contributing to the transfection activity of the formulated PDTMG complexes, perhaps the pDNA complexation ability of these cationic peptide enhancers were more likely to be the reason for the transfection activity of the formulated PDTMG complexes. The relation between the pDNA complexation and transfection activity is more evident when compared to the PDTMG complexes formulated from zwitterionic targeting RGD peptide enhancers (P_A) that revealed significantly lower transfection activity than the PDTMG complexes formulated from cationic peptide enhancers (i.e., P_B, P_C, P_D, P_E, P_F, P_G). Therefore, it can be reasonably argued that the comparable pDNA complexation of the cationic peptide enhancers resulting from small differences on their net positive charges (at neutral pH, the net positive charge of the cationic peptide enhancers ranging from 0.5-6.3; Table 2.2) led to similar transfection properties of the formulated PDTMG complexes. In accordance with this research, Welser *et al*. reported that the Arg- or Lys-rich peptides significantly improved the transfection efficiency of lipopolyplexes (formulated with DOTMA and DOPE) [326]. Further, the author showed His-rich peptides did not significantly contribute to the endosomal release of lipopolyplexes, and concluded that the "proton-sponge" effect, previously described for His-rich peptides formulated as polyplexes [298, 328], had a negligible impact in the lipopolyplexe formulations [326]. Taken these together, it can be expected that the higher complexation of pDNA mediated by the

electrostatic interactions between the positively charged side chains of the cationic peptide enhancers and the negatively charged phosphate backbone of pDNA in the PDTMG formulation can perhaps introduce more pDNA per cell; hence, resulting in higher GFP expression levels. However, it is believed that the endosomal release of the PDTMG components is mediated by the synergistic effects of the gemini surfactants and DOPE lipid, as described in the following sections (refer to Section 4.3.4 and 4.3.5).

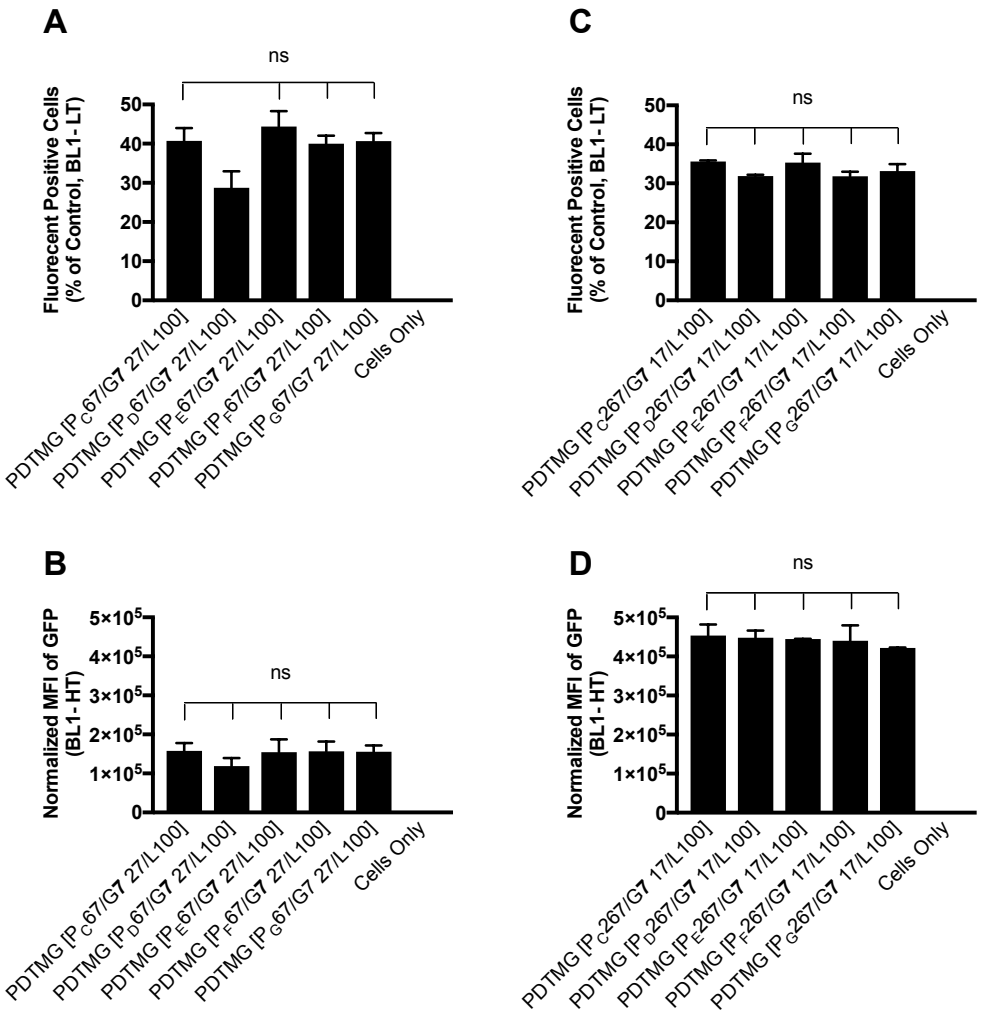

Fig. 4.17. The transfection activities of PDTMG complexes formulated using various cationic peptide enhancers (i.e., P_C, P_D, P_E, P_F, P_G) in combination with RGDG-18 (G**7**) and DOPE lipid at $\rho_{\pm} = 1.7$ and 1.1 (prepared at $M_G = 27$ μM and 17 μM, respectively). Results are presented as mean ± SD from one experiment (n = 3 for graphs (A) and (B); n = 2 for graphs (C) and (D)) performed in 24-well plates. (A) and (C) The percentage of the transfected cells, and (B) and (D) the intensity of GFP expression level were normalized to untreated control (cells only).

4.3.3.2 Cell viability

The PDTMG complexes formulated from zwitterionic P_A peptide enhancers showed significant reduction in 3T3 cell viability (cell viability: ≈ 63% and ≈ 57% for cells treated with PDTMG [P_A62/G**7** 31/L 100] and [P_A308/G**7** 31/L 100] formulations, respectively) compared to untreated control (Fig. 4.18 (A)). However, PDTMG complexes formulated from cationic P_B or P_C exhibited lower cytotoxicity (cell viability: ≈ 72% and ≈ 77% for cells treated with PDTMG [P_B62/G**7** 31/L 100] and [P_C62/G**7** 31/L 100] formulations, respectively) than the PDTMG complexes formulated from zwitterionic P_A peptide enhancers. These suggest that the lower association of zwitterionic P_A peptide enhancers compared to cationic peptide enhancers for pDNA complexation and the resulting dispersion effect in formation of the PDTMG complexes could be the reason for the increased cytotoxicity.

As shown in Figure 4.18 (B) and (C), reducing the amounts of gemini surfactant and/or increasing the amounts of cationic peptide enhancers (i.e., P_C, P_D, P_E, P_F, P_G), the formulated PDTMG complexes resulted in minimal reduction (from ~ 20% to non-toxic) in cell viability compared to untreated control.

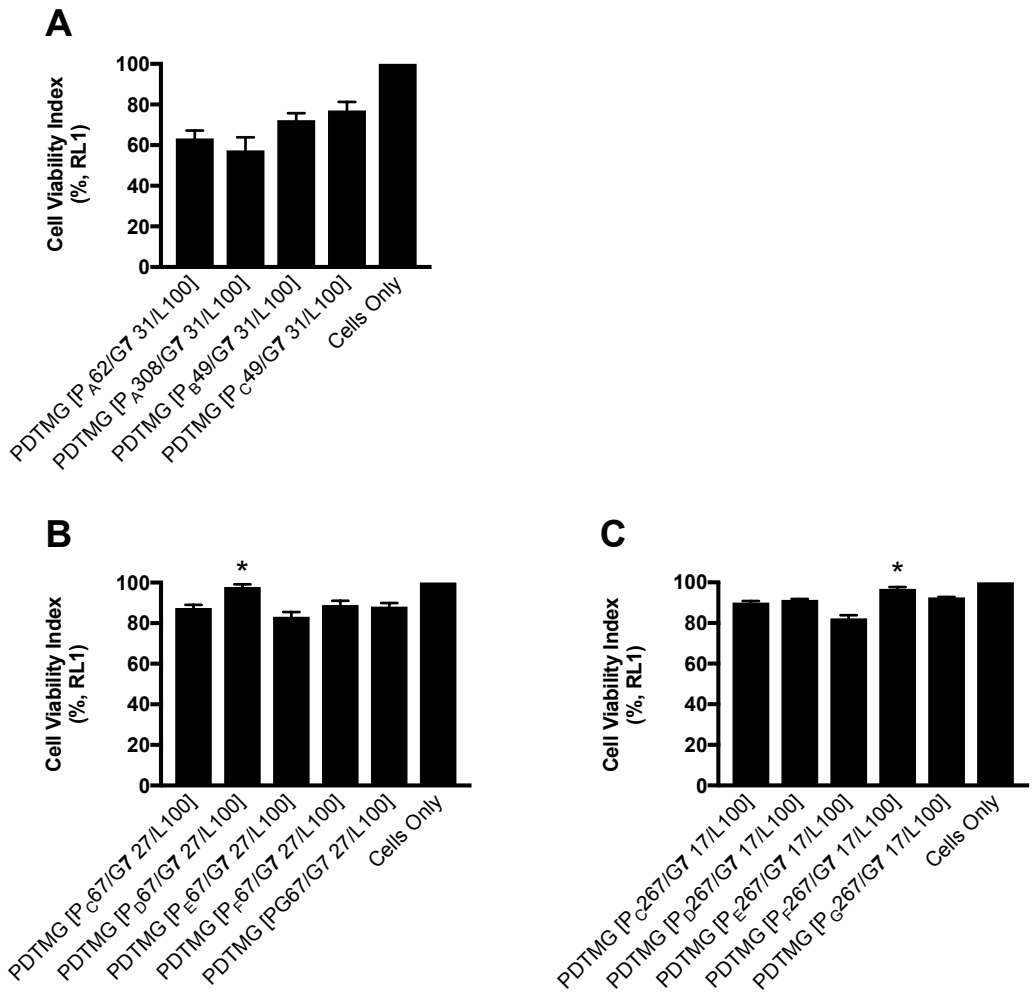

Fig. 4.18. MitoTracker staining for measuring the cytotoxicity of PDTMG complexes formulated from peptide enhancers $P_{A\text{-}G}$, RGDG-18 (G**7**) gemini surfactant and DOPE lipid. Results are presented as mean ± SD from one experiment (n = 3 for graphs (A) and (B); n = 2 for graph (C)) performed in 24-well plates. *Asterisks* represent no significant difference from untreated (100%) control (cells only) ($p > 0.05$).

4.3.4 The impact of gemini surfactants of varying alkyl chain lengths, spacer groups and functional headgroups on transfection portfolio of PDTMG nanoparticles

4.3.4.1 *In vitro* transfection activities of PDTMG nanoparticles formulated using m-3-m, m-7NH-m or m-7N(RGDG)-m

As previously shown (Sections 4.3.2 and 4.3.3), the optimization of the PDTMG [P_C/G**7**/L] formulation showed the highest transfection activity for the PDTMG complexes prepared at M_P = 267 μM, M_G = 17 μM and M_L = 113 μM ($\rho_\pm$ = 1.1 and r = 6.8), and further it was observed that the PDTMG complexes formulated from the cationic P_B, P_C, P_D, P_E, P_F, P_G peptide enhancers demonstrated similar transfection activities. To further investigate the impact of gemini surfactants on transfection properties of the PDTMG complexes, *in vitro* transfection studies of various PDTMG delivery systems were performed using G**1**-G**7** gemini surfactants (Table 2.1) which differ in the alkyl chain lengths (m = saturated 12C or 18C) and/or spacer groups (s = 3, 7NH, 7NR) and/or functional headgroups (R = R_1 (imidazolepropionyl), R_2 (thiopropionyl), R_3 (RGDG peptide)).

As presented in the Figure 4.19 (A), the PDTMG [P_C 267/G 17/L 113] complexes formulated at $\rho_\pm$ = 1.1 and r = 6.8 from 12-7NH-12 (G**2**) or RGDG-12 (G**6**) gemini surfactants showed insignificant increase in the percentages of the transfected cells and the MFI compared to control-untreated cells ($p > 0.05$). Increasing the amounts of G**6** gemini surfactant by increasing $\rho_\pm$ from 1.1 to 1.7, as shown in Figure 4.20 and Figure D5 (Appendix D), the transfection percentage of the PDTMG [P_C 267/G**6** 27/L 100] complexes was slightly improved compared to the PDTMG [P_C 267/G**6** 17/L 113] complexes (though statistically significant, $p < 0.05$), while the MFI was significantly increased for the PDTMG [P_C 267/G**6** 27/L 100] complexes compared to the PDTMG

[P_C 267/G**6** 17/L 113] complexes ($p < 0.0001$). This could be explained by the internalization of the G**6**-based PDTMG nanoparticles at $\rho_{\pm} = 1.7$ into the cells to mediate the downstream events including rupturing the endosome and release its pDNA cargo into the cell cytoplasm. By further increasing the $\rho_{\pm}$ from 1.7 to 2.1, the slight increase in the transfection percentage of the PDTMG [P_C 267/G**6** 33/L 100] complexes compared to the PDTMG [P_C 267/G**6** 27/L 100] complexes ($p > 0.05$; Fig 4.20 (A)) was accompanied with significant decrease in the MFI ($p < 0.05$; Fig 4.20 (B)). This suggests that the tighter compaction with higher amounts of G**6** gemini surfactants in formulating the PDTMG complexes hindered the endosomal release of pDNA.

Increasing the length of the alkyl tails using gemini surfactants with saturated 18C alkyl tails resulted in higher internalization of the formulated PDTMG nanoparticles (Fig. 4.19 (A)). The PDTMG complexes formulated from 18-7NH-18 (G**3**) gemini surfactants (i.e., PDTMG [P_C 267/G**3** 17/L 113]) showed significantly higher transfection activity compared to 18-3-18 (G**1**) counterpart complexes, as indicated by both higher the transfection percentage ($p < 0.0001$) and the MFI ($p < 0.01$) (Fig. 4.19 (A) and (B)). Compared to G**3**-based PDTMG complexes, the PDTMG complexes formulated from imidazolepropionyl-functionalized G**4** gemini surfactants resulted in significant increase ($p < 0.01$) in the intensity of the GFP expression level with similar transfection percentage (Fig. 4.19 (A) and (B)). However, the thiolpropionyl-functionalized G**5**-based PDTMG showed significant reduction in the GFP expression level as compared to the counterpart PDTMG complexes formulated with the parent G**3** gemini surfactants. As shown in Figure 4.19 and Figure D4 (Appendix D), the PDTMG complexes formulated from the RDGD-functionalized G**7** gemini surfactants demonstrated superior transfection activity, exhibited the highest transfection percentage and MFI as compared to the counterpart G**1**-G**6** lipopolyplexes. Compared to the PDTMG complexes formulated from G**6** gemini surfactant, the PDTMG

complexes formulated from G**7** (with the same headgroup but 18C alkyl tails) showed a 23-fold increase in the transfection percentage and a 39-fold increase in the MFI (Fig 4.19 (A) and (B)). The above data indicates that the G**7**-based PDTMG nanoparticles could more efficiently internalize and more effectively release the pDNA into the cell cytoplasm compared to the PDTMG nanoparticles formulated from G**1**-G**6** (Fig D4, Appendix D). The higher cell penetration activity of the G**7**-based PDTMG complexes is, therefore, inferred to be attributed to both the long C18 alkyl tails of G**7** gemini surfactants and their functional RDGD headgroups. It is thought that the electrostatic interaction as well as hydrogen bond formation between the positive guanidine group of arginine residue from the RGDG functional headgroups of gemini surfactants and the negatively charged phosphate and sulphate of cell surface membrane resulted in high penetration activity of the G**7**-based PDTMG nanoparticles. As shown in Figure 4.19 and Figure D4 (Appendix D), the G**7**-based PDTMG nanoparticles also demonstrated comparable transfection activity with the positive control Lipofectamine 3000 transfection reagent. Further details on the impact of the functional headgroups for endosomal release of pDNA will be described in the Section 4.3.5.

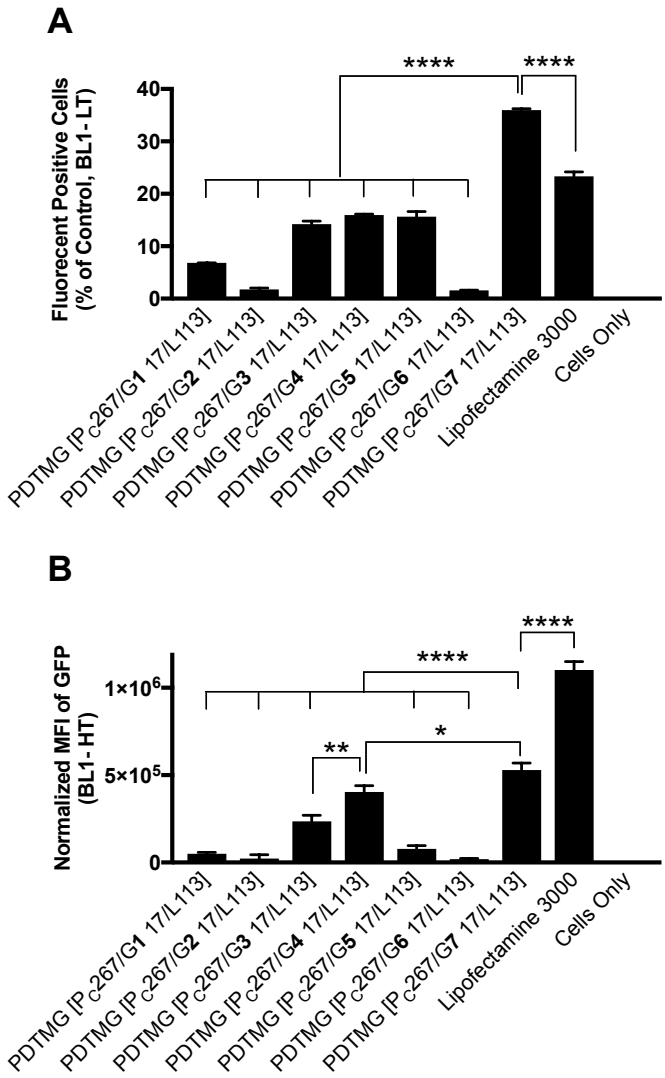

Fig. 4.19. The impact of alkyl chain length, spacer group and functional headgroup of gemini surfactants on transfection activities of PDTMG complexes formulated from cationic P_C peptide enhancer, various gemini surfactants (i.e., 18-3-18 (G**1**), 12-7NH-12 (G**2**), 18-7NH-18 (G**3**), imid-18 (G**4**), thiol-18 (G**5**), RGDG-12 (G**6**), RGDG-18 (G**7**)) and DOPE lipid. Results are presented as mean ± SD from one experiment (n = 2) performed in 24-well plates. (A) The percentage of the transfected cells and (B) the intensity of GFP expression level were normalized to untreated control (cells only) (* $p < 0.05$, ** $p < 0.01$ and **** $p < 0.0001$).

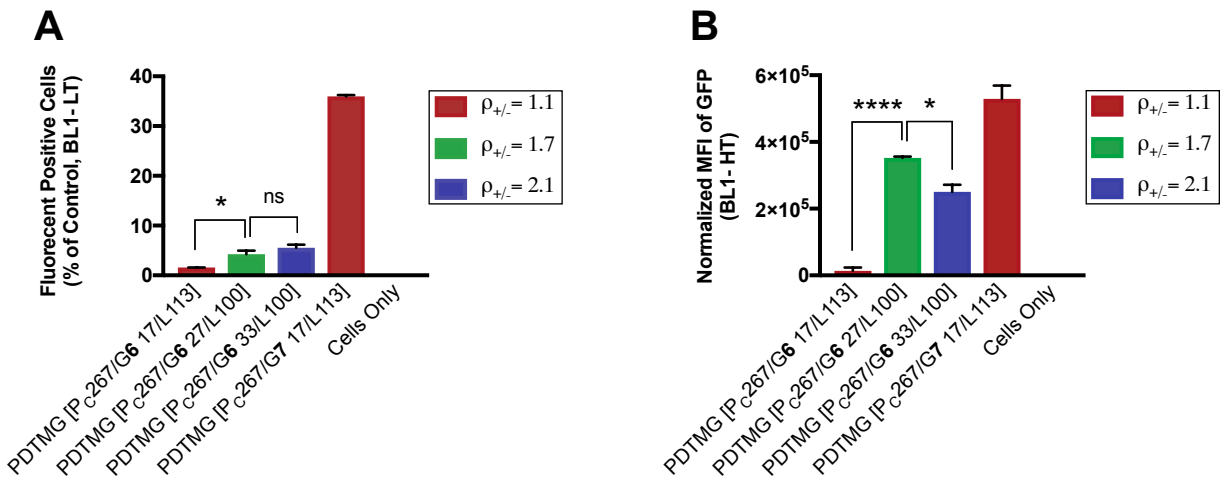

Fig. 4.20. Transfection activities of PDTMG complexes formulated from P_C peptide enhancer, RGDG-12 (G**6**) and DOPE at $\rho_{\pm}$ = 2.1, 1.7, 1.1 (prepared at M_G = 33 μM, 27 μM and 17 μM, respectively) as compared to RGDG-18 (G**7**)-based PDTMG complexes formulated at $\rho_{\pm}$ = 1.1 (i.e., PDTMG [P_C 267/G**7** 17/L 113]). (A) The percentage of the transfected cells and (B) the intensity of GFP expression level were normalized to untreated control (cells only) (* $p < 0.05$, ** $p < 0.01$ and **** $p < 0.0001$). Results are presented as mean ± SD from one experiments (n = 2) performed in 24-well plates.

4.3.4.2 Cell viability

The PDTMG [P_C 267/G 17/L 113] complexes formulated from G**1**, G**2**, G**5** or G**6** gemini surfactants, previously shown to have insignificant transfection activities (as indicated by their MFIs; Fig. 4.19 (B)), were also non-toxic to the cells (Fig. 4.21). As shown in Figure 4.21, Lipofectamine 3000 transfection reagent showed no significant reduction in the cell viability, while the G**3**- and G**7**-based PDTMG complexes caused slight reduction (approximately 8% and 16%, respectively) of the 3T3 cell viability compared to the untreated control. Interestingly, the PDTMG complexes formulated from G**4** gemini surfactants, which previously showed higher transfection activity than the G**3**-based PDTMG complexes (Figure 4.19 (B)), revealed no significant cell viability reduction compared to the untreated control. This is perhaps due to the better charge distribution of imidazole group [319] of the G**4** gemini surfactants compared to the parental G**3** gemini surfactant.

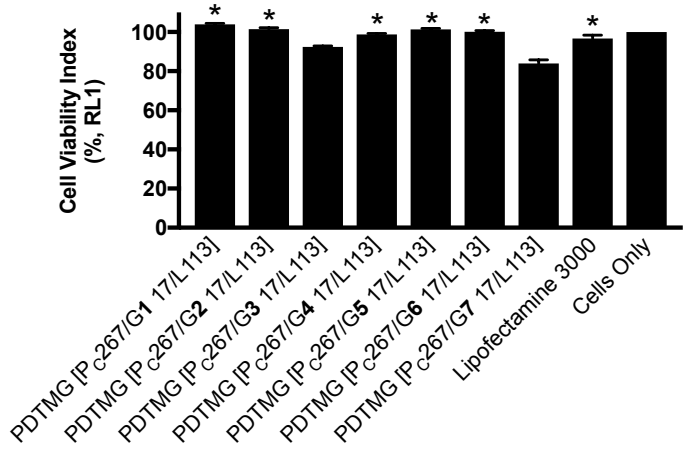

Fig. 4.21. MitoTracker staining for measuring the cytotoxicity of PDTMG complexes formulated from G**1**-G**7**. Results are presented as mean ± SD from one experiment (n = 2) performed in 24-well plates. *Asterisks* represent that there is no significant toxicity compared with untreated (100%) control ($p > 0.05$).

4.3.5 Understanding the mechanism of pDNA release from PDTMG nanoparticles by designing various peptide-functionalized gemini surfactants

4.3.5.1 *In vitro* transfection activity of the PDTMG delivery systems using peptide-functionalized gemini surfactants

To better understand the synergistic effects of the compositional elements of the PDTMG delivery system and elucidate the structure-activity relationships, *in vitro* transfection study of various PDTMG delivery systems were investigated by modifying the structure of the hydrophilic headgroups of gemini surfactants.

As shown in Section 4.3.3, the non-covalent addition of several cationic peptide enhancers including bifunctional RGD-$(R)_6$-$(H)_3$ peptide enhancers (i.e., P_C), pH sensitive cationic $(H)_5$ peptide enhancers (i.e., P_D), bi-functional cationic RDG-$(H)_5$ peptide enhancers (i.e., P_E) in formulating the PDTMG delivery systems demonstrated similar transfection activities, while significantly higher transfection activities as compared to the non-covalent addition of the zwitterionic RGD peptide enhancers (i.e., P_A). Further, it was shown (Section 4.3.4) that the PDTMG delivery systems formulated from gemini surfactants with 18C alkyl tails have higher penetration activity as compared to those formulated with C12 gemini surfactants. In this section, the effect of G**8**, G**9** and G**10** surfactants with P_A, P_D or P_E peptide functional headgroup, respectively, will be evaluated on the transfection properties of the formulated PDTMG complexes. In addition, further understanding of the pDNA release from the PDTMG complexes will be assessed by systematically modifying the arginine-rich peptide functionalities using G**11**, G**12**, G**13** and G**14** gemini surfactants.

As shown in Figure 4.22, in contrast to the effect of non-covalent addition of P_A peptide enhancers as explained before, the P_A-functionalized gemini (G**8**)-based PDTMG complexes showed

comparable transfection activity with the G**7**-based PDTMG complexes and Lipofectamine 3000 transfection reagent.

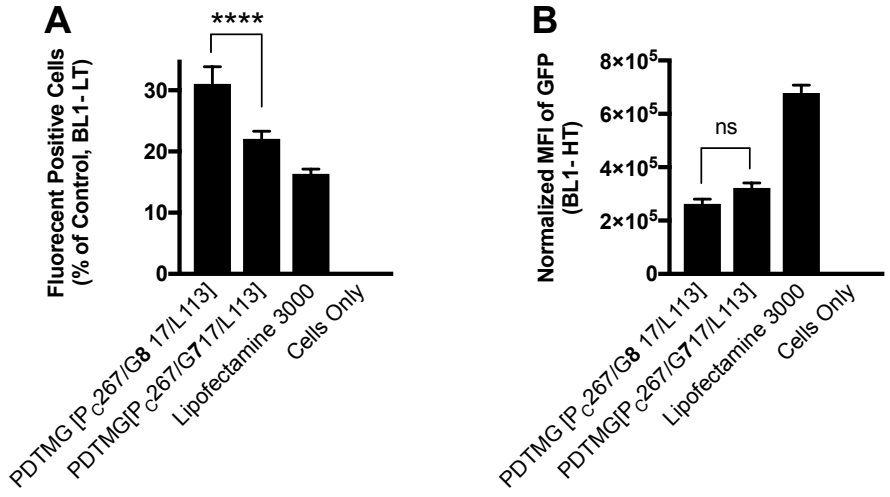

Fig. 4.22. Transfection activities of RGDG-18 (G**7**)- and GRGDSPG-18 (G**8**)-based PDTMG complexes as compared to Lipofectamine 3000. Results are presented as mean ± SD from one experiment (n = 3) performed in 24-well plates. (A) The percentage of the transfected cells and (B) the intensity of GFP expression level were normalized to untreated control (cells only) (**** $p < 0.0001$).

However, the P_D-functionalized gemini surfactants (G**9)** and the P_E-functionalized gemini surfactants (G**10)** formulated in the PDTMG complexes (i.e., [P_C267/G 17/L 113]) showed significantly lower penetration activities as compared to the counterpart G**7**-based PDTMG complexes (Fig. 4.23 (A)). The observed lower penetration activities were perhaps due to the increased repulsive forces between cationic headgroups of the gemini surfactants (i.e., G**9**, G**10)** resulting from the increased positive charge density associated with the glutamic acid linkers containing positive α-ammonium groups. As shown in Figure 4.23 (A), the P_E-functionalized

gemini (G**10**)-based PDTMG nanoparticles showed higher penetration activity compared to the P_D-functionalized gemini (G**10**)-based PDTMG nanoparticles. While increasing the $\rho_{\pm}$ from 1.1 to 2.5 restored and significantly increased the penetration activities of the formulated G**9**- and G**10**-based PDTMG nanoparticles (i.e., [P_C267/G 40/L 100]) (Fig 4.23 (A)), their MFIs did not change and indicated negligible GFP expression levels as compared to the G**7**-based PDTMG nanoparticles ($p < 0.00001$) (Fig 4.23 (B)). The data above suggests that there is a totally different scenario between the non-covalent addition and the covalent linking of the peptide moieties (e.g., P_A, P_D, P_E) to gemini surfactants in formulating the PDTMG complexes. Comparing the transfection activities of the PDTMG [P_C267/G**7** 17/L 100], PDTMG [P_D267/G**7** 17/L 100], PDTMG [P_E267/G**7** 17/L 100] complexes, as shown in Figure 4.17 (see Section 4.3.3), vs. PDTMG [P_C267/G**7** 17/L 113], PDTMG [P_C267/G**9** 17/L 113], PDTMG [P_C267/G**10** 17/L 113] complexes, as shown in Figure 4.23, it can be inferred that by covalently linking the peptide functionalities to gemini surfactants, the small changes in the arrangement of the amino acid residues have a determining impact on the pDNA release from the PDTMG complexes.

As mentioned above, by increasing the $\rho_{\pm}$ from 1.1 to 2.5, the increased amounts of G**9** and G**10** gemini surfactants containing pH sensitive $(H)_5$ peptide motifs in the PDTMG complexes showed no improvement in GFP expression levels as compared to control-untreated cells, suggesting that the "proton-sponge" effect had no significant impact on the pDNA release from the G**9**- and G**10**-based PDTMG complexes into the cell cytoplasm. Further, it was shown that the PDTMG complexes formulated at $\rho_{\pm}$ = 1.1 from RGDG-functionalized gemini surfactants (G**7**) or GRGDSPG-functionalized gemini surfactants (G**8**), which did not contain the pH sensitive $(H)_5$ peptide motifs, accommodated the pDNA release and resulted in high GFP expression levels. Taken together, it can be inferred that following the internalization of the PDTMG complexes in

the cells, the ability of the cationic gemini surfactants to induce the well-known inverted hexagonal phase [117, 130, 329, 330] is most likely to be responsible for the downstream events including fusion and disruption of the endosomal membrane and release of pDNA into the cell cytoplasm. However, further research such as SAXS experiments requires to further validate this hypothesis.

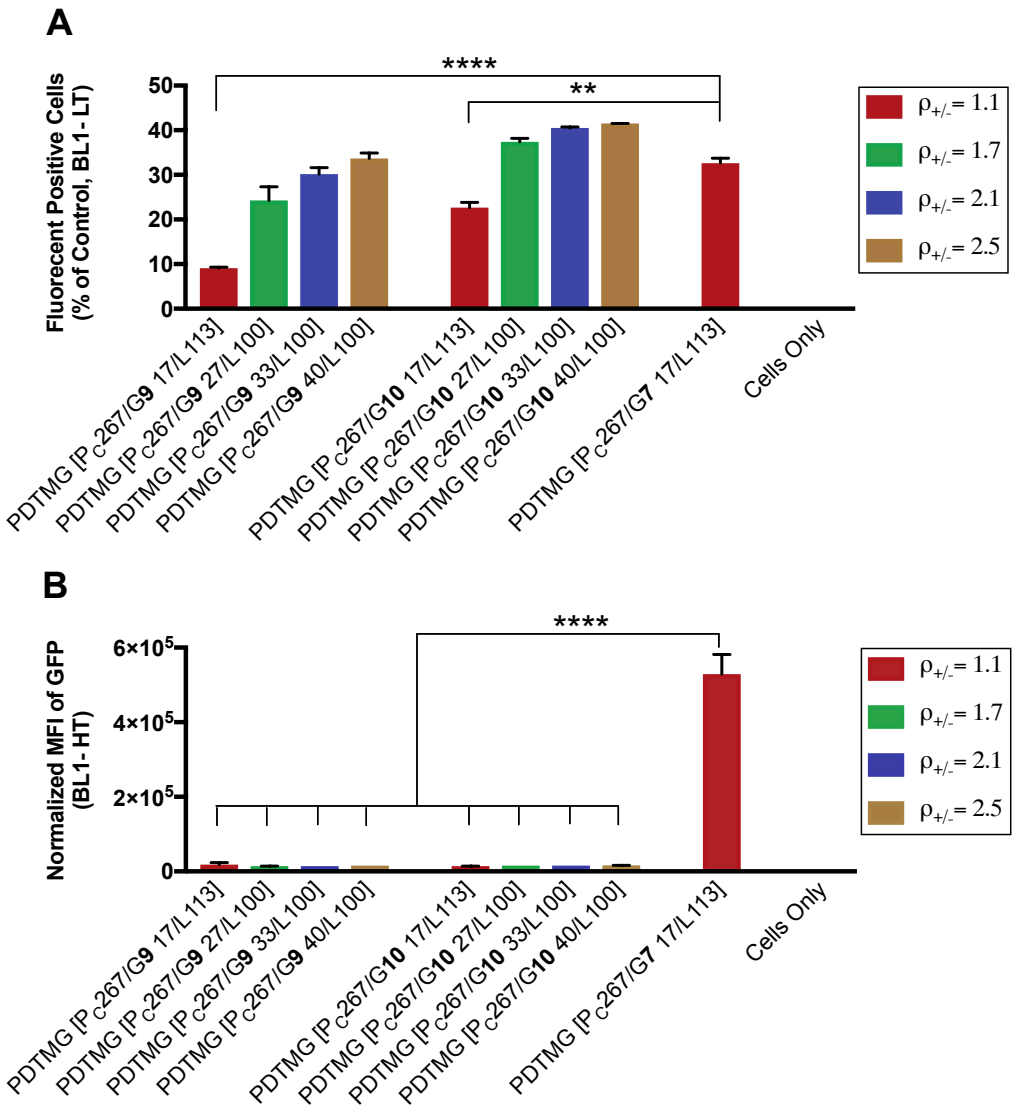

Fig. 4.23. Transfection activities of 18-E-PepD (G**9**)- and 18-E-PepE (G**10**)-based PDTMG complexes formulated at $\rho_{\pm}$ = 2.5, 2.1, 1.7 and 1.1 (prepared at M_G = 40 µM, 33 µM, 27 µM and 17 µM, respectively) as compared to RGDG-18 (G**7**)-based PDTMG complexes formulated at $\rho_{\pm}$ = 1.1 (i.e., PDTMG [P_C267/G**7** 17/L 113]). Results are presented as mean ± SD from one experiments (n = 2) performed in 24-well plates. (A) The percentage of the transfected cells and (B) the intensity of GFP expression level were normalized to untreated control (cells only) (** $p < 0.01$ and **** $p < 0.0001$).

As shown above, while the covalent functionalization of gemini surfactants with RGDG (i.e., G**7**) and GRGDGSPG (i.e., G**8**) motifs resulted in pDNA release from the PDTMG complexes and high GFP expression levels, the covalent functionalization of gemini surfactants with $E(H)_5$ (i.e., G**9**) and $EGRGDSPG(H)_5$ (i.e., G**10**) revealed total loss of GFP expression levels, suggesting no pDNA release from the PDTMG complexes into the cell cytoplasm. These experiments may suggest that the fusogenic inverted hexagonal phase structures for endosomal release of pDNA are not induced by the targeting sequence (i.e., GRGDSPG) or the nature of the amino acid residues (e.g., His-rich peptides) of the peptide-functionalized gemini surfactants but rather promoted by the molecular architecture of gemini surfactants (Fig. 3.4) in the PDTMG complexes.

To further test the effect of molecular architectures of gemini surfactants, several peptide-functionalized gemini surfactants (G**11**- G**14**) were designed and produced that include Arg, Asp, Glu, Gly residues. As shown in Figure 4.24 (A), the conjugation of $(E)_2G(R)_2$, $(E)_2G(R)_3$, $(E)_2(G)_3(R)_3$ or $DE(G)_3(R)_3$ peptide motifs to gemini surfactants via succinic acid linkers (for producing G**11**-G**14**, respectively), all the G**11**-, G**12**-, G**13**- and G**14**-based PDTMG complexes formulated at $\rho_{\pm} = 1.1$ showed similar penetration activities as compared to the counterpart G**7**-based PDTMG complexes (i.e., PDTMG [P_C 267/G**7** 17/ L 113]). However, the GFP expression levels of the PDTMG complexes formulated from either G**11**, G**12**, G**13,** or G**14** were significantly lower compared to the PDTMG complexes formulated from G**7** ($p < 0.00001$) (Fig. 4.24 (B)). In addition, it was found that the MFI of the PDTMG complexes formulated from the G**11** or G**12** gemini surfactants at $\rho_{\pm} = 1.1$ (i.e., [P_C 267/G 17/ L 113]) were similar, but about 2-fold higher compared to the counterpart PDTMG complexes formulated from G**13** or G**14** (i.e., G**13** and G**14** containing increased number of Gly residues compared to G**11** and G**12**) (though statistically insignificant; Fig. 4.24 (B)). This supports the hypothesis that the molecular architecture of the

gemini surfactants, rather than the nature of the amino acid residues (e.g., His, Arg, Asp, Glu, Gly) of the peptide-functionalized gemini surfactants, is more likely to be responsible to effectively destabilize the endosome; and hence, release pDNA from the PDTMG complexes in to the cell cytoplasm. Further, as shown in Figure 4.24 (B), slight increase of the $\rho_{\pm}$ from 1.1 to 1.7, resulted in the total loss of GFP expression levels for all the G**11**-, G**12**-, G**13**- and G**14**-based PDTMG complexes.

In general, it was observed that peptide functionalization of gemini surfactants can significantly improve the internalization of the PDTMG complexes into the cells. However, the PDTMG complexes can either significantly improve or decrease the GFP expression levels that were observed to be dependent on the arrangement of the amino acid residues and the molecular structure of the peptide-functionalized gemini surfactants as well as the density of the peptide functionalities. Therefore, it may be reasonably concluded that due to the reduced steric hindrance of the RGDG and GRGDSPG peptide motifs of the G**7** and G**8** gemini surfactants, respectively, the internalized G**7**- and G**8**-based PDTMG complexes in the endosomal vesicles could effectively disassemble by forming fusogenic inverted hexagonal phase structure, and release their pDNA cargo into the cell cytoplasm.

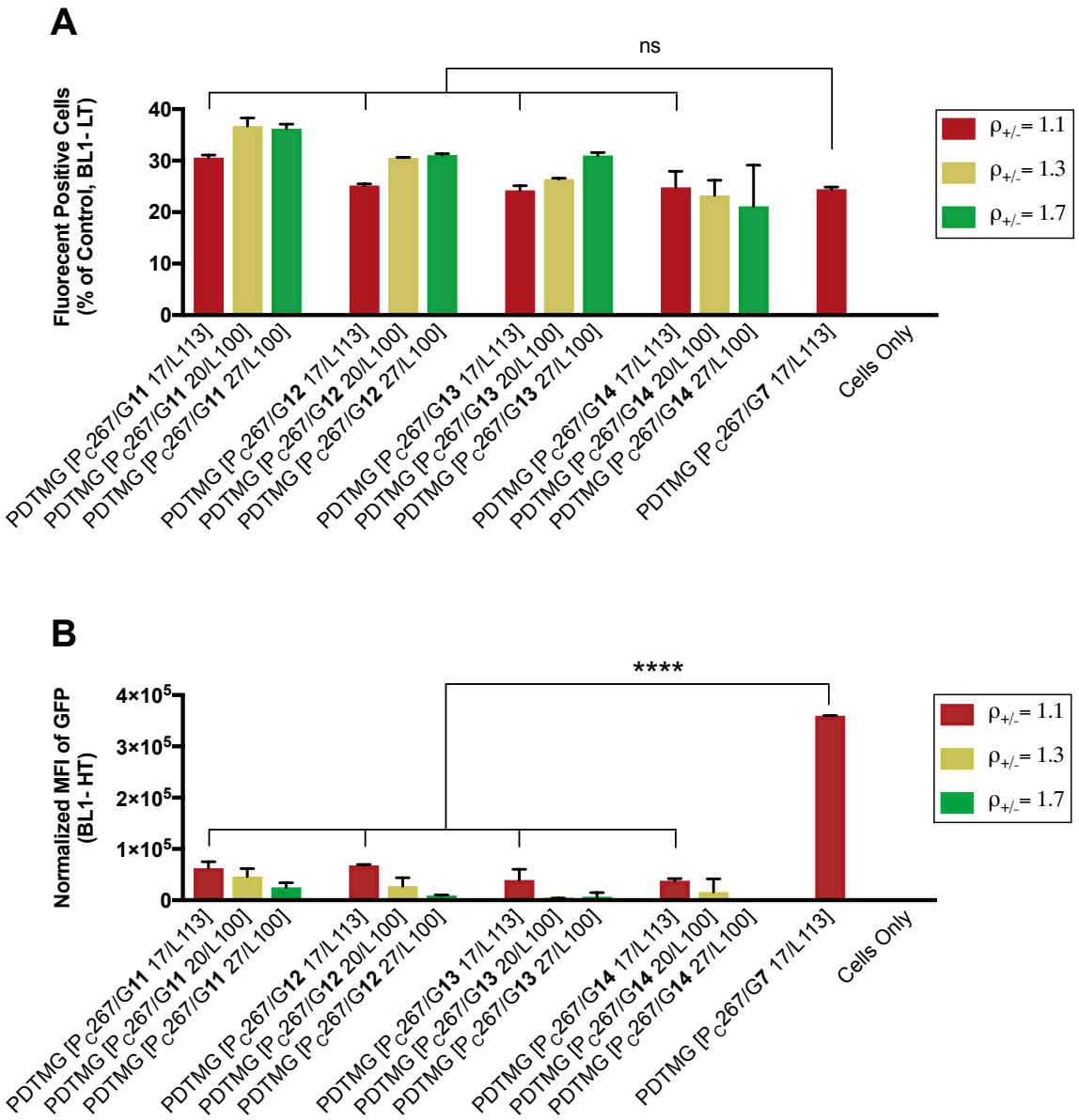

Fig. 4.24. Transfection activities of 18-Suc-E_2GR_2 (G**11**)-, 18-Suc-E_2GR_3 (G**12**)-, 18-Suc-$E_2G_3R_3$ (G**13**)- and 18-Suc-DEG_3R_3 (G**14**)-based PDTMG complexes formulated at $\rho_{\pm}$ = 1.7, 1.3 and 1.1 (prepared at M_G = 27 µM, 20 µM and 17 µM, respectively) as compared to RGDG-18 (G**7**)-based PDTMG complexes formulated at $\rho_{\pm}$ = 1.1 (i.e., PDTMG [P_C267/G**7** 17/L 113]). Results are presented as mean ± SD from one experiments (n = 2) performed in 24-well plates. (A) The percentage of the transfected cells and (B) the intensity of GFP expression level were normalized to untreated control (cells only) (**** $p < 0.0001$).

4.3.5.2 Cell viability

As presented in Figure 4.25, the PDTMG complexes formulated from G**9**-G**14**, which previously showed to have high cell penetration activities but no significant transfection activities, caused negligible cell cytotoxicity. However, the G**8**- and G**7**-based PDTMG complexes with high transfection profile caused slight reduction (from 17% to 4%-varies depending on the cells age) in cell viability. The higher cytotoxicity of the G**8**- and G**7**-based PDTMG complexes is most likely to be due to the efficient endosomal disruption associated with the amino acid arrangement of peptide headgroup and molecular shape of G**7** and G**8** compared to G**9**-G**14** gemini surfactants.

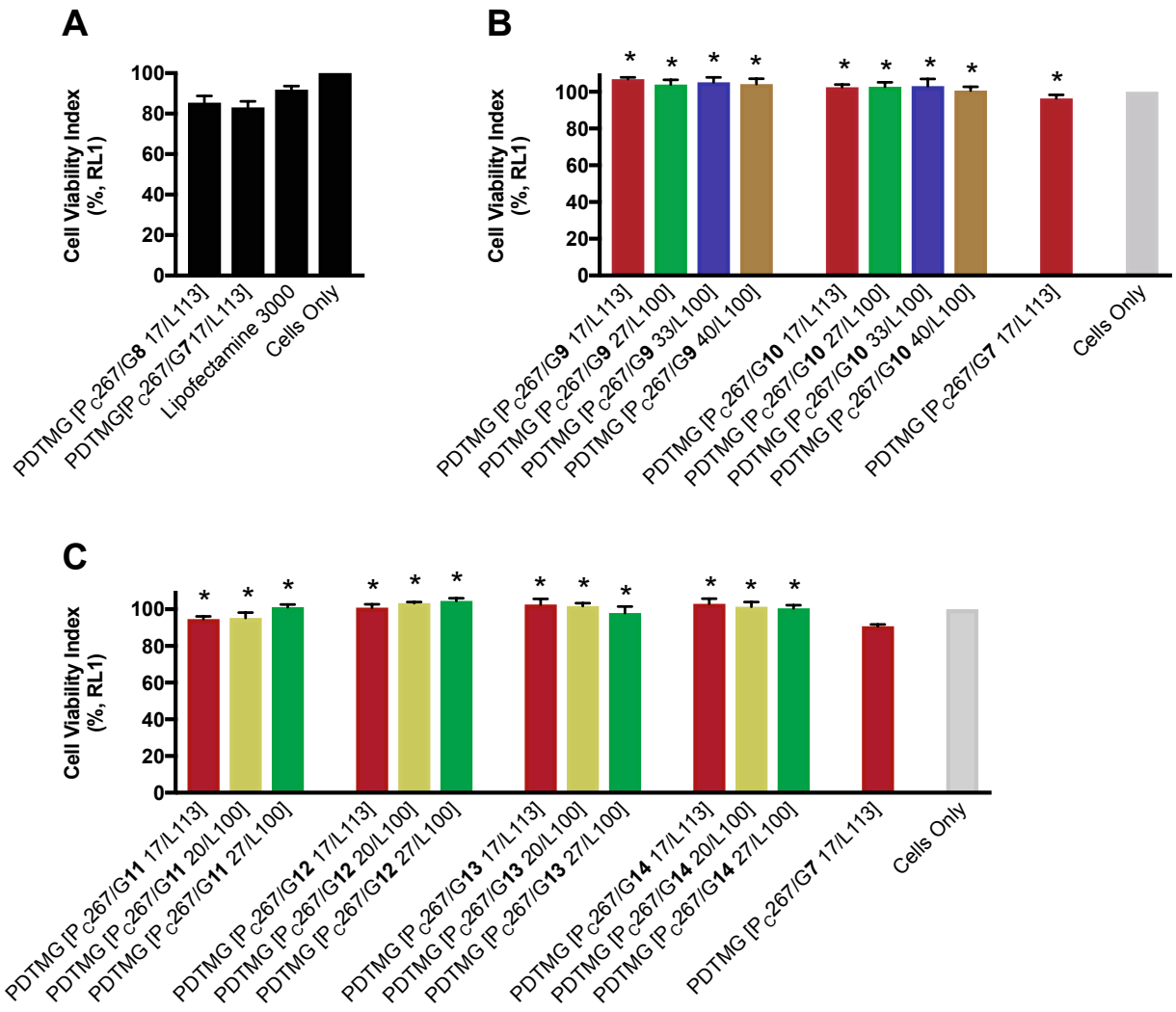

Fig. 4.25. MitoTracker staining for measuring the cytotoxicity of PDTMG complexes formulated from G**7**-G**14**. Results are presented as mean ± SD (n = 2 for experiments (A) and (B); n = 3 for experiment (C)) performed in 24-well plates. *Asterisks* represent that there is no significant difference from untreated (100%) control ($p > 0.05$).

Chapter 5

Discussion

5.1 Gemini-based lipoplexes

To efficiently and effectively deliver pDNA, the negatively charged genetic materials need to be condensed into stable positively charged particles (or neutral particles in the presence of targeting moieties) to 1- protect them against enzymatic degradation, 2- facilitate their uptake across the negatively charged cell surface membrane via different mechanisms (e.g., clathrin, caveolae, micropinocytosis, and other endocytosis pathways), and following internalization, 3- destabilize and rupture the endosomal vesicles, and 4- release their pDNA cargo into the cytoplasm, from where the pDNA can reach the cell's nucleus to be transcribed, and later translated into the encoding proteins [113, 319]. Therefore, in the first part of this project, the effects of lipoplex formulations incorporating gemini surfactants of varying alkyl tails, spacer groups, and functional headgroups (i.e., m-3-m, m-7NH-m, m-7N(RGDG)-m; m = saturated C12 or C18) were investigated for pDNA compaction, cellular internalization, and endosomal escape. The physicochemical characterization, size and zeta potential measurements by DLS, in conjunction with the transfection properties and cytotoxicity profile of lipoplex formulations identified the essential parameters for development of efficient and effective gene delivery systems.

It was shown that lipoplexes formulated from m-3-m, m-7NH-m or m-7N(RGDG)-m gemini surfactants (m = saturated C12 or C18) at $\rho_{\pm} = 10$ (i.e., prepared at $M_G = 154$ μM) resulted in negligible GFP expression levels (as indicated by their MFIs at LT and HT analysis; Fig. 4.3 (B), 4.6 (B), 4.11 (B)). Although these lipoplex formulations promoted the cellular uptake of pDNA, the limited expression of reporter GFP gene suggested the entrapment of pDNA in endosomes,

leading to their eventual degradation [115, 224]. By decreasing the $\rho_{\pm}$ values from 10 to 2, however, the intensity of GFP expression levels for all the lipoplexes formulated from m-3-m, m-7NH-m or m-7N(RGDG)-m gemini surfactants were significantly improved (either statistically significant or statistically insignificant) (Fig. 4.3 (B)). Further reduction in lipid density, RGDG-18 (G**7**)-based lipoplexes formulated at $\rho_{\pm} = 2$ and r = 3.3 (i.e., prepared at $M_G = 31$ μM and $M_L = 100$ μM) demonstrated the highest transfection activity compared to the counterpart complexes formulated using gemini surfactants with saturated 12C alkyl tails (i.e., 12-7NH-12 (G**2**) and RGDG-12 (G**6**)) or parental 18-7NH-18 (G**3**) gemini surfactant (Fig. 4.5 (A) and (B); Fig. D2, Appendix D). This suggests that RGDG peptide functionalization of gemini surfactant having long C18 alkyl tails could complex pDNA at low lipid density (i.e., $\rho_{\pm} = 2$ and r = 3.3), enhance internalization of lipoplexes, effectively destabilize endosomal vesicles and disassemble lipoplexes, and hence release the pDNA into the cell cytoplasm. Comparing with the G**7**-based lipoplexes formulated at high lipid density with $\rho_{\pm} = 10$ and r = 3.3 (i.e., BM [G**7** 154/L 500]), the penetration activity of the G**7**-based lipoplexes formulated at low lipid density with $\rho_{\pm} = 2$ and r = 3.3 (i.e., BM [G**7** 31/L 100]) was significantly lower, while the MFI (HT analysis) was approximately 20-fold higher. This is most likely due to the degree of pDNA compaction for GFP expression level, which associated primarily with the amount of G**7** gemini surfactants, as formulating the lipoplexes by decreasing or increasing the amount of DOPE lipids at $\rho_{\pm} = 10$ had no significant impact on the MFI, and revealed negligible GFP expression levels (refer to Section 4.2.2.2 and Fig 4.6 (B) and Fig D3 (Appendix D)). These observations are in agreement with the physical properties of the lipoplexes measured by DLS, which showed the tight pDNA compaction using G**7** gemini surfactant at $\rho_{\pm} = 10$ when compared to counterparts formulated at $\rho_{\pm} = 2$, as indicated by the zeta potential of the complexes (e.g., ζ-potential: +63.4 ± 1.3 mV and +38.3 ± 0.5

mV for BM [G**7** 154/L 500] and BM [G**7** 31/L 100] formulations, respectively) (Fig. 4.2 and Fig. D3 (Appendix D)). It was shown that increasing the $\rho_{\pm}$ value above 2 or 3, depending on the length of the alkyl tails of gemini surfactants (i.e., saturated C12 or C18) demonstrated by G**6**- and G**7**-based lipoplexes in Figure 4.4, the tight compaction hindered the cytoplasmic release of pDNA. Considering the higher penetration activity of the gemini surfactants with longer alkyl tails (i.e., C18 vs C12), fine tuning of r values by adjusting the DOPE lipid molarity at $\rho_{\pm} = 2$ not only further increased the transfection activities of the lipoplexes (Fig. 4.5 and Fig. D2 (Appendix D)), but also generated more stable particles. For example, the G**7**-based lipoplexes formulated at $\rho_{\pm} = 2$ and r = 3.3 (i.e., BM [G**7** 31/L 100]) generated more stable particles compared to those formulated at $\rho_{\pm}$ = 2 and r = 16.2 (i.e., BM [G**7** 31/L 500]), as indicated by both the hydrodynamic size and the zeta potential of the complexes (Z-average size: 289.4 ± 8.8 nm vs. 3738.7 ± 172.4 nm; ζ-potential: +38.3 ± 0.5 mV vs. −14.1 ± 0.5 mV for the BM [G**7** 31/L 100] formulation and the BM [G**7** 31/L 500] formulation, respectively) (Fig. 4.2). Considering the limitation in increasing the lipid density (controlled by $\rho_{\pm}$ and r values) both in terms of stability and transfection activity of the lipoplexes, as stated above, the RGDG peptide functionalization of gemini surfactants demonstrated the high penetration activity with enhanced intensity of GFP expression level for the BM [G**7** 31/L 100] lipoplexes compared to the BM [G**3** 31/L 100] lipoplexes (Fig. D2, Appendix D). In terms of cytotoxicity, the BM [G**7** 31/L 100] lipoplexes caused minimal reduction in cell viability (~ 10%) compared to control-untreated group (Fig. 4.15).

5.2 PDTMG complexes: peptide-based lipopolyplexes

To improve pDNA complexation, stability, and penetration activity of the complexes while enhance their endosomal release functionality, in the present project various peptide-based lipopolyplexes, named PDTMG, were developed and studied by the non-covalent addition of peptide enhancers (P_A-P_G) and covalent functionalization of gemini surfactants with various functional groups (G**4**-G**14**) formulated in combination with DOPE lipid.

The physical characterization of PDTMG complexes formulated at $\rho_{\pm} = 2$ and r = 3.3 from cationic peptide enhancers, gemini surfactants of varying saturated alkyl tail lengths (as demonstrated by G**6** and G**7** gemini surfactant), and DOPE lipid, showed higher pDNA complexation, forming more stable particles compared to their corresponding lipoplexes, as indicated by the size, PDI and zeta potential of the complexes (e.g., Z-average size: 195.2 ± 1.6 nm vs. 289.4 ± 8.8 nm; PDI: 0.174 ± 0.017 vs. 0.475 ± 0.006; ζ-potential: +46.9 ± 0.2 mV vs. +38.3 ± 0.5 mV, for the PDTMG [P_C49/G**7** 31/L 100] formulation and the BM [G**7** 31/L 100] formulation, respectively). This is due to the effective pDNA complexation by association of cationic peptide enhancers in conjunction with gemini and DOPE. In agreement with DLS measurements, the flow cytometry quantification of the percentage of the fluorescent positive cells and the intensity of GFP expression levels revealed higher transfection activity for the G**6**- or G**7**-based PDTMG complexes compared to the counterpart lipoplexes (Fig. 4.11 and 4.12). For example, the transfection activity of the PDTMG [P_C49/G**7** 31/L 100] formulation was shown to be approximately 3-fold higher compared to the BM [G**7** 31/L 100] formulation (Fig. 5.1 (A) and (B)). Compared to the lipoplexes (prepared at $\rho_{\pm}$ = 2 and r = 3.3), the PDTMG complexes with the increased zeta potentials demonstrated stable delivery system with enhanced penetration activity and endosomal rupturing functionality.

By reducing the $\rho_{\pm}$ value from 2 to 1.1, along with increasing the amount of cationic peptide enhancers, and fine tuning the r = 6.8, the transfection activity of the G**7**-based PDTMG complexes (i.e., PDTMG [P_C267/G**7** 17/L 113]) was further improved (Fig. 4.13). This indicates the synergistic activity between the components of the G**7**-based PDTMG complexes for effective pDNA complexation, internalization, and release into the cell cytoplasm.

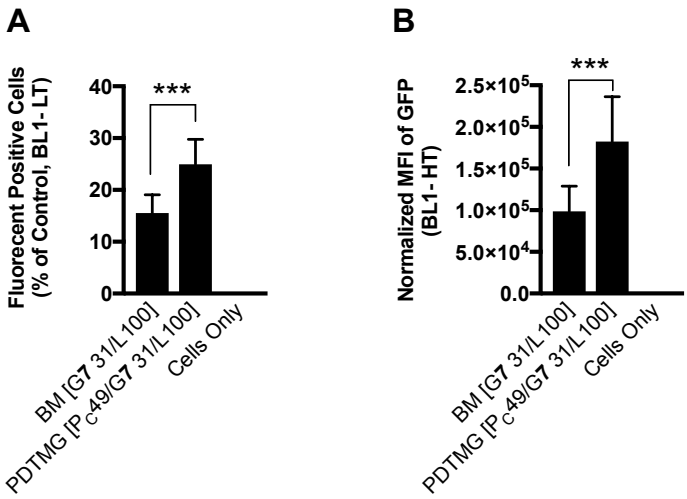

Fig. 5.1. Comparing (A) the transfection percentage, (B) the intensity of GFP expression level of G**7**-based PDTMG complexes with the counterpart lipoplex formulation. Results are presented as mean ± SD from two to three independent experiments (n = 3 per experiment) performed in 24-well plates) (*** $p < 0.001$).

In addition, at $\rho_{\pm}$ = 1.1, the impact of RGDG-functionalized gemini surfactant having saturated 18C alkyl tails (i.e., G**7**) on transfection activity of the PDTMG complexes is more pronounced when compared with counterpart PDTMG complexes formulated from gemini surfactants having saturated 12C alkyl tails (G**2** or G**6**, without or with RGDG peptide functional headgroups, respectively), or gemini surfactants having 18C without RGDG peptide functional headgroups (i.e., G**1**, G**3**-G**5**) (Fig. 5.2 (A.1) and (B.1)). This indicates that the peptide functionalization of the

gemini surfactant with long alkyl tails can improve the internalization and endosomal release of pDNA complexes.

5.2.1 Model mechanism for pDNA release from PDTMG complexes

Further investigation on the impact of peptide functionalization of gemini surfactants with saturated 18C-alkyl tails using G**7**, G**9**, and G**10**, showed that despite small differences in the physical properties (size and zeta potential) of the G**7**-, G**9**-, G**10**-based PDTMG complexes (Fig. 4.10), significant differences on their transfection activities were observed (Fig. 4. 23 (A) and (B)). As presented in Figure 5.2 (B.2-3), the peptide-functionalization of gemini surfactants with: $E(H)_5$; $EGRGDSPG(H)_5$; succinyl-$(E)_2G(R)_2$; succinyl-$(E)_2G(R)_3$; succinyl-$(E)_2(G)_3(R)_3$; succinyl-$DE(G)_3(R)_3$ (i.e., the functional headgroups of G**9**-G**14**, respectively), resulted in negligible transfection activity of G**9**-G**14**-based PDTMG complexes. The G**7** and G**8** gemini surfactants with RGDG and GRGDSPG peptide functional headgroups, respectively, and with saturated 18C-alkyl tails, however, demonstrated remarkable transfection activities (Fig. 5.2 (A.1-4) and (B.1-4)). Taken together, it can be concluded that while the peptide functionalization of gemini surfactants can improve the cellular uptake of the PDTMG complexes, the release of pDNA cargo into the cell cytoplasm depends on the molecular flexibility of the peptide-functionalized gemini surfactants to permit and induce the formation of fusogenic inverted lipid phase structure.

As illustrated in Figure 5.3, the following model mechanism is proposed for pDNA release from the lipopolyplexes, PDTMG delivery systems. After cellular uptake, the destabilization of the PDTMG complexes inside the endosomal vesicles is triggered by the inward compression exerted by actin polymerization [331] and/or by acidification of the endosomal vesicles, in which it is believed that depending on the molecular flexibility and molecular architecture of the gemini

surfactants, the induction of the inverted lipid phase structures destabilize the endosomal membrane, and hence release pDNA cargo into the cell cytoplasm. This suggested model mechanism was supported by covalently functionalizing gemini surfactants with various functional headgroups (R_1-R_{10}; Fig. 3.2) and their transfection activities formulated in the PDTMG complexes. It was observed that the increased steric hindrance of the functional headgroups (i.e., R_5-R_{10}, the peptide functional headgroups of G**9**-G**14**, respectively), resulted in negligible GFP expression levels. However, in the case of short RGDG and GRGDSPG peptide motifs linked to gemini surfactants with saturated 18C alkyl tails (i.e., R_3 and R_4, the peptide functional headgroups of G**7** and G**8**, respectively), the G**7**- and G**8**-based PDTMG complexes not only exhibited enhanced cell penetration activities but also demonstrated endosomal rupturing functionalities in response to cellular environment. From this, it can be concluded that the reduced steric hindrance associated with the amino acid arrangement of the RGDG and GRGDSPG caused the G**7**- and G**8**-based PDTMG complexes to effectively disassemble inside the endosomal compartments and release pDNA into the cell cytoplasm; while the bulky peptide functionalities in turn stiffened the G**9**-G**14**-based PDTMG complexes and hence, lead to the entrapment and degradation of pDNA in endosomal vesicles.

These experiments indicated the importance of peptide functionalization of gemini surfactants for cellular internalization and their impact on the GFP expression level. The G**7**- and G**8**-based PDTMG complexes demonstrated comparable transfection activities with the commercial gold-standard Lipofectamine 3000 reagent. The targeting ability of the peptide-decorated PDTMG complexes signifies the major advantages of this technology [309, 310] over Lipofectamine 3000 and provided a rationale in designing its versatile derivatives for targeted gene therapy.

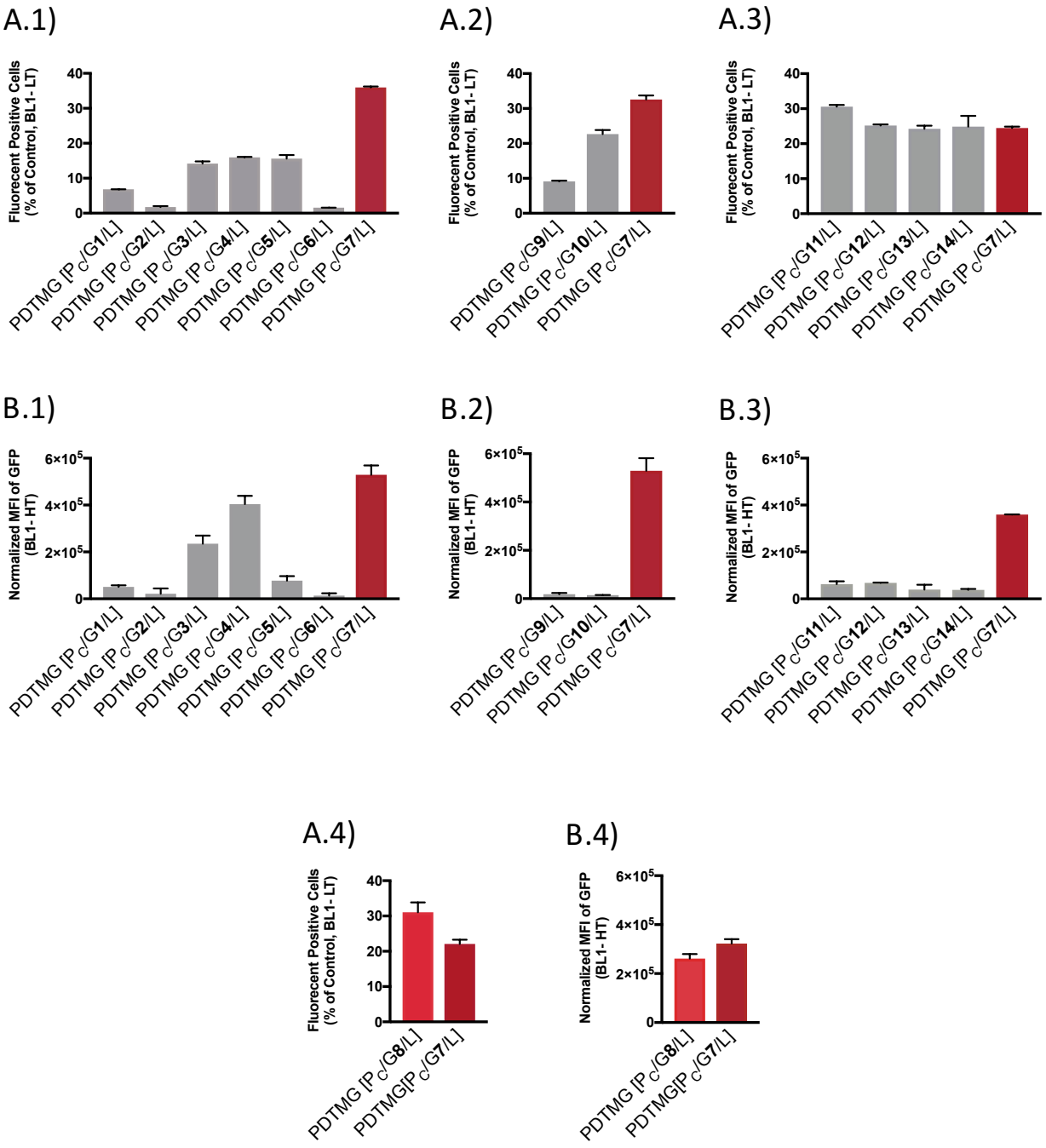

Fig. 5.2. Summary graphs for transfection activities of PDTMG complexes formulated from P_C peptide enhancer, G**1**-G**14** gemini surfactant, and DOPE lipid at $\rho_{\pm} = 1.1$ and $r = 6.8$ (prepared at $M_P = 267$, $M_G = 17$ and $M_L = 113$). (A.1-4) The percentage of the transfected cells and (B.1-4) the intensity of GFP expression level were normalized to untreated control (cells only).

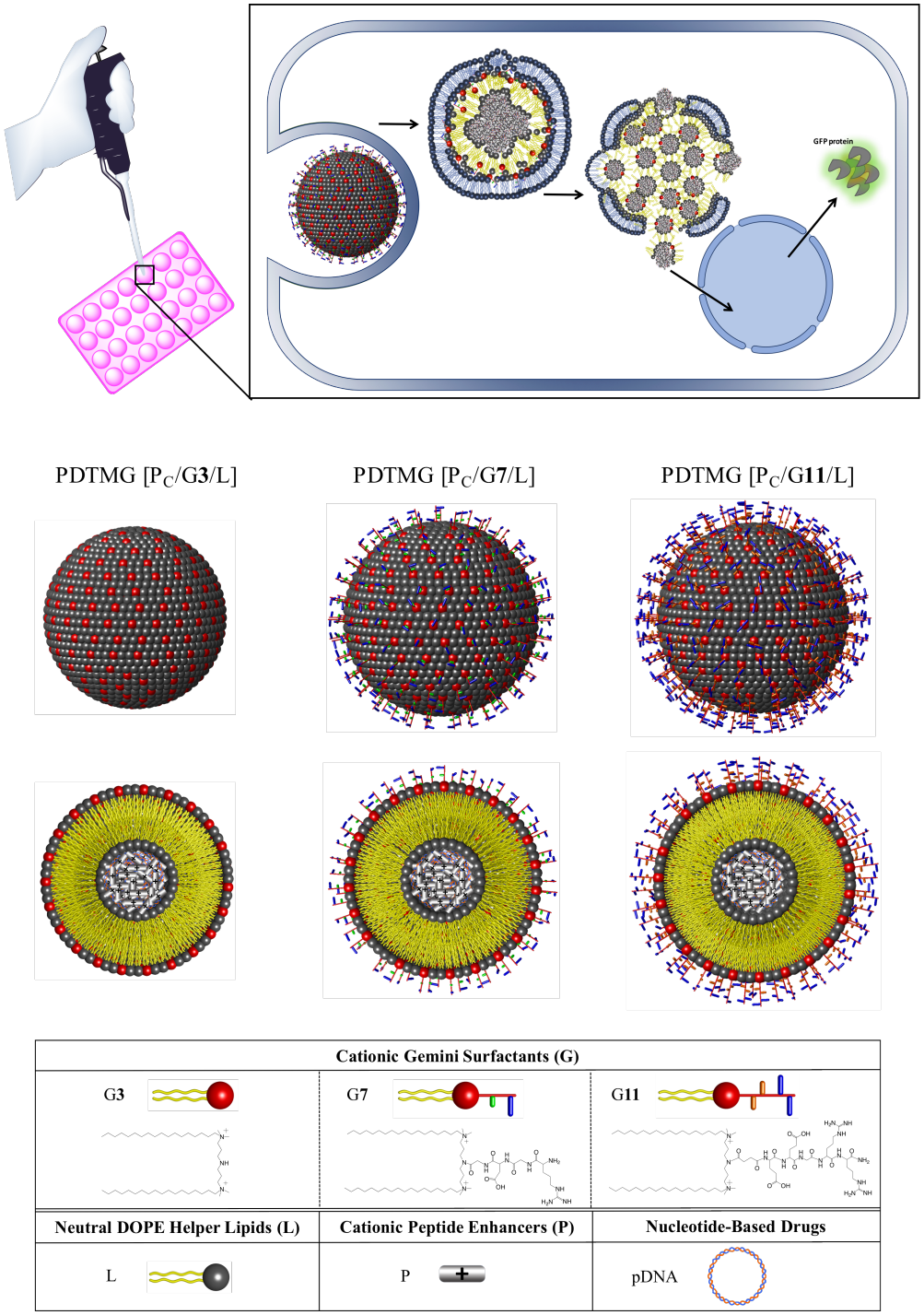

Fig. 5.3. Schematic depiction of 18-7NH-18 (G**3**)-, RGDG-18 (G**7**)-, 18-Suc-E_2GR_2 (G**11**)-based PDTMG nanoparticles (top: from the surface view; bottom: from the horizontal plane view). The peptide functional headgroups of G**7** and G**11** gemini surfactants provide higher penetration activities compared to G**3** gemini surfactant. In addition, the RGDG functional headgroup of the

G**7** gemini surfactants present a reduced steric hindrance at the surface of the PDTMG nanoparticles compared to G**11** gemini surfactants. This is believed to allow G**7** gemini surfactants the molecular flexibly to induce lipid phase transition in the endosomal vesicles and effectively disassemble and rupture the endosome and release pDNA cargo into the cell cytoplasm. The peptide functionality of G**11** gemini surfactants, however, it is believed to stiffen the G**11**-based PDTMG nanoparticles in which the bulky peptide functionality (i.e., with side chain groups of amino acid residues at both sides of the peptide backbone plane according to the primary structure of the peptide) of G**11** may be locked into position, thus avoiding the inverted phase transition inside the endosomes and; hence resulted in pDNA entrapment and/or low release from endosomes. This proposed model mechanism may explain the high MFI of the G**7**-based PDTMG nanoparticles.

Chapter 6

Conclusion and Future Directions

In the present study, several designed peptide enhancers and novel functionalized gemini surfactants were developed and their transfection properties, alone or in combination with or without DOPE lipid, were investigated. The physicochemical properties along with transfection activity and cytotoxicity of various gene delivery systems were evaluated to identify the elements for efficient uptake, effective DNA complexation and release into the cell cytoplasm.

The success for development of a potent gene delivery system is reliant on the amount, concentration (i.e., formulation aspect), as well as the structure-activity relationship of the compositional elements for DNA compaction and release. It was shown that the formation of large aggregates are not particularly detrimental for the *in vitro* transfection activity [303], since, for example, the large complexes of the BM [G**3** 31/L 500] formulation (prepared at $\rho_{\pm} = 2$ and r = 16.2) showed significant transfection activity when compared to untreated control cells (Fig. 4.3). However, the physical properties (i.e., size, PDI, and zeta potential) of the complexes are imperative indications for the particle stability, and essential for *in vivo* gene therapy applications. In this project, the transfection study of 7 peptide enhancers (P_A-P_G) and 15 different gemini surfactants (G**0**-G**14**) differing in spacer groups and/or functional headgroups and/or alkyl tail lengths were evaluated in different formulations.

It was shown that non-covalent addition of cationic peptide enhancers (i.e., P_B-P_G) formulated with gemini surfactants and DOPE lipid can significantly improve the transfection activity of gene delivery complexes when compared to uni-modal (i.e., UM [G], UM [P]) and bi-modal (i.e., BM [G/L], BM [P/L], BM [P/G]) complexes. This indicates that the high association of the cationic

peptide enhancers to pDNA provided a peptide-pDNA core platform for effective compaction of pDNA by gemini surfactant and DOPE lipid in the tri-modal gene delivery system (PDTMG). While the transfection activities of the PDTMG complexes formulated from cationic peptide enhancers were shown to be higher than those formulated from zwitterionic P_A peptide enhancers, there were no significant differences amongst transfection activities of the PDTMG complexes formulated from the cationic P_B-P_G peptide enhancers. This is partly attributed to the comparable pDNA complexation using the cationic P_B-P_G peptide enhancers resulting from small differences on their net positive charges ranging from 0.5-6.3. The impact of cationic peptide enhancers for effective pDNA compaction and their *in vitro* transfection activities in the PDTMG formulations can further be studied by increasing the number of Arg or Lys residues with or without RGD targeting or His-rich motifs, as listed in Table 6.1. The impact of non-covalent addition of the peptide enhancers on morphology of the lipopolyplexes will also require further detail investigation by TEM, SNAS and SAXS [258, 259, 326, 332].

Table. 6.1. Future possibilities for designing cationic peptide enhancers to investigate the extent of transfection improvements in comparison with P_C peptide enhancers in the PDTMG formulations.

Peptide enhancer	Name	Sequence (N- to C-terminus)
P_C (17a.a.)	RGD-$(R)_6$-H_3	GRGDSPGH$(R)_3$H$(R)_3$HG
P_H (12a.a.)	$(R)_{12}$	RRRRRRRRRRRR
P_I (12a.a.)	$(K)_{12}$	KKKKKKKKKKKK
P_J (19a.a.)	RGD-$(R)_{12}$	GRGDSPGRRRRRRRRRRRR
P_K (19a.a.)	RGD-$(K)_{12}$	GRGDSPGKKKKKKKKKKKK
P_L (19a.a.)	$(H)_7$-$(K)_{12}$	HHHHHHHKKKKKKKKKKKK
P_M (20a.a.)	$(K)_{20}$	KKKKKKKKKKKKKKKKKKKK

Further, it was shown that among the gemini surfactants studied in this project, the G**7**- and G**8**-based PDTMG delivery systems formulated at $\rho_{\pm} = 1.1$ and r = 6.8 (prepared at $M_P = 267$ μM, $M_G = 17$ μM, $M_L = 113$ μM) demonstrated superior transfection activities comparable to Lipofectamine 3000 transfection reagent. It is believed that the short RGDG and GRGDSPG peptide motifs covalently linked to gemini surfactants with saturated 18C alkyl tails not only resulted in enhanced penetration of the complexes but also provided reduced steric hindrance on the surface of the PDTMG complexes, allowing the complexes to effectively disassemble inside the cells, and release their pDNA cargo into the cell cytoplasm. The impact of molecular architecture of peptide-functionalized gemini surfactants in relation to the stability, transfection activity, and cell cytotoxicity of the tri-modal gene delivery complexes can be further studied for development of versatile delivery systems. For example, the derivatives of G**7** gemini surfactant can be produced by alteration of the primary structure of the peptide headgroups [333] using method (B) and/or the alkyl chain geometry, as shown in Fig. 6.1, to further investigate their structure-function relationships. The synthesis of the peptide-functionalized gemini surfactants on-resin using solid phase peptide synthesis (i.e., method (B)) could be advantageous in that the facile manufacturing of a library of gemini surfactants of varying peptide motif headgroups can be prepared using high-throughput automated peptide synthesis [334, 335]. The versatile development of active peptide-decorated PDTMG complexes can further be investigated for targeted gene delivery of various cell lines, including keratinocytes, retinal cells, neuronal cells, and lymphocytes for eventual *ex vivo* and *in vivo* applications.

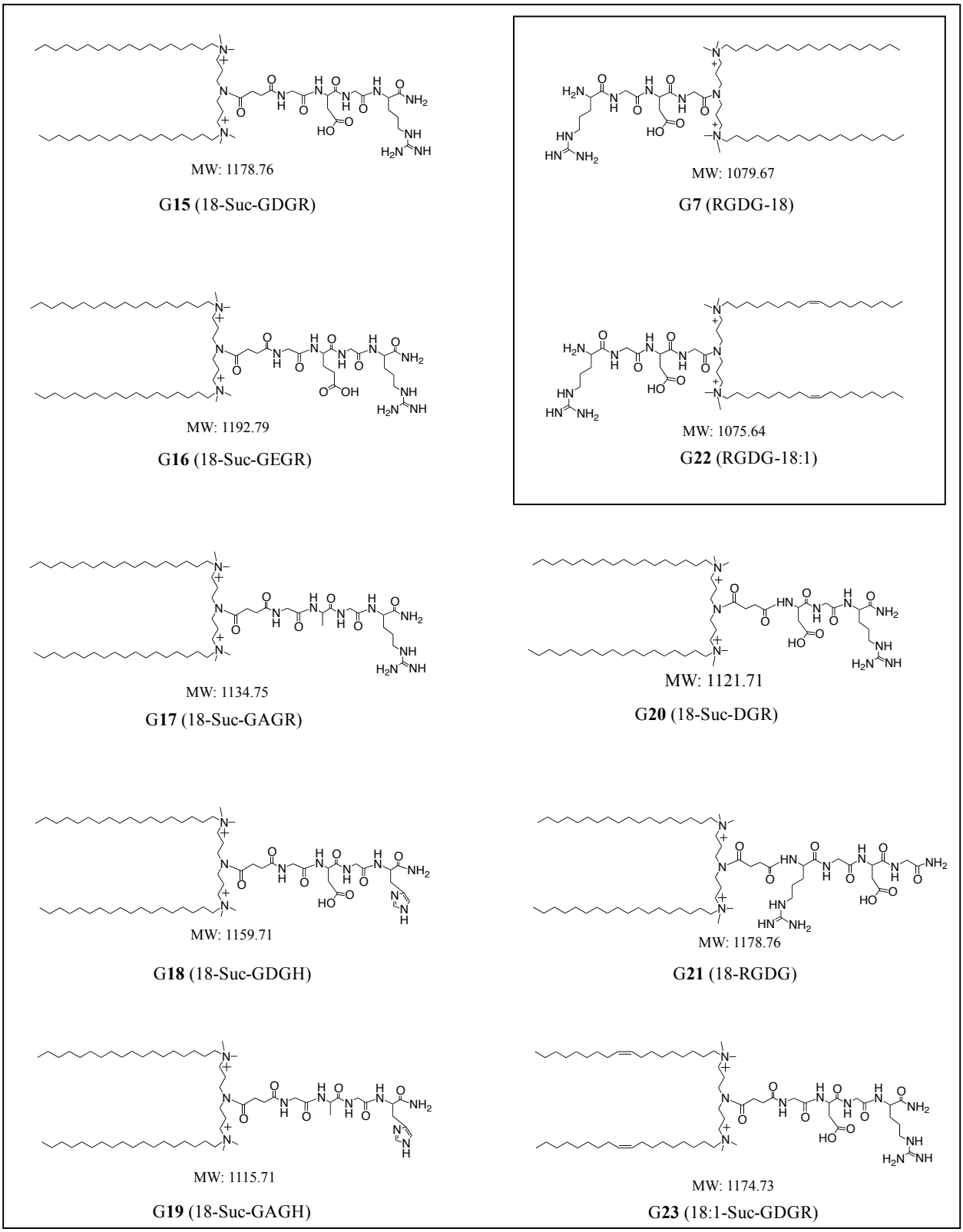

Fig. 6.1. Chemical structures for future congeners of G**7** gemini surfactants.

Letter of Copyright Permission

Title: Biophysical Characterization of an Integrin-Targeted Lipopolyplex Gene Delivery Vector

Author: M. Firouz Mohd Mustapa, Paul C. Bell, Christopher A. Hurley, et al

Publication: Biochemistry

Publisher: American Chemical Society

Date: Nov 1, 2007

LOGIN

If you're a copyright.com user, you can login to RightsLink using your copyright.com credentials.

Already **a RightsLink user** or want to learn more?

PERMISSION/LICENSE IS GRANTED FOR YOUR ORDER AT NO CHARGE

This type of permission/license, instead of the standard Terms & Conditions, is sent to you because no fee is being charged for your order. Please note the following:

- Permission is granted for your request in both print and electronic formats, and translations.
- If figures and/or tables were requested, they may be adapted or used in part.
- Please print this page for your records and send a copy of it to your publisher/graduate school.
- Appropriate credit for the requested material should be given as follows: "Reprinted (adapted) with permission from (COMPLETE REFERENCE CITATION). Copyright (YEAR) American Chemical Society." Insert appropriate information in place of the capitalized words.
- One-time permission is granted only for the use specified in your request. No additional uses are granted (such as derivative works or other editions). For any other uses, please submit a new request.

If credit is given to another source for the material you requested, permission must be obtained from that source.

BACK CLOSE WINDOW

Bibliography

1. Walsh, C.E., *Hemophilia gene therapy*, Translating Gene Therapy to the Clinic. 2015, Elsevier. p. 207-213.
2. Cavazzana-Calvo, M., et al., *Transfusion independence and HMGA2 activation after gene therapy of human β-thalassaemia.* Nature, 2010. **467**(7313): p. 318.
3. Griesenbach, U., K.M. Pytel, and E.W. Alton, *Cystic fibrosis gene therapy in the UK and elsewhere.* Human Gene Therapy, 2015. **26**(5): p. 266-275.
4. Braun, C.J., et al., *Gene therapy for Wiskott-Aldrich syndrome—long-term efficacy and genotoxicity.* Science Translational Medicine, 2014. **6**(227): p. 227ra33-227ra33.
5. Kerr, D., *Clinical development of gene therapy for colorectal cancer.* Nature Reviews Cancer, 2003. **3**(8): p. 615.
6. Cross, D. and J.K. Burmester, *Gene therapy for cancer treatment: past, present and future.* Clinical Medicine & Research, 2006. **4**(3): p. 218-227.
7. Hu, W., et al., *RNA-directed gene editing specifically eradicates latent and prevents new HIV-1 infection.* Proceedings of the National Academy of Sciences, 2014. **111**(31): p. 11461-11466.
8. O'Connor, D.M. and N.M. Boulis, *Gene therapy for neurodegenerative diseases.* Trends in Molecular Medicine, 2015. **21**(8): p. 504-512.
9. Rincon, M.Y., T. VandenDriessche, and M.K. Chuah, *Gene therapy for cardiovascular disease: advances in vector development, targeting, and delivery for clinical translation.* Cardiovascular Research, 2015. **108**(1): p. 4-20.
10. Lombardo, A., et al., *Gene editing in human stem cells using zinc finger nucleases and integrase-defective lentiviral vector delivery.* Nature Biotechnology, 2007. **25**(11): p. 1298.

11. Jinek, M., et al., *A programmable dual-RNA–guided DNA endonuclease in adaptive bacterial immunity.* Science, 2012. **337**(6096): p. 816-821.

12. Gaj, T., C.A. Gersbach, and C.F. Barbas, *ZFN, TALEN, and CRISPR/Cas-based methods for genome engineering.* Trends in Biotechnology, 2013. **31**(7): p. 397-405.

13. Hsu, P.D., E.S. Lander, and F. Zhang, *Development and applications of CRISPR-Cas9 for genome engineering.* Cell, 2014. **157**(6): p. 1262-1278.

14. Doudna, J.A. and E. Charpentier, *The new frontier of genome engineering with CRISPR-Cas9.* Science, 2014. **346**(6213): p. 1258096.

15. Stribley, J.M., et al., *Gene therapy and reproductive medicine.* Fertility and Sterility, 2002. **77**(4): p. 645-657.

16. Ibraheem, D., A. Elaissari, and H. Fessi, *Gene therapy and DNA delivery systems.* International Journal of Pharmaceutics, 2014. **459**(1): p. 70-83.

17. Munson, R. and L.H. Davis, *Germ-line gene therapy and the medical imperative.* Kennedy Institute of Ethics Journal, 1992. **2**(2): p. 137-158.

18. Liang, P., et al., *CRISPR/Cas9-mediated gene editing in human tripronuclear zygotes.* Protein & Cell, 2015. **6**(5): p. 363-372.

19. Lanphier, E. and F. Urnov, *Don't edit the human germ line.* Nature, 2015. **519**(7544): p. 410.

20. Baltimore, D., et al., *A prudent path forward for genomic engineering and germline gene modification.* Science, 2015. **348**(6230): p. 36-38.

21. Miller, H.I., *Germline gene therapy: We're ready.* Science, 2015. **348**(6241): p. 1325-1325.

22. Porteus, M.H. and C.T. Dann, *Genome editing of the germline: broadening the discussion.* Molecular Therapy, 2015. **23**(6): p. 980-982.

23. Ormond, K.E., et al., *Human germline genome editing.* The American Journal of Human Genetics, 2017. **101**(2): p. 167-176.

24. Anderson, W.F., *Prospects for human gene therapy.* Science, 1984. **226**(4673): p. 401-409.

25. Foldvari, M., et al., *Non-viral gene therapy: gains and challenges of non-invasive administration methods.* Journal of Controlled Release, 2016. **240**: p. 165-190.

26. Liu, C., et al., *Delivery strategies of the CRISPR-Cas9 gene-editing system for therapeutic applications.* Journal of Controlled Release, 2017.

27. Miller, J.C., et al., *A TALE nuclease architecture for efficient genome editing.* Nature Biotechnology, 2011. **29**(2): p. 143-148.

28. Wang, H.-X., et al., *CRISPR/Cas9-based genome editing for disease modeling and therapy: challenges and opportunities for nonviral delivery.* Chemical Reviews, 2017. **117**(15): p. 9874-9906.

29. Rosenberg, S.A., et al., *Gene transfer into humans—immunotherapy of patients with advanced melanoma, using tumor-infiltrating lymphocytes modified by retroviral gene transduction.* New England Journal of Medicine, 1990. **323**(9): p. 570-578.

30. Blaese, R.M., et al., *T lymphocyte-directed gene therapy for ADA− SCID: initial trial results after 4 years.* Science, 1995. **270**(5235): p. 475-480.

31. Ginn, S.L., et al., *Gene therapy clinical trials worldwide to 2017: An update.* The Journal of Gene Medicine, 2018. **20**(5): p. e3015.

32. Pearson, S., H. Jia, and K. Kandachi, *China approves first gene therapy*. 2004, Nature Publishing Group.

33. Ylä-Herttuala, S., *Endgame: glybera finally recommended for approval as the first gene therapy drug in the European union*. 2012, Nature Publishing Group.

34. Aiuti, A., M.G. Roncarolo, and L. Naldini, *Gene therapy for ADA-SCID, the first marketing approval of an ex vivo gene therapy in Europe: paving the road for the next generation of advanced therapy medicinal products.* EMBO Molecular Medicine, 2017: p. e201707573.

35. Ledford, H., *Engineered cell therapy for cancer gets thumbs up from FDA advisers.* Nature, 2017. **547**(7663): p. 270.

36. Wilson, J.M., *2017 Was the Year We Have Been Waiting For*. 2017, Mary Ann Liebert, Inc. 140 Huguenot Street, 3rd Floor New Rochelle, NY 10801 USA.

37. Senior, M., *After Glybera's withdrawal, what's next for gene therapy?* 2017, Nature Publishing Group.

38. Sharfstein, S.T., *Non-protein biologic therapeutics.* Current Opinion in Biotechnology, 2018. **53**: p. 65-75.

39. Morrison, C., *Landmark gene therapy poised for US approval*. 2017, Nature Publishing Group.

40. Fischer, A. and A. Stark. *FDA approval brings first gene therapy to the United States*. 2017; Available from: https://www.fda.gov/NewsEvents/Newsroom/PressAnnouncements/ucm574058.htm.

41. Prasad, V., *Immunotherapy: Tisagenlecleucel—the first approved CAR-T-cell therapy: implications for payers and policy makers.* Nature Reviews Clinical Oncology, 2018. **15**(1): p. 11.

42. Fischer, A. *FDA approves CAR-T cell therapy to treat adults with certain types of large B-cell lymphoma*. 2017; Available from: https://www.fda.gov/NewsEvents/Newsroom/PressAnnouncements/ucm581216.htm.

43. Fischer, A. *FDA approves novel gene therapy to treat patients with a rare form of inherited vision loss*. 2017; Available from: https://www.fda.gov/NewsEvents/Newsroom/PressAnnouncements/ucm589467.htm.

44. Smalley, E., *First AAV gene therapy poised for landmark approval*. 2017, Nature Publishing Group.

45. Hacein-Bey-Abina, S., et al., *LMO2-associated clonal T cell proliferation in two patients after gene therapy for SCID-X1.* Science, 2003. **302**(5644): p. 415-419.

46. McCormack, M.P. and T.H. Rabbitts, *Activation of the T-cell oncogene LMO2 after gene therapy for X-linked severe combined immunodeficiency.* New England Journal of Medicine, 2004. **350**(9): p. 913-922.

47. Thomas, C.E., A. Ehrhardt, and M.A. Kay, *Progress and problems with the use of viral vectors for gene therapy.* Nature Reviews Genetics, 2003. **4**(5): p. 346-358.

48. Marshall, E., *Gene therapy on trial.* Science, 2000. **288**(5468): p. 951-957.

49. Check, E., *Gene therapy: a tragic setback.* Nature, 2002. **420**(6912): p. 116-118.

50. Couzin, J. and J. Kaiser, *As Gelsinger case ends, gene therapy suffers another blow*. 2005, American Association for the Advancement of Science.

51. Budde, L.E. and J.A. Zaia, *CD19 CAR-T therapy and sepsis: dancing with the devil.* Blood, 2018. **131**(1): p. 7-8.

52. Nayak, S. and R.W. Herzog, *Progress and prospects: immune responses to viral vectors.* Gene therapy, 2010. **17**(3): p. 295.

53. Ylä-Herttuala, S., *Glybera's second act: the curtain rises on the high cost of therapy.* Molecular Therapy, 2015. **23**(2): p. 217-218.

54. Merten, O.-W., et al., *Manufacturing of viral vectors for gene therapy: part I. Upstream processing.* Pharmaceutical Bioprocessing, 2014. **2**(2): p. 183-203.

55. Neumann, E., et al., *Gene transfer into mouse lyoma cells by electroporation in high electric fields.* The EMBO journal, 1982. **1**(7): p. 841-845.

56. Sanford, J.C., et al., *Delivery of substances into cells and tissues using a particle bombardment process.* Particulate Science and Technology, 1987. **5**(1): p. 27-37.

57. Kim, H.J., et al., *Ultrasound-mediated transfection of mammalian cells.* Human Gene Therapy, 1996. **7**(11): p. 1339-1346.

58. Budker, V., et al., *The efficient expression of intravascularly delivered DNA in rat muscle.* Gene therapy, 1998. **5**(2): p. 272-276.

59. Gao, X., K.-S. Kim, and D. Liu, *Nonviral gene delivery: what we know and what is next.* The AAPS Journal, 2007. **9**(1): p. E92-E104.

60. Mellott, A.J., M.L. Forrest, and M.S. Detamore, *Physical non-viral gene delivery methods for tissue engineering.* Annals of Biomedical Engineering, 2013. **41**(3): p. 446-468.

61. Morille, M., et al., *Progress in developing cationic vectors for non-viral systemic gene therapy against cancer.* Biomaterials, 2008. **29**(24-25): p. 3477-3496.

62. Yin, H., et al., *Non-viral vectors for gene-based therapy.* Nature Reviews Genetics, 2014. **15**(8): p. 541.

63. Chen, J., et al., *Production and clinical development of nanoparticles for gene delivery.* Molecular Therapy-Methods & Clinical Development, 2016. **3**: p. 16023.

64. Wagner, E., *Strategies to improve DNA polyplexes for in vivo gene transfer: will "artificial viruses" be the answer?* Pharmaceutical Research, 2004. **21**(1): p. 8-14.

65. Mastrobattista, E., et al., *Artificial viruses: a nanotechnological approach to gene delivery.* Nature reviews Drug discovery, 2006. **5**(2): p. 115.

66. Miyata, K., N. Nishiyama, and K. Kataoka, *Rational design of smart supramolecular assemblies for gene delivery: chemical challenges in the creation of artificial viruses.* Chemical Society Reviews, 2012. **41**(7): p. 2562-2574.

67. Kawabata, K., Y. Takakura, and M. Hashida, *The fate of plasmid DNA after intravenous injection in mice: involvement of scavenger receptors in its hepatic uptake.* Pharmaceutical Research, 1995. **12**(6): p. 825-830.

68. Mintzer, M.A. and E.E. Simanek, *Nonviral vectors for gene delivery.* Chemical Reviews, 2008. **109**(2): p. 259-302.

69. Tang, M. and F. Szoka, *The influence of polymer structure on the interactions of cationic polymers with DNA and morphology of the resulting complexes.* Gene Therapy, 1997. **4**(8).

70. Plank, C., et al., *Activation of the complement system by synthetic DNA complexes: a potential barrier for intravenous gene delivery.* Human Gene Therapy, 1996. **7**(12): p. 1437-1446.

71. Zhang, J.-S., F. Liu, and L. Huang, *Implications of pharmacokinetic behavior of lipoplex for its inflammatory toxicity.* Advanced Drug Delivery Reviews, 2005. **57**(5): p. 689-698.

72. Klibanov, A.L., et al., *Amphipathic polyethyleneglycols effectively prolong the circulation time of liposomes.* FEBS Letters, 1990. **268**(1): p. 235-237.

73. Wang, T., J.R. Upponi, and V.P. Torchilin, *Design of multifunctional non-viral gene vectors to overcome physiological barriers: dilemmas and strategies.* International Journal of Pharmaceutics, 2012. **427**(1): p. 3-20.

74. Maeda, H., et al., *Tumor vascular permeability and the EPR effect in macromolecular therapeutics: a review.* Journal of Controlled Release, 2000. **65**(1): p. 271-284.

75. Mishra, S., P. Webster, and M.E. Davis, *PEGylation significantly affects cellular uptake and intracellular trafficking of non-viral gene delivery particles.* European Journal of Cell Biology, 2004. **83**(3): p. 97-111.

76. Hatakeyama, H., H. Akita, and H. Harashima, *A multifunctional envelope type nano device (MEND) for gene delivery to tumours based on the EPR effect: a strategy for overcoming the PEG dilemma.* Advanced Drug Delivery Reviews, 2011. **63**(3): p. 152-160.

77. Khalil, I.A., et al., *Uptake pathways and subsequent intracellular trafficking in nonviral gene delivery.* Pharmacological Reviews, 2006. **58**(1): p. 32-45.

78. Elouahabi, A. and J.-M. Ruysschaert, *Formation and intracellular trafficking of lipoplexes and polyplexes.* Molecular Therapy, 2005. **11**(3): p. 336-347.

79. Häcker, U., K. Nybakken, and N. Perrimon, *Heparan sulphate proteoglycans: the sweet side of development.* Nature Reviews. Molecular cell biology, 2005. **6**(7): p. 530.

80. Rehman, Z.u., D. Hoekstra, and I.S. Zuhorn, *Mechanism of polyplex-and lipoplex-mediated delivery of nucleic acids: real-time visualization of transient membrane destabilization without endosomal lysis.* ACS Nano, 2013. **7**(5): p. 3767-3777.

81. Summerford, C. and R.J. Samulski, *Membrane-associated heparan sulfate proteoglycan is a receptor for adeno-associated virus type 2 virions.* Journal of Virology, 1998. **72**(2): p. 1438-1445.

82. Giroglou, T., et al., *Human papillomavirus infection requires cell surface heparan sulfate.* Journal of Virology, 2001. **75**(3): p. 1565-1570.

83. Tuve, S., et al., *Role of cellular heparan sulfate proteoglycans in infection of human adenovirus serotype 3 and 35.* PLoS Pathogens, 2008. **4**(10): p. e1000189.

84. Hussein, H.A., et al., *Beyond RGD: virus interactions with integrins.* Archives of Virology, 2015. **160**(11): p. 2669-2681.

85. Schaffer, D.V. and D.A. Lauffenburger, *Optimization of cell surface binding enhances efficiency and specificity of molecular conjugate gene delivery.* Journal of Biological Chemistry, 1998. **273**(43): p. 28004-28009.

86. Pack, D.W., et al., *Design and development of polymers for gene delivery.* Nature Reviews Drug discovery, 2005. **4**(7): p. 581.

87. Sakurai, Y., et al., *RNAi-mediated gene knockdown and anti-angiogenic therapy of RCCs using a cyclic RGD-modified liposomal-siRNA system.* Journal of Controlled Release, 2014. **173**: p. 110-118.

88. Lee, D.-J., et al., *Systemic delivery of folate-PEG siRNA lipopolyplexes with enhanced intracellular stability for in vivo gene silencing in leukemia.* Bioconjugate Chemistry, 2017. **28**(9): p. 2393-2409.

89. Zhang, W., et al., *Combination of sequence-defined oligoaminoamides with transferrin-polycation conjugates for receptor-targeted gene delivery.* The journal of Gene Medicine, 2015. **17**(8-9): p. 161-172.

90. Ruan, G.-X., et al., *Macrophage mannose receptor-specific gene delivery vehicle for macrophage engineering.* Acta Biomaterialia, 2014. **10**(5): p. 1847-1855.

91. Duan, Y., et al., *A tumor targeted gene vector modified with G250 monoclonal antibody for gene therapy.* Journal of Controlled Release, 2008. **127**(2): p. 173-179.

92. Wickham, T.J., et al., *Integrins αvβ3 and αvβ5 promote adenovirus internalization but not virus attachment.* Cell, 1993. **73**(2): p. 309-319.

93. Bergelson, J.M., et al., *Identification of the integrin VLA-2 as a receptor for echovirus 1.* Science, 1992. **255**(5052): p. 1718-1720.

94. Logan, D., et al., *Structure of a major immunogenic site on foot-and-mouth disease virus.* Nature, 1993. **362**(6420): p. 566.

95. Ng, Q.K., et al., *Engineering clustered ligand binding into nonviral vectors: αvβ3 targeting as an example.* Molecular Therapy, 2009. **17**(5): p. 828-836.

96. Hee-Dong, H., et al., *Targeted gene silencing using RGD-labeled chitosan nanoparticles.* Clinical Cancer Research, 2010: p. clincanres. 0005. subyr.

97. Danhier, F., A. Le Breton, and V.r. Préat, *RGD-based strategies to target alpha (v) beta (3) integrin in cancer therapy and diagnosis.* Molecular Pharmaceutics, 2012. **9**(11): p. 2961-2973.

98. Kim, Y.-M., S.-C. Park, and M.-K. Jang, *Targeted gene delivery of polyethyleneimine-grafted chitosan with RGD dendrimer peptide in αvβ3 integrin-overexpressing tumor cells.* Carbohydrate Polymers, 2017. **174**: p. 1059-1068.

99. Liu, Z., F. Wang, and X. Chen, *Integrin αvβ3-targeted cancer therapy.* Drug Development Research, 2008. **69**(6): p. 329-339.

100. Schiffelers, R.M., et al., *Cancer siRNA therapy by tumor selective delivery with ligand-targeted sterically stabilized nanoparticle.* Nucleic Acids Research, 2004. **32**(19): p. e149-e149.

101. Vercauteren, D., et al., *The use of inhibitors to study endocytic pathways of gene carriers: optimization and pitfalls.* Molecular Therapy, 2010. **18**(3): p. 561-569.

102. Medina-Kauwe, L., J. Xie, and S. Hamm-Alvarez, *Intracellular trafficking of nonviral vectors.* Gene therapy, 2005. **12**(24): p. 1734-1751.

103. Xiang, S., et al., *Uptake mechanisms of non-viral gene delivery.* Journal of Controlled Release, 2012. **158**(3): p. 371-378.

104. El-Sayed, A. and H. Harashima, *Endocytosis of gene delivery vectors: from clathrin-dependent to lipid raft-mediated endocytosis.* Molecular Therapy, 2013. **21**(6): p. 1118-1130.

105. Kiss, A.L. and E. Botos, *Endocytosis via caveolae: alternative pathway with distinct cellular compartments to avoid lysosomal degradation?* Journal of Cellular and Molecular Medicine, 2009. **13**(7): p. 1228-1237.

106. Rewatkar, P.V., et al., *Are caveolae a cellular entry route for non-viral therapeutic delivery systems?* Advanced Drug Delivery Reviews, 2015. **91**: p. 92-108.

107. Ferrari, A., et al., *Caveolae-mediated internalization of extracellular HIV-1 tat fusion proteins visualized in real time.* Molecular Therapy, 2003. **8**(2): p. 284-294.

108. Hillaireau, H. and P. Couvreur, *Nanocarriers' entry into the cell: relevance to drug delivery.* Cellular and Molecular Life Sciences, 2009. **66**(17): p. 2873-2896.

109. Lim, J.P. and P.A. Gleeson, *Macropinocytosis: an endocytic pathway for internalising large gulps.* Immunology and Cell Biology, 2011. **89**(8): p. 836-843.

110. Rabinovitch, M., *Professional and non-professional phagocytes: an introduction.* Trends in Cell Biology, 1995. **5**(3): p. 85-87.

111. Gupta, B., T.S. Levchenko, and V.P. Torchilin, *Intracellular delivery of large molecules and small particles by cell-penetrating proteins and peptides.* Advanced Drug Delivery Reviews, 2005. **57**(4): p. 637-651.

112. Koren, E. and V.P. Torchilin, *Cell-penetrating peptides: breaking through to the other side.* Trends in Molecular Medicine, 2012. **18**(7): p. 385-393.

113. Jones, C.H., et al., *Overcoming nonviral gene delivery barriers: perspective and future.* Molecular Pharmaceutics, 2013. **10**(11): p. 4082-4098.

114. Sahay, G., et al., *Efficiency of siRNA delivery by lipid nanoparticles is limited by endocytic recycling.* Nature Biotechnology, 2013. **31**(7): p. 653-658.

115. Remaut, K., et al., *Lysosomal capturing of cytoplasmic injected nanoparticles by autophagy: An additional barrier to non viral gene delivery.* Journal of Controlled Release, 2014. **195**: p. 29-36.

116. Zabner, J., et al., *Cellular and molecular barriers to gene transfer by a cationic lipid.* Journal of Biological Chemistry, 1995. **270**(32): p. 18997-19007.

117. Xu, Y. and F.C. Szoka, *Mechanism of DNA release from cationic liposome/DNA complexes used in cell transfection.* Biochemistry, 1996. **35**(18): p. 5616-5623.

118. Cullis, P.R., M.J. Hope, and C.P. Tilcock, *Lipid polymorphism and the roles of lipids in membranes.* Chemistry and Physics of Lipids, 1986. **40**(2): p. 127-144.

119. Litzinger, D.C. and L. Huang, *Phosphatodylethanolamine liposomes: drug delivery, gene transfer and immunodiagnostic applications.* Biochimica et Biophysica Acta (BBA)-Reviews on Biomembranes, 1992. **1113**(2): p. 201-227.

120. Farhood, H., N. Serbina, and L. Huang, *The role of dioleoyl phosphatidylethanolamine in cationic liposome mediated gene transfer.* Biochimica et Biophysica Acta (BBA)-Biomembranes, 1995. **1235**(2): p. 289-295.

121. Seth, P., M.C. Willingham, and I. Pastan, *Binding of adenovirus and its external proteins to Triton X-114. Dependence on pH.* Journal of Biological Chemistry, 1985. **260**(27): p. 14431-14434.

122. Dmitriev, I., et al., *An adenovirus vector with genetically modified fibers demonstrates expanded tropism via utilization of a coxsackievirus and adenovirus receptor-independent cell entry mechanism.* Journal of Virology, 1998. **72**(12): p. 9706-9713.

123. Medina-Kauwe, L.K., *Endocytosis of adenovirus and adenovirus capsid proteins.* Advanced Drug Delivery Reviews, 2003. **55**(11): p. 1485-1496.

124. Neumann, R., J. Chroboczek, and B. Jacrot, *Determination of the nucleotide sequence for the penton-base gene of human adenovirus type 5.* Gene, 1988. **69**(1): p. 153-157.

125. Zuhorn, I.S., et al., *Nonbilayer phase of lipoplex–membrane mixture determines endosomal escape of genetic cargo and transfection efficiency.* Molecular Therapy, 2005. **11**(5): p. 801-810.

126. Johnsson, M. and K. Edwards, *Phase behavior and aggregate structure in mixtures of dioleoylphosphatidylethanolamine and poly (ethylene glycol)-lipids.* Biophysical Journal, 2001. **80**(1): p. 313-323.

127. Israelachvili, J.N., D.J. Mitchell, and B.W. Ninham, *Theory of self-assembly of hydrocarbon amphiphiles into micelles and bilayers.* Journal of the Chemical Society, Faraday Transactions 2: Molecular and Chemical Physics, 1976. **72**: p. 1525-1568.

128. Hafez, I.M. and P.R. Cullis, *Roles of lipid polymorphism in intracellular delivery.* Advanced Drug Delivery Reviews, 2001. **47**(2): p. 139-148.

129. Rädler, J.O., et al., *Structure of DNA-cationic liposome complexes: DNA intercalation in multilamellar membranes in distinct interhelical packing regimes.* Science, 1997. **275**(5301): p. 810-814.

130. Koltover, I., et al., *An inverted hexagonal phase of cationic liposome-DNA complexes related to DNA release and delivery.* Science, 1998. **281**(5373): p. 78-81.

131. Boussif, O., et al., *A versatile vector for gene and oligonucleotide transfer into cells in culture and in vivo: polyethylenimine.* Proceedings of the National Academy of Sciences, 1995. **92**(16): p. 7297-7301.

132. Behr, J.-P., *The proton sponge: a trick to enter cells the viruses did not exploit.* CHIMIA International Journal for Chemistry, 1997. **51**(1-2): p. 1-2.

133. Thomas, M. and A. Klibanov, *Non-viral gene therapy: polycation-mediated DNA delivery.* Applied Microbiology and Biotechnology, 2003. **62**(1): p. 27-34.

134. Ciftci, K. and R.J. Levy, *Enhanced plasmid DNA transfection with lysosomotropic agents in cultured fibroblasts.* International Journal of Pharmaceutics, 2001. **218**(1-2): p. 81-92.

135. Cheng, J., et al., *Structure− function correlation of chloroquine and analogues as transgene expression enhancers in nonviral gene delivery.* Journal of Medicinal Chemistry, 2006. **49**(22): p. 6522-6531.

136. Mochizuki, S., et al., *The role of the helper lipid dioleoylphosphatidylethanolamine (DOPE) for DNA transfection cooperating with a cationic lipid bearing ethylenediamine.* Biochimica et Biophysica Acta (BBA)-Biomembranes, 2013. **1828**(2): p. 412-418.

137. Funhoff, A.M., et al., *Endosomal escape of polymeric gene delivery complexes is not always enhanced by polymers buffering at low pH.* Biomacromolecules, 2004. **5**(1): p. 32-39.

138. Benjaminsen, R.V., et al., *The possible "proton sponge" effect of polyethylenimine (PEI) does not include change in lysosomal pH.* Molecular Therapy, 2013. **21**(1): p. 149-157.

139. Wagner, E., et al., *Influenza virus hemagglutinin HA-2 N-terminal fusogenic peptides augment gene transfer by transferrin-polylysine-DNA complexes: toward a synthetic virus-like gene-transfer vehicle.* Proceedings of the National Academy of Sciences, 1992. **89**(17): p. 7934-7938.

140. Subbarao, N.K., et al., *The pH-dependent bilayer destabilization by an amphipathic peptide.* Biochemistry, 1987. **26**(11): p. 2964-2972.

141. Sasaki, K., et al., *An artificial virus-like nano carrier system: enhanced endosomal escape of nanoparticles via synergistic action of pH-sensitive fusogenic peptide derivatives.* Analytical and Bioanalytical Chemistry, 2008. **391**(8): p. 2717-2727.

142. Martin, M.E. and K.G. Rice, *Peptide-guided gene delivery.* The AAPS Journal, 2007. **9**(1): p. E18-E29.

143. Deshayes, S., et al., *Cell-penetrating peptides: tools for intracellular delivery of therapeutics.* Cellular and Molecular Life Sciences CMLS, 2005. **62**(16): p. 1839-1849.

144. Lear, J.D. and W.F. DeGrado, *Membrane binding and conformational properties of peptides representing the NH2 terminus of influenza HA-2.* Journal of Biological Chemistry, 1987. **262**(14): p. 6500-6505.

145. Wagner, E., et al., *Transferrin-polycation-DNA complexes: the effect of polycations on the structure of the complex and DNA delivery to cells.* Proceedings of the National Academy of Sciences, 1991. **88**(10): p. 4255-4259.

146. Miller, A.M. and D.A. Dean, *Tissue-specific and transcription factor-mediated nuclear entry of DNA.* Advanced Drug Delivery Reviews, 2009. **61**(7-8): p. 603-613.

147. Stoffler, D., B. Fahrenkrog, and U. Aebi, *The nuclear pore complex: from molecular architecture to functional dynamics.* Current Opinion in Cell Biology, 1999. **11**(3): p. 391-401.

148. Sebestyén, M.G., et al., *DNA vector chemistry: the covalent attachment of signal peptides to plasmid DNA.* Nature Biotechnology, 1998. **16**(1): p. 80.

149. Ludtke, J.J., et al., *A nuclear localization signal can enhance both the nuclear transport and expression of 1 kb DNA.* Journal of Cell Science, 1999. **112**(12): p. 2033-2041.

150. Dean, D.A., et al., *Sequence requirements for plasmid nuclear import.* Experimental Cell Research, 1999. **253**(2): p. 713-722.

151. Young, J.L., J.N. Benoit, and D.A. Dean, *Effect of a DNA nuclear targeting sequence on gene transfer and expression of plasmids in the intact vasculature.* Gene Therapy, 2003. **10**(17): p. 1465.

152. Brandén, L.J., A.J. Mohamed, and C.E. Smith, *A peptide nucleic acid–nuclear localization signal fusion that mediates nuclear transport of DNA.* Nature Biotechnology, 1999. **17**(8): p. 784.

153. Chan, C.K. and D.A. Jans, *Enhancement of polylysine-mediated transferrinfection by nuclear localization sequences: polylysine does not function as a nuclear localization sequence.* Human Gene Therapy, 1999. **10**(10): p. 1695-1702.

154. Wu, G.Y. and C.H. Wu, *Receptor-mediated in vitro gene transformation by a soluble DNA carrier system.* Journal of Biological Chemistry, 1987. **262**(10): p. 4429-4432.

155. Wu, G.Y. and C.H. Wu, *Receptor-mediated gene delivery and expression in vivo.* Journal of Biological Chemistry, 1988. **263**(29): p. 14621-14624.

156. Nayerossadat, N., T. Maedeh, and P.A. Ali, *Viral and nonviral delivery systems for gene delivery.* Advanced Biomedical Research, 2012. **1**.

157. Alexis, F., et al., *Factors affecting the clearance and biodistribution of polymeric nanoparticles.* Molecular Pharmaceutics, 2008. **5**(4): p. 505-515.

158. Leamon, C.P., D. Weigl, and R.W. Hendren, *Folate copolymer-mediated transfection of cultured cells.* Bioconjugate Chemistry, 1999. **10**(6): p. 947-957.

159. Harbottle, R.P., et al., *An RGD-oligolysine peptide: a prototype construct for integrin-mediated gene delivery.* Human Gene Therapy, 1998. **9**(7): p. 1037-1047.

160. Suh, W., et al., *Anti-JL1 antibody-conjugated poly (L-lysine) for targeted gene delivery to leukemia T cells.* Journal of Controlled Release, 2001. **72**(1-3): p. 171-178.

161. Neu, M., D. Fischer, and T. Kissel, *Recent advances in rational gene transfer vector design based on poly (ethylene imine) and its derivatives.* The Journal of Gene Medicine, 2005. **7**(8): p. 992-1009.

162. Ferrari, S., et al., *ExGen 500 is an efficient vector for gene delivery to lung epithelial cells in vitro and in vivo.* Gene Therapy, 1997. **4**(10): p. 1100.

163. Erbacher, P., J. Remy, and J. Behr, *Gene transfer with synthetic virus-like particles via the integrin-mediated endocytosis pathway.* Gene Therapy, 1999. **6**(1): p. 138.

164. Zanta, M.-A., et al., *In vitro gene delivery to hepatocytes with galactosylated polyethylenimine.* Bioconjugate Chemistry, 1997. **8**(6): p. 839-844.

165. Kircheis, R., et al., *Coupling of cell-binding ligands to polyethylenimine for targeted gene delivery.* Gene Therapy, 1997. **4**(5): p. 409.

166. Petersen, H., et al., *Polyethylenimine-graft-poly (ethylene glycol) copolymers: influence of copolymer block structure on DNA complexation and biological activities as gene delivery system.* Bioconjugate Chemistry, 2002. **13**(4): p. 845-854.

167. Kunath, K., et al., *Integrin targeting using RGD-PEI conjugates for in vitro gene transfer.* The journal of Gene Medicine, 2003. **5**(7): p. 588-599.

168. Sagara, K. and S.W. Kim, *A new synthesis of galactose-poly (ethylene glycol)-polyethylenimine for gene delivery to hepatocytes.* Journal of Controlled Release, 2002. **79**(1-3): p. 271-281.

169. Jin, L., et al., *Current progress in gene delivery technology based on chemical methods and nano-carriers.* Theranostics, 2014. **4**(3): p. 240.

170. Mellet, C.O., J.M.G. Fernández, and J.M. Benito, *Cyclodextrin-based gene delivery systems.* Chemical Society Reviews, 2011. **40**(3): p. 1586-1608.

171. Taira, K., K. Kataoka, and T. Niidome, *Non-viral gene therapy*. 2014: Springer.

172. Buschmann, M.D., et al., *Chitosans for delivery of nucleic acids.* Advanced Drug Delivery Reviews, 2013. **65**(9): p. 1234-1270.

173. Sato, T., T. Ishii, and Y. Okahata, *In vitro gene delivery mediated by chitosan. Effect of pH, serum, and molecular mass of chitosan on the transfection efficiency.* Biomaterials, 2001. **22**(15): p. 2075-2080.

174. Ishii, T., Y. Okahata, and T. Sato, *Mechanism of cell transfection with plasmid/chitosan complexes.* Biochimica et Biophysica Acta (BBA)-Biomembranes, 2001. **1514**(1): p. 51-64.

175. Roy, K., et al., *Oral gene delivery with chitosan–DNA nanoparticles generates immunologic protection in a murine model of peanut allergy.* Nature Medicine, 1999. **5**(4): p. 387.

176. Kumar, M., et al., *Intranasal gene transfer by chitosan–DNA nanospheres protects BALB/c mice against acute respiratory syncytial virus infection.* Human Gene Therapy, 2002. **13**(12): p. 1415-1425.

177. Bowman, K. and K.W. Leong, *Chitosan nanoparticles for oral drug and gene delivery.* International Journal of Nanomedicine, 2006. **1**(2): p. 117.

178. Dang, J.M. and K.W. Leong, *Natural polymers for gene delivery and tissue engineering.* Advanced Drug Delivery Reviews, 2006. **58**(4): p. 487-499.

179. Bowman, K., et al., *Gene transfer to hemophilia A mice via oral delivery of FVIII–chitosan nanoparticles.* Journal of Controlled Release, 2008. **132**(3): p. 252-259.

180. Lai, W.-F. and M.C.-M. Lin, *Nucleic acid delivery with chitosan and its derivatives.* Journal of Controlled Release, 2009. **134**(3): p. 158-168.

181. Thanou, M., et al., *Quaternized chitosan oligomers as novel gene delivery vectors in epithelial cell lines.* Biomaterials, 2002. **23**(1): p. 153-159.

182. Cheng, M., et al., *Synthesis and efficient hepatocyte targeting of galactosylated chitosan as a gene carrier in vitro and in vivo.* Journal of Biomedical Materials Research Part B: Applied Biomaterials, 2011. **99**(1): p. 70-80.

183. Jiang, H.-L., et al., *The suppression of lung tumorigenesis by aerosol-delivered folate–chitosan-graft-polyethylenimine/Akt1 shRNA complexes through the Akt signaling pathway.* Biomaterials, 2009. **30**(29): p. 5844-5852.

184. Morris, V.B. and C.P. Sharma, *Folate mediated histidine derivative of quaternised chitosan as a gene delivery vector.* International Journal of Pharmaceutics, 2010. **389**(1-2): p. 176-185.

185. Chang, K.-L., et al., *Efficient gene transfection by histidine-modified chitosan through enhancement of endosomal escape.* Bioconjugate Chemistry, 2010. **21**(6): p. 1087-1095.

186. Ghosn, B., et al., *Efficient gene silencing in lungs and liver using imidazole-modified chitosan as a nanocarrier for small interfering RNA.* Oligonucleotides, 2010. **20**(3): p. 163-172.

187. Moreira, C., et al., *Improving chitosan-mediated gene transfer by the introduction of intracellular buffering moieties into the chitosan backbone.* Acta Biomaterialia, 2009. **5**(8): p. 2995-3006.

188. Kim, T.H., et al., *Efficient gene delivery by urocanic acid-modified chitosan.* Journal of Controlled Release, 2003. **93**(3): p. 389-402.

189. Lu, B., et al., *Low molecular weight polyethylenimine grafted N-maleated chitosan for gene delivery: properties and in vitro transfection studies.* Biomacromolecules, 2008. **9**(10): p. 2594-2600.

190. Lai, W.-F., *Cyclodextrins in non-viral gene delivery.* Biomaterials, 2014. **35**(1): p. 401-411.

191. Raemdonck, K., et al., *Polysaccharide-based nucleic acid nanoformulations.* Advanced Drug Delivery Reviews, 2013. **65**(9): p. 1123-1147.

192. Azzam, T., et al., *Polysaccharide− oligoamine based conjugates for gene delivery.* Journal of Medicinal Chemistry, 2002. **45**(9): p. 1817-1824.

193. De la Fuente, M., B. Seijo, and M. Alonso, *Bioadhesive hyaluronan–chitosan nanoparticles can transport genes across the ocular mucosa and transfect ocular tissue.* Gene Therapy, 2008. **15**(9): p. 668.

194. Patnaik, S., et al., *PEI-alginate nanocomposites as efficient in vitro gene transfection agents.* Journal of Controlled Release, 2006. **114**(3): p. 398-409.

195. Jo, J.-i., et al., *Liver targeting of plasmid DNA with a cationized pullulan for tumor suppression.* Journal of Nanoscience and Nanotechnology, 2006. **6**(9-10): p. 2853-2859.

196. Katav, T., et al., *Modified pectin-based carrier for gene delivery: cellular barriers in gene delivery course.* Journal of Controlled Release, 2008. **130**(2): p. 183-191.

197. Takedatsu, H., et al., *A new therapeutic approach using a schizophyllan-based drug delivery system for inflammatory bowel disease.* Molecular Therapy, 2012. **20**(6): p. 1234-1241.

198. Yang, J., et al., *Surface-engineered dendrimers in gene delivery.* Chemical Reviews, 2015. **115**(11): p. 5274-5300.

199. Tomalia, D.A., et al., *A new class of polymers: starburst-dendritic macromolecules.* Polymer Journal, 1985. **17**(1): p. 117.

200. Hawker, C.J. and J.M. Frechet, *Preparation of polymers with controlled molecular architecture. A new convergent approach to dendritic macromolecules.* Journal of the American Chemical Society, 1990. **112**(21): p. 7638-7647.

201. Haensler, J. and F.C. Szoka Jr, *Polyamidoamine cascade polymers mediate efficient transfection of cells in culture.* Bioconjugate Chemistry, 1993. **4**(5): p. 372-379.

202. Kim, T.-i., et al., *Arginine-conjugated polypropylenimine dendrimer as a non-toxic and efficient gene delivery carrier.* Biomaterials, 2007. **28**(11): p. 2061-2067.

203. Merkel, O.M., et al., *Triazine dendrimers as nonviral gene delivery systems: effects of molecular structure on biological activity.* Bioconjugate Chemistry, 2009. **20**(9): p. 1799-1806.

204. Perisé-Barrios, A.J., et al., *Carbosilane dendrimers as gene delivery agents for the treatment of HIV infection.* Journal of Controlled Release, 2014. **184**: p. 51-57.

205. Loup, C., et al., *Preparation of water-soluble cationic phosphorus-containing dendrimers as DNA transfecting agents.* Chemistry–A European Journal, 1999. **5**(12): p. 3644-3650.

206. Shcharbin, D., et al., *Fourth generation phosphorus-containing dendrimers: prospective drug and gene delivery carrier.* Pharmaceutics, 2011. **3**(3): p. 458-473.

207. Toth, I., et al., *Novel cationic lipidic peptide dendrimer vectors in vitro gene delivery.* STP Pharma Sciences, 1999. **9**(1): p. 93-99.

208. Ohsaki, M., et al., *In vitro gene transfection using dendritic poly (L-lysine).* Bioconjugate Chemistry, 2002. **13**(3): p. 510-517.

209. Kitchens, K.M., et al., *Endocytosis inhibitors prevent poly (amidoamine) dendrimer internalization and permeability across Caco-2 cells.* Molecular Pharmaceutics, 2008. **5**(2): p. 364-369.

210. Santos, J.L., et al., *Receptor-mediated gene delivery using PAMAM dendrimers conjugated with peptides recognized by mesenchymal stem cells.* Molecular Pharmaceutics, 2010. **7**(3): p. 763-774.

211. Santos, J.L., et al., *Functionalization of poly (amidoamine) dendrimers with hydrophobic chains for improved gene delivery in mesenchymal stem cells.* Journal of Controlled Release, 2010. **144**(1): p. 55-64.

212. Zhang, Y., et al., *Cationic dendron-bearing lipids: investigating structure–activity relationships for small interfering RNA delivery.* Biomacromolecules, 2013. **14**(12): p. 4289-4300.

213. Arima, H., et al., *Enhancement of gene expression by polyamidoamine dendrimer conjugates with α-, β-, and γ-cyclodextrins.* Bioconjugate Chemistry, 2001. **12**(4): p. 476-484.

214. Kim, K., et al., *Bifunctional compounds for targeted hepatic gene delivery.* Gene Therapy, 2007. **14**(8): p. 704.

215. Sadler, K. and J.P. Tam, *Peptide dendrimers: applications and synthesis.* Reviews in Molecular Biotechnology, 2002. **90**(3-4): p. 195-229.

216. Yang, S., et al., *Cellular uptake of self-assembled cationic peptide–DNA complexes: multifunctional role of the enhancer chloroquine.* Journal of Controlled Release, 2009. **135**(2): p. 159-165.

217. Taratula, O., et al., *Surface-engineered targeted PPI dendrimer for efficient intracellular and intratumoral siRNA delivery.* Journal of Controlled Release, 2009. **140**(3): p. 284-293.

218. Chen, J., et al., *Peptide-Based and Polypeptide-Based Gene Delivery Systems.* Topics in Current Chemistry, 2017. **375**(2): p. 32.

219. Martinez-Fong, D., et al., *Neurotensin-SPDP-poly-L-lysine conjugate: a nonviral vector for targeted gene delivery to neural cells.* Molecular Brain Research, 1999. **69**(2): p. 249-262.

220. Gonzalez-Barrios, J.A., et al., *Neurotensin polyplex as an efficient carrier for delivering the human GDNF gene into nigral dopamine neurons of hemiparkinsonian rats.* Molecular Therapy, 2006. **14**(6): p. 857-865.

221. Kim, S.H., et al., *LHRH receptor-mediated delivery of siRNA using polyelectrolyte complex micelles self-assembled from siRNA-PEG-LHRH conjugate and PEI.* Bioconjugate Chemistry, 2008. **19**(11): p. 2156-2162.

222. Park, J., et al., *A review of RGD-functionalized nonviral gene delivery vectors for cancer therapy.* Cancer Gene Therapy, 2012. **19**(11): p. 741-748.

223. Chiu, S.-J., N.T. Ueno, and R.J. Lee, *Tumor-targeted gene delivery via anti-HER2 antibody (trastuzumab, Herceptin®) conjugated polyethylenimine.* Journal of Controlled Release, 2004. **97**(2): p. 357-369.

224. Wan, Y., et al., *Nanosized, peptide-based multicomponent DNA delivery systems: optimization of endosome escape activity.* Nanomedicine, 2016. **11**(8): p. 907-919.

225. Fawell, S., et al., *Tat-mediated delivery of heterologous proteins into cells.* Proceedings of the National Academy of Sciences, 1994. **91**(2): p. 664-668.

226. Derossi, D., et al., *The third helix of the Antennapedia homeodomain translocates through biological membranes.* Journal of Biological Chemistry, 1994. **269**(14): p. 10444-10450.

227. Pooga, M., M. Hällbrink, and M. Zorko, *Cell penetration by transportan.* The FASEB Journal, 1998. **12**(1): p. 67-77.

228. Copolovici, D.M., et al., *Cell-penetrating peptides: design, synthesis, and applications.* ACS Nano, 2014. **8**(3): p. 1972-1994.

229. Elliott, G. and P. O'Hare, *Intercellular trafficking and protein delivery by a herpesvirus structural protein.* Cell, 1997. **88**(2): p. 223-233.

230. Oehlke, J., et al., *Cellular uptake of an α-helical amphipathic model peptide with the potential to deliver polar compounds into the cell interior non-endocytically.* Biochimica et Biophysica Acta (BBA)-Biomembranes, 1998. **1414**(1-2): p. 127-139.

231. Morris, M.C., et al., *A peptide carrier for the delivery of biologically active proteins into mammalian cells.* Nature Biotechnology, 2001. **19**(12): p. 1173.

232. Wender, P.A., et al., *The design, synthesis, and evaluation of molecules that enable or enhance cellular uptake: peptoid molecular transporters.* Proceedings of the National Academy of Sciences, 2000. **97**(24): p. 13003-13008.

233. Wyman, T.B., et al., *Design, synthesis, and characterization of a cationic peptide that binds to nucleic acids and permeabilizes bilayers.* Biochemistry, 1997. **36**(10): p. 3008-3017.

234. Gottschalk, S., et al., *A novel DNA-peptide complex for efficient gene transfer and expression in mammalian cells.* Gene Therapy, 1996. **3**(5): p. 448-457.

235. Rittner, K., et al., *New basic membrane-destabilizing peptides for plasmid-based gene delivery in vitro and in vivo.* Molecular Therapy, 2002. **5**(2): p. 104-114.

236. Pichon, C., C. Gonçalves, and P. Midoux, *Histidine-rich peptides and polymers for nucleic acids delivery.* Advanced Drug Delivery Reviews, 2001. **53**(1): p. 75-94.

237. McKenzie, D.L., et al., *Low molecular weight disulfide cross-linking peptides as nonviral gene delivery carriers.* Bioconjugate Chemistry, 2000. **11**(6): p. 901-909.

238. Lanford, R.E., P. Kanda, and R.C. Kennedy, *Induction of nuclear transport with a synthetic peptide homologous to the SV40 T antigen transport signal.* Cell, 1986. **46**(4): p. 575-582.

239. Robbins, J., et al., *Two interdependent basic domains in nucleoplasmin nuclear targeting sequence: identification of a class of bipartite nuclear targeting sequence.* Cell, 1991. **64**(3): p. 615-623.

240. Schreiber, V., et al., *The human poly (ADP-ribose) polymerase nuclear localization signal is a bipartite element functionally separate from DNA binding and catalytic activity.* The EMBO Journal, 1992. **11**(9): p. 3263-3269.

241. Subramanian, A., P. Ranganathan, and S.L. Diamond, *Nuclear targeting peptide scaffolds for lipofection of nondividing mammalian cells.* Nature Biotechnology, 1999. **17**(9): p. 873.

242. Ewert, K., et al., *Cationic lipid-DNA complexes for gene therapy: understanding the relationship between complex structure and gene delivery pathways at the molecular level.* Current Medicinal Chemistry, 2004. **11**(2): p. 133-149.

243. Balazs, D.A. and W. Godbey, *Liposomes for use in gene delivery.* Journal of Drug Delivery, 2011. **2011**.

244. Fraley, R., et al., *Introduction of liposome-encapsulated SV40 DNA into cells.* Journal of Biological Chemistry, 1980. **255**(21): p. 10431-10435.

245. Felgner, P.L., et al., *Lipofection: a highly efficient, lipid-mediated DNA-transfection procedure.* Proceedings of the National Academy of Sciences, 1987. **84**(21): p. 7413-7417.

246. Behr, J.-P., et al., *Efficient gene transfer into mammalian primary endocrine cells with lipopolyamine-coated DNA.* Proceedings of the National Academy of Sciences, 1989. **86**(18): p. 6982-6986.

247. Stamatatos, L., et al., *Interactions of cationic lipid vesicles with negatively charged phospholipid vesicles and biological membranes.* Biochemistry, 1988. **27**(11): p. 3917-3925.

248. Leventis, R. and J.R. Silvius, *Interactions of mammalian cells with lipid dispersions containing novel metabolizable cationic amphiphiles.* Biochimica et Biophysica Acta (BBA)-Biomembranes, 1990. **1023**(1): p. 124-132.

249. Gao, X. and L. Huang, *A novel cationic liposome reagent for efficient transfection of mammalian cells.* Biochemical and Biophysical Research Communications, 1991. **179**(1): p. 280-285.

250. Gebeyehu, G., et al., *Cationic lipids*. 1994, Google Patents.

251. Gao, X. and L. Huang, *Potentiation of cationic liposome-mediated gene delivery by polycations.* Biochemistry, 1996. **35**(3): p. 1027-1036.

252. Rezaee, M., et al., *Progress in the development of lipopolyplexes as efficient non-viral gene delivery systems.* Journal of Controlled Release, 2016. **236**: p. 1-14.

253. Hart, S.L., et al., *Lipid-mediated enhancement of transfection by a nonviral integrin-targeting vector.* Human Gene Therapy, 1998. **9**(4): p. 575-585.

254. Jenkins, R., et al., *An integrin-targeted non-viral vector for pulmonary gene therapy.* Gene Therapy, 2000. **7**(5): p. 393.

255. Colin, M., et al., *Liposomes enhance delivery and expression of an RGD-oligolysine gene transfer vector in human tracheal cells.* Gene Therapy, 1998. **5**(11): p. 1488.

256. Jenkins, R., et al., *Formation of LID vector complexes in water alters physicochemical properties and enhances pulmonary gene expression in vivo.* Gene Therapy, 2003. **10**(12): p. 1026.

257. Kudsiova, L., et al., *Lipid chain geometry of C14 glycerol-based lipids: effect on lipoplex structure and transfection.* Molecular BioSystems, 2011. **7**(2): p. 422-436.

258. Kudsiova, L., et al., *Lipopolyplex ternary delivery systems incorporating C14 glycerol-based lipids.* Molecular Pharmaceutics, 2011. **8**(5): p. 1831-1847.

259. Mustapa, M.F.M., et al., *Biophysical characterization of an integrin-targeted lipopolyplex gene delivery vector.* Biochemistry, 2007. **46**(45): p. 12930-12944.

260. Tagawa, T., et al., *Characterisation of LMD virus-like nanoparticles self-assembled from cationic liposomes, adenovirus core peptide μ (mu) and plasmid DNA.* Gene Therapy, 2002. **9**(9): p. 564.

261. Kirby, A.J., et al., *Gemini surfactants: new synthetic vectors for gene transfection.* Angewandte Chemie International Edition, 2003. **42**(13): p. 1448-1457.

262. Draghici, B. and M.A. Ilies, *Synthetic nucleic acid delivery systems: present and perspectives.* Journal of Medicinal Chemistry, 2015. **58**(10): p. 4091-4130.

263. Wettig, S.D., R.E. Verrall, and M. Foldvari, *Gemini surfactants: a new family of building blocks for non-viral gene delivery systems.* Current Gene Therapy, 2008. **8**(1): p. 9-23.

264. Menger, F.M. and C. Littau, *Gemini-surfactants: synthesis and properties.* Journal of the American Chemical Society, 1991. **113**(4): p. 1451-1452.

265. Menger, F.M. and J.S. Keiper, *Gemini surfactants.* Angewandte Chemie International Edition, 2000. **39**(11): p. 1906-1920.

266. Bunton, C.A., et al., *Catalysis of nucleophilic substitutions by micelles of dicationic detergents.* The Journal of Organic Chemistry, 1971. **36**(16): p. 2346-2350.

267. Devinsky, F., Ľ. Masárová, and I. Lacko, *Surface activity and micelle formation of some new bisquaternary ammonium salts.* Journal of Colloid and Interface Science, 1985. **105**(1): p. 235-239.

268. Zhu, Y.-p., A. Masuyama, and M. Okahara, *Preparation and surface active properties of amphipathic compounds with two sulfate groups and two lipophilic alkyl chains.* Journal of the American Oil Chemists' Society, 1990. **67**(7): p. 459-463.

269. Esumi, K., M. Goino, and Y. Koide, *Adsorption and adsolubilization by monomeric, dimeric, or trimeric quaternary ammonium surfactant at silica/water interface.* Journal of Colloid and Interface Science, 1996. **183**(2): p. 539-545.

270. McGregor, C., et al., *Rational approaches to the design of cationic gemini surfactants for gene delivery.* Journal of the American Chemical Society, 2001. **123**(26): p. 6215-6220.

271. Zana, R., M. Benrraou, and R. Rueff, *Alkanediyl-. alpha.,. omega.-bis (dimethylalkylammonium bromide) surfactants. 1. Effect of the spacer chain length on the critical micelle concentration and micelle ionization degree.* Langmuir, 1991. **7**(6): p. 1072-1075.

272. Rosen, M.J. and L.D. Song, *Dynamic surface tension of aqueous surfactant solutions 8. Effect of spacer on dynamic properties of gemini surfactant solutions.* Journal of Colloid and Interface Science, 1996. **179**(1): p. 261-268.

273. Wettig, S. and R. Verrall, *Thermodynamic studies of aqueous m–s–m gemini surfactant systems.* Journal of Colloid and Interface Science, 2001. **235**(2): p. 310-316.

274. Wettig, S.D., et al., *Structural and transfection properties of amine-substituted gemini surfactant-based nanoparticles.* The Journal of Gene Medicine, 2007. **9**(8): p. 649-658.

275. Bombelli, C., et al., *Gemini surfactant based carriers in gene and drug delivery.* Current Medicinal Chemistry, 2009. **16**(2): p. 171-183.

276. Rosen, M.J. and D.J. Tracy, *Gemini surfactants.* Journal of Surfactants and Detergents, 1998. **1**(4): p. 547-554.

277. Zana, R., *Dimeric (gemini) surfactants: effect of the spacer group on the association behavior in aqueous solution.* Journal of Colloid and Interface Science, 2002. **248**(2): p. 203-220.

278. Danino, D., Y. Talmon, and R. Zana, *Alkanediyl-. alpha.,. omega.-bis (dimethylalkylammonium bromide) surfactants (dimeric surfactants). 5. Aggregation and microstructure in aqueous solutions.* Langmuir, 1995. **11**(5): p. 1448-1456.

279. Hait, S. and S. Moulik, *Gemini surfactants: a distinct class of self-assembling molecules.* Current Science-Bangalore, 2002. **82**(9): p. 1101-1111.

280. Bernheim-Groswasser, A., R. Zana, and Y. Talmon, *Sphere-to-cylinder transition in aqueous micellar solution of a dimeric (gemini) surfactant.* The Journal of Physical Chemistry B, 2000. **104**(17): p. 4005-4009.

281. Israelachvili, J.N., *Intermolecular and surface forces*. 2011: Academic Press.

282. Sharma, V.D. and M.A. Ilies, *Heterocyclic Cationic Gemini Surfactants: A Comparative Overview of Their Synthesis, Self-assembling, Physicochemical, and Biological Properties.* Medicinal Research Reviews, 2014. **34**(1): p. 1-44.

283. Rosenzweig, H.S., V.A. Rakhmanova, and R.C. MacDonald, *Diquaternary ammonium compounds as transfection agents.* Bioconjugate Chemistry, 2001. **12**(2): p. 258-263.

284. Badea, I., et al., *In vivo cutaneous interferon-γ gene delivery using novel dicationic (gemini) surfactant-plasmid complexes.* The Journal of Gene Medicine, 2005. **7**(9): p. 1200-1214.

285. Wang, H. and S.D. Wettig, *Synthesis and aggregation properties of dissymmetric phytanyl-gemini surfactants for use as improved DNA transfection vectors.* Physical Chemistry Chemical Physics, 2011. **13**(2): p. 637-642.

286. Vijayanathan, V., et al., *Formation of DNA nanoparticles in the presence of novel polyamine analogues: a laser light scattering and atomic force microscopic study.* Nucleic Acids Research, 2004. **32**(1): p. 127-134.

287. Wettig, S.D., et al., *Thermodynamic and aggregation properties of aza-and imino-substituted gemini surfactants designed for gene delivery.* Physical Chemistry Chemical Physics, 2007. **9**(7): p. 871-877.

288. Wettig, S.D., et al., *Structural and transfection properties of amine-substituted gemini surfactant-based nanoparticles.* The Journal of Gene Medicine, 2007. **9**(8): p. 649-658.

289. Donkuru, M., et al., *Designing pH-sensitive gemini nanoparticles for non-viral gene delivery into keratinocytes.* Journal of Materials Chemistry, 2012. **22**(13): p. 6232-6244.

290. Yang, P., et al., *Enhanced gene expression in epithelial cells transfected with amino acid-substituted gemini nanoparticles.* European Journal of Pharmaceutics and Biopharmaceutics, 2010. **75**(3): p. 311-320.

291. Cardoso, A.M., et al., *Gemini surfactant dimethylene-1, 2-bis (tetradecyldimethylammonium bromide)-based gene vectors: a biophysical approach to transfection efficiency.* Biochimica et Biophysica Acta (BBA)-Biomembranes, 2011. **1808**(1): p. 341-351.

292. Li, X., et al., *Synthesis and solution properties of gemini surfactants containing oleyl chains.* Physical Chemistry Chemical Physics, 2005. **7**(17): p. 3172-3178.

293. Sharma, V.D., et al., *Interfacial engineering of pyridinium gemini surfactants for the generation of synthetic transfection systems.* Biomaterials, 2013. **34**(28): p. 6906-6921.

294. Collins, K.D. and M.W. Washabaugh, *The Hofmeister effect and the behaviour of water at interfaces.* Quarterly Reviews of Biophysics, 1985. **18**(4): p. 323-422.

295. Bajaj, A., P. Kondiah, and S. Bhattacharya, *Design, synthesis, and in vitro gene delivery efficacies of novel cholesterol-based gemini cationic lipids and their serum compatibility:*

A structure− activity investigation. Journal of Medicinal Chemistry, 2007. **50**(10): p. 2432-2442.

296. Zuber, G., M. Dontenwill, and J.-P. Behr, *Synthetic viruslike particles for targeted gene delivery to αvβ3 integrin-presenting endothelial cells.* Molecular Pharmaceutics, 2009. **6**(5): p. 1544-1552.

297. Pack, D.W., D. Putnam, and R. Langer, *Design of imidazole-containing endosomolytic biopolymers for gene delivery.* Biotechnology and Bioengineering, 2000. **67**(2): p. 217-223.

298. Midoux, P., et al., *Chemical vectors for gene delivery: a current review on polymers, peptides and lipids containing histidine or imidazole as nucleic acids carriers.* British Journal of Pharmacology, 2009. **157**(2): p. 166-178.

299. Lin, C., et al., *Random and block copolymers of bioreducible poly (amido amine) s with high-and low-basicity amino groups: study of DNA condensation and buffer capacity on gene transfection.* Journal of Controlled Release, 2007. **123**(1): p. 67-75.

300. Lo, S.L. and S. Wang, *An endosomolytic Tat peptide produced by incorporation of histidine and cysteine residues as a nonviral vector for DNA transfection.* Biomaterials, 2008. **29**(15): p. 2408-2414.

301. Dunehoo, A.L., et al., *Cell adhesion molecules for targeted drug delivery.* Journal of Pharmaceutical Sciences, 2006. **95**(9): p. 1856-1872.

302. Varga, C.M., T.J. Wickham, and D.A. Lauffenburger, *Receptor-mediated targeting of gene delivery vectors: Insights from molecular mechanisms for improved vehicle design.* Biotechnology and Bioengineering, 2000. **70**(6): p. 593-605.

303. Majzoub, R.N., et al., *Uptake and transfection efficiency of PEGylated cationic liposome–DNA complexes with and without RGD-tagging.* Biomaterials, 2014. **35**(18): p. 4996-5005.

304. Gailit, J., et al., *Human fibroblasts bind directly to fibrinogen at RGD sites through integrin αvβ3.* Experimental Cell Research, 1997. **232**(1): p. 118-126.

305. Du, Z., et al., *The role of the helper lipid on the DNA transfection efficiency of lipopolyplex formulations.* Scientific Reports, 2014. **4**: p. 7107.

306. Wan, Y., et al., *Multifunctional peptide-lipid nanocomplexes for efficient targeted delivery of DNA and siRNA into breast cancer cells.* Acta Biomaterialia, 2017. **59**: p. 257-268.

307. Kogure, K., et al., *Development of a non-viral multifunctional envelope-type nano device by a novel lipid film hydration method.* Journal of Controlled Release, 2004. **98**(2): p. 317-323.

308. Ahmed, T., A.O. Kamel, and S.D. Wettig, *Interactions between DNA and Gemini surfactant: impact on gene therapy: part I.* Nanomedicine, 2016. **11**(3): p. 289-306.

309. Rafiee, A., *Tri-Modal nucleic acid delivery systems*. 2017: US Patent, Application Number:15/696,945

310. Rafiee, A., *Tri-Modal nucleic acid delivery systems*. 2018: Canadian Patent, Application Number: 3,009,829.

311. Rafiee, A., et al., *Synthesis and Characterization of Luteinizing Hormone-Releasing Hormone (LHRH)-Functionalized Mini-Dendrimers.* International Journal of Organic Chemistry, 2013. **3**(1): p. 51-57.

312. Varamini, P., et al., *Development of New Gonadotropin-Releasing Hormone-Modified Dendrimer Platforms with Direct Antiproliferative and Gonadotropin Releasing Activity.* Journal of Medicinal Chemistry, 2017.

313. Valeur, E. and M. Bradley, *Amide bond formation: beyond the myth of coupling reagents.* Chemical Society Reviews, 2009. **38**(2): p. 606-631.

314. Alqawlaq, S., et al., *Preclinical development and ocular biodistribution of gemini-DNA nanoparticles after intravitreal and topical administration: towards non-invasive glaucoma gene therapy.* Nanomedicine: Nanotechnology, Biology and Medicine, 2014. **10**(8): p. 1637-1647.

315. Gharagozloo, M., et al., *A flow cytometric approach to study the mechanism of gene delivery to cells by gemini-lipid nanoparticles: an implication for cell membrane nanoporation.* Journal of Nanobiotechnology, 2015. **13**(1): p. 62.

316. Cottet-Rousselle, C., et al., *Cytometric assessment of mitochondria using fluorescent probes.* Cytometry Part A, 2011. **79**(6): p. 405-425.

317. Śliwka, L., et al., *The comparison of MTT and CVS assays for the assessment of anticancer agent interactions.* PloS One, 2016. **11**(5): p. e0155772.

318. Alsina, J. and F. Albericio, *Solid-phase synthesis of C-terminal modified peptides.* Peptide Science, 2003. **71**(4): p. 454-477.

319. Sharma, V.D., et al., *Modulation of pyridinium cationic lipid–DNA complex properties by pyridinium gemini surfactants and its impact on lipoplex transfection properties.* Molecular Pharmaceutics, 2014. **11**(2): p. 545-559.

320. Al-Dulaymi, M.A., et al., *Di-peptide-modified Gemini surfactants as Gene delivery vectors: exploring the role of the alkyl tail in their physicochemical behavior and biological activity.* The AAPS Journal, 2016. **18**(5): p. 1168-1181.

321. Holmberg, K., et al., *Surfactants and polymers in aqueous solution*. Vol. 2. 2003: Wiley Online Library.

322. Dias, R.S., et al., *Interaction between DNA and cationic surfactants: effect of DNA conformation and surfactant headgroup.* The Journal of Physical Chemistry B, 2008. **112**(46): p. 14446-14452.

323. Wadhwa, M.S., et al., *Peptide-mediated gene delivery: influence of peptide structure on gene expression.* Bioconjugate Chemistry, 1997. **8**(1): p. 81-88.

324. Plank, C., et al., *Branched cationic peptides for gene delivery: role of type and number of cationic residues in formation and in vitro activity of DNA polyplexes.* Human Gene Therapy, 1999. **10**(2): p. 319-332.

325. Schaffer, D.V., et al., *Vector unpacking as a potential barrier for receptor-mediated polyplex gene delivery.* Biotechnology and Bioengineering, 2000. **67**(5): p. 598-606.

326. Welser, K., et al., *Gene delivery using ternary lipopolyplexes incorporating branched cationic peptides: the role of peptide sequence and branching.* Molecular Pharmaceutics, 2012. **10**(1): p. 127-141.

327. Kudsiova, L., et al., *Delivery of siRNA using ternary complexes containing branched cationic peptides: the role of peptide sequence, branching and targeting.* Molecular BioSystems, 2016. **12**(3): p. 934-951.

328. Leng, Q. and A.J. Mixson, *Modified branched peptides with a histidine-rich tail enhance in vitro gene transfection.* Nucleic Acids Research, 2005. **33**(4): p. e40-e40.

329. Ma, B., et al., *Lipoplex morphologies and their influences on transfection efficiency in gene delivery.* Journal of Controlled Release, 2007. **123**(3): p. 184-194.

330. Bell, P.C., et al., *Transfection mediated by gemini surfactants: engineered escape from the endosomal compartment.* Journal of the American Chemical Society, 2003. **125**(6): p. 1551-1558.

331. Giardini, P.A., D.A. Fletcher, and J.A. Theriot, *Compression forces generated by actin comet tails on lipid vesicles.* Proceedings of the National Academy of Sciences, 2003. **100**(11): p. 6493-6498.

332. Caracciolo, G., et al., *Factors determining the superior performance of lipid/DNA/protammine nanoparticles over lipoplexes.* Journal of Medicinal Chemistry, 2011. **54**(12): p. 4160-4171.

333. Cavalli, S., F. Albericio, and A. Kros, *Amphiphilic peptides and their cross-disciplinary role as building blocks for nanoscience.* Chemical Society Reviews, 2010. **39**(1): p. 241-263.

334. Berndt, P., G.B. Fields, and M. Tirrell, *Synthetic lipidation of peptides and amino acids: monolayer structure and properties.* Journal of the American Chemical Society, 1995. **117**(37): p. 9515-9522.

335. Ewert, K.K., et al., *Synthesis of linear and cyclic peptide–PEG–lipids for stabilization and targeting of cationic liposome–DNA complexes.* Bioorganic & Medicinal Chemistry Letters, 2016. **26**(6): p. 1618-1623.

Appendices

Appendix A: Flow Cytometry Analysis

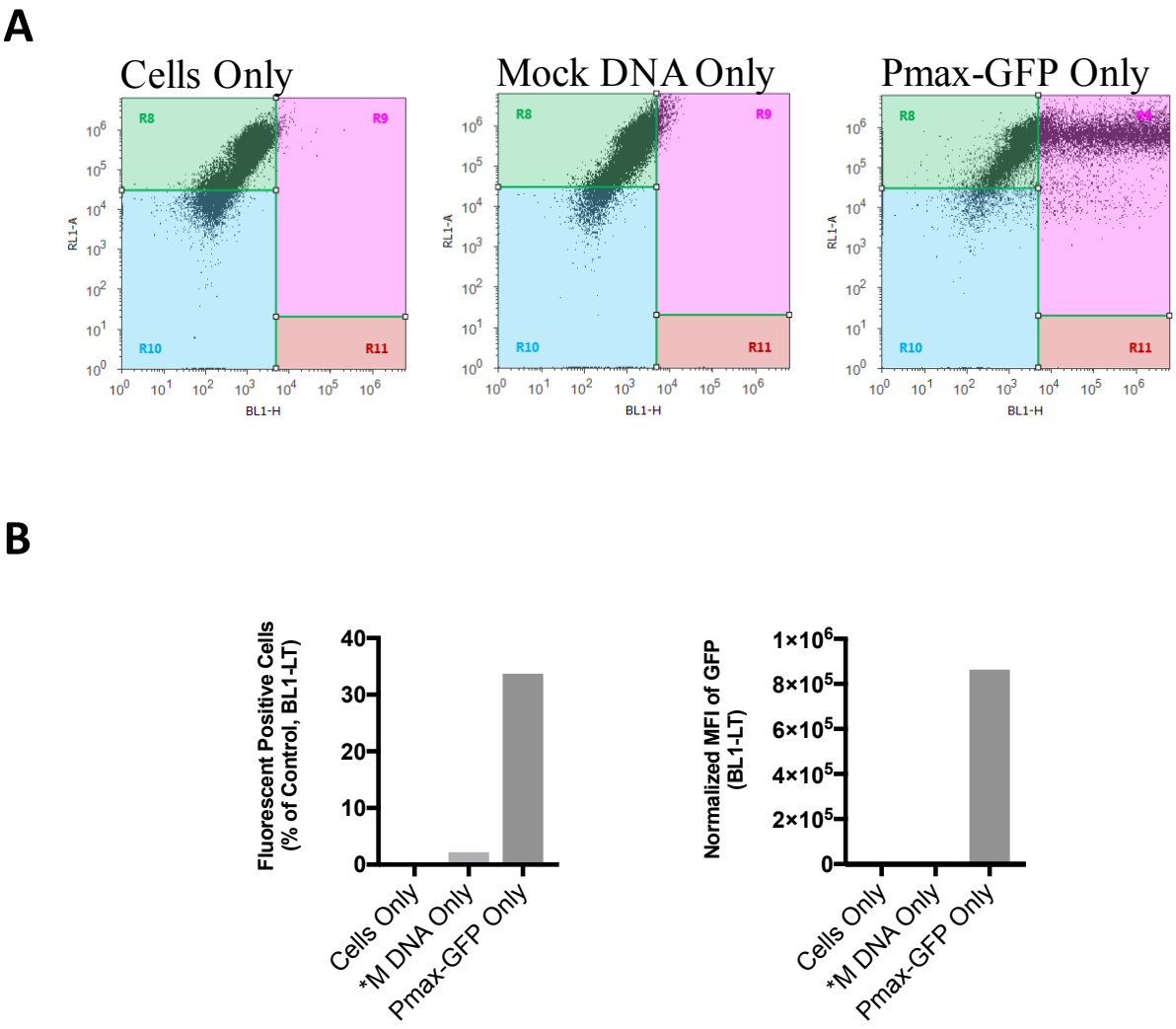

Fig. A1. Setting up flow cytometry parameters according to control-untreated cells and transfected cells with *mock pDNA and Pmax-GFP^{TM} pDNA using electroporation. (A) the flow cytometry 2D *dot plot*, presenting control-untreated cell, Mock pDNA- and Pmax-GFP pDNA-transfected cells, and (B) the flow cytometry quantitative measurement of the transfection percentage and the intensity of GFP expression level (MFI).

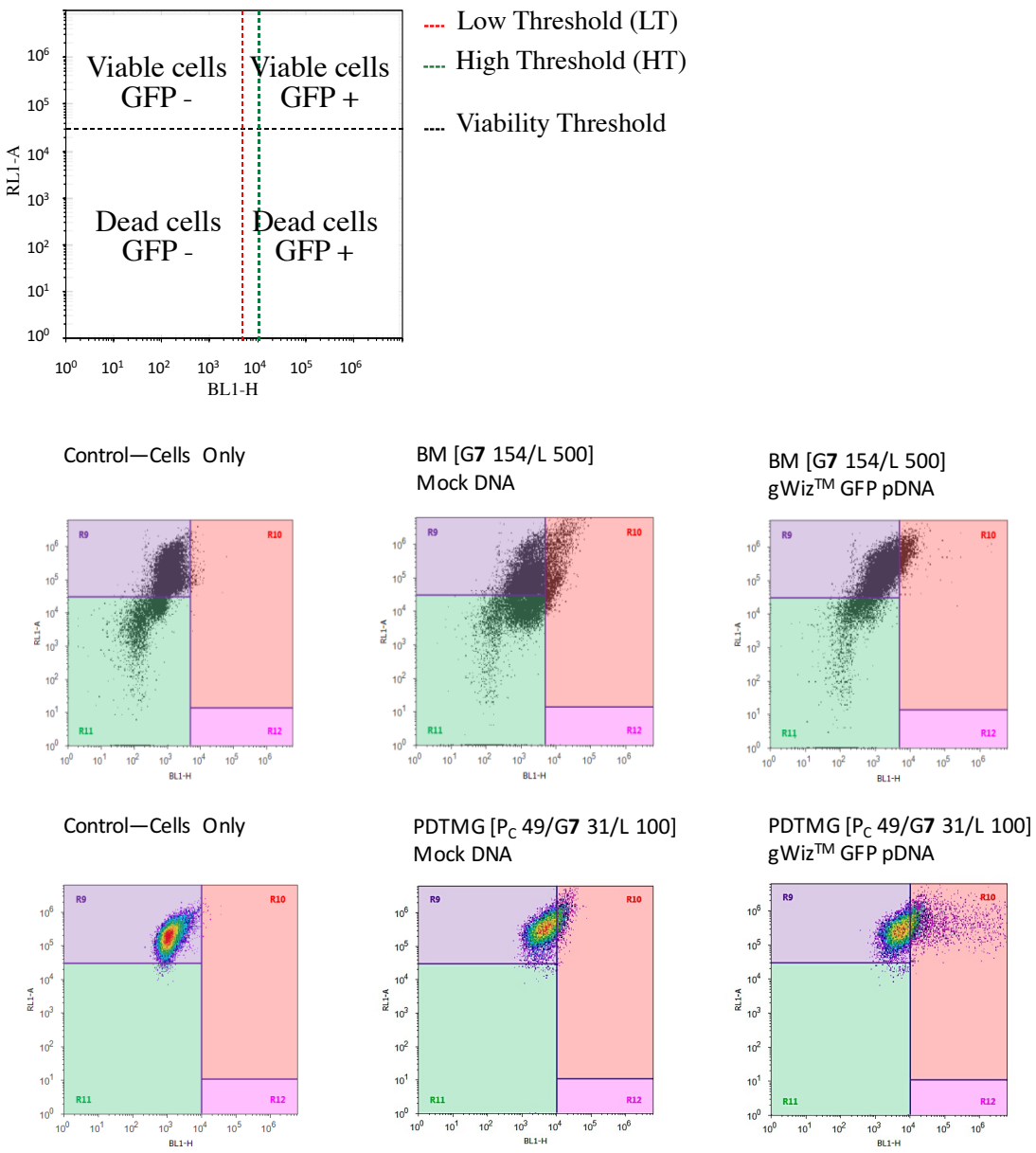

Fig. A2. Flow cytometry data analysis. The quantification of transfection percentages at low threshold (LT analysis by setting the outlier at 5,000 on the BL1 axis), while the MFI analysis at two different thresholds: at low threshold and high threshold (HT analysis by setting the outlier at 10,000 on the BL1 axis). The HT analyses reduce the effect of the skewing of the MFI by the background noise, which detected below 10,000 fluorescence intensity on the BL1 axis, as demonstrated by the cells transfected with mock pDNA using BM [G/L] and PDTMG complexes.

Appendix B: Covalent Functionalization of Gemini Surfactants

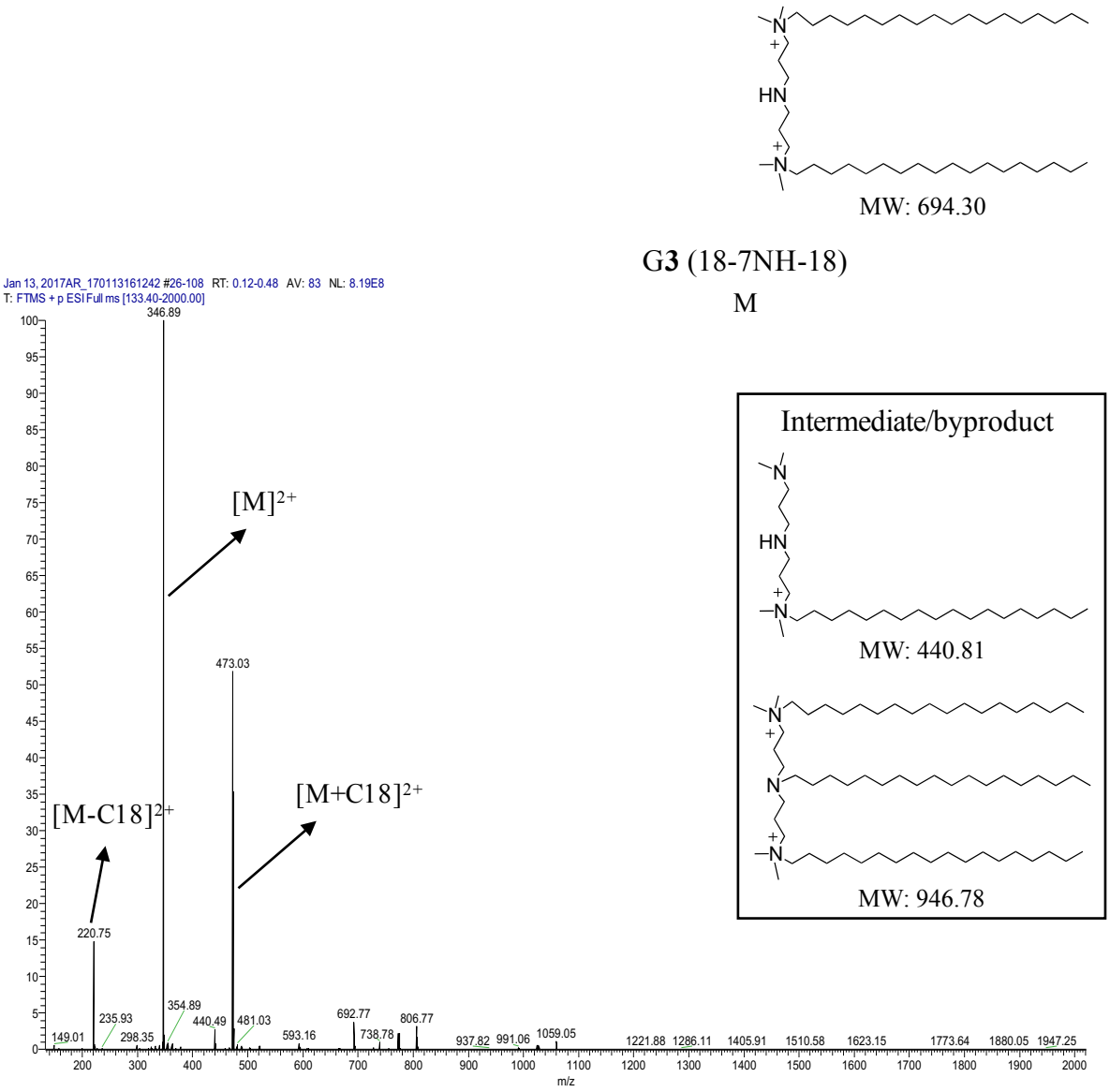

Fig. B1. ESI-MS data confirmed the identity of synthesized 18-7NH-18 (G**3**) gemini surfactants.

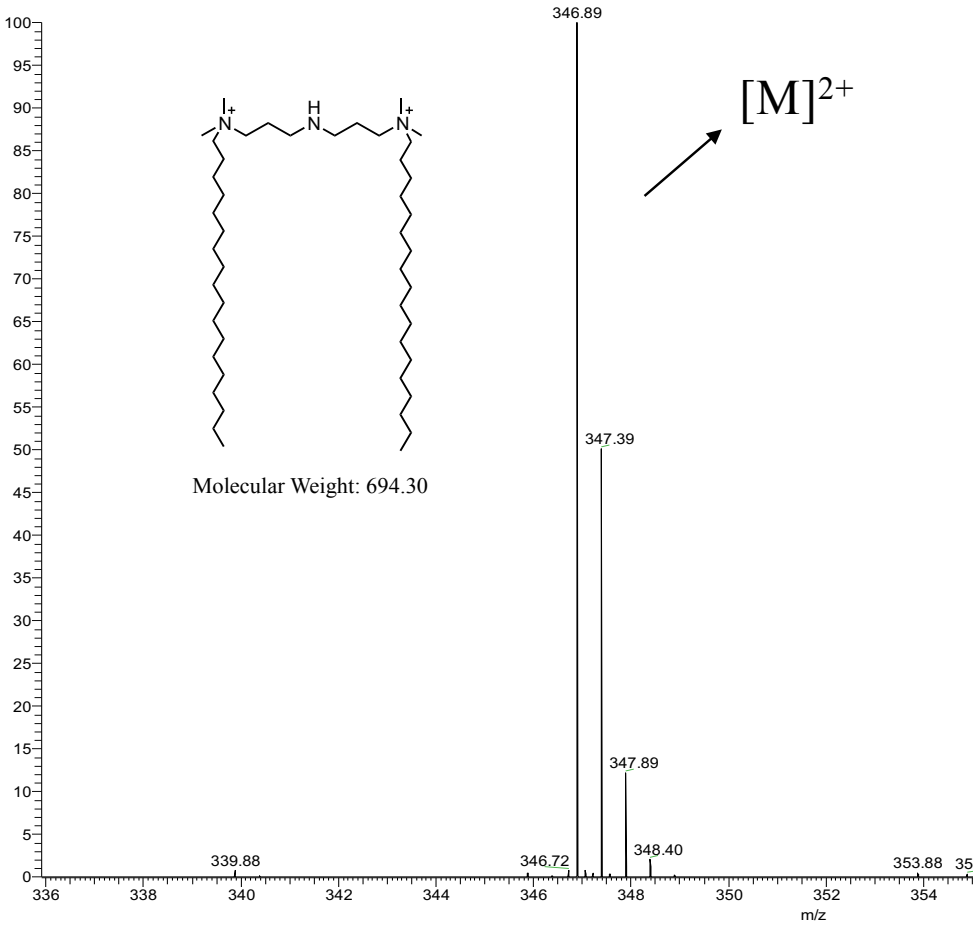

Fig. B2. High-resolution mass spectrometry (*m/z*) displays the doubly-charged ions to two decimal places for 18-7NH-18 (G**3**) gemini surfactants.

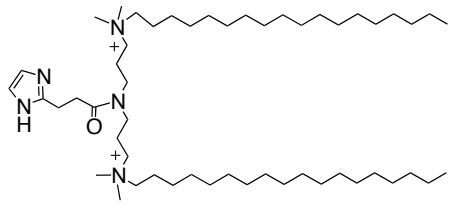

MW: 816.42

G**4** (Imid-18)

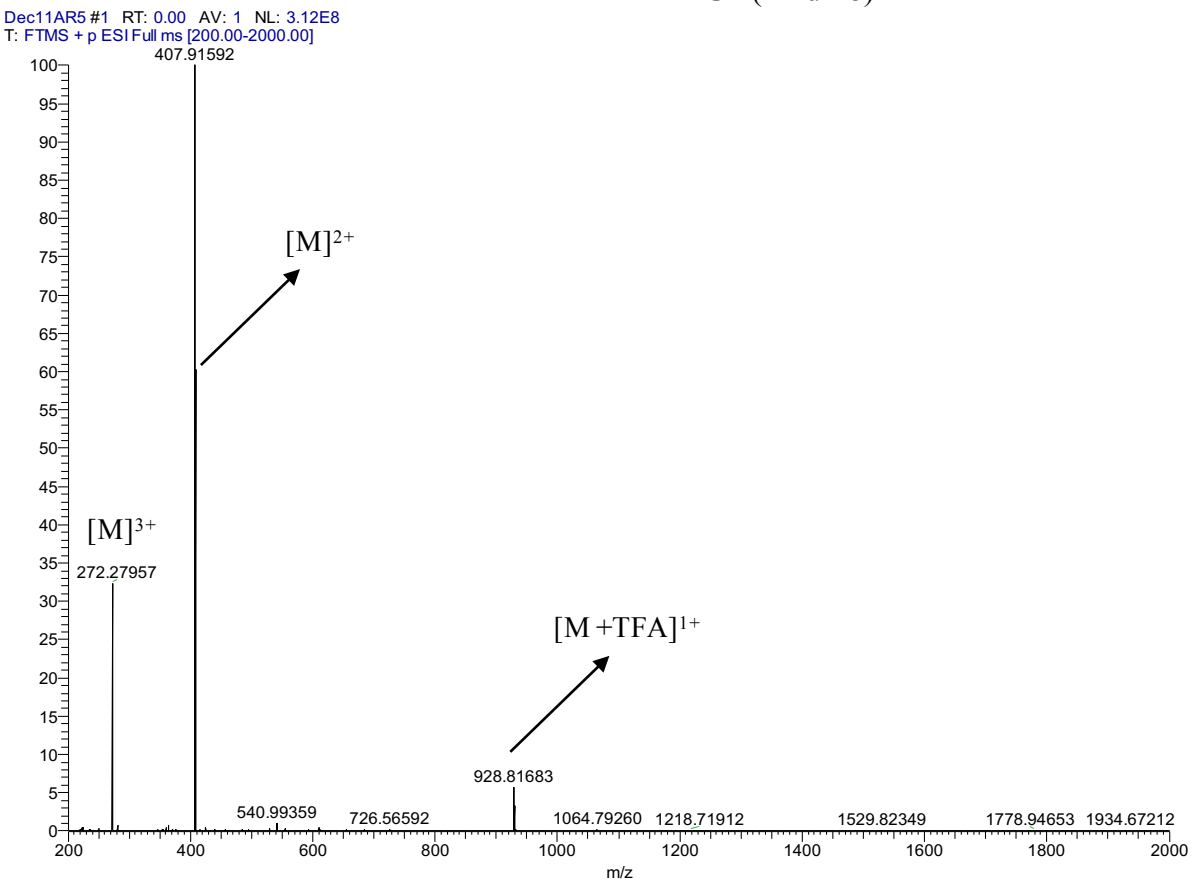

Fig. B3. ESI-MS data confirmed the identity of synthesized imid-18 (G**4**) gemini surfactants.

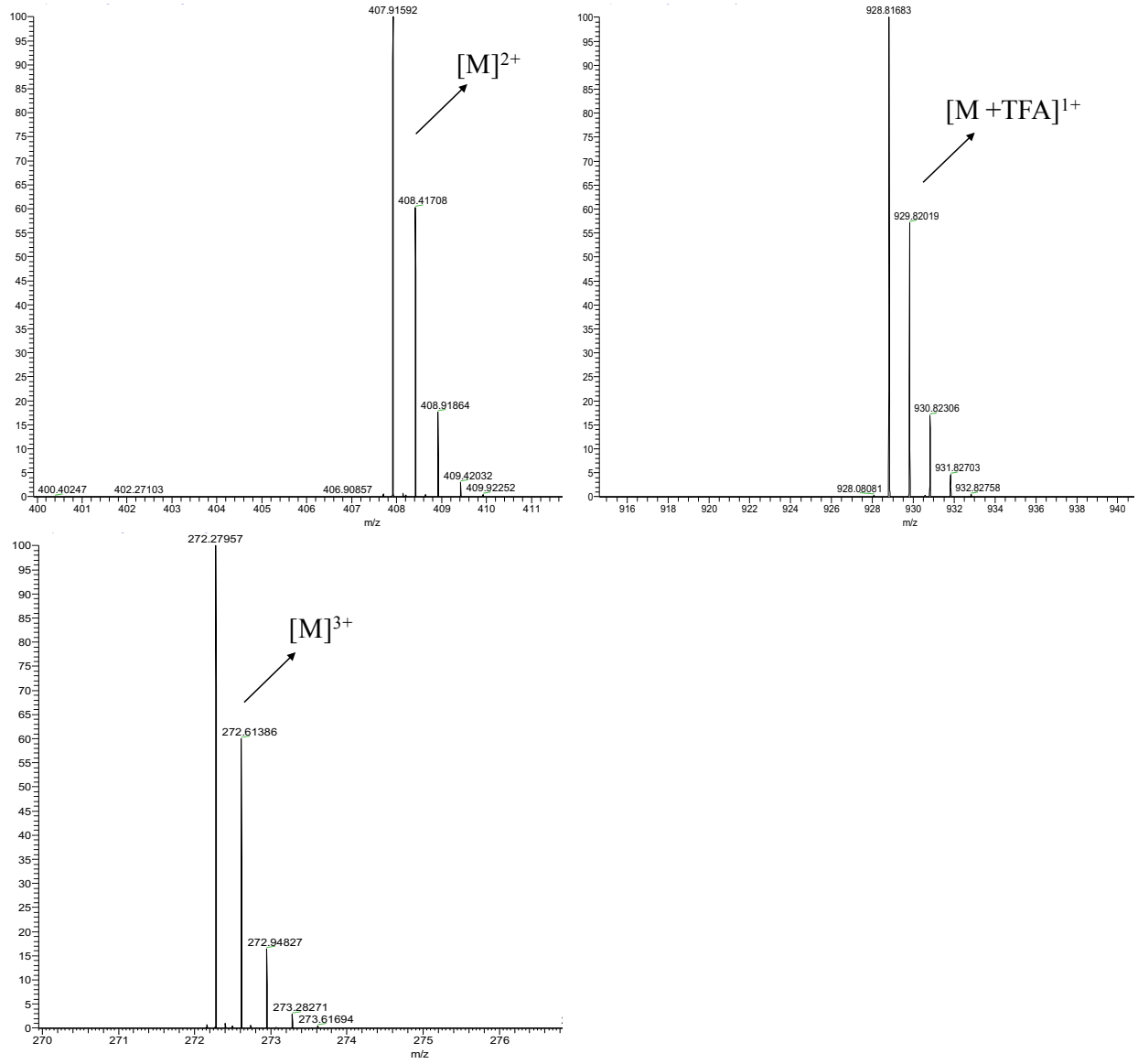

Fig. B4. High-resolution mass spectrometry (*m/z*) displays the singly- (as the TFA salt), doubly-, and triply-charged ions to five decimal places for imid-18 (G**4**) gemini surfactants.

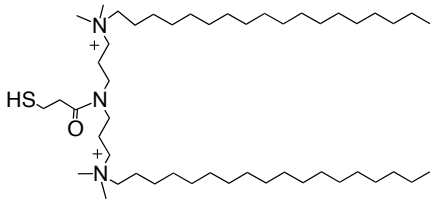

MW: 782.43

G**5** (Thiol-18)

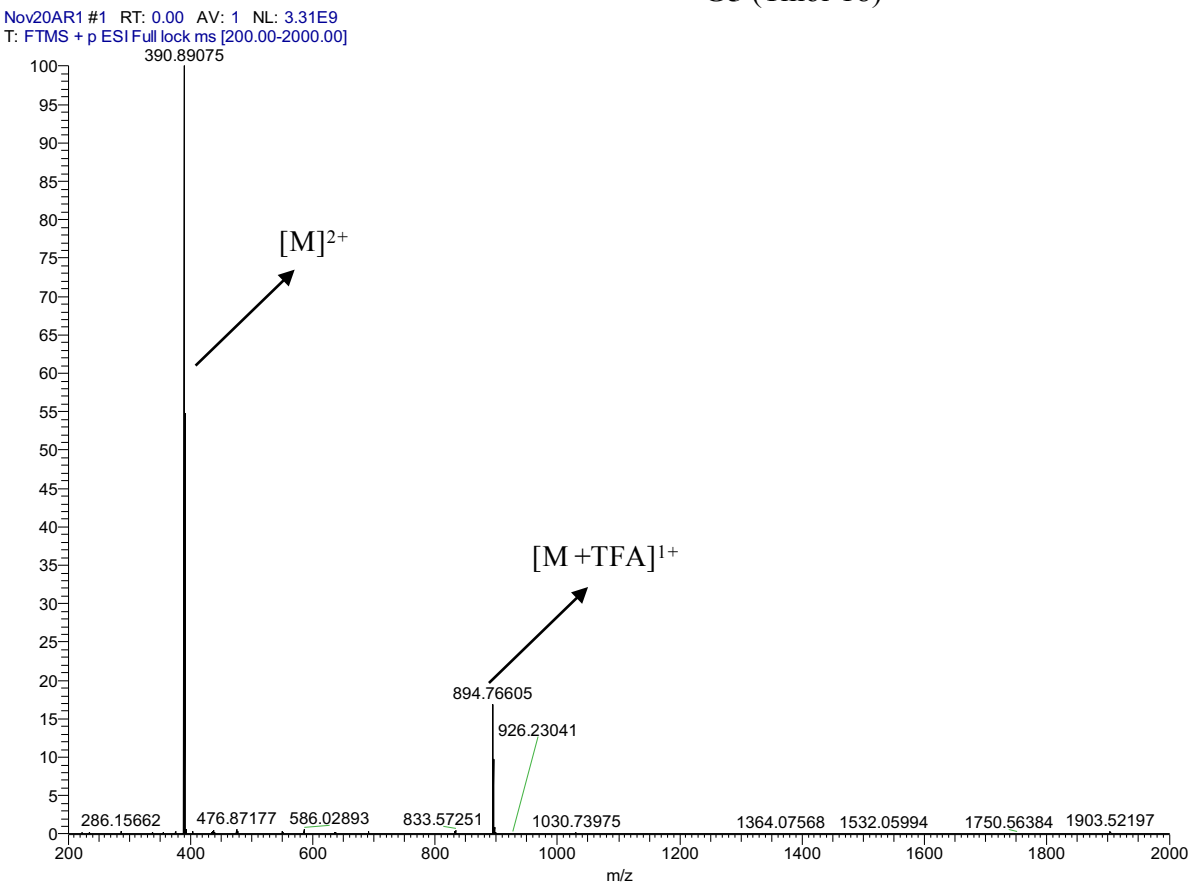

Fig. B5. ESI-MS data confirmed the identity of synthesized thiol-18 (G**5**) gemini surfactants.

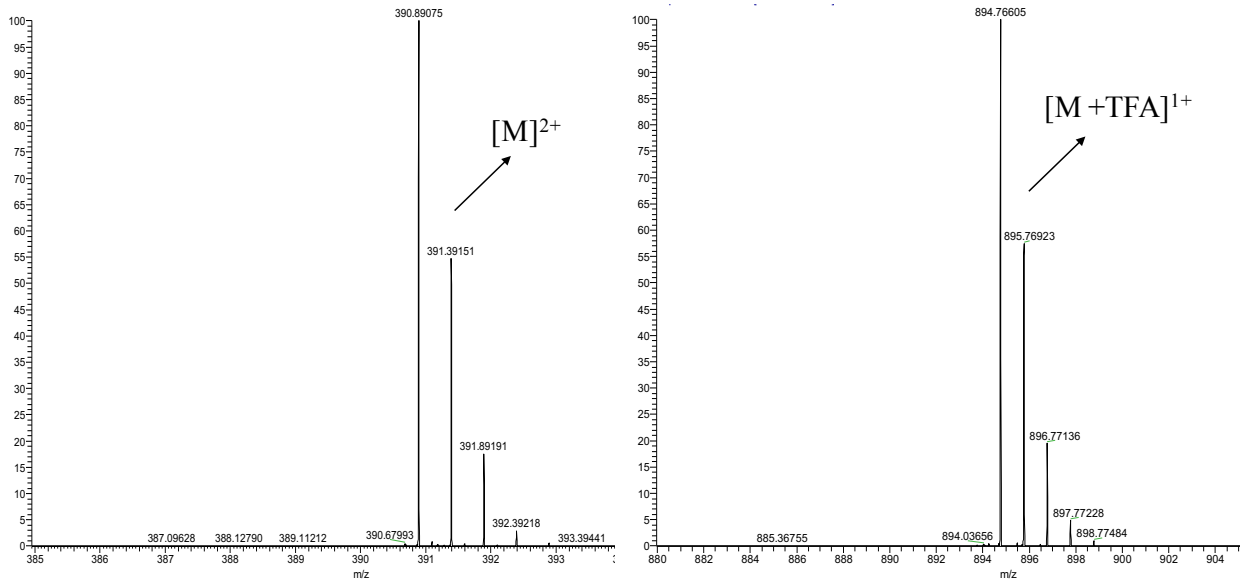

Fig. B6. High-resolution mass spectrometry (*m/z*) displays the singly- (as the TFA salt), and doubly-charged ions to five decimal places for thiol-18 (G**5**) gemini surfactants.

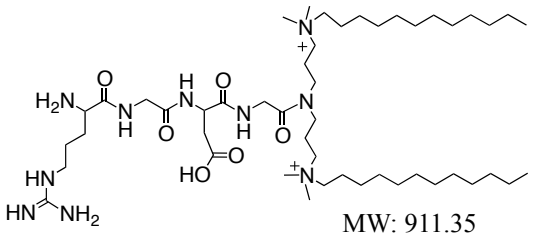

MW: 911.35

G**6** (RGDG-12)

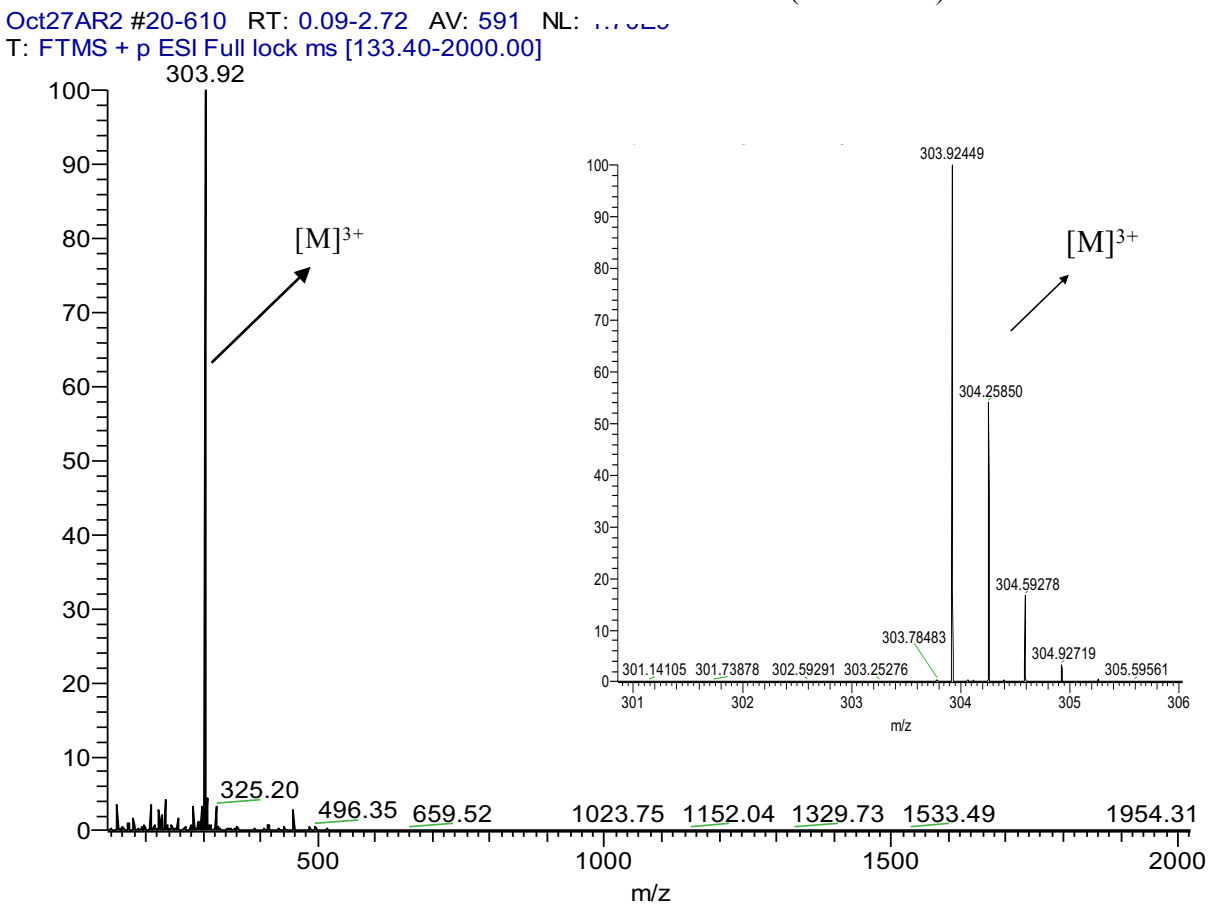

Fig. B7. ESI-MS data confirmed the identity of synthesized RGDG-12 (G**6**) gemini surfactants. High-resolution mass spectrometry (*m/z*) displays the triply-charged ions to five decimal places for RGDG-12 (G**6**) gemini surfactants.

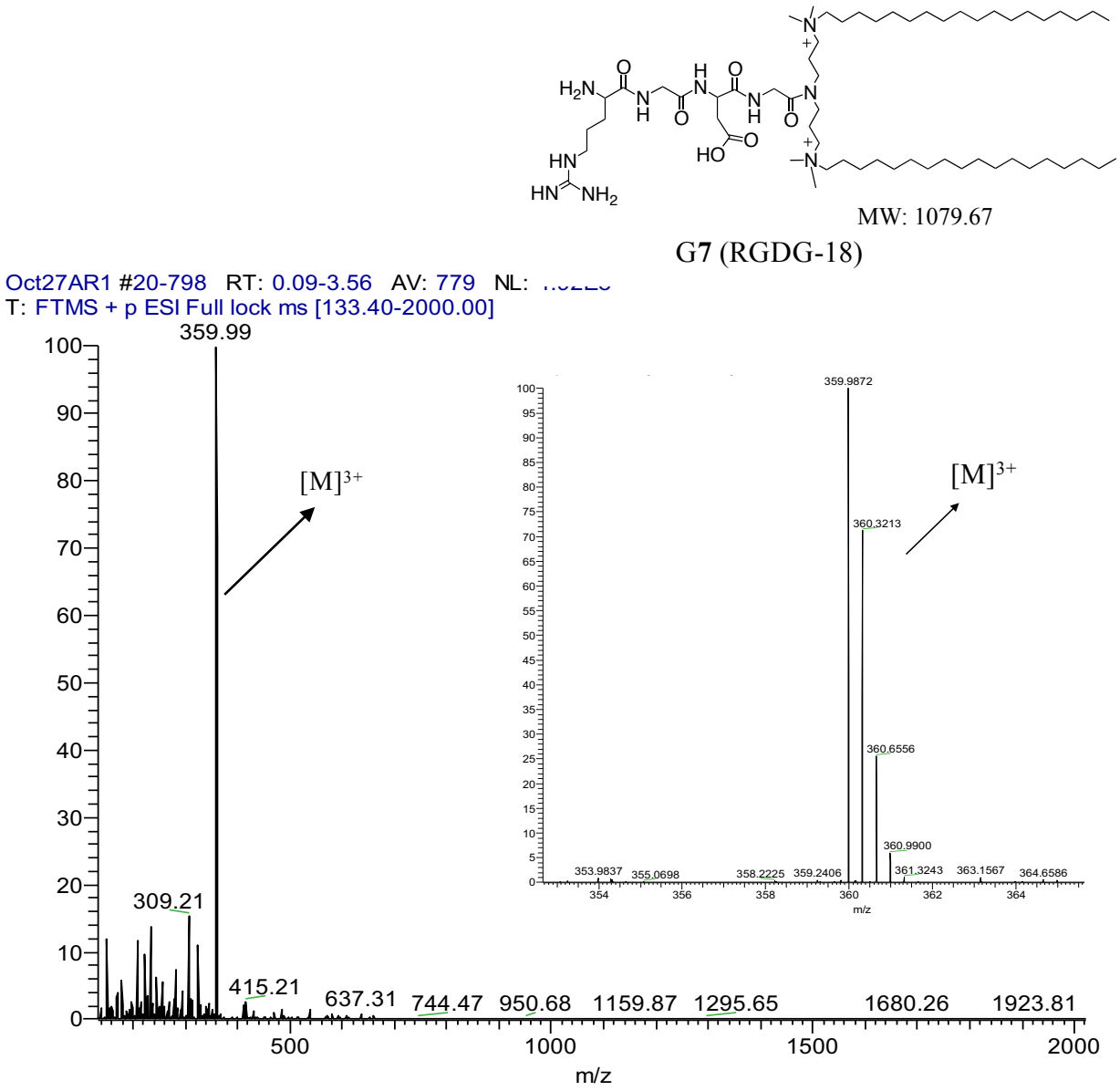

Fig. B8. ESI-MS data confirmed the identity of synthesized RGDG-18 (G**7**) gemini surfactants. High-resolution mass spectrometry (*m/z*) displays the triply-charged ions to four decimal places for RGDG-18 (G**7**) gemini surfactants.

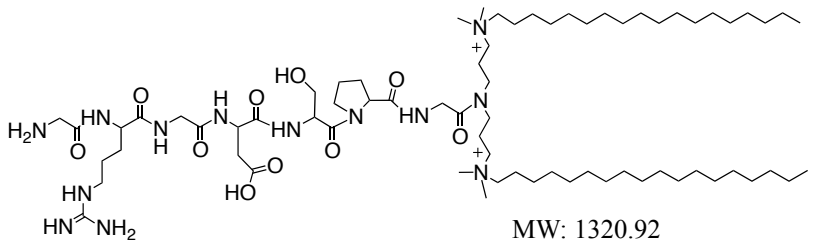

MW: 1320.92

G**8** (GRGDSPG-18)

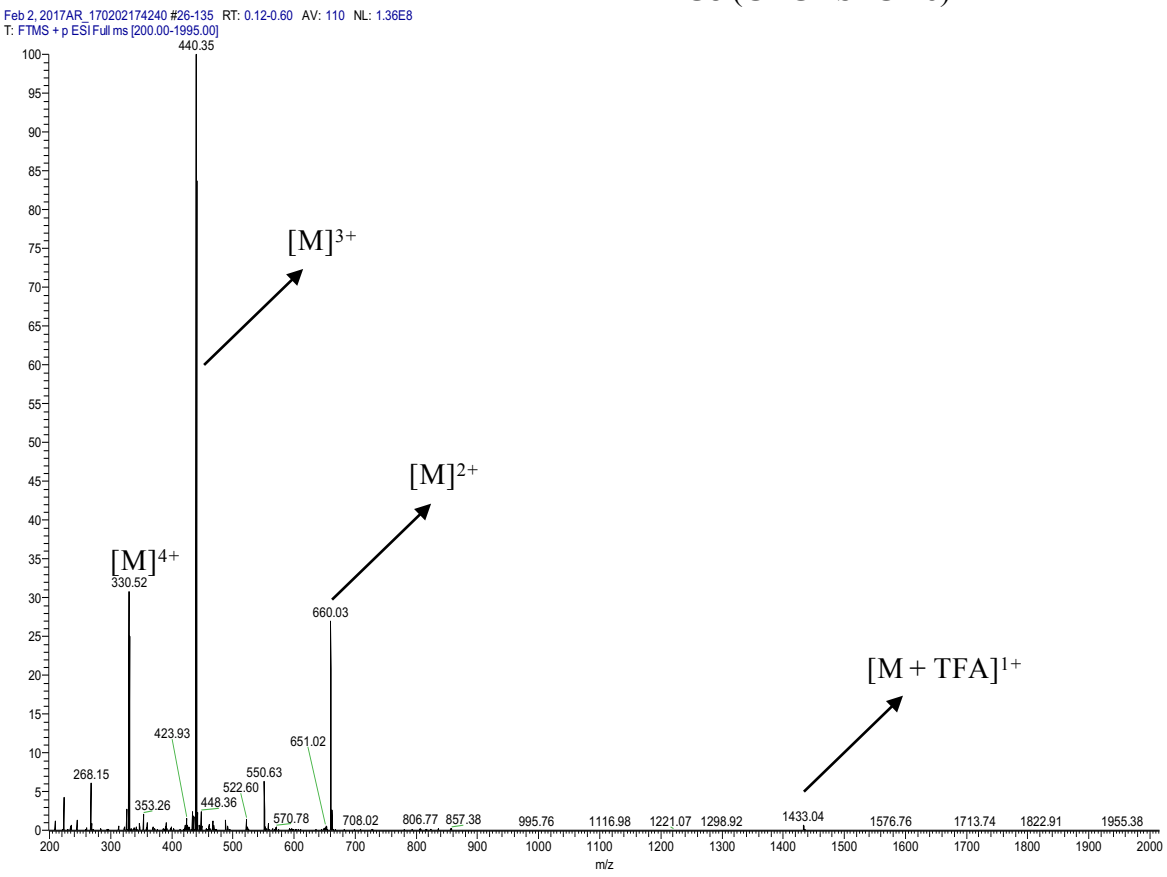

Fig. B9. ESI-MS data confirmed the identity of synthesized GRGDSPG-18 (G**8**) gemini surfactants.

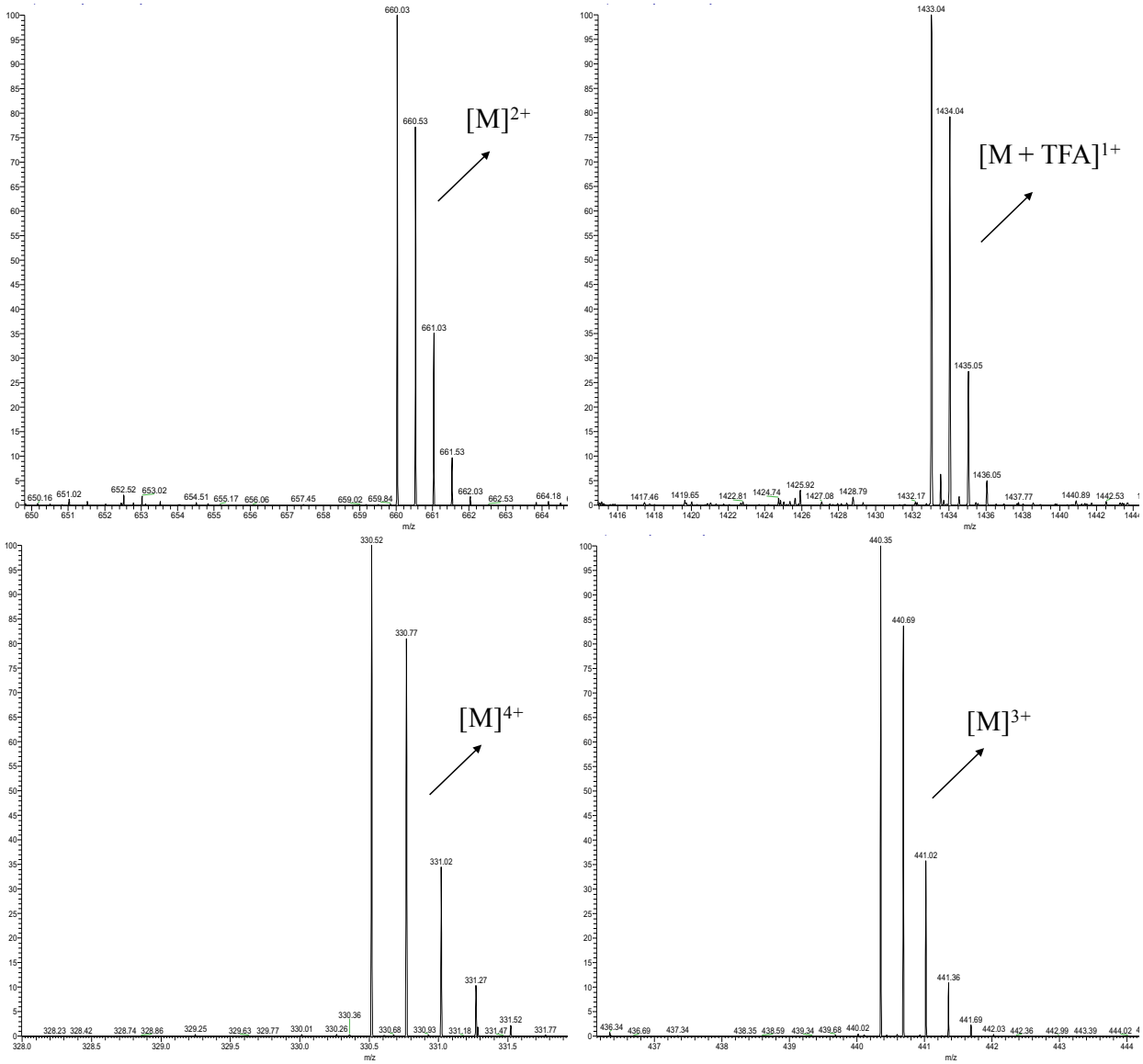

Fig. B10. High-resolution mass spectrometry (*m/z*) displays the singly- (as the TFA salt), doubly-, triply-, and quadruply-charged ions to two decimal places for GRGDSPG-18 (G**8**) gemini surfactants.

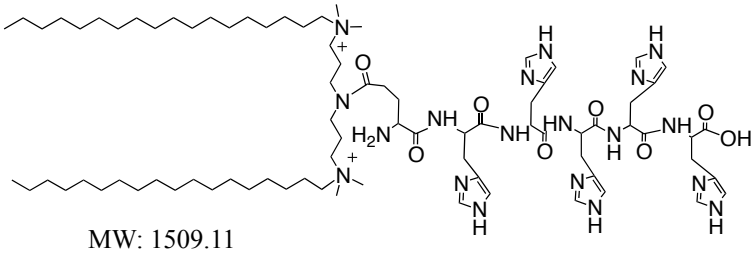

MW: 1509.11

G**9** (18-E-PepD)

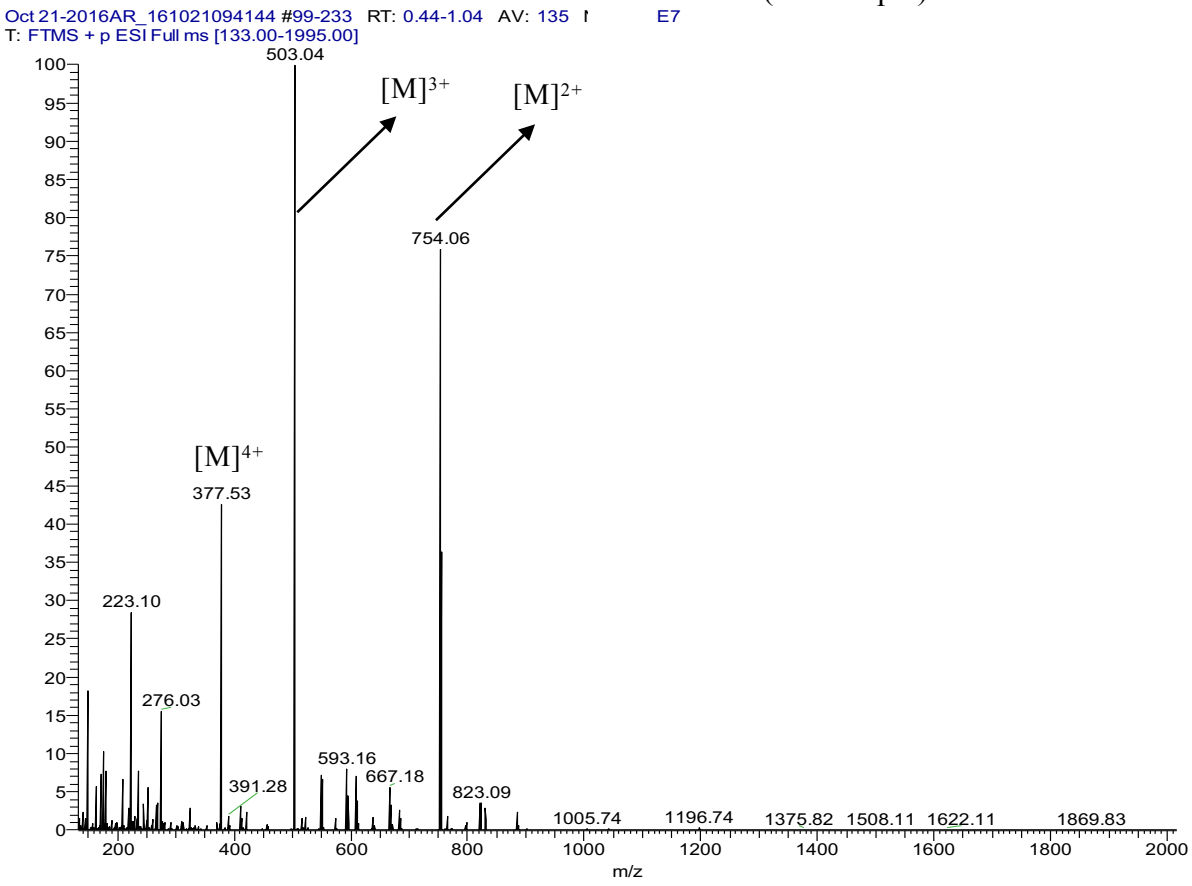

Fig. B11. ESI-MS data confirmed the identity of synthesized 18-E-PepD (G**9**) gemini surfactants.

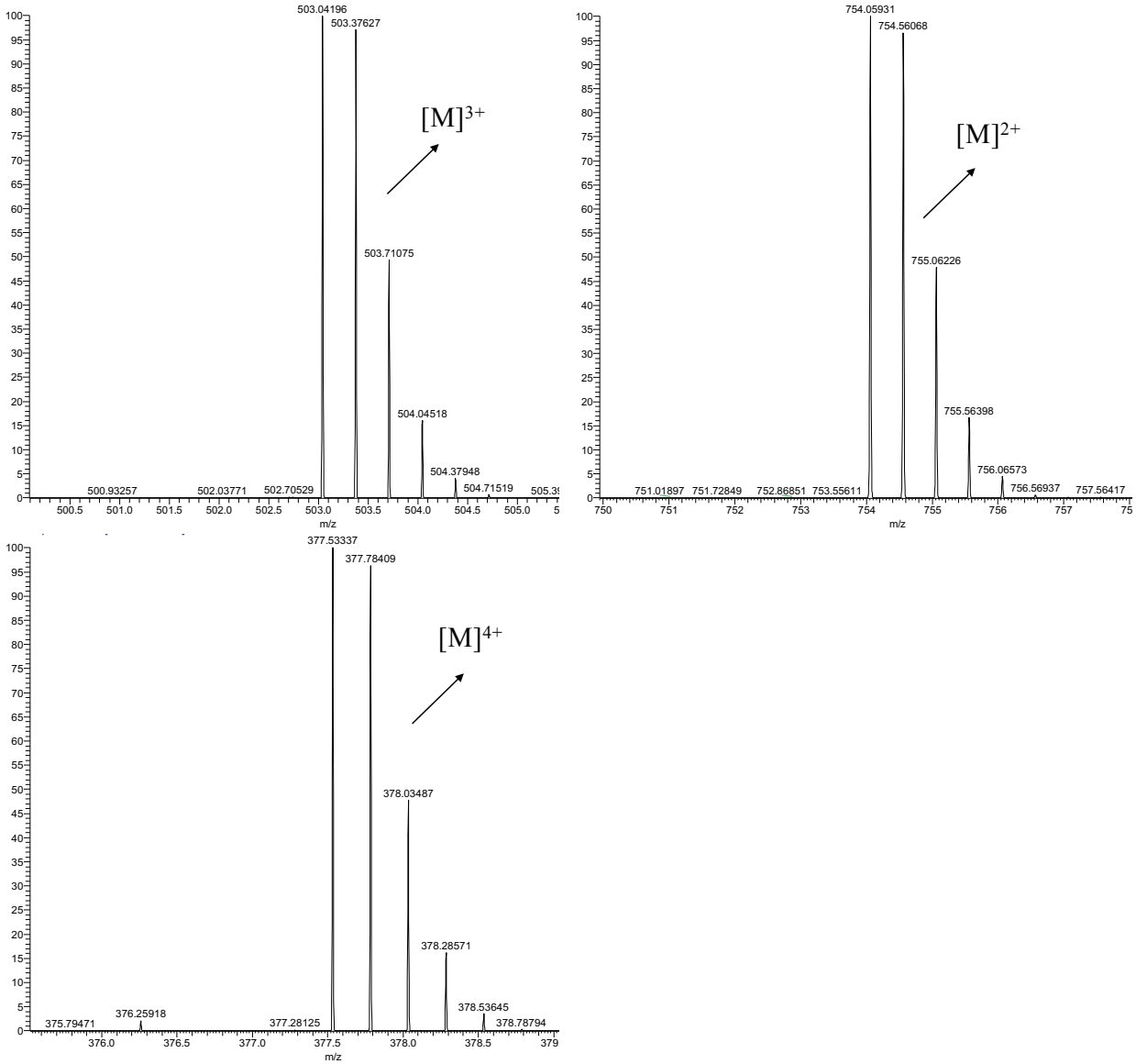

Fig. B12. High-resolution mass spectrometry (*m/z*) displays the doubly-, triply-, and quadruply-charged ions to five decimal places for 18-E-PepD (G**9**) gemini surfactants.

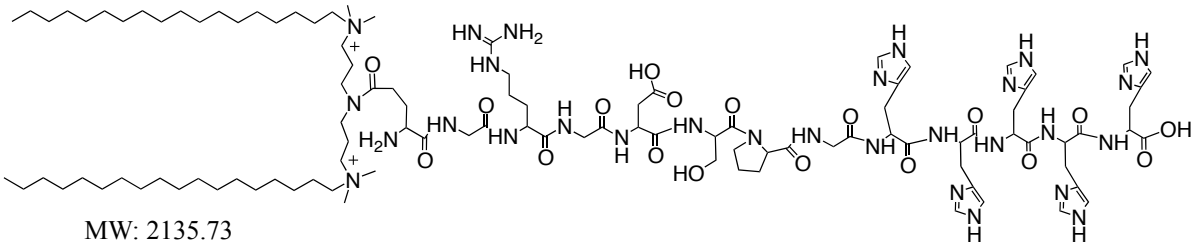

G**10** (18-E-PepE)

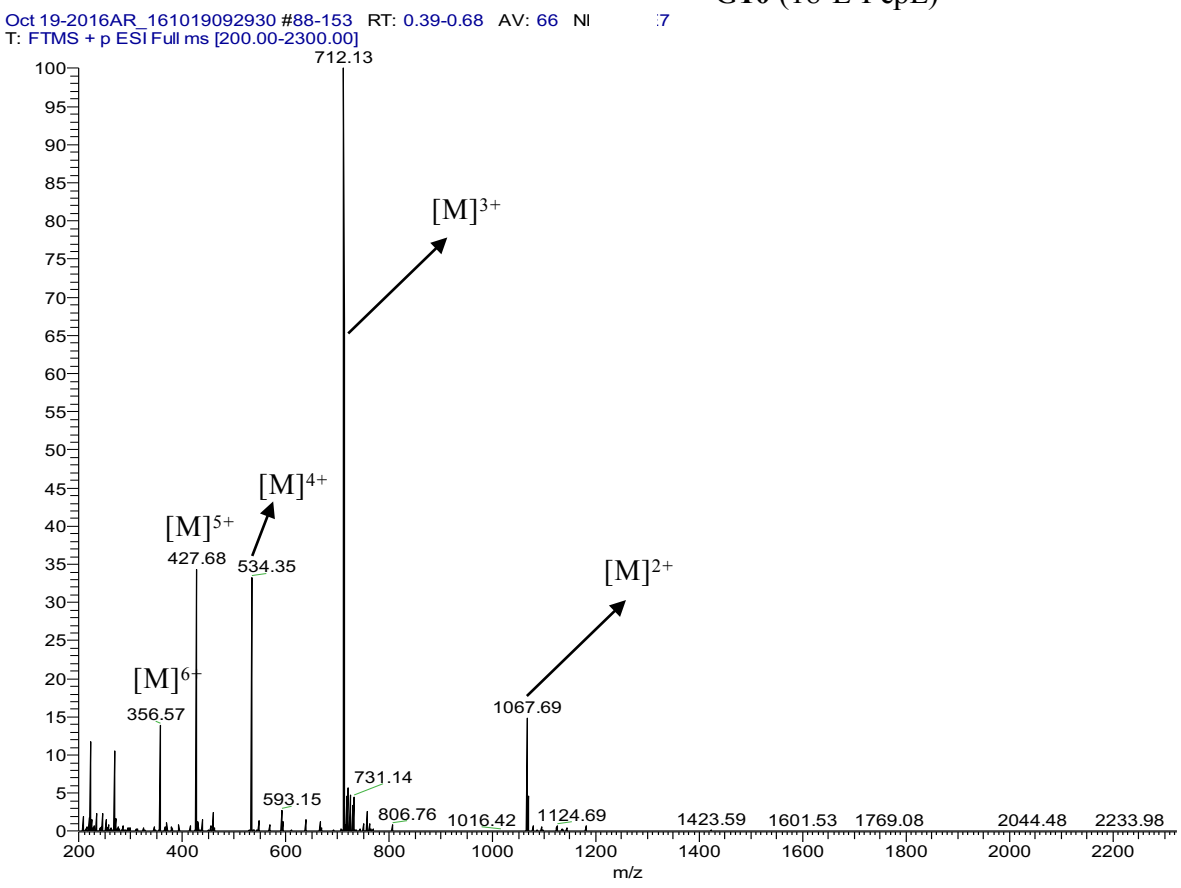

Fig. B13. ESI-MS data confirmed the identity of synthesized 18-E-PepE (G**10**) gemini surfactants.

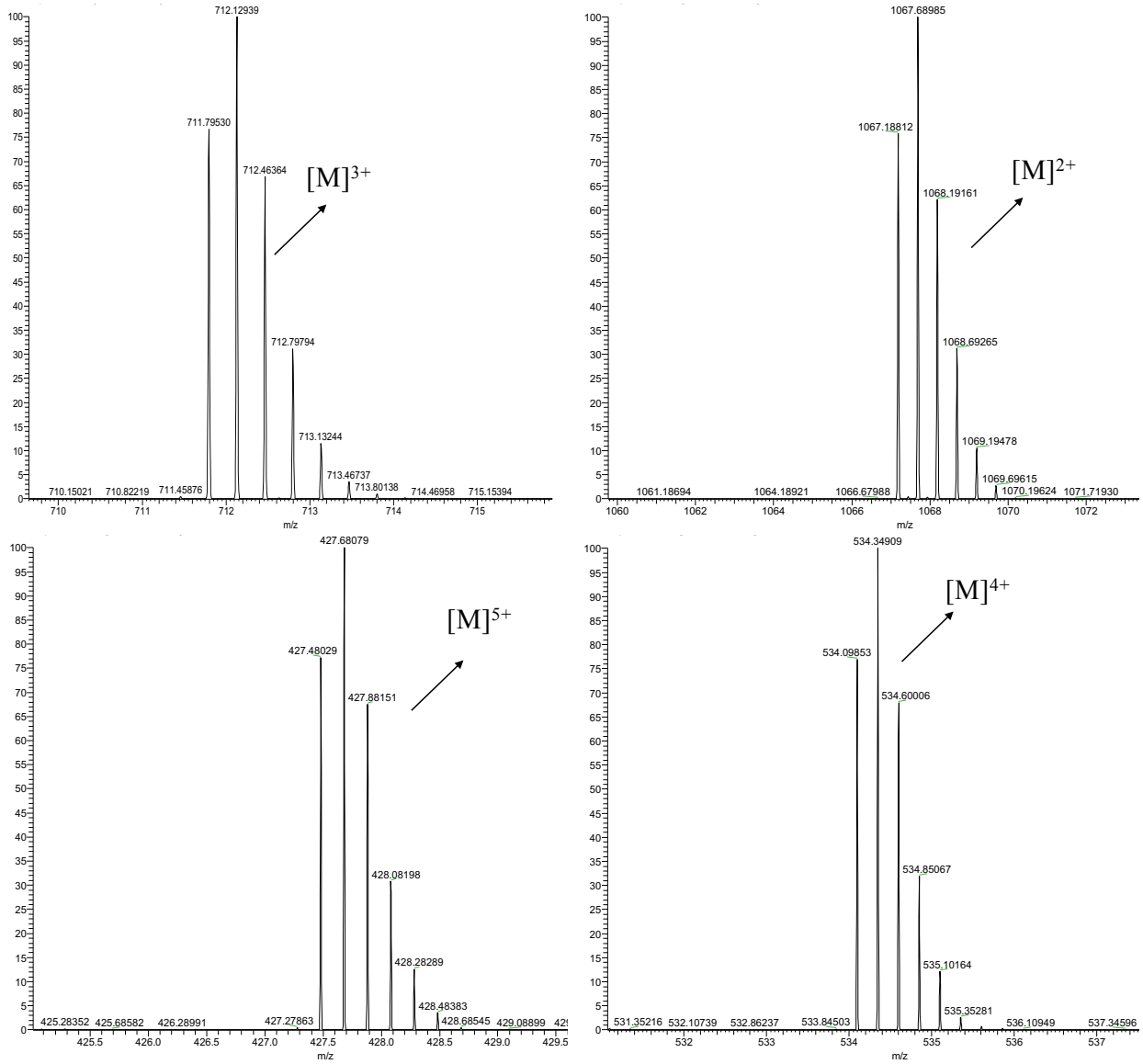

Fig. B14. High-resolution mass spectrometry (*m/z*) displays the doubly-, triply-, quadruply-, and quintuply-charged ions to five decimal places for 18-E-PepE (G**10**) gemini surfactants.

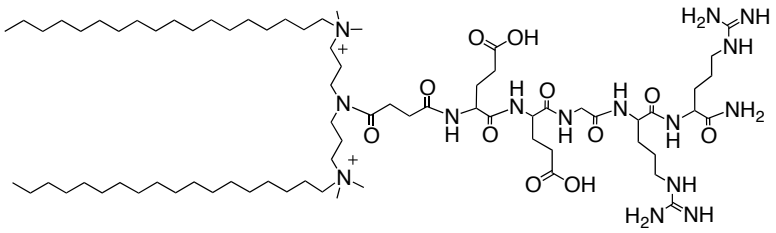

MW: 1421.04

G**11** (18-Suc-E_2GR_2)

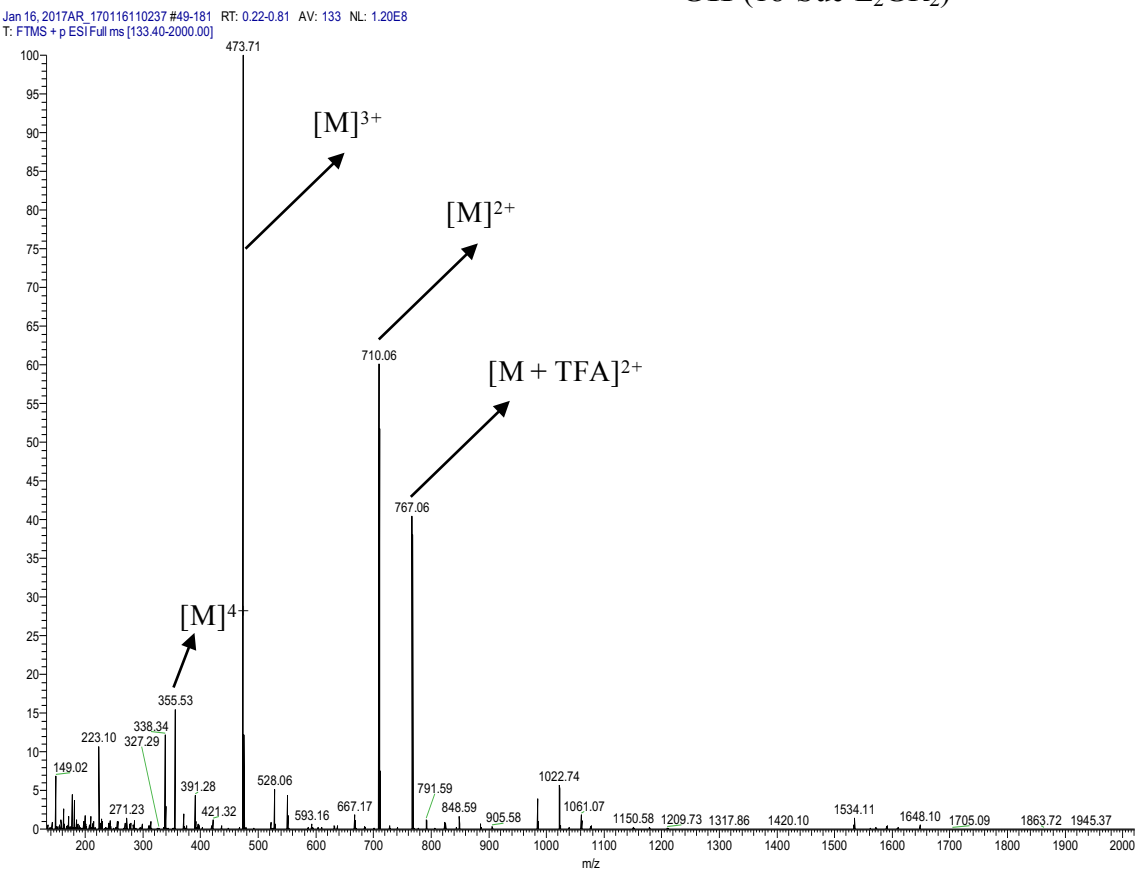

Fig. B15. ESI-MS data confirmed the identity of synthesized 18-Suc-E_2GR_2 (G**11**) gemini surfactants.

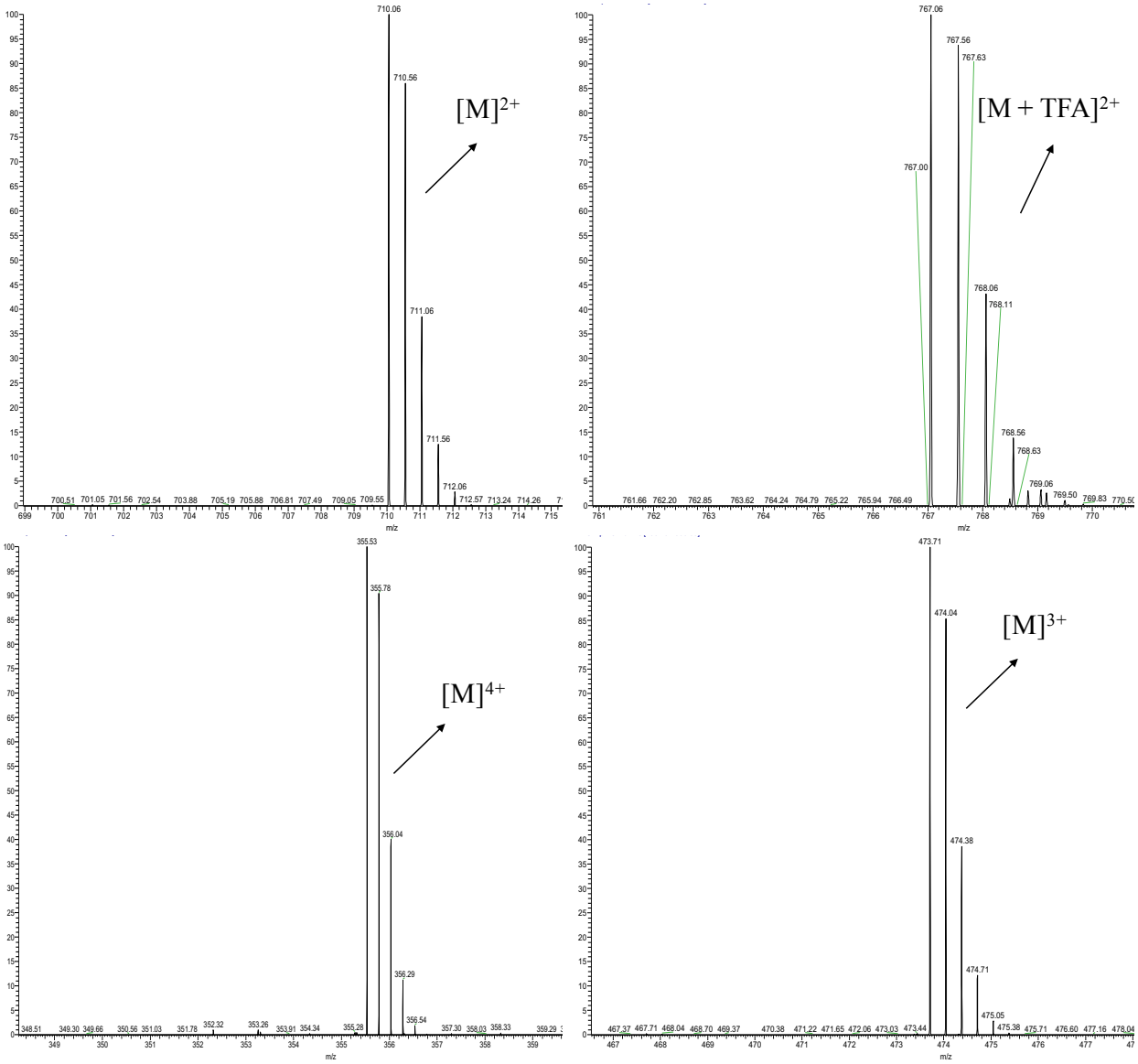

Fig. B16. High-resolution mass spectrometry (*m/z*) displays the doubly- (with or without TFA counterion), triply-, and quadruply-charged ions to two decimal places for 18-Suc-E_2GR_2 (G**11**) gemini surfactants.

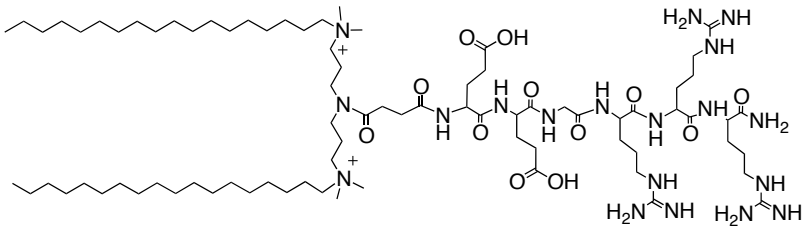

MW: 1577.22

G**12** (18-Suc-E_2GR_3)

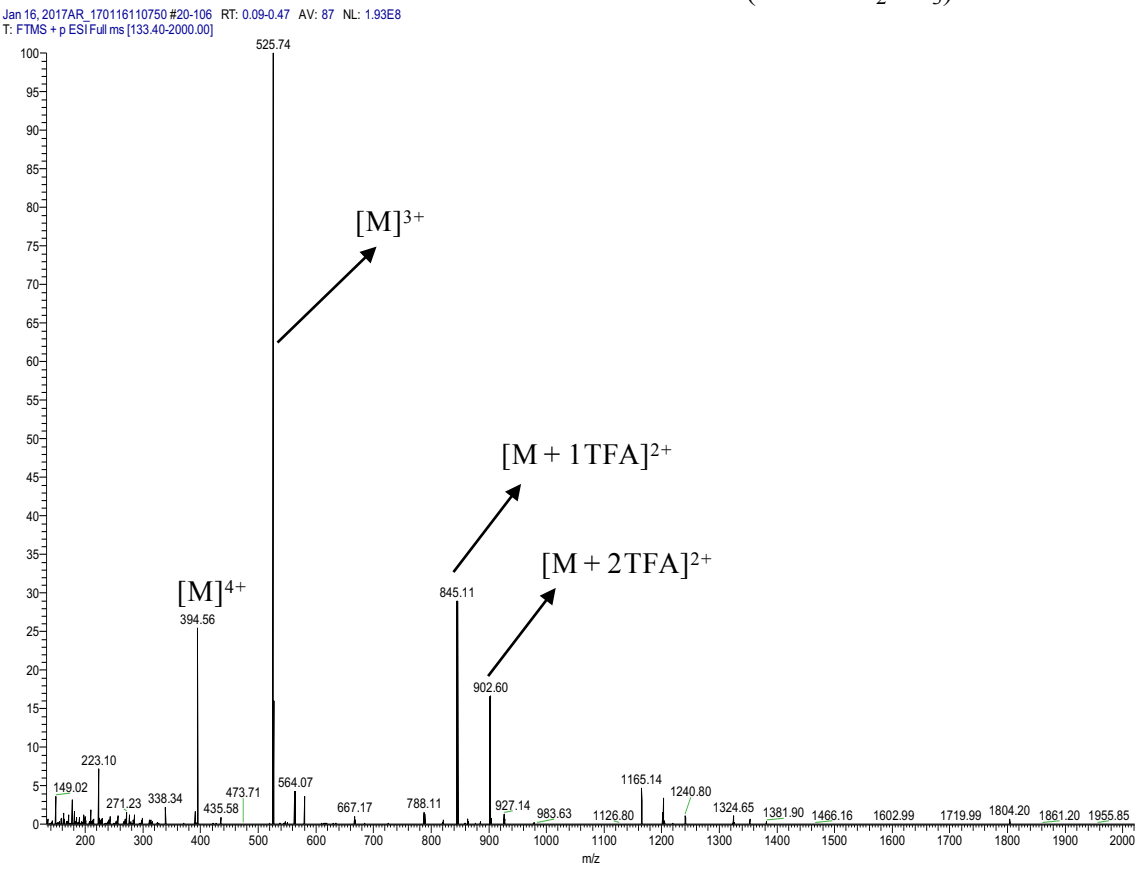

Fig. B17. ESI-MS data confirmed the identity of synthesized 18-Suc-E_2GR_3 (G**12**) gemini surfactants.

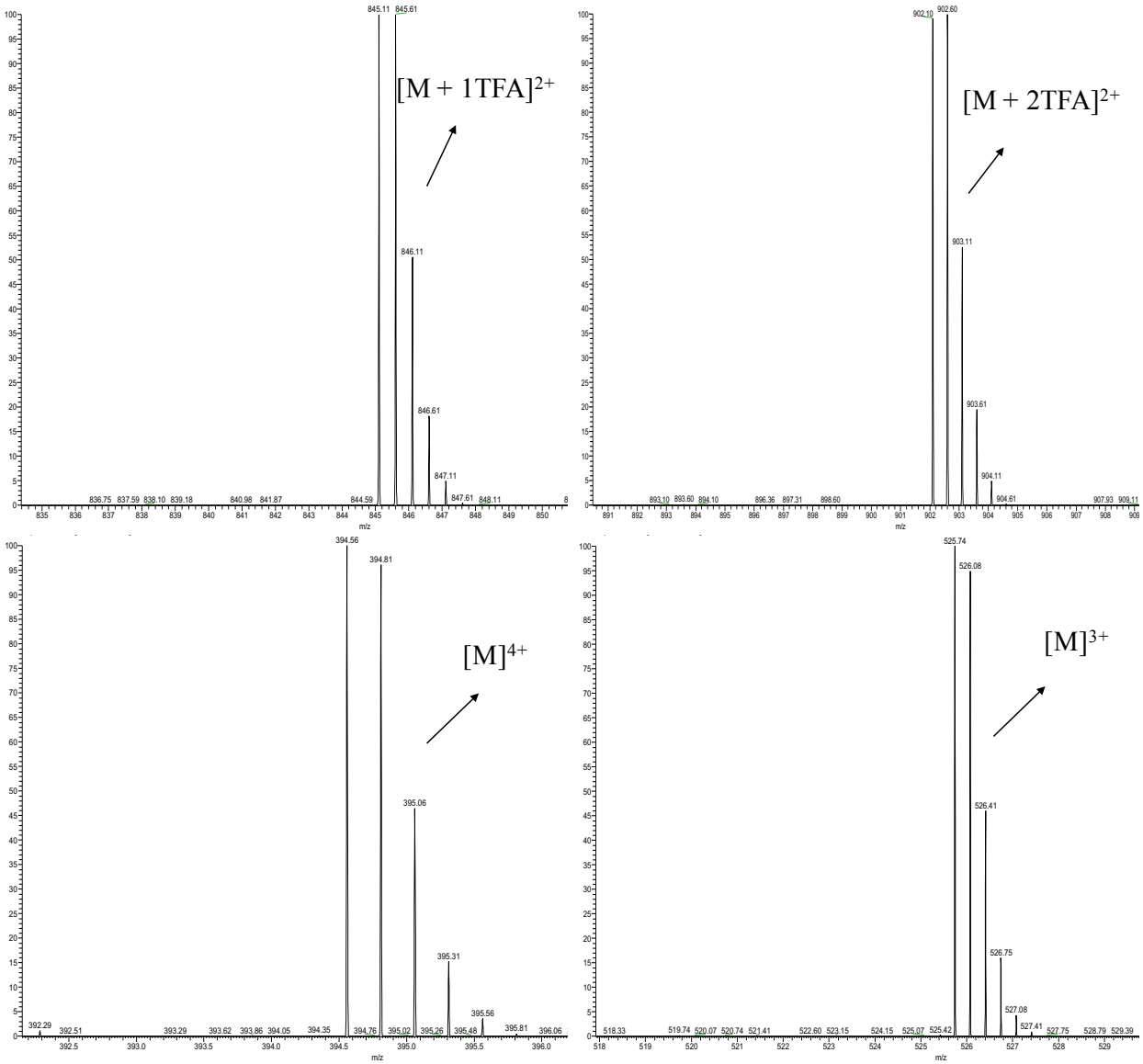

Fig. B18. High-resolution mass spectrometry (*m/z*) displays the doubly- (with one or two TFA counterions), triply-, and quadruply-charged ions to two decimal places for 18-Suc-E_2GR_3 (G**12**) gemini surfactants.

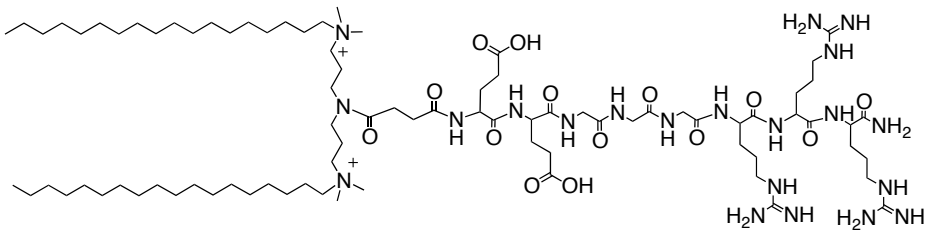

MW: 1691.32

G**13** (18-Suc-$E_2G_3R_3$)

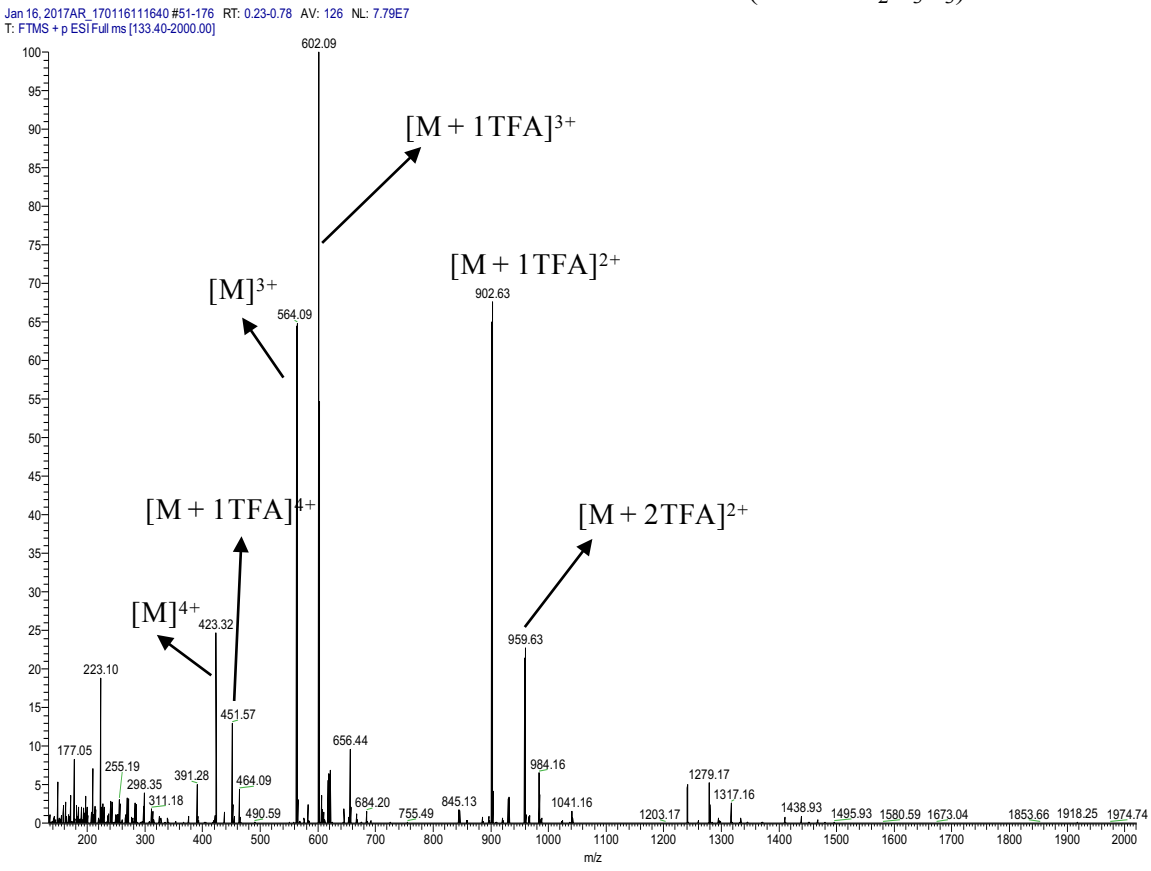

Fig. B19. ESI-MS data confirmed the identity of synthesized 18-Suc-$E_2G_3R_3$ (G**13**) gemini surfactants.

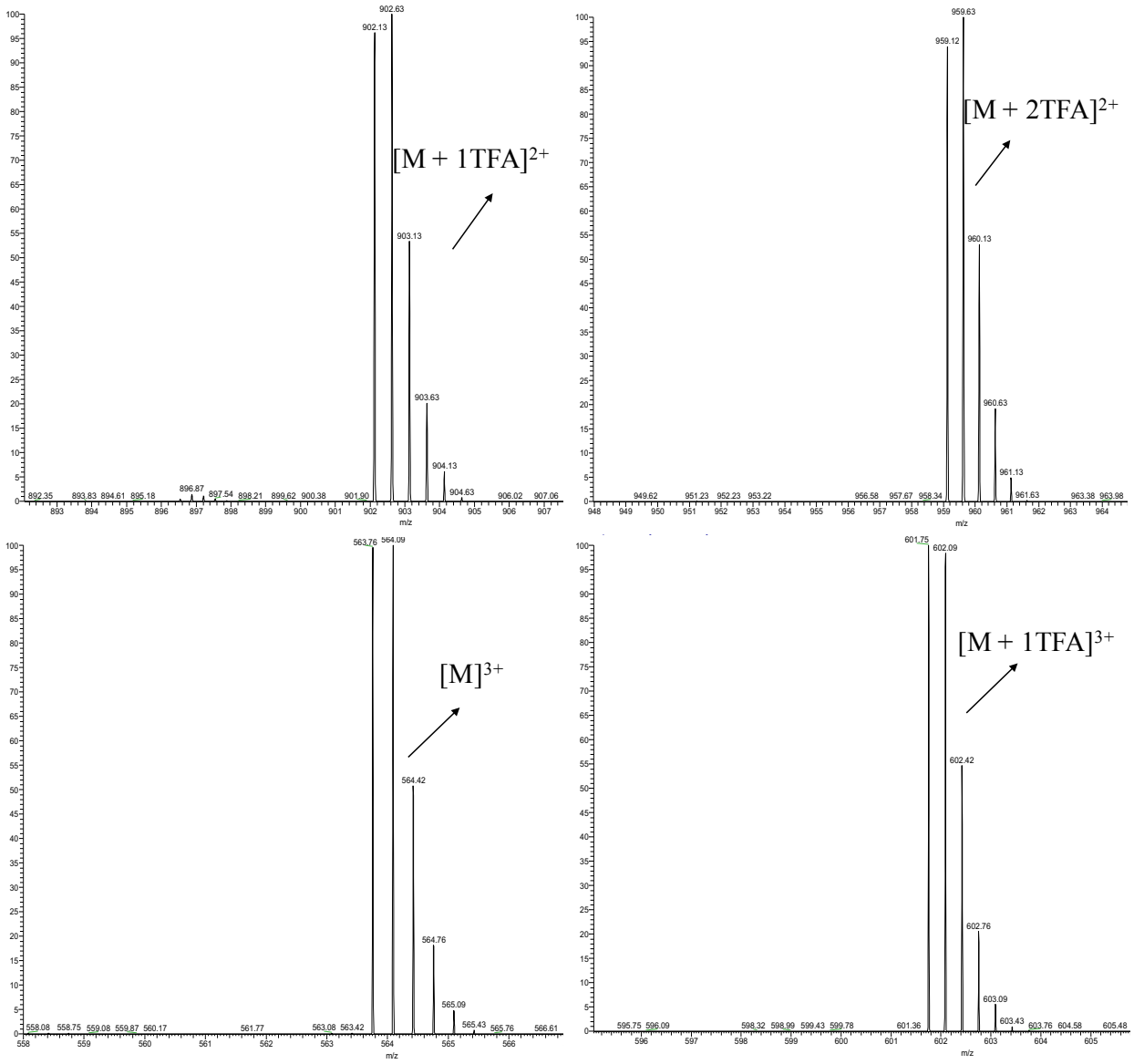

Fig. B20. High-resolution mass spectrometry (*m/z*) displays the doubly- (with one or two TFA counterions), and triply- (with or without TFA counterion) charged ions to two decimal places for 18-Suc-$E_2G_3R_3$ (G**13**) gemini surfactants.

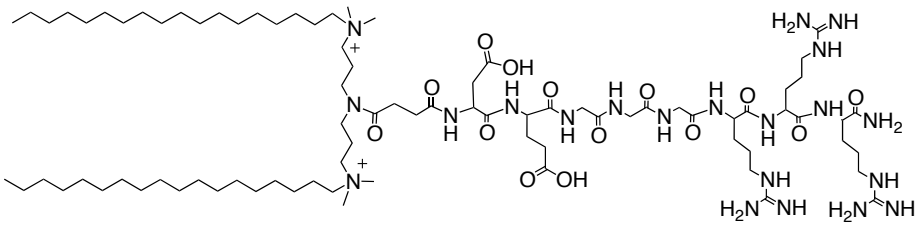

MW: 1677.30

G**14** (18-Suc-DEG$_3$R$_3$)

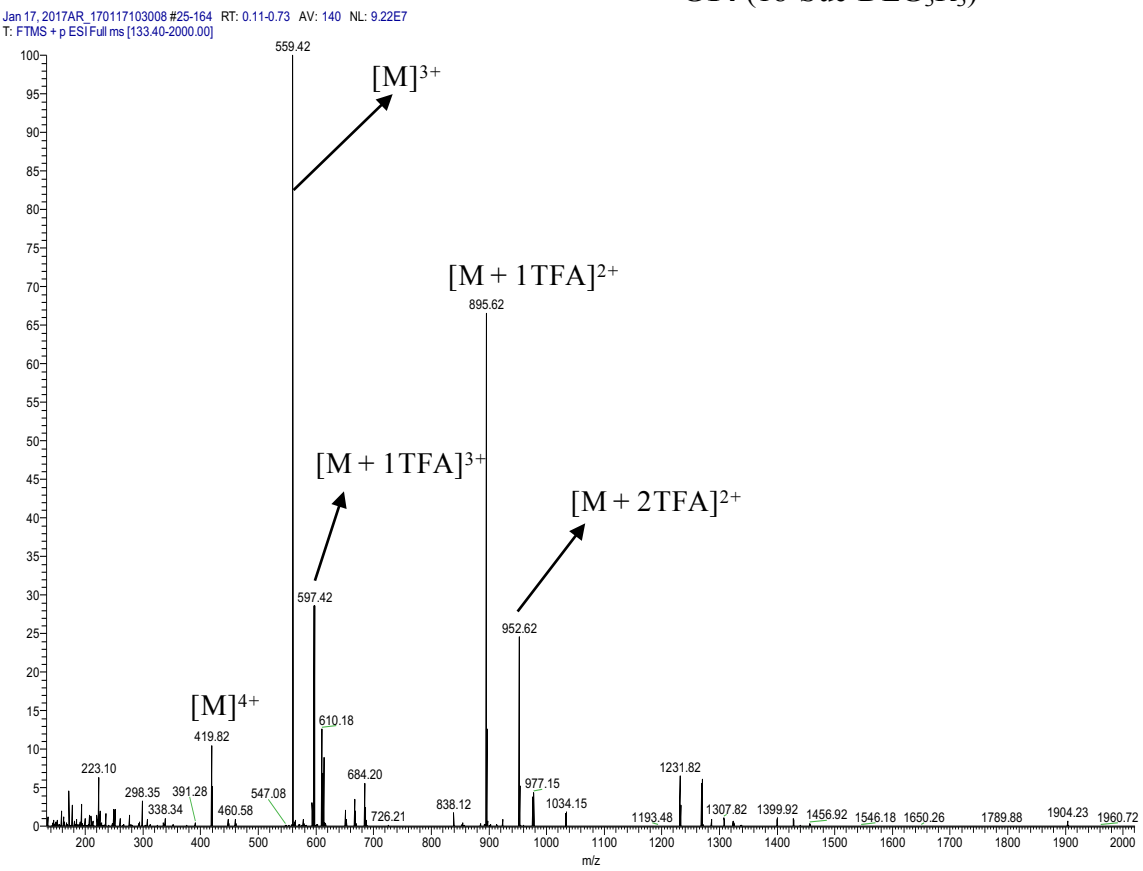

Fig. B21. ESI-MS data confirmed the identity of synthesized 18-Suc-DEG$_3$R$_3$ (G**14**) gemini surfactants.

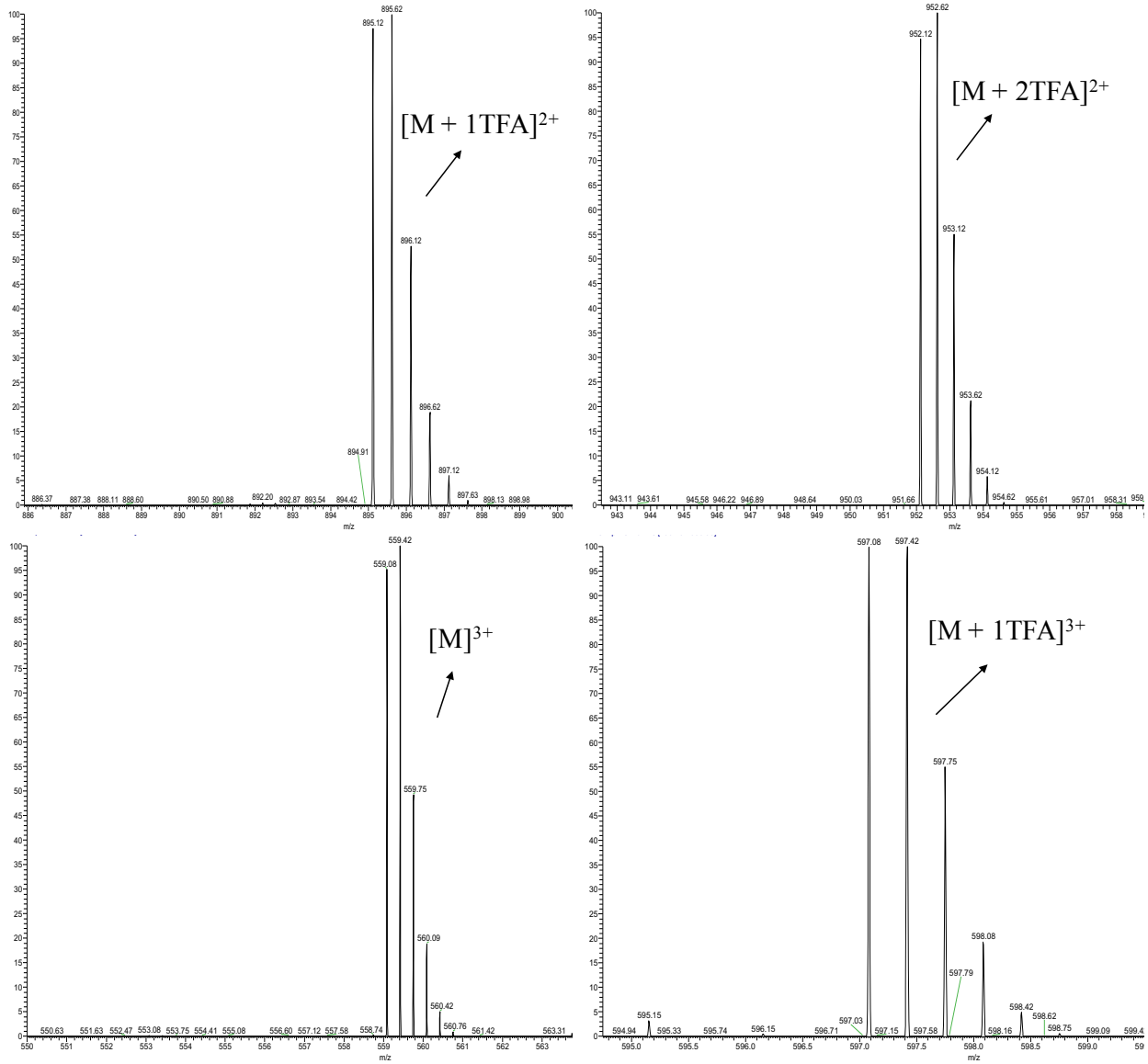

Fig. B22. High-resolution mass spectrometry (*m/z*) displays the doubly- (with one or two TFA counterions), and triply- (with or without TFA counterion) charged ions to two decimal places for 18-Suc-DEG$_3$R$_3$ (G**14**) gemini surfactants.

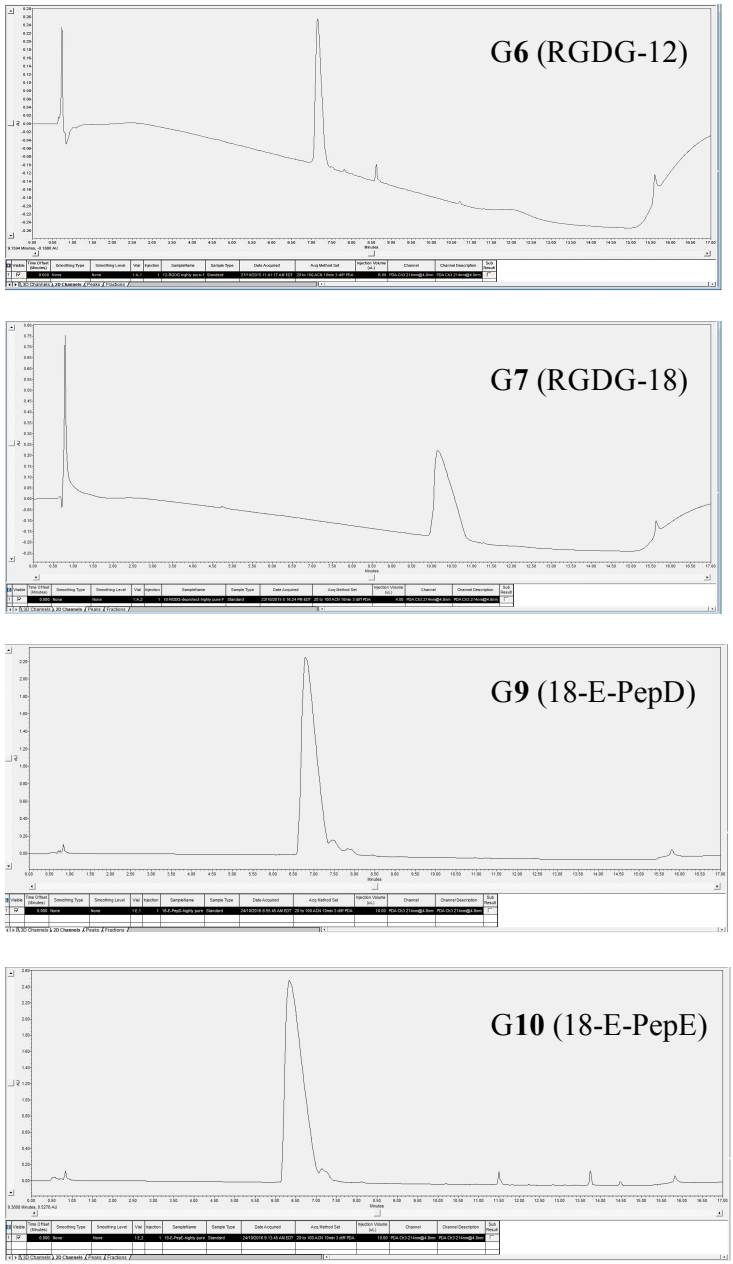

Fig. B23. RP-UPLC data for RGDG-12 (G**6**) and RGDG-18 (G**7**), synthesized using Method (A), and for 18-E-PepD (G**9**) and 18-E-PepE (G**10**), synthesized using Method (B). The purity of the products was confirmed by RP-UPLC using a linear gradient of solvent B (MeCN/TFA: 99.9/0.1, v/v) from 20% to 100% over 10 min on ACQUITY UPLC BEH C18 column (130 Å pore size, 1.7 μm particle size, 2.1 mm × 50 mm) (flow rate: 0.2 mL/min; UV detection wavelength: 214 nm).

Appendix C: Non-Covalent Addition of Peptide Enhancers (7 Types)

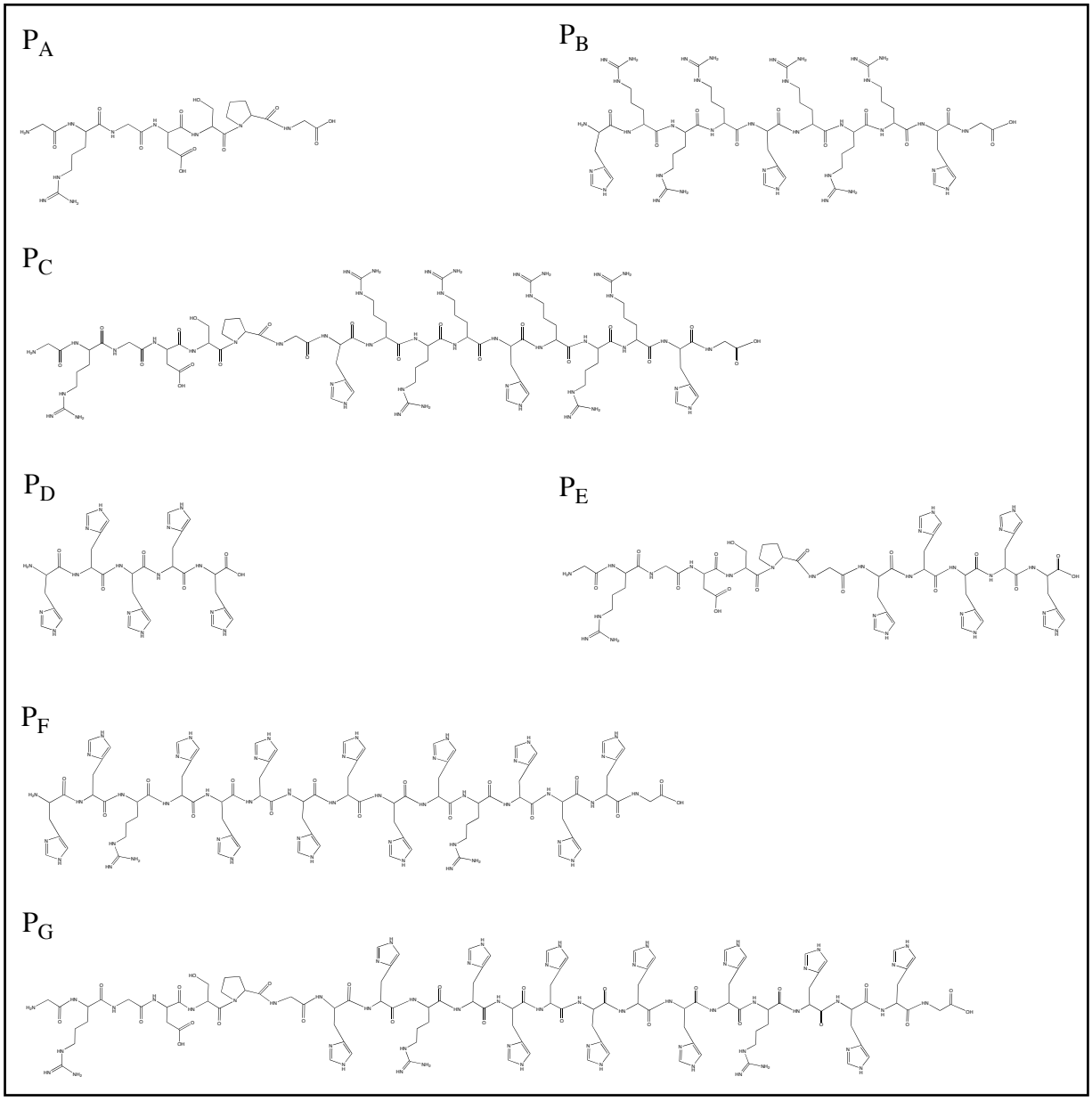

Fig. C1. Chemical structure of the peptide enhancers (P_A-P_G) studied in this research.

Appendix D: Flow Cytometry Dot-Plots

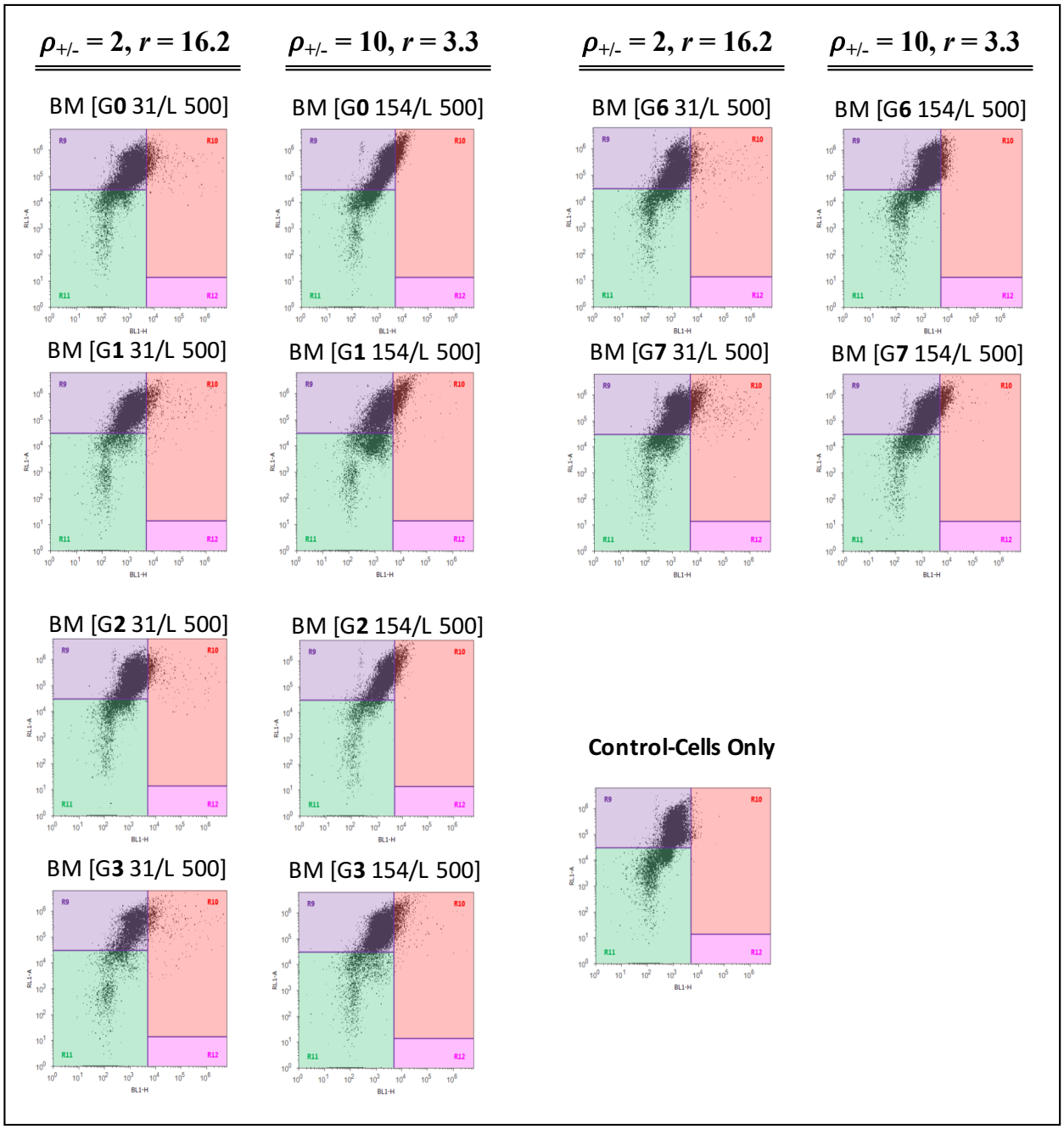

Fig. D1. Flow cytometry *dot plot* of GFP expression levels in 3T3 fibroblasts after transfection (in 96-well plate) with BM [G/L] lipoplexes formulated using 12-3-12 (G**0**), 18-3-13 (G**1**), 12-7NH-12 (G**2**), 18-7NH-18 (G**3**), RGDG-12 (G**6**) and RGDG-18 (G**7**) as a function of $\rho_{\pm}$ = 10, 2 (M_G = 154 μM, 31 μM, respectively) with identical DOPE molarity at M_L = 500 μM.

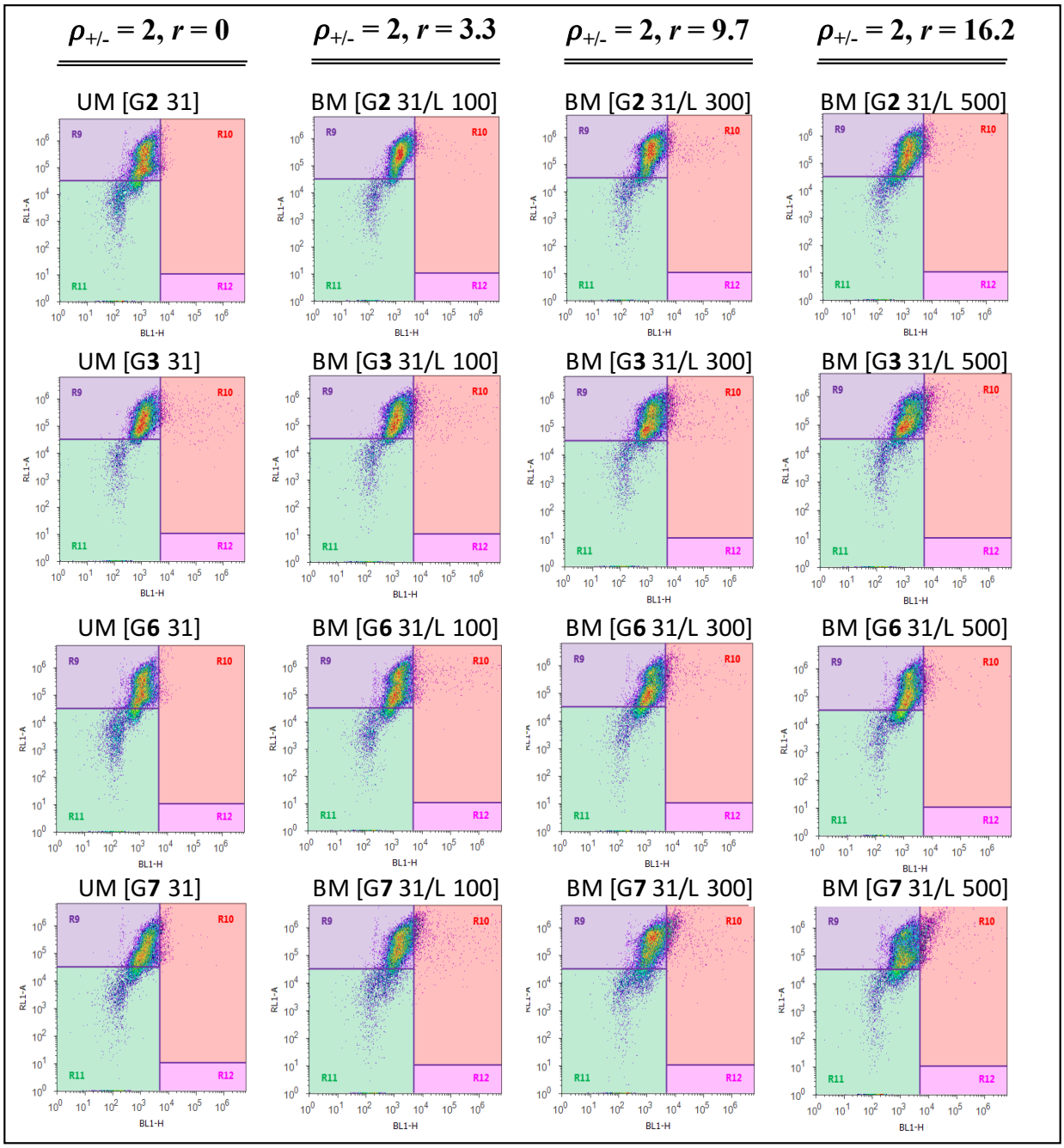

Fig. D2. Flow cytometry *density plot* of GFP expression levels in 3T3 fibroblasts after transfection (in 96-well plate) with BM [G/L] lipoplexes formulated using 12-7NH-12 (G**2**), 18-7NH-18 (G**3**), RGDG-12 (G**6**) and RGDG-18 (G**7**) as a function of r = 16.2, 9.7, 3.3, 0 (prepared at M_L = 500 µM, 300 µM, 100 µM, 0 µM, respectively) with identical $\rho_{\pm} = 2$ (prepared at M_G = 31 µM).

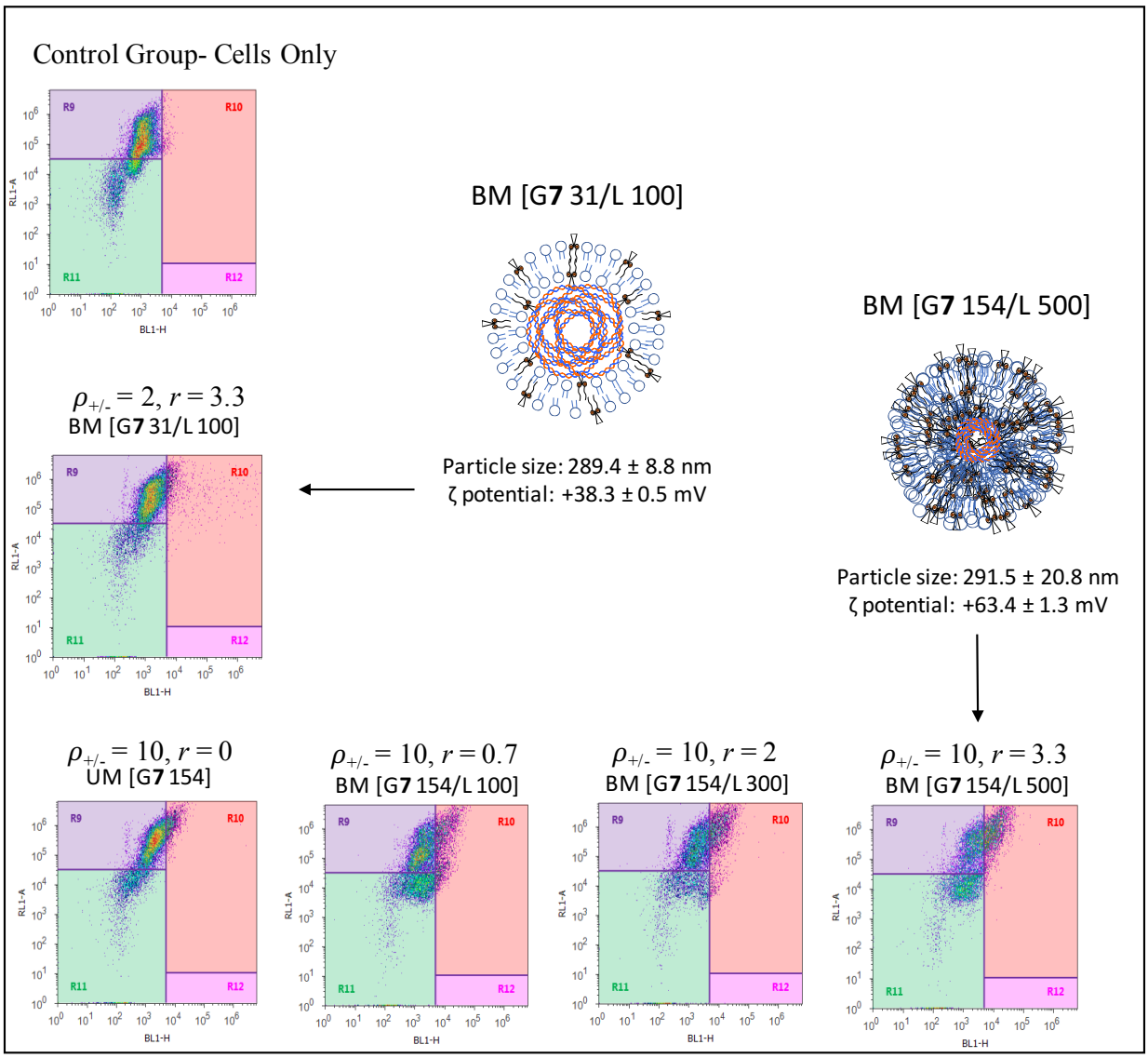

Fig. D3. Flow cytometry *density plot* of GFP expression in 3T3 fibroblasts, performed in 96-well plate. The correlation between the transfection efficacy of the gemini-based lipoplexes with the degree of pDNA compaction (as determined by the size and zeta potential of the complexes) using G7 gemini surfactants at $\rho_{\pm} = 10, 2$ (prepared at $M_G = 154\ \mu M, 31\ \mu M$, respectively).

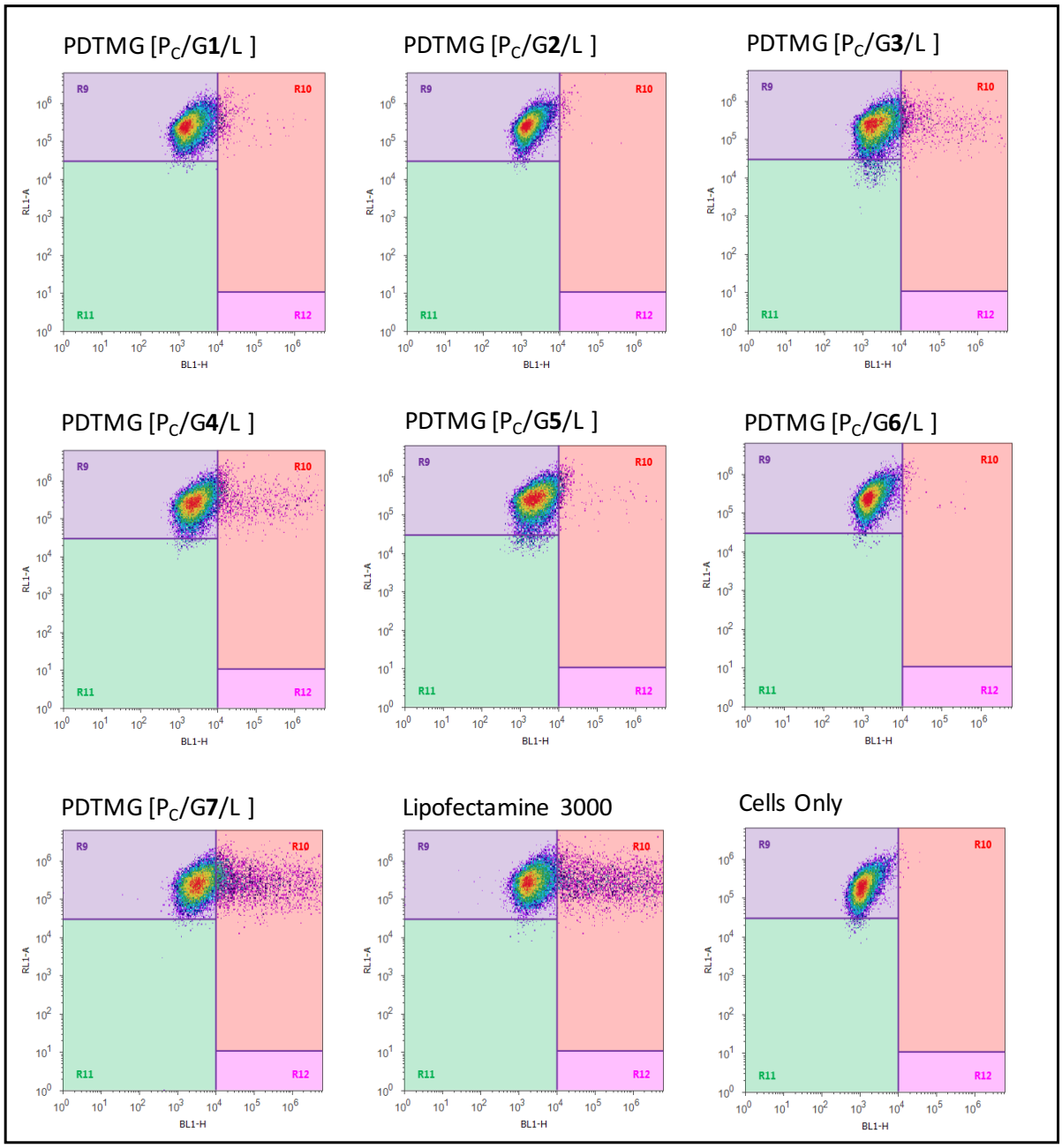

Fig. D4. Flow cytometry *density plot* of GFP expression in 3T3 fibroblasts after transfection (in 24-well plates) with PDTMG complexes formulated using P_C peptide enhancer at M_P = 267, and G**1**-G**7** gemini surfactants and DOPE lipid at $\rho_{\pm}$ = 1.1 and r = 6.8 (M_G = 17 μM and M_L = 113 μM).

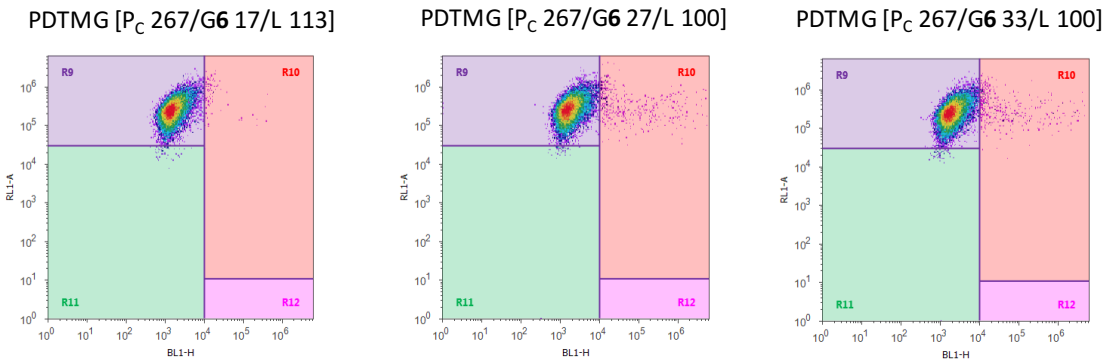

Fig. D5. Flow cytometry *density plot* of GFP expression in 3T3 fibroblasts transfected using G**6**-based PDTMG complexes formulated at varying $\rho_{\pm}$ (1.1, 1.7, 2.1).

Appendix E: Optimization of PDTMG Nanoparticles

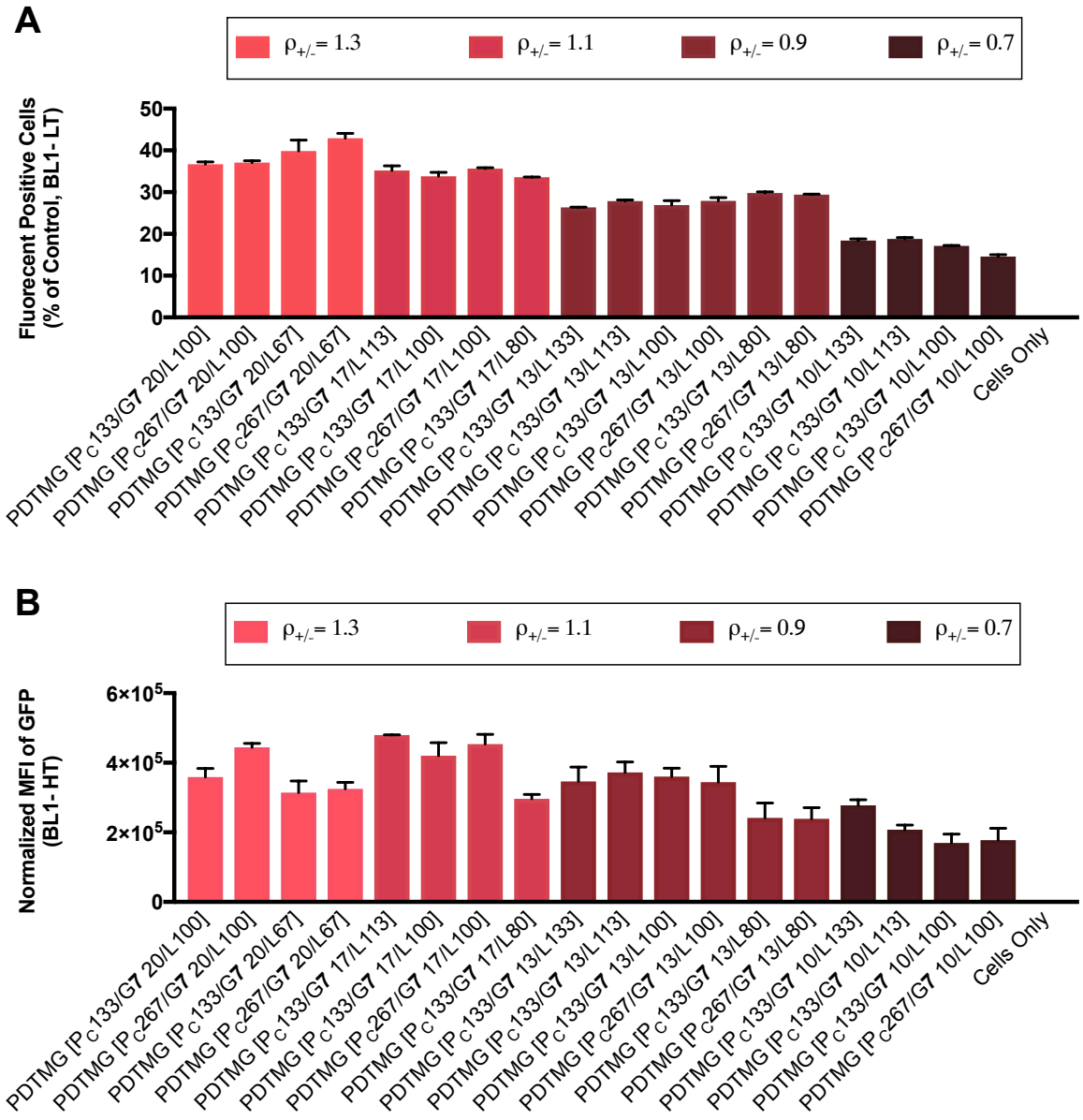

Fig. E1. Optimization study- results are presented as mean ± SD from one experiment (n = 3) performed in 24-well plates. (A) The percentage of the transfected cells and (B) the intensity of GFP expression level were normalized to untreated control (cells only).

Appendix F: Size distributions for UM, BM and PDTMG complexes

Table. F1. Particle size and PDI of UM [G] and BM [G/L] formulations as measured by DLS.

Type	Sample Name	Repeats	T	Z-Ave	PdI	Pk 1 Mean Int	Pk 2 Mean Int	Pk 3 Mean Int	Pk 1 Area Int	Pk 2 Area Int	Pk 3 Area Int
			°C	d.nm		d.nm	d.nm	d.nm	Percent	Percent	Percent
Size	UM [G**6** 31]	1	25	1299	0.648	726.9	0	0	100	0	0
Size		2	25	2256	0.294	1148	0	0	100	0	0
Size		3	25	2221	0.327	1053	0	0	100	0	0
Size	BM [G**6** 31/L 100]	1	25	469.8	0.493	628.7	114.3	0	73	27	0
Size		2	25	449.1	0.405	652.5	119.9	0	75.2	24.8	0
Size		3	25	512.5	0.442	699.8	125.4	0	71.8	28.2	0
Size	BM [G**6** 31/L 500]	1	25	1846	0.968	240.2	0	0	100	0	0
Size		2	25	1271	0.887	238.9	0	0	100	0	0
Size		3	25	1334	0.804	448.3	63.56	0	88.6	11.4	0
Size	UM [G**7** 31]	1	25	403.7	0.434	461.9	62.38	5430	89.6	8.2	2.2
Size		2	25	397.1	0.532	704.9	152.5	5420	73.5	25	1.5
Size		3	25	423.4	0.584	632.1	125.1	5426	77.7	19.9	2.4
Size	BM [G**7** 31/L 100]	1	25	282.9	0.471	408.1	4803	0	94	6	0
Size		2	25	275.9	0.488	714.7	144	4808	60.6	36.5	2.9
Size		3	25	309.3	0.467	535.4	109.9	5249	72.9	24.4	2.8
Size	BM [G**7** 31/L 500]	1	25	4011	0.153	669.2	0	0	100	0	0
Size		2	25	3351	0.889	1319	0	0	100	0	0
Size		3	25	3854	1	1614	0	0	100	0	0
Size	UM [G**6** 154]	1	25	2207	0.283	1974	0	0	100	0	0
Size		2	25	2729	0.451	1579	0	0	100	0	0
Size		3	25	2229	0.274	2035	0	0	100	0	0
Size	BM [G**6** 154/L 100]	1	25	735	0.534	744.3	81.29	5560	89.8	9	1.2
Size		2	25	632.6	0.414	604.9	0	0	100	0	0
Size		3	25	1206	0.501	1492	111.8	5463	86.1	11.3	2.6
Size	BM [G**6** 154/L 500]	1	25	629.4	0.616	652.9	91.21	0	79.3	20.7	0
Size		2	25	476.3	0.545	637.1	108.7	17.68	78.4	21.2	0.4
Size		3	25	446.7	0.387	399	0	0	100	0	0
Size	UM [G**7** 154]	1	25	176.6	0.391	176.4	1652	0	77.4	22.6	0
Size		2	25	192.1	0.436	130.4	605.9	4588	51.7	44.7	3.6
Size		3	25	174.6	0.387	249.7	4881	0	96.9	3.1	0
Size	BM [G**7** 154/L 100]	1	25	179.7	0.411	265.3	4715	0	95.4	4.6	0
Size		2	25	177.8	0.394	221.7	3398	29.42	86.6	11.4	2
Size		3	25	186.6	0.374	221.2	3864	0	89.3	10.7	0
Size	BM [G**7** 154/L 500]	1	25	332.5	0.358	225	65.05	0	76.2	23.8	0
Size		2	25	292.9	0.32	222.3	60.24	0	79.4	20.6	0
Size		3	25	249.2	0.338	259.5	79.39	0	67	33	0

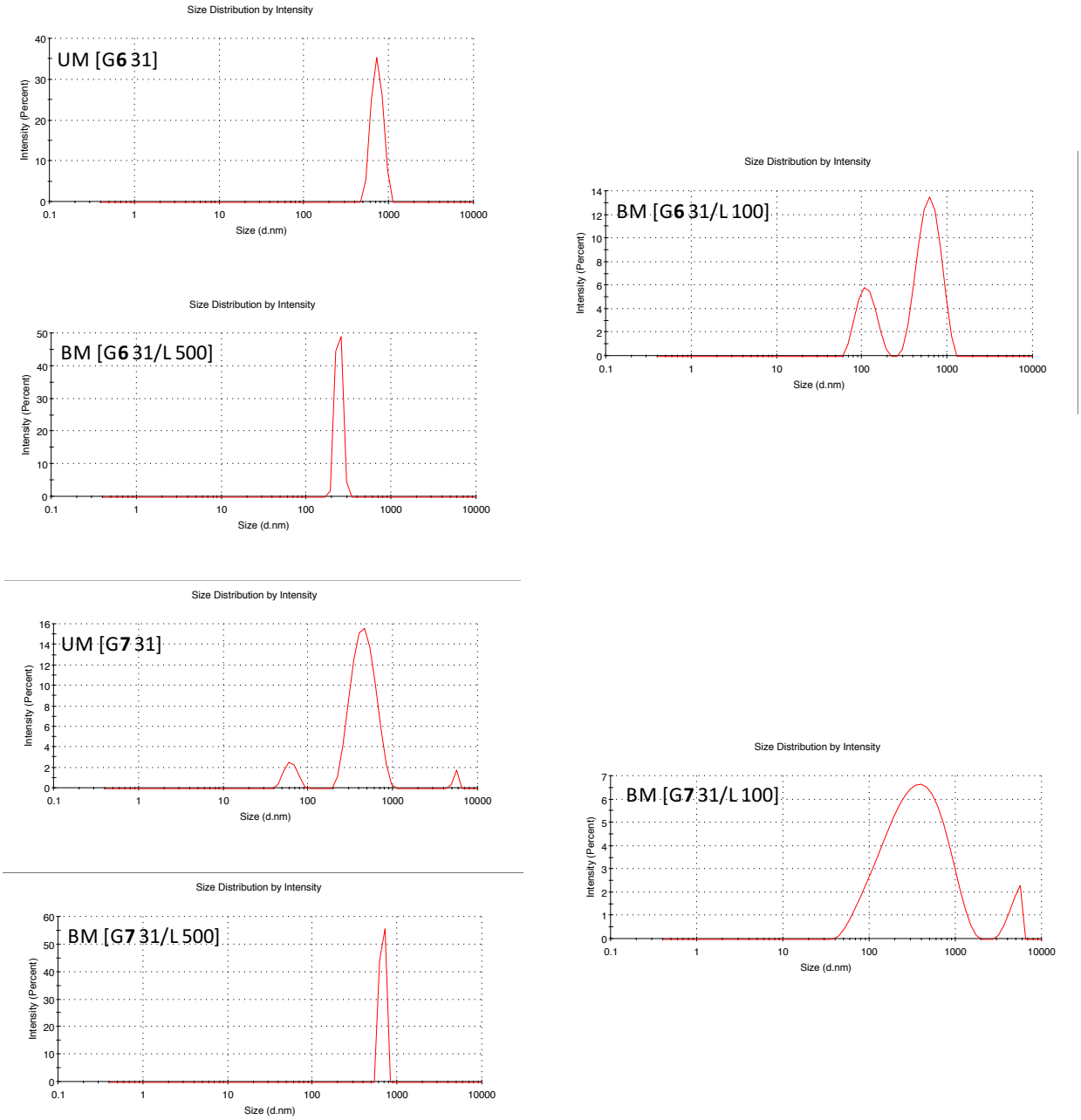

Fig. F1. The intensity-based size distribution of UM [G] and BM [G/L] formulated with G**6** or G**7** gemini surfactants at $\rho_{\pm} = 2$ and r = 16.2, 3.3, and 0 (i.e., 500/31, 100/31, and 0/31, respectively).

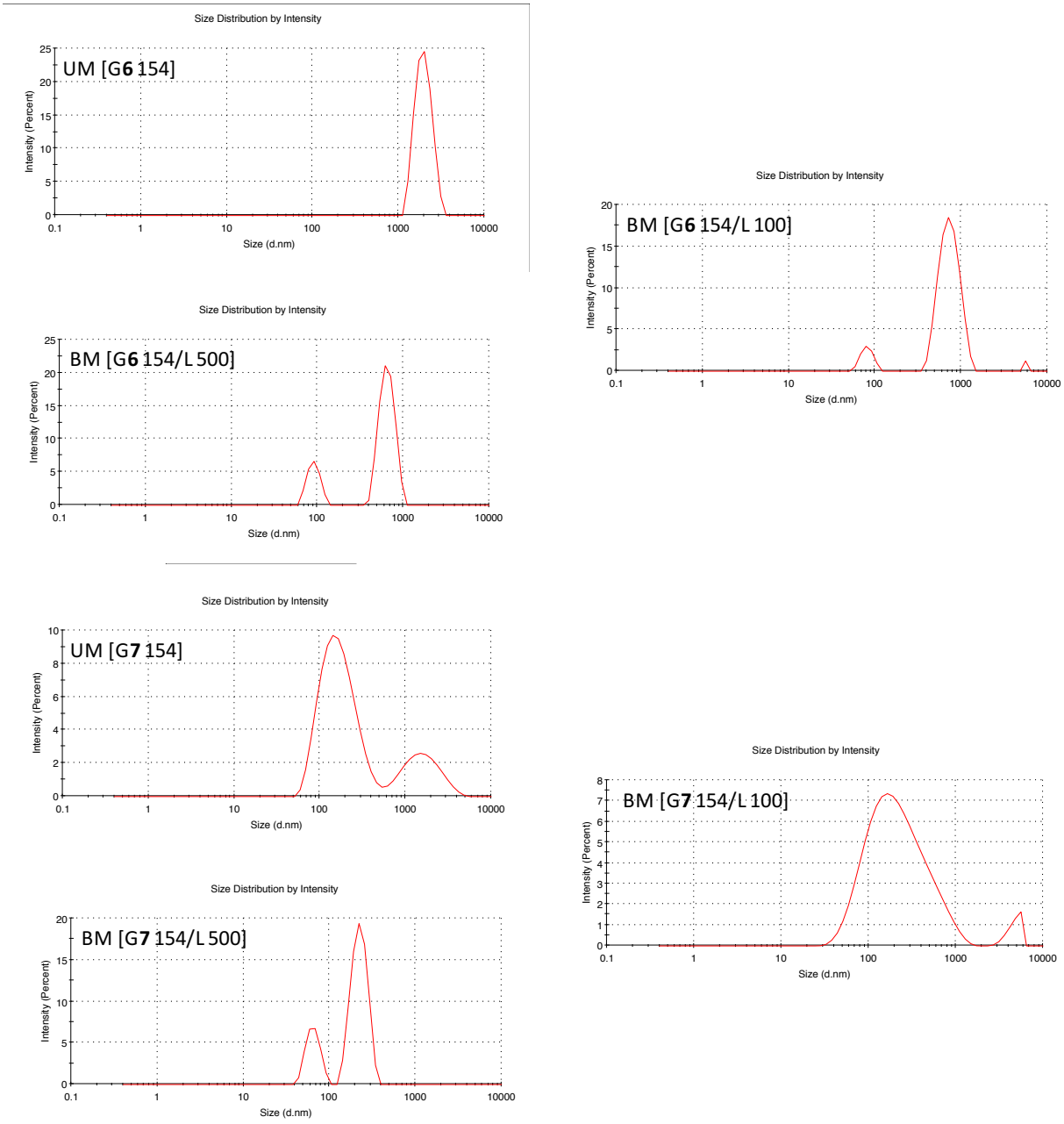

Fig. F2. The intensity-based size distribution of UM [G] and BM [G/L] formulated with G**6** or G**7** gemini surfactants at $\rho_{\pm}$ = 10 and r = 3.3, 0.7, and 0 (i.e., 500/154, 100/154, and 0/154, respectively).

Table. F2. Particle size and PDI of UM [P] formulations as measured by DLS.

Type	Sample Name	Repeats	T	Z-Ave	PdI	Pk 1 Mean Int	Pk 2 Mean Int	Pk 3 Mean Int	Pk 1 Area Int	Pk 2 Area Int	Pk 3 Area Int
			°C	d.nm		d.nm	d.nm	d.nm	Percent	Percent	Percent
Size	UM [P_A 62]	1	25	145.6	0.471	378	0	0	100	0	0
Size		2	25	150.5	0.502	509.6	82.87	0	63.1	36.9	0
Size		3	25	145.6	0.52	194.5	3037	0.8014	78.2	15.3	6.4
Size	UM [P_A 154]	1	25	128.4	0.531	274.9	0	0	100	0	0
Size		2	25	128	0.515	266	19.35	0	93.3	6.7	0
Size		3	25	235.7	0.253	233	24.27	5224	82.8	10.7	6.5
Size	UM [P_A 308]	1	25	135.4	0.669	588.8	57.01	0	65.3	34.7	0
Size		2	25	110.2	0.467	371	66.93	0	57.6	42.4	0
Size		3	25	112	0.429	244.9	3723	0	97.5	2.5	0
Size	UM [P_B 10]	1	25	340.6	0.456	668.3	194.2	5174	59.5	37.8	2.7
Size		2	25	279.2	0.367	434.8	4722	0	98.6	1.4	0
Size		3	25	272.4	0.282	538.3	0	0	100	0	0
Size	UM [P_B 25]	1	25	265.8	0.287	421.9	118.8	0	78.9	21.1	0
Size		2	25	266.7	0.269	335.7	74.05	0	92.1	7.9	0
Size		3	25	293.7	0.403	485.2	126.9	0	76.1	23.9	0
Size	UM [P_B 49]	1	25	239.3	0.364	478.9	126.4	0	69.6	30.4	0
Size		2	25	237.5	0.322	284.4	61.82	5029	92.7	4.1	3.2
Size		3	25	245.3	0.387	313.6	4547	0	94.2	5.8	0
Size	UM [P_B 98]	1	25	182.7	0.374	219.5	4584	0	93.3	6.7	0
Size		2	25	170.1	0.347	137	507.6	0	59.6	40.4	0
Size		3	25	175.2	0.331	208.8	5012	0	96.4	3.6	0
Size	UM [P_C 10]	1	25	212.4	0.239	242.5	5161	0	97.9	2.1	0
Size		2	25	205.1	0.261	257.6	4060	40.11	95.7	4.1	0.3
Size		3	25	210.8	0.247	285.2	66.25	0	91.7	8.3	0
Size	UM [P_C 25]	1	25	208.4	0.208	234.5	5291	0	98.9	1.1	0
Size		2	25	214.1	0.239	269.7	5041	0	98.8	1.2	0
Size		3	25	220.6	0.262	246.6	4783	0	95.7	4.3	0
Size	UM [P_C 49]	1	25	161.3	0.204	199.4	0	0	100	0	0
Size		2	25	157.6	0.197	195.9	0	0	100	0	0
Size		3	25	160.9	0.205	182.2	4865	0	98	2	0
Size	UM [P_C 98]	1	25	158.9	0.224	171	4817	0	96.4	3.6	0
Size		2	25	158.3	0.196	197.4	0	0	100	0	0
Size		3	25	152.5	0.188	189.9	0	0	100	0	0

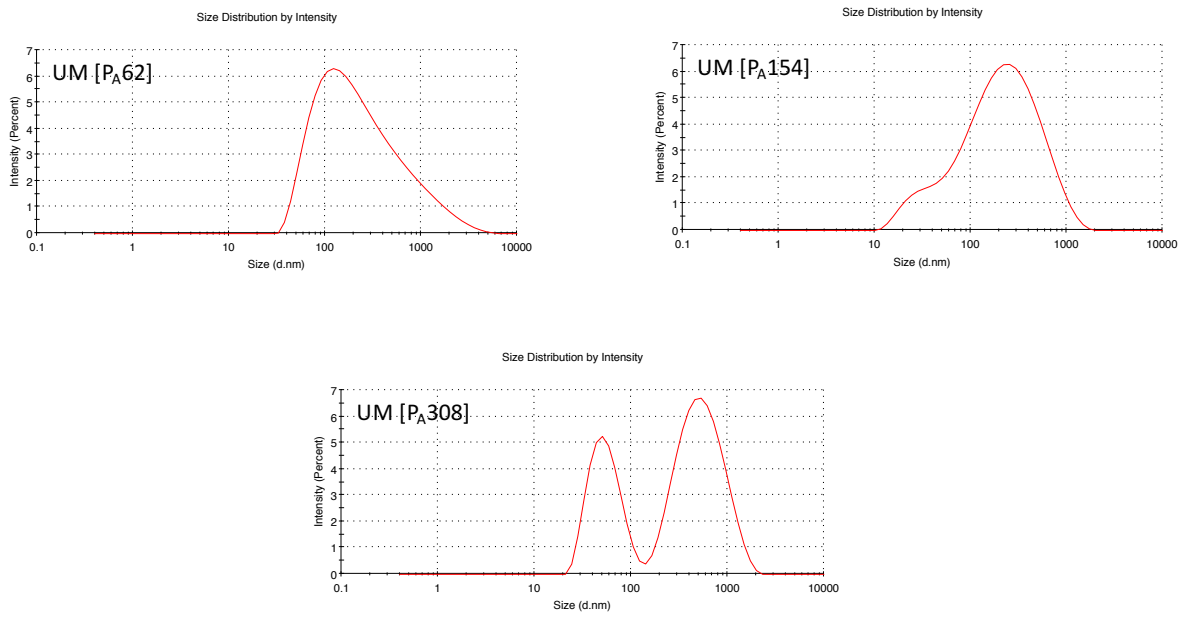

Fig. F3. The intensity-based size distribution of UM [P] formulated with zwitterionic P_A peptide enhancer (at M_P = 62 μM, 154 μM, 308 μM).

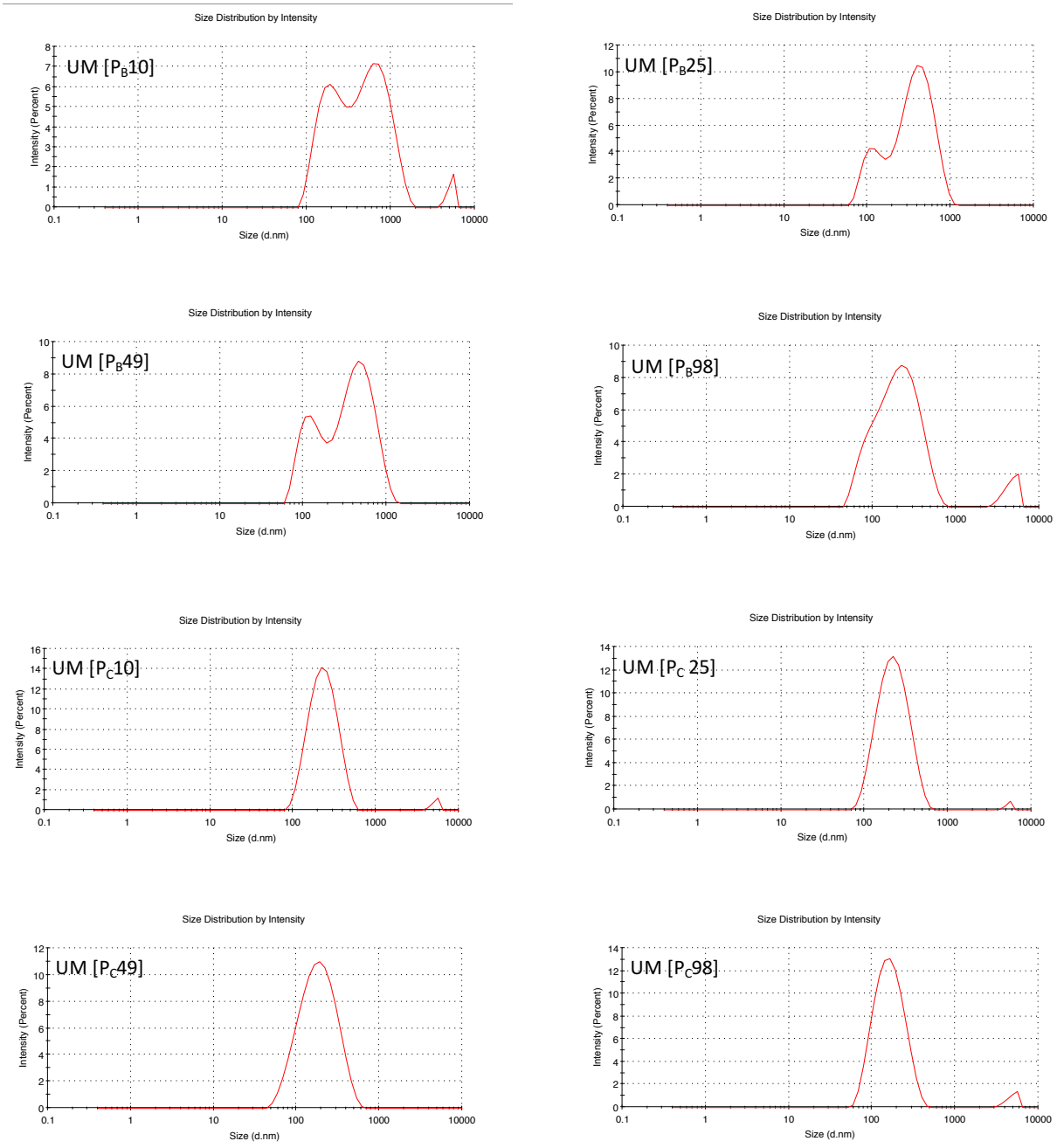

Fig. F4. The intensity-based size distribution of UM [P] formulated with cationic P_B and P_C peptide enhancers (at M_P = 10 µM, 25 µM, 49 µM, 98 µM).

Table. F3. Particle size and PDI of BM [P/L] formulations as measured by DLS.

Type	Sample Name	Repeats	T	Z-Ave	PdI	Pk 1 Mean Int	Pk 2 Mean Int	Pk 3 Mean Int	Pk 1 Area Int	Pk 2 Area Int	Pk 3 Area Int
			°C	d.nm		d.nm	d.nm	d.nm	Percent	Percent	Percent
Size	BM [P_A 62/L 500]	1	25	112.1	0.236	140.6	4589	0	98.5	1.5	0
Size		2	25	110.6	0.229	144.7	0	0	100	0	0
Size		3	25	110.9	0.234	146.4	0	0	100	0	0
Size	BM [P_A 154/L 500]	1	25	112.8	0.243	130.7	4758	0	97	3	0
Size		2	25	109.2	0.238	140.1	21.76	0	98.3	1.7	0
Size		3	25	110.7	0.218	143.4	0	0	100	0	0
Size	BM [P_A 308/L 500]	1	25	114.6	0.253	155.9	0	0	100	0	0
Size		2	25	113.7	0.223	147	0	0	100	0	0
Size		3	25	111.8	0.231	140.8	4785	22.3	98.2	1.2	0.6
Size	BM [P_B 10/L 500]	1	25	139.1	0.228	163	4896	0	97.9	2.1	0
Size		2	25	141.8	0.231	156.9	4672	0	96.5	3.5	0
Size		3	25	138	0.236	199.5	0	0	100	0	0
Size	BM [P_B 25/L 500]	1	25	463.7	0.332	538.2	118.2	0	91.4	8.6	0
Size		2	25	427.2	0.341	825.2	0	0	100	0	0
Size		3	25	454	0.377	1109	288.4	0	59.3	40.7	0
Size	BM [P_B 49/L 500]	1	25	2664	0.624	591.9	0	0	100	0	0
Size		2	25	2925	0.104	1032	0	0	100	0	0
Size		3	25	2636	0.195	1155	0	0	100	0	0
Size	BM [P_B 98/L 500]	1	25	2940	0.987	512.2	0	0	100	0	0
Size		2	25	3462	0.461	683.9	0	0	100	0	0
Size		3	25	3615	1	1363	0	0	100	0	0
Size	BM [P_C 10/L 500]	1	25	171.8	0.176	211.5	0	0	100	0	0
Size		2	25	167.6	0.181	209.6	0	0	100	0	0
Size		3	25	167.5	0.185	210.5	0	0	100	0	0
Size	BM [P_C 25/L 500]	1	25	692.8	0.566	407	0	0	100	0	0
Size		2	25	692.1	0.421	481.7	0	0	100	0	0
Size		3	25	687.8	0.44	491.4	0	0	100	0	0
Size	BM [P_C 49/L 500]	1	25	3294	0.011	889.6	0	0	100	0	0
Size		2	25	5163	1	1219	0	0	100	0	0
Size		3	25	4006	1	1518	0	0	100	0	0
Size	BM [P_C 98/L 500]	1	25	4155	0.19	839.3	0	0	100	0	0
Size		2	25	5093	0.392	793.7	0	0	100	0	0
Size		3	25	3778	0.507	1002	0	0	100	0	0
Size	BM [P_B 98/L 100]	1	25	249.4	0.298	243.9	0	0	100	0	0
Size		2	25	257.1	0.276	281.3	61.48	0	94.6	5.4	0
Size		3	25	276.8	0.375	338.2	124.4	0	76.7	23.3	0
Size	BM [P_C 98/L 100]	1	25	319.3	0.449	462.4	174.7	0	61.3	38.7	0
Size		2	25	337.5	0.375	475.1	156.3	5376	71	26.9	2.1
Size		3	25	368.9	0.39	479.6	141.4	0	78.7	21.3	0

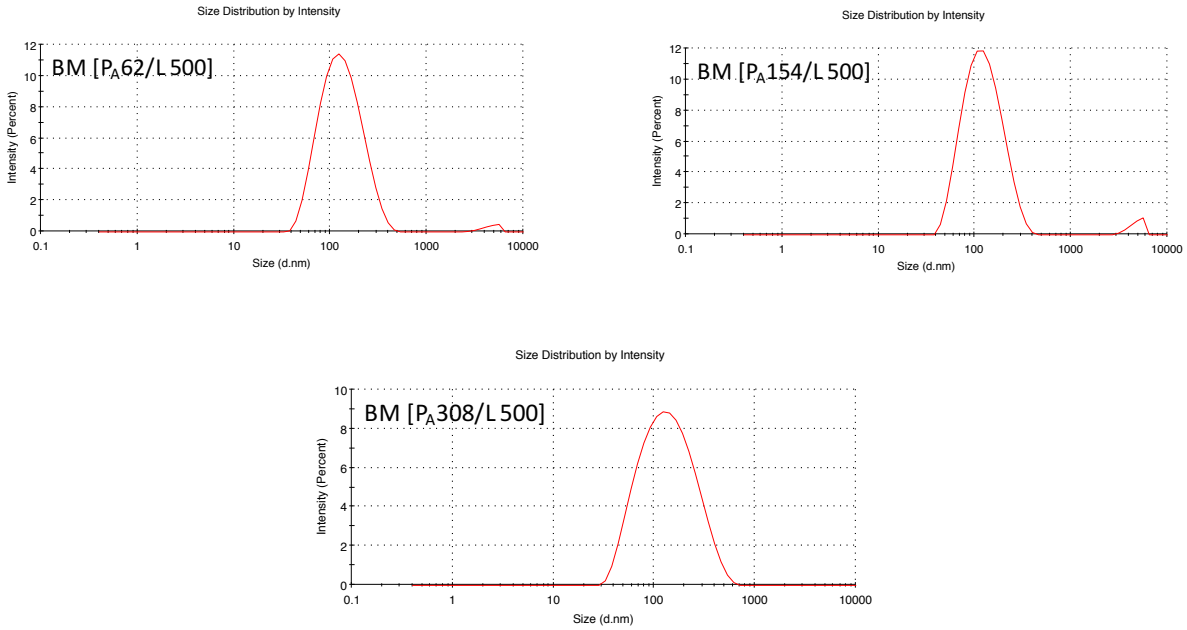

Fig. F5. The intensity-based size distribution of BM [P/L] formulated with zwitterionic P_A peptide enhancer (at M_P = 62 µM, 154 µM, 308 µM) and DOPE helper lipid (at M_L = 500µM).

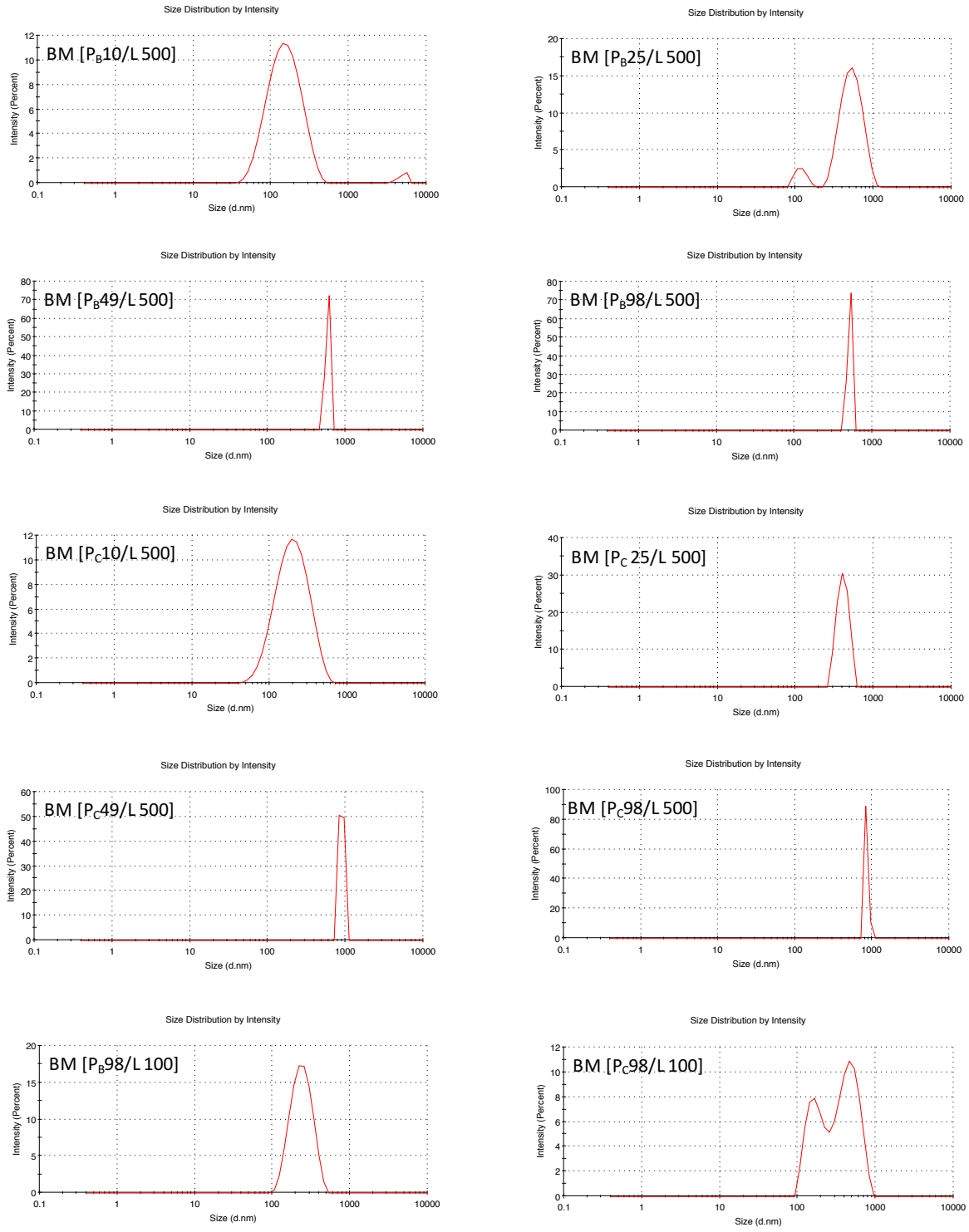

Fig. F6. The intensity-based size distribution of BM [P/L] formulated using cationic P_B and P_C peptide enhancers (at M_P = 10 μM, 25 μM, 49 μM, 98 μM) and DOPE helper lipid (at M_L = 500μM, 100 μM).

Table. F4. Particle size and PDI of BM [P/G] formulations as measured by DLS.

Type	Sample Name	Repeats	T	Z-Ave	PdI	Pk 1 Mean Int	Pk 2 Mean Int	Pk 3 Mean Int	Pk 1 Area Int	Pk 2 Area Int	Pk 3 Area Int
			°C	d.nm		d.nm	d.nm	d.nm	Percent	Percent	Percent
Size	BM [P_B 49/G**6** 31]	1	25	228.8	0.266	300.6	4612	39.63	95.8	2.1	2.1
Size		2	25	234.6	0.303	288.3	4845	0	97.1	2.9	0
Size		3	25	239.9	0.296	307.8	4801	0	97.2	2.8	0
Size	BM [P_B 98/G**6** 31]	1	25	263.8	0.52	345.8	5401	0	97.8	2.2	0
Size		2	25	243.9	0.451	489.4	96.71	0	75.7	24.3	0
Size		3	25	244.9	0.452	507.8	93.73	0	76.2	23.8	0
Size	BM [P_C 49/G**6** 31]	1	25	164.4	0.294	194.4	5156	0	97.7	2.3	0
Size		2	25	169.5	0.254	217.5	4796	0	98.5	1.5	0
Size		3	25	164.1	0.253	180.2	4633	0	95.4	4.6	0
Size	BM [P_C 98/G**6** 31]	1	25	167.6	0.352	218.8	5006	0	97.1	2.9	0
Size		2	25	156.7	0.17	164	0	0	100	0	0
Size		3	25	161.9	0.173	169.4	0	0	100	0	0
Size	BM [P_B 49/G**7** 31]	1	25	181.6	0.237	242.3	0	0	100	0	0
Size		2	25	187.4	0.245	248.9	0	0	100	0	0
Size		3	25	191	0.265	240.9	4005	0	96	4	0
Size	BM [P_B 98/G**7** 31]	1	25	148.3	0.221	187.1	3657	0	97.7	2.3	0
Size		2	25	151.9	0.215	181.5	4964	0	98.6	1.4	0
Size		3	25	151.5	0.225	180.5	38.36	4838	95.9	2.2	1.9
Size	BM [P_C 49/G**7** 31]	1	25	239.5	0.326	263.8	5132	0	96.1	3.9	0
Size		2	25	224.7	0.263	235.6	5103	0	96.5	3.5	0
Size		3	25	215	0.238	236	4414	0	94.8	5.2	0
Size	BM [P_C 98/G**7** 31]	1	25	138.9	0.278	194.6	4822	0	98.9	1.1	0
Size		2	25	137.1	0.265	203.8	0	0	100	0	0
Size		3	25	131.6	0.31	182.5	4290	0	97	3	0

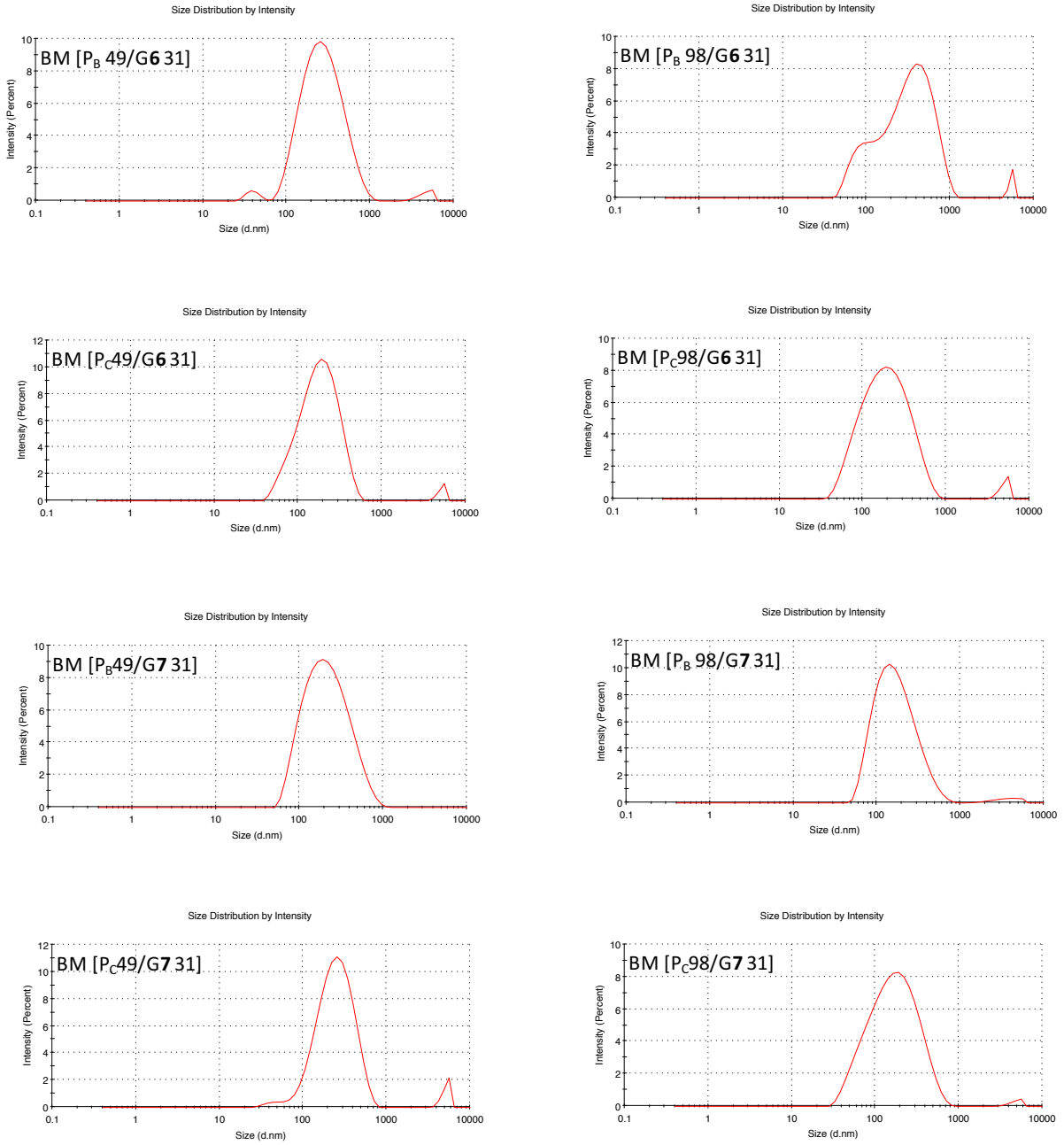

Fig. F7. The intensity-based size distribution of BM [P/G] formulated with cationic P_B and P_C peptide enhancers (at M_P = 49 μM, 98 μM) and G**6** or G**7** gemini surfactants at $\rho_{\pm}$ = 2 (M_G = 31 μM).

Table. F5. Particle size and PDI of PDTMG [P/G/L] formulations as measured by DLS.

Type	Sample Name	Repeats	T	Z-Ave	PdI	Pk 1 Mean Int	Pk 2 Mean Int	Pk 3 Mean Int	Pk 1 Area Int	Pk 2 Area Int	Pk 3 Area Int
			°C	d.nm		d.nm	d.nm	d.nm	Percent	Percent	Percent
Size	PDTMG [P_A 308/G**6** 31/L100]	1	25	2186	0.315	1673	0	0	100	0	0
Size		2	25	1748	0.277	1631	0	0	100	0	0
Size		3	25	1921	0.257	2039	0	0	100	0	0
Size	PDTMG [P_B 49/G**6** 31/L100]	1	25	265.5	0.131	215.5	0	0	100	0	0
Size		2	25	230.8	0.388	207.9	0	0	100	0	0
Size		3	25	240.1	0.466	196.2	5192	0	91.8	8.2	0
Size	PDTMG [P_B 98/G**6** 31/L100]	1	25	151	0.218	166.8	0	0	100	0	0
Size		2	25	146.6	0.217	160.9	0	0	100	0	0
Size		3	25	148.5	0.231	155.3	0	0	100	0	0
Size	PDTMG [P_C 49/G**6** 31/L100]	1	25	205.7	0.95	175.1	0	0	100	0	0
Size		2	25	191.1	0.748	173.7	0	0	100	0	0
Size		3	25	177.2	0.345	159.2	0	0	100	0	0
Size	PDTMG [P_C 98/G**6** 31/L100]	1	25	139.5	0.248	141.5	0	0	100	0	0
Size		2	25	140.8	0.253	137.1	5413	0	98.7	1.3	0
Size		3	25	141.5	0.254	138.4	0	0	100	0	0
Size	PDTMG [P_A 308/G**7** 31/L100]	1	25	280.5	0.443	410.5	5048	0	96.4	3.6	0
Size		2	25	283.2	0.452	690.9	176.1	4912	54.1	43	2.9
Size		3	25	342	0.445	159.1	686.5	0	50.9	49.1	0
Size	PDTMG [P_B 49/G**7** 31/L100]	1	25	191.5	0.168	199.2	0	0	100	0	0
Size		2	25	193.9	0.109	216.2	0	0	100	0	0
Size		3	25	191.5	0.134	210.3	0	0	100	0	0
Size	PDTMG [P_B 98/G**7** 31/L100]	1	25	166.2	0.079	176.1	0	0	100	0	0
Size		2	25	158.1	0.182	172.7	0	0	100	0	0
Size		3	25	153.7	0.194	169.1	0	0	100	0	0
Size	PDTMG [P_C 49/G**7** 31/L100]	1	25	196.2	0.213	200.7	0	0	100	0	0
Size		2	25	191.7	0.16	208.8	0	0	100	0	0
Size		3	25	197.7	0.148	215.5	0	0	100	0	0
Size	PDTMG [P_C 98/G**7** 31/L100]	1	25	161.6	0.222	155.3	0	0	100	0	0
Size		2	25	163.9	0.011	169.8	0	0	100	0	0
Size		3	25	150.9	0.199	166.9	0	0	100	0	0

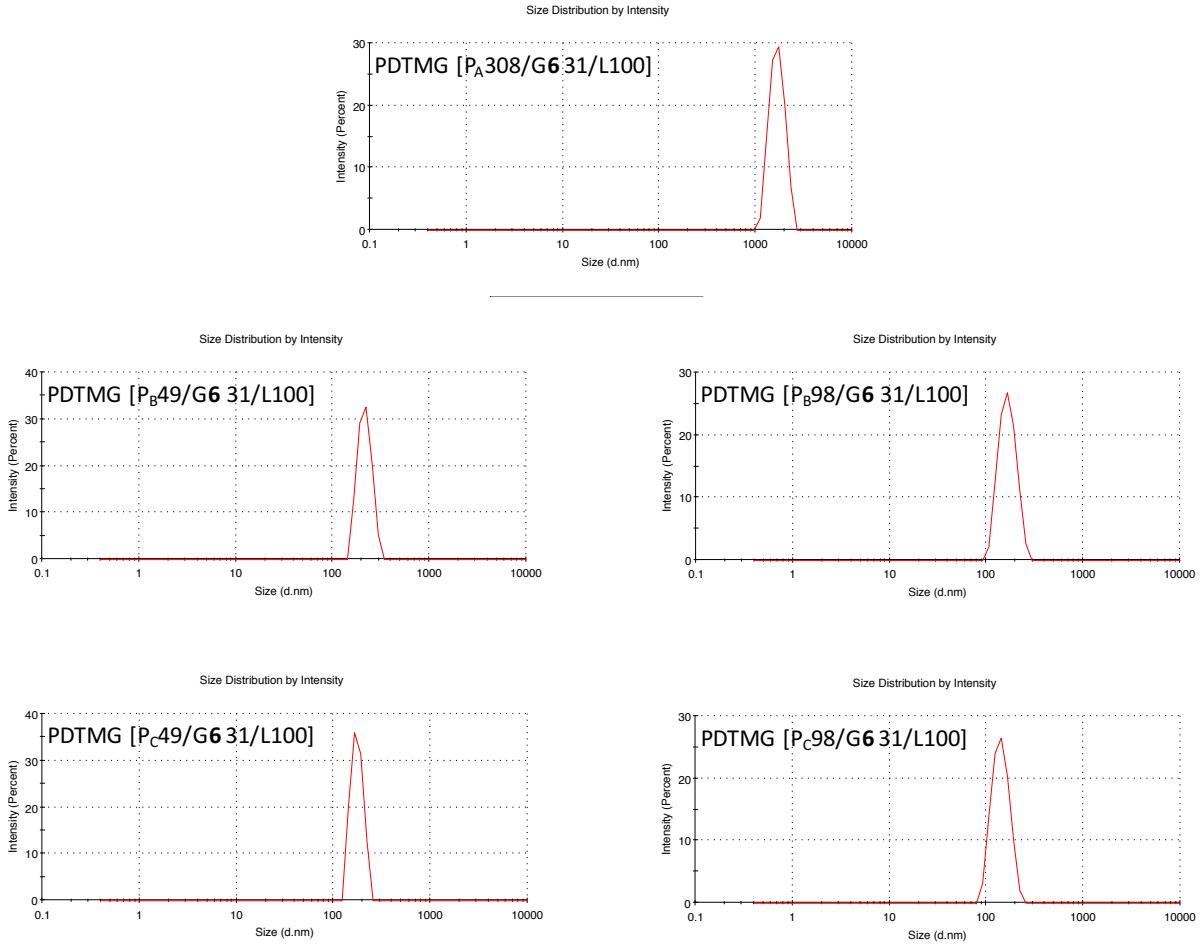

Fig. F7. The intensity-based size distribution of PDTMG [P/G/L] formulated with zwitterionic P_A (at M_P = 308 μM), cationic P_B or P_C peptide enhancers (at M_P = 49 μM, 98 μM), G**6** gemini surfactants, and DOPE lipid at $\rho_{\pm} = 2$ and r = 3.3.

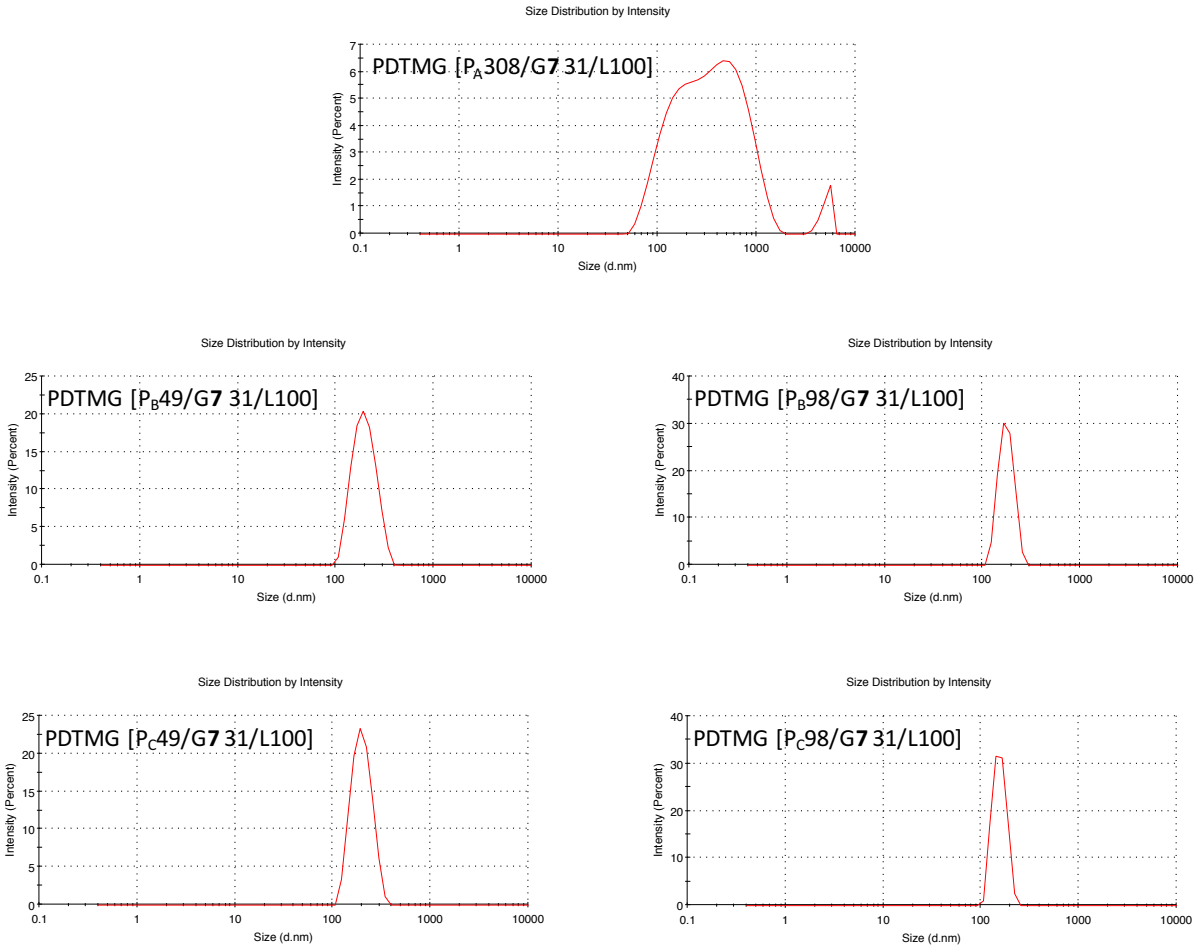

Fig. F8. The intensity-based size distribution of PDTMG [P/G/L] formulated with zwitterionic P_A (at M_P = 308 μM), cationic P_B or P_C peptide enhancers (at M_P = 49 μM, 98 μM), G**7** gemini surfactants, and DOPE lipid at $\rho_{\pm} = 2$ and r = 3.3.

Table. F6. Particle size and PDI of PDTMG [P/G/L] formulations using P_C-P_G peptide enhancers as measured by DLS.

Type	Sample Name	Repeats	T	Z-Ave	PdI	Pk 1 Mean Int	Pk 2 Mean Int	Pk 3 Mean Int	Pk 1 Area Int	Pk 2 Area Int	Pk 3 Area Int
			°C	d.nm		d.nm	d.nm	d.nm	Percent	Percent	Percent
Size	PDTMG [P_C 67/G**7** 27/L100]	1	25	161.6	0.25	218.1	4797	0	98.9	1.1	0
Size		2	25	158.4	0.237	187.2	4140	0	96.2	3.8	0
Size		3	25	155.1	0.221	208.4	0	0	100	0	0
Size	PDTMG [P_D 67/G**7** 27/L100]	1	25	445.2	0.487	613.2	118.2	0	77.4	22.6	0
Size		2	25	375.6	0.575	463.2	101.1	5392	80.5	15.8	3.7
Size		3	25	335.8	0.472	534.5	3763	0	89	11	0
Size	PDTMG [P_E 67/G**7** 27/L100]	1	25	283.8	0.286	435.1	0	0	100	0	0
Size		2	25	284.3	0.306	552.4	141	0	70.5	29.5	0
Size		3	25	269.8	0.312	328.2	4630	59	92.3	4.4	3.2
Size	PDTMG [P_F 67/G**7** 27/L100]	1	25	164.1	0.286	216	4873	0	98.9	1.1	0
Size		2	25	164.7	0.287	218.7	4777	0	97.7	2.3	0
Size		3	25	155	0.265	194.7	4878	0	98.2	1.8	0
Size	PDTMG [P_G 67/G**7** 27/L100]	1	25	157.3	0.248	206.8	42.63	0	95.1	4.9	0
Size		2	25	156.4	0.261	192.6	4503	0	96.5	3.5	0
Size		3	25	149.5	0.284	217.1	0	0	100	0	0
Size	PDTMG [P_C 67/G**7** 20/L100]	1	25	168.6	0.205	195.7	5005	0	98.7	1.3	0
Size		2	25	162.8	0.193	208.5	0	0	100	0	0
Size		3	25	161	0.179	197.5	0	0	100	0	0
Size	PDTMG [P_C 133/G**7** 20/L100]	1	25	169.1	0.232	227.1	0	0	100	0	0
Size		2	25	162.5	0.19	202.4	0	0	100	0	0
Size		3	25	163.7	0.164	196.2	0	0	100	0	0

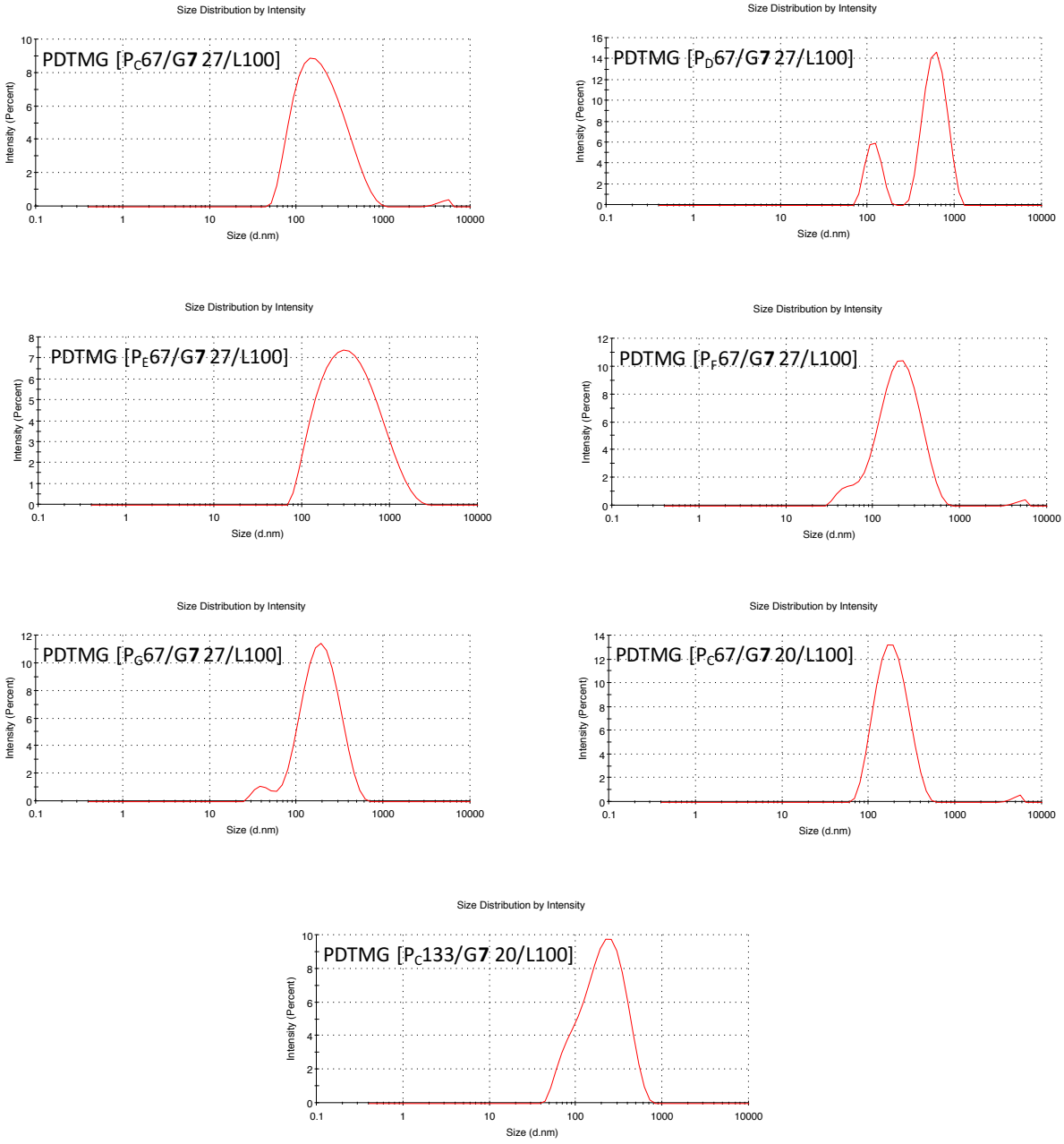

Fig. F9. The intensity-based size distribution of PDTMG [P/G/L] formulated with cationic P_C-P_G peptide enhancers, G**7** gemini surfactants, and DOPE lipid.

Table. F7. Particle size and PDI of PDTMG [P/G/L] formulations using cationic P_C peptide enhancer, with G**7**, G**9** or G**10** gemini surfactants, and DOPE lipid as measured by DLS.

Type	Sample Name	Repeats	T	Z-Ave	PdI	Pk 1 Mean Int	Pk 2 Mean Int	Pk 3 Mean Int	Pk 1 Area Int	Pk 2 Area Int	Pk 3 Area Int
			°C	d.nm		d.nm	d.nm	d.nm	Percent	Percent	Percent
Size	PDTMG [P_C 267/G**9** 17/L113]	1	25	170.4	0.216	216.1	0	0	100	0	0
Size		2	25	176.5	0.224	210.6	0	0	100	0	0
Size		3	25	175	0.24	228.7	0	0	100	0	0
Size	PDTMG [P_C 267/G**9** 27/L100]	1	25	149.3	0.205	191.7	0	0	100	0	0
Size		2	25	153.1	0.229	206.1	0	0	100	0	0
Size		3	25	149.6	0.247	208.6	0	0	100	0	0
Size	PDTMG [P_C 267/G**9** 33/L100]	1	25	150.3	0.234	201.9	0	0	100	0	0
Size		2	25	150.8	0.242	175.8	4851	0	97.4	2.6	0
Size		3	25	150.2	0.247	191.5	4942	0	98.6	1.4	0
Size	PDTMG [P_C 267/G**9** 40/L100]	1	25	148.6	0.244	242	0	0	100	0	0
Size		2	25	151.7	0.263	184	4892	0	97.3	2.7	0
Size		3	25	159.5	0.336	161.2	758	0	74.9	25.1	0
Size	PDTMG [P_C 267/G**10** 17/L113]	1	25	166.3	0.221	217.3	0	0	100	0	0
Size		2	25	164.9	0.164	199.7	41.48	0	97.7	2.3	0
Size		3	25	165	0.228	219.8	0	0	100	0	0
Size	PDTMG [P_C 267/G**10** 27/L100]	1	25	166.9	0.252	236.9	0	0	100	0	0
Size		2	25	173.4	0.203	221.1	0	0	100	0	0
Size		3	25	175.4	0.256	221.4	41.3	5183	93.2	5.6	1.2
Size	PDTMG [P_C 267/G**10** 33/L100]	1	25	146.8	0.236	161.1	4940	0	96.9	3.1	0
Size		2	25	148.1	0.23	202.4	0	0	100	0	0
Size		3	25	150.8	0.204	190.7	0	0	100	0	0
Size	PDTMG [P_C 267/G**10** 40/L100]	1	25	149.8	0.23	194.8	0	0	100	0	0
Size		2	25	146.9	0.232	193.6	31.28	0	98.9	1.1	0
Size		3	25	144.7	0.244	185.2	4770	0	98.3	1.7	0
Size	PDTMG [P_C 267/G**7** 17/L113]	1	25	169	0.255	160.1	0	0	100	0	0
Size		2	25	169.6	0.165	208.5	0	0	100	0	0
Size		3	25	167.3	0.144	201.2	0	0	100	0	0

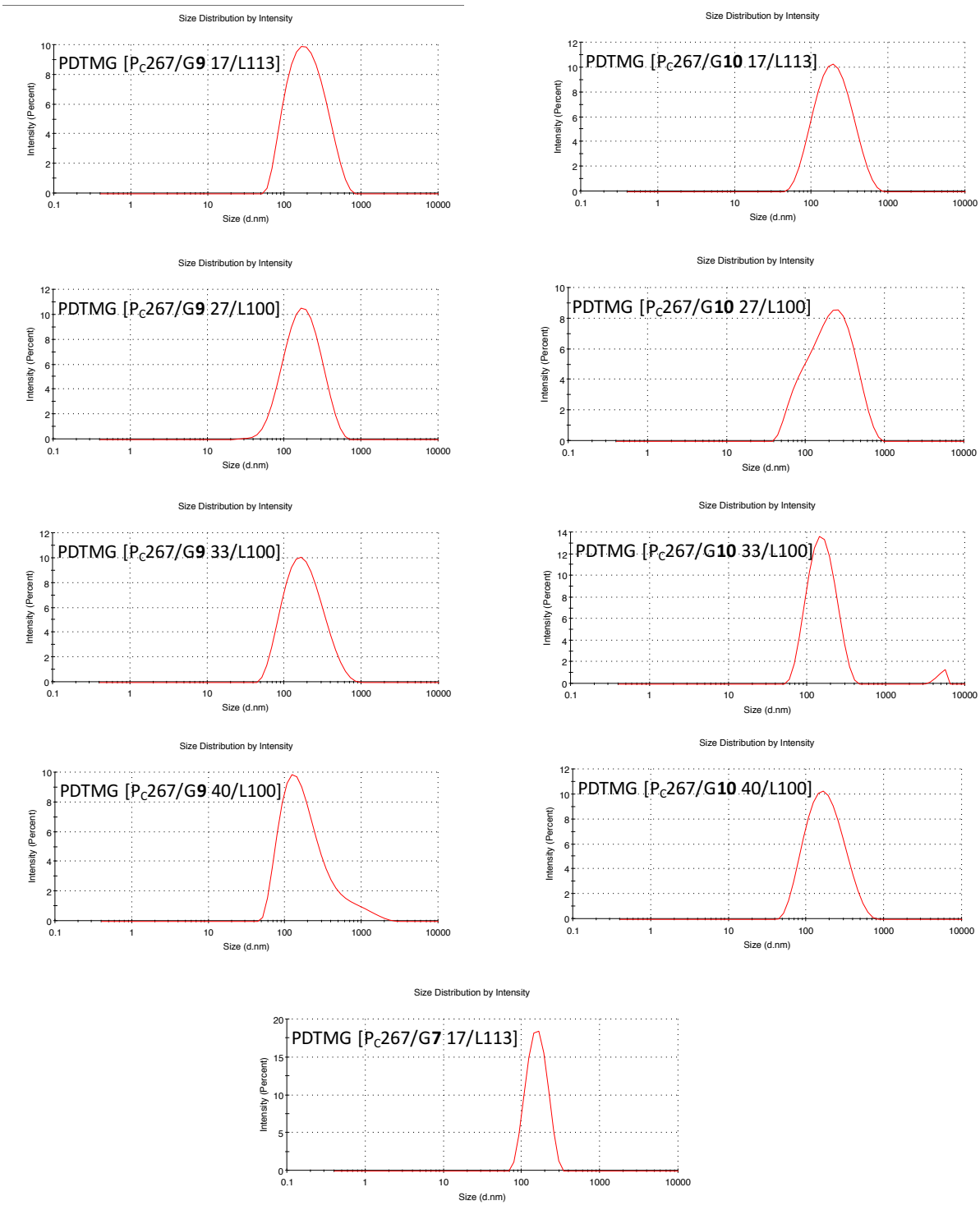

Fig. F10. The intensity-based size distribution of PDTMG [P/G/L] formulated using cationic P_C peptide enhancers in combination with G**7**, G**9** or G**10** gemini surfactants, and DOPE lipid at $\rho_{\pm}$ = 2.5, 2.1, 1.7 and 1.1 (prepared at M_G = 40 µM, 33 µM, 27 µM, 17 µM, respectively).